NMR investigation on molecular mobility of poly(ethylene glycol / oxide) and dendrimer probes in casein dispersions and gels

Souad Salami

ANNÉE 2013

THÈSE / UNIVERSITÉ DE RENNES 1
sous le sceau de l'Université Européenne de Bretagne

pour le grade de

DOCTEUR DE L'UNIVERSITÉ DE RENNES 1

Mention Chimie

Ecole doctorale Vie-Agro-Santé

présentée par

Souad Salami

Préparée à l'unité de recherche :
Technologie des équipements agroalimentaires, Irstea

NMR investigation on molecular mobility of poly(ethylene glycol/oxide) and dendrimer probes in casein dispersions and gels

Thèse soutenue à Irstea
le 21 Février 2013

devant le jury composé de :

Milena CORREDIG
Professeur ● Université de Guelph / *rapporteur*

Armel GUILLERMO
Chargé de recherche (CNRS) ● CEA, Grenoble/ *rapporteur*

Taco NICOLAI
Directeur de recherche (CNRS) ● Université du Maine / *examinateur*

Ronan LEFORT
Maître de conférences ● Université de Rennes 1/ *examinateur*

François MARIETTE
Directeur de recherche ● Irstea de Rennes / *directeur de thèse*

John-van DUYNHOVEN
Professeur ● Wageningen University -Unilever/ *co-directeur de thèse*

Acknowledgments

Acknowledgements

This project was the subject of a scientific and financial cooperation between Irstea (Rennes) and Unilever (The Netherlands) in which the Regional Council of Brittany was financially involved. I wish to thank each side for providing financial assistance.

This dissertation would not have been possible without the guidance and the help of several individuals who, in one way or another, contributed and extended their valuable assistance in the preparation and completion of this study.

First and foremost, my deepest sense of **G**ratitude (with a capital and bold g) to my advisor, Francois Mariette, for his continuous support during my PhD studies, for his patience, motivation, enthusiasm, efficiency, immense knowledge, sense of humor, kindness and great humanity. His guidance helped me throughout the research and writing of this thesis. I could not have imagined having a better advisor for my PhD study.

My warm thanks also go to:

Corinne Rondeau and John van Duynhoven, who co-directed this thesis. Thank you for helping to shape and guide the direction of the work with your careful and instructive comments and for all that you had taught me.

The jury members who honored me by accepting to read and judge this work: as rapporteurs, Prof. Milena Corredig and Armel Guillermo; and as examiners, Taco Nicolai and Ronan Lefort.

Taco Nicolai for valuable and very interesting discussions regarding my project.

Armel Guillermo for providing me with training sessions at the beginning of my thesis in the use of pulsed magnetic field gradients in high-resolution NMR and for valuable discussions regarding my project.

Arnaud Bondon for access to the NMR facilities of the PRISM Research Platform (Rennes), for his valuable help, his extreme reactivity each time I had a problem with the NMR spectrometer, and for everything that he has taught me.

Myriam Barhoum, for helping me in the NMR and microscopy experiments, for her kindness and good work as an intern.

Marie-Helene Famelart and Florence Rousseau (INRA Rennes, UMR STLO) for their assistance with the rheological and dynamic light scattering experiments.

Finally, the members of Irstea for their friendliness, courtesy, hospitality and helpfulness.

In loving memory of my grandmother,

List of contents

Introduction

Introduction

Researchers in the domain of food structure are seeking to unravel the structural organization and dynamics of components in foodstuffs. This represents a challenge due to the wide range of distance and time scales that are involved. An array of spectroscopic and microscopic techniques are used in the food science field, but NMR has distinguished itself by covering a very broad length of scales and by its ability to assess dynamic events in a non-invasive manner. ^{1}H NMR diffusometry and relaxometry are proven methods for the rapid and quantitative assessment of microstructural parameters in foods.

The ^{1}H NMR relaxation and diffusion properties of water and solutes (probes or components of foodstuffs) are often used to probe food microstructures. Water and solute diffusion, as well as the identification of the physical and chemical factors involved in it, have been addressed by different authors in the dairy sector. Concerning casein matrices, studies were carried out within the framework of three PhD theses that were conducted at the Irstea laboratory (Rennes, France). The first one [1] dealt with the diffusion of water in casein systems in order to evaluate the effects of the microstructure by taking the effect of the different components (water, caseins, fat content and the dispersing aqueous phase) into account. A model has been proposed that includes the effect of composition on water diffusion that made it possible to conclude that the microstructure has a small effect on water diffusion. The second one [2] also dealt with the diffusion of water in suspensions and gels of dairy proteins (whey and casein micelle protein), but the study has been extended to investigate the diffusion of polyethyleneglycols (PEGs) of various sizes used as molecular probes. This thesis originally made it possible to highlight the high sensitivity of the probe diffusion to microstructural changes that take place in native phosphocaseinate and whey protein suspensions and gels. The diffusion of linear and deformable PEG probes in native phosphocaseinate suspensions and gels was further studied in the third PhD thesis [3]. In addition to static measurements, a continuous investigation of probe diffusion by NMR during the formation of casein gels was also addressed during this thesis. Two PEG sizes (a 615 and a 96750 g/mol) were selected and their diffusion coefficients were measured throughout the rennet, acid and combined coagulation processes. The results obtained were explained by considering that PEGs can or cannot diffuse through casein particles, depending on their size.

The large probes could only diffuse around casein particles. As a result, they will diffuse faster after coagulation due to the increase in gel porosity, which is known to take place during aging and whose intensity is highly dependent on the type of coagulation, whereas the small PEG will diffuse through the casein particles. After coagulation, casein aggregates become denser and the "through the casein aggregate" diffusion component is reduced. In conclusion, these results showed that there are two characteristic length scales of structure to be considered to explain probe diffusion. For large PEGs, the voluminosity of casein particles and the network porosity are the most important elements, whereas for small PEGs, the internal porosity of the casein particle is the preponderant factor. Such a model was proposed because casein particles are known to be porous and highly hydrated. On the other hand, because PEGs are flexible, they are easily deformable and can change their shape according to their environment. They can therefore diffuse through small spaces compared to their hydrodynamic diameter by adopting a more elongated conformation.

Despite the gains achieved during the third thesis, the mechanisms explaining the relationship between the diffusion of these probes and the structure of casein matrices are still poorly understood. Is the molecular diffusion of probes in casein suspensions and gels modulated by the flexibility of the probe? How does the probe ^{1}H NMR relaxation time change in relation to casein concentration? How would a treatment such as acid precipitation of the micelle, leading to the formation of smaller subunits of approximately 11 nm, affect the probe diffusion? How does the mobility of the matrix affect the mobility of the probe? How can these variations in diffusion be explained?

This project follows in the footsteps of the other projects conducted in our laboratory. It aims to validate the interpretations of Le Feunteun [3] and to improve the understanding of the phenomena that may affect the diffusion of the probe, including the flexibility of the probe, the structure and the mobility of the matrix and the relationship that exists between the size of the probe and the structure of the matrix. This aim was achieved by investigating the mobility of flexible PEG probes and spherical dendrimer probes in two different casein systems (native phosphocaseinate "NPC" and sodium caseinate "SC" systems) using different NMR techniques (^{1}H NMR relaxometry and PFG-NMR diffusometry). The results of this project are enclosed as one published paper and two submitted papers presented as chapters in the present report:

Chapter I presents an overview of previous work on related topics that provides the necessary background for the purpose of this research. The literature review concentrates on three topics (i) milk, caseins and dairy gels; (ii) the use of Nuclear Magnetic Resonance as a tool for the determination of the mobility of molecules in different matrices, with a brief section reviewing the application of other techniques to measure self-diffusion coefficients; and (iii) the mobility of PEG and dendrimer probes in different matrices, including suspensions and gels of the native phosphocaseinate system.

Chapter II describes the materials and methods used in this project.

Chapter III, which includes **Paper I**, presents the results of self-diffusion coefficient measurements of PEG probes with different sizes and casein proteins in both casein systems (NPC and SC). The aim of this study was: (i) to understand the effect of casein supramolecular organization and mobility in determining the diffusion behavior of PEG probes; and (ii) to validate or invalidate the intra-micellar diffusion mechanism already adopted in NPC suspensions to explain the diffusion of probes.

Chapter IV examines the effects of the shape and size of probes on their mobility in NPC suspensions and rennet casein gels with the intent of providing an answer to the following question: "Is the molecular diffusion in systems composed of casein micelles or micellar aggregates modulated by the flexibility of the probe?" Self-diffusion and T_2 relaxation times of spherical dendrimer probes were thus measured and compared with those of flexible PEG probes in NPC suspensions and in a concentrated rennet casein gel (15 g/100 g H_2O). Moreover, both static and real-time NMR measurements were undertaken in this study and were performed at a gel casein concentration of 15 g/100 g H_2O. (**Paper II**)

Chapter V provides an NMR study of the mobility of a PEG/dendrimer couple (R_h~7nm) in dispersions and acid gels of casein protein organized in the form of sodium caseinate, with the aim to understand the respective effects of protein crowding and coagulation on translational and rotational diffusion of these probes. (**Paper III**)

The results of all three papers are discussed in C***hapter VI***. Finally, conclusions are drawn and future perspectives are considered.

1. Métais, A., Caractérisation des coefficients d'auto-diffusion de l'eau par RMN dans les gels laitiers en relation avec leur composition et leur structure. 2003, ENSAR. p. 225.
2. Colsenet, R., Etude par RMN de la diffusion moléculaire : influence de la structure des protéines laitières à l'état liquide et gélifié. 2005, Nantes. p. 237.
3. Le Feunteun, S., Diffusion de sondes moléculaires mesurée par RMN à gradient de champ pulsé : application à l'étude de l'évolution de la structure des systèmes caséiques au cours de la formation des gels. 2007, Nantes. p. 222. (http://tel.archives-ouvertes.fr/docs/00/34/70/02/PDF/these.pdf)

Chapter I

Bibliographic review and objectives

1. Milk, caseins and dairy gels

1.1. Milk and casein micelles

Milk is a complex system containing numerous different components. The main components beside water are lactose (~ 4.6%), fat (~ 4.3%), proteins (~ 3.3%) and minerals (~ 0.7%). Lactose is a disaccharide formed by glucose and galactose. Milk fat consists mainly of triglycerides in a very complex mixture in which the fatty acids highly vary in chain length (2-20 C-atoms) and in saturation. Approximately 80% of the proteins are caseins. The other proteins are β-lactoglobulin, α-lactalbumin, bovine serum albumin and immune globulins [1]. Milk is a heterogeneous aqueous system that contains various phases:

- An aqueous phase that is also known as milk serum and that contains lactose, soluble proteins, mineral salts, hydrosoluble vitamins and other elements (peptides, amino acids, urea, etc.).
- An emulsion of fat globules in the aqueous phase with a diameter of between 1 and 8 micrometers.
- A micellar phase that consists of a suspension of colloidal particles made up of caseins.

The function of caseins is assumed to be primarily nutritional. Owing to their commercial importance, they have been extensively studied and are among the most well characterized food protein systems. There are four major types of casein molecules, α_{s1}, α_{s2}, β and κ, in a proportion of 3:1:3:1 [2], which exhibit microheterogeneity that arises from differences in the degree of phosphorylation or glycosylation (κ-), cysteine content and hydrophobic character [3]. Most casein in milk (94%) exists as large colloidal particles suspended in the aqueous phase, 50-600 nm in diameter, referred to as "casein micelles". They are composed of several thousand individual molecules of all four types of caseins, as well as minerals (6%), essentially calcium and phosphate, referred to as colloidal calcium phosphate (CCP), which enables cross-linkage between caseins and contributes to the structure of the micelle [3-4]. The stability of these colloidal particles is provided by a ''hairy'' surface layer of the protein, κ-casein, part of which (C-terminal side) protrudes into the aqueous phase of the milk and provides steric and

electrostatic stabilization of the particles [5-6]. Casein micelles are considered to be in "dynamic equilibrium" because they are highly dependent on environmental conditions such as pH and temperature. For example, at 20°C, 94% of the caseins are in the micelle [7], whereas at 4°C, approximately 50% of the caseins are in the aqueous phase [8].

The average physical characteristics of casein micelles are presented in Table **1**:

Characteristic	Value
Mean diameter[9]	In the order of 200 nm
Surface area	8×10^{-10} cm^2
Volume	2.1×10^{-15} cm^3
Density (hydrated)	1.0632 g cm^{-3}
Mass	2.2×10^{-15} g
Water content	63%
Hydration[10]	3.6 g H_2O g^{-1} protein
Voluminosity[10]	4.2 cm^3. g^{-1} protein
Molecular mass (hydrated)	1.3×10^9 Da
Molecular mass (dehydrated)	5×10^8 Da
No. of peptide chains	5×10^3
No. of particles per mL milk	10^{14}-10^{16}
Surface of micelles per mL milk	5×10^4 cm^2
Mean free distance	240 nm

Table 1: Average characteristics of casein micelles [4, 9-10].

Casein micelles are heterogeneous, both in composition and size, with a much greater polydispersity than many other protein assemblies. The majority of the micelles have a diameter of between 100 and 200 nm [9]. Due to this polydispersity, many techniques are not appropriate to precisely measure the size of the micelles. The two most commonly used techniques are electron microscopy and light scattering. Other methods such as electroacoustic [11] and diffusion wave spectroscopy [12-13] have been implemented for this purpose, and the measured size (a mean diameter of between 180 and 200 nm) was in agreement with the values determined using photon correlation spectroscopy. Moreover, the size of the micelles is subjected to a natural variability linked to the race and to the lactation period of the animal [14]. The fractionation of casein micelles by exclusion chromatography [15] or by differential ultracentrifugation [7, 16] showed an inverse relationship between the size of the micelles and their kappa casein content. These variations are compensated for by the opposite behavior of α_s and β caseins according to

exclusion chromatography, whereas differential ultracentrifugation revealed that only β casein was involved.

Casein micelles are roughly spherical, very porous, highly hydrated and sponge-like colloidal particles that contain approximately 3.6 g H_2O/g protein [10]. Casein micelle hydration can be directly determined by measuring the dry extract of micelles sedimented by ultracentrifugation[15] or indirectly by measuring their voluminosity [17]. The voluminosity can be estimated by electron microscopy, light scattering, measurement of the intrinsic viscosity, or from the diffusion coefficient of casein micelles [18]. Depending on the method used, the values of the voluminosity vary between 1.5 and 7.1 cm^3/g [19]. Recently, de Kruif et al. [10] and Morris et al. [20] reported a voluminosity of 4.2-4.4 ml/g, on the basis of viscosity measurements, which corresponds to a micellar hydration of 3.6-3.4 g H_2O/g protein.

Regardless of the method used, casein micelles have a higher hydration rate than other proteins in solution [21]. This characteristic could be attributed to the porous character of casein micelles as well as to their strong surface hydration. The porosity of micelles was demonstrated by showing that large molecules such as β-casein (24000 g/mol) [22] or transglutaminase (45000 g/mol) [23-24] can enter and exit the casein micelle. The surface hydration was attributed to the presence of a "hairy layer" constituted of negatively charged[18] hydrophilic peptidic chains whose flexibility was revealed by ^{1}H NMR [25].

1.2. Structure of casein micelles

1.2.1. Internal structure

Due to the importance of the role of casein micelles in relation to many of the physico-chemical properties of milk and dairy products, their structure and properties, as well as the effects of compositional and processing factors, have been extensively studied. Since the discovery of the micelle-stabilizing protein, κ-casein, in 1956, several models of the casein micelle have been proposed and refined. Yet their structure is still a puzzle and is continuously the subject of debates among the scientific community. Based on the biochemical properties of the micelles, two types of models have been proposed: the submicelle model [26-30] and the open structure model [6, 21, 31-33]. Both are in agreement that the molecular chain of the C-terminal end of κ-

casein protrudes from the micelle surface, forming a so-called hairy layer, and that colloidal calcium phosphate plays an active role in the micellar structure.

The most enduring of the early attempts is the submicelle model which, though with refinement and rethinking, still remains largely as described by Slattery and Evard [34] and Slattery [35] with chief elaboration by Schmidt [36]. In the submicelle model, the caseins first aggregate via hydrophobic interaction into subunits (15-30 nm) of 15-20 molecules each. The pattern of interaction is such that it brings about a variation in the κ-casein content of these submicelles. Those rich in κ-casein congregate on the micelle surface, whereas those that are poor or totally deficient in κ-casein remain inside the micelle. The submicelles are linked together via the CCP as depicted in **Figure 1**. The elaboration of Schmidt is to link these interior submicelles by colloidal calcium phosphate. It is hypothesized that support for the submicelle was found in the shoulder in the SANS spectra at Q~0.35 nm^{-1}, leading to a correlation length of approximately 18.6 nm in radius.

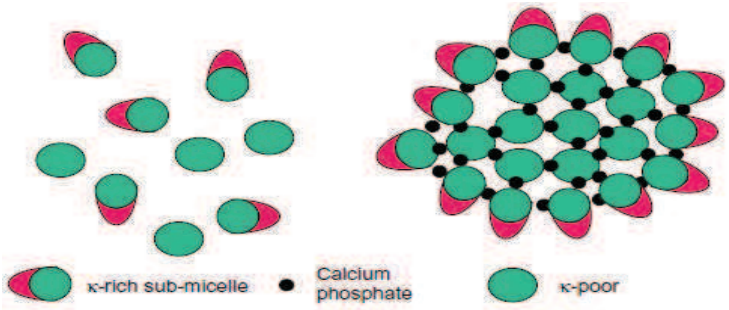

Figure 1. Schematic diagram of the submicelle model of the casein micelle (extracted from Horne [31]).

The second type of model represents the micelle as an open, spherical and porous structure. In this model, the subunits are nanoclusters of CCP, randomly distributed in a homogeneous web of caseins. As illustrated in **Figure 2**, both of these models depict the micelle as being made up of casein molecules linked together by CCP nanoclusters and a collection of weak interactions, but they differ in detail. The term of weak interactions is explicitly used as a collective term for hydrophobic interactions, hydrogen bonding, ion bonding, weak electrostatic interactions and other interactions leading to self-association. This multiplicity of binding interactions probably plays a role in maintaining supramolecular integrity, as well as giving casein micelles a level of

elasticity and making them resistant to complete dissociation if only a single interaction is eliminated.

a b

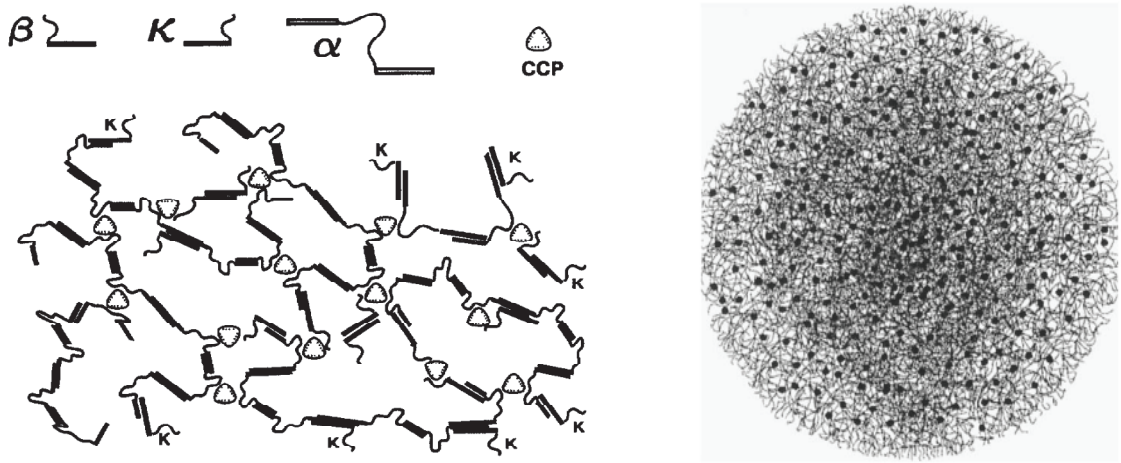

Figure 2. (a) Micellar structure model according to Horne [33]; (b) Micellar structure model according to Holt (extracted from Farrell [37]).

Although κ-casein molecules can interact via their hydrophobic domains with the hydrophobic regions of the other caseins, further growth beyond the k-caseins is not possible because they possess neither a phosphoserine cluster for linkage via colloidal calcium phosphate, nor another hydrophobic anchor point to extend the chain via the established route. κ-casein acts as a terminator for both types of growth and unless it is circumvented by the growing network, it will become part of the surface structure of the micelle. Hence, its surface location arises naturally in this model. The size of the casein micelles would therefore be inversely proportional to the amount of κ-casein.

At the same time as the physico-chemical studies, electron microscopy of the particles was also used to directly study the shapes and structures of the micelles. The open structure model shows a high degree of correspondence with the transmission electron micrographs of McMahon and Marchin et al. [38-39], while the submicelle model was effectively eliminated as a result of the detailed electron microscopy studies of these authors.

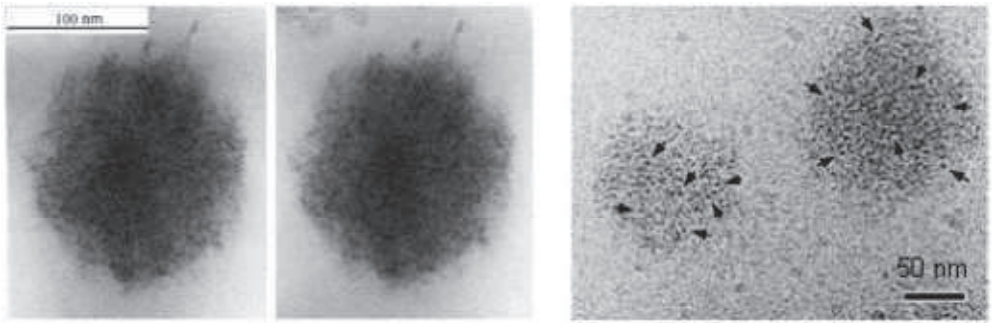

Figure 3. Transmission electron micrographs of casein micelles extracted from McMahon et al. [38] (left) and from Marchin et al. [39] (right).

Early electron microscopy studies gave pictures of casein micelles with a raspberry-like appearance and lent support to the submicelle model [40-41]. Such structures were shown to be artifacts of sample preparation and treatment [38]. Stereo images of casein micelles (**Figure 3**) obtained by cryo-transmission electron microscopy (cryo-TEM) showed an inhomogeneous internal structure within the micelle, but no electron-dense particles larger than 8-10 nm, with most individual areas only 2-3 nm [38]. Marchin et al. [39] (**Figure 3**) also demonstrated that the only substructures characterized by cryo-TEM and small angle x-ray scattering (SAXS) were attributed to calcium phosphate nanoclusters of approximately 3 nm in diameter. The high resolution field-emission scanning electron microscopy (FE-SEM) study [42] (**Figure 4**) shows no evidence of spherical subunits, but instead suggests an organization of the caseins into tubular structures protruding from the surface and originating from within the micelle.

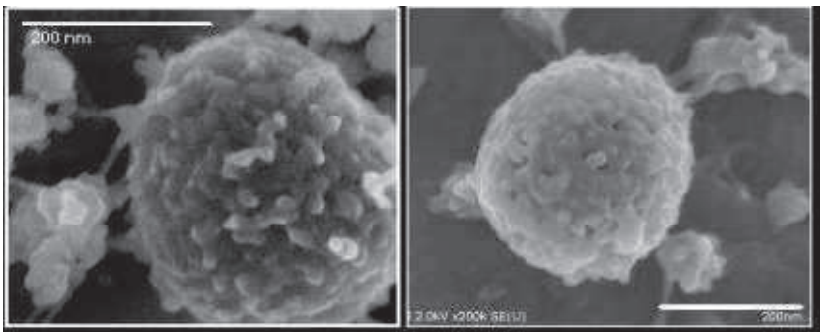

Figure 4. Electron micrograph of an individual casein micelle made using field-emission scanning electron microscopy (extracted from Dalgleish et al.[42]).

In a similar manner, Pignon et al. [43], using an exceptionally wide scattering vector range (SAXS and USAXS "Ultra-Small-Angle X-ray Scattering") allowing the characterization of the whole casein micelle, showed that casein micelles were organized as an entangled network rather than an agglomeration of globular submicelles, casting still more doubts on the submicelle model. On the other hand, the open structure models [2, 44] are mainly theoretical models and have weaknesses as well. Moreover, such a network model does not fully explain the combination of particulate or thread-like structures observed in the transmission electron microscopy (TEM) cross-sectional freeze-fracture replica images reported by Heertje et al. [45] or, more recently, by Karlsson et al. [46]. Cross-sectional TEM images of rat mammary glands have also shown the presence of particulate aggregates during the bioassembly of casein micelles in Golgi-associated vacuoles. Evidence for the particulate aggregates was also provided by Hojou et al. [47] who used ion beam sputtering and etching to disintegrate casein micelles into star-like particles of approximately 7 to 13 nm in diameter, observed by using TEM, in contrast with the results obtained by Marchin et al. [39].

More recently, McMahon et al. [48] proposed a new model structure for casein micelles that includes both protein chains and protein-calcium phosphate aggregates. An interlocking lattice model of the casein micelle supramolecule is proposed from their interpretation of high-resolution TEM micrographs of freeze-dried, immobilized, uranyl oxalate-stained casein micelles (**Figure 5**).

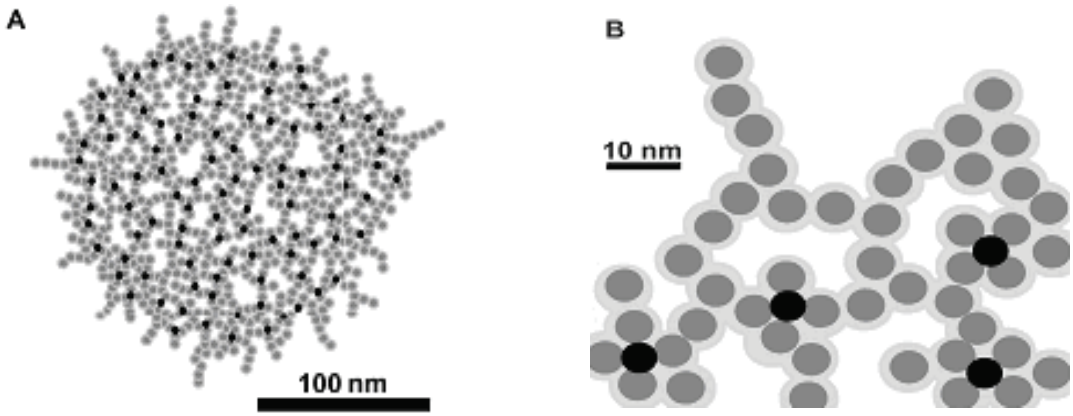

Figure 5. Schematic diagram of an interlocking lattice model of the casein micelle. (A) The complete supramolecule; (B) A portion of the supramolecule periphery (extracted from McMahon et al. [48]).

Proteins are represented as spheres of 8 nm in diameter that both surround the calcium phosphate nanoclusters (represented as spheres of 4.8 nm in diameter) and extend as short chains between the interlocking points and out from the periphery of the supramolecule. These calcium phosphate-casein aggregates, in the size range of 7 to 13 nm as observed by Hojou et al., serve as structure-forming sites to which other caseins can be bound, forming short chains between them.

However, Horne's model [33] made it possible for the first time to explain several phenomena concerning not only some properties of casein in solution, but the influence of various parameters on the physical properties of dairy gels as well [49-52]. As a result, it was suggested that this model is the prevailing model in comparison to other open structure models. Further refinement of these models can be expected, especially as electron microscopes are improved.

1.2.2. Surface structure of casein micelles

On the basis of the recent studies of Dalgleish et al. [42] and Marchin et al. [39], the casein micelle surface seems to be more complex than that of a simple sphere surrounded by a hairy layer. Due to the high resolution of scanning microscopy (FE-SEM) and cryo-TEM, the authors showed that the surface consisted of tubules extending to the exterior, with large gaps in between (**Figure 4**). The amount of κ-casein in milk (10%) [3] is insufficient to cover the micellar surface on its own, especially if the surface is not smooth. According to these authors, κ-casein would be grouped at the extremity of the tubules rather than forming a surrounding continuous brush on a hard sphere, so that other caseins can be well exposed to the exterior at the surface of the casein micelles. A new analytical tool known as Biacore has recently been developed, based on surface Plasmon resonance technology. This technique makes it possible to study the interactions between two molecules such as antigens and antibodies. Marchin et al. [53] showed that Biacore can be used to obtain information about the composition of the casein micelle surface. Their results confirmed the preferential location of κ-casein at the surface, in agreement with previous studies on ^{1}H NMR [25], and showed that all caseins seem to be accessible at the surface, with a lower accessibility for α_{s2}-casein, in agreement with the idea that the casein micelle surface is a natural extension of the internal casein network with a termination role of κ-casein.

1.3.The casein micelle: a stable structure?

Casein micelles form a system that is remarkably stable when subjected to the principal treatments that milk undergoes during industrial processes. They can withstand a very high-temperature thermal treatment and aggregation is only induced when the temperature is equal to or greater than 140°C for 15-20 mn at the natural pH of the milk, due to dephosphorylation of caseins and/or cleavage of the κ-casein part rich in carbohydrates. They support compaction, i.e., they can be sedimented by ultracentrifugation and then redispersed by agitation. The micelles also support the addition of Ca^{2+} (at least up to 200 mM) without being aggregated [6, 21, 26]. However, under certain conditions, the micelles may be destabilized. The stability of casein micelles may be divided into two categories: intermicellar and intramicellar stability.

The intermicellar, or colloidal stability, of casein micelles refers to the stability of casein micelles in terms of aggregation, e.g., under the influence of heat, ethanol, acid or rennet. Such stabilities are well characterized and, in some cases, form the basis of the conversion of milk into other dairy products, e.g., rennet- or acid-induced coagulation of milk forms the basis of the manufacture of cheese and yogurt, respectively (**Section 1.3.2.**).

Whereas, the intramicellar stability is the ability of the casein micelle to maintain its internal structural integrity under the influence of environmental changes. Colloidal calcium phosphate (CCP) and hydrophobic interactions are primary features in maintaining micellar integrity. Solubilization of CCP, most easily achieved through the addition of a calcium-chelating agent or by acidification, results in the disintegration of the casein micelles into small, hydrophobically-bound casein aggregates. Furthermore, treatment of milk at high hydrostatic pressure can result in considerable disruption of casein micelles, although through solubilization of CCP. Dissociation of casein micelles can also be achieved through disruption of hydrophobic interactions, e.g., through the addition of urea or SDS, or heating milk to > 60°C in the presence of > 30% ethanol [3, 54]. The present project has only addressed acid precipitation, which will therefore be the only one discussed in **section 1.3.2.**.

1.3.1. Coagulation of milk

a. Rennet coagulation

Milk can be coagulated by enzymes of animal, plant and microbial origin. However, the most commonly used enzyme is rennet. There seems to be a consensus in the literature that rennet-induced milk coagulation is the result of three underlying stages with different mechanisms (**Figure 6**):

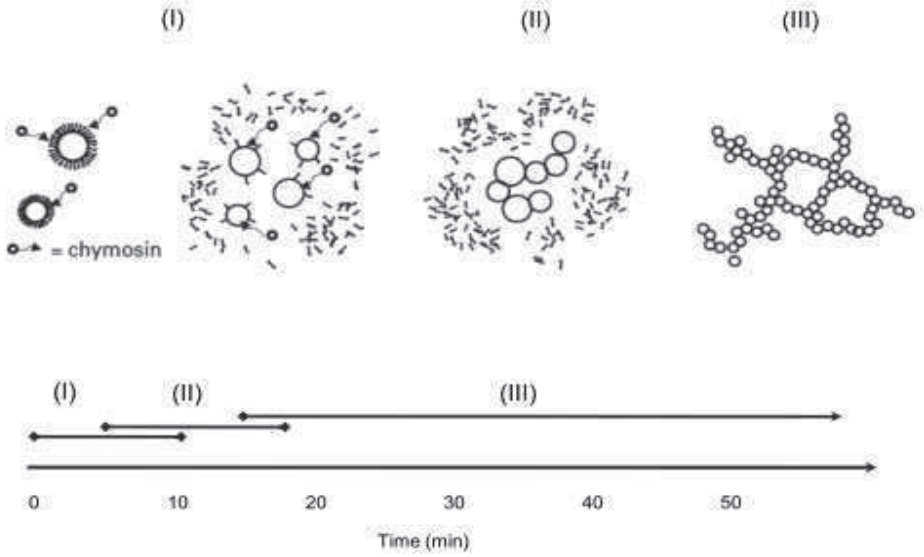

Figure 6. Illustration of the rennet coagulation process. (I) κ-casein removal by chymosin; (II) para-casein aggregation; (III) gel network formation (modified from Dalgleish, 1993 [55]).

I. Enzymatic hydrolysis of κ -casein

The chymosin cleaves the Phe^{105}-Met^{106} peptide bond of κ-caseins, leading to the formation of κ-para-casein and to the release the C-terminal peptide residues 106-169, known as caseinomacropeptides (CMP). The hydrophilic CMP is strongly negatively charged. It is the κ-casein part that is responsible for steric and electrostatic repulsions between the casein particles. The action of the chymosin therefore corresponds to the suppression of this stabilizing hairy layer

and to the destabilization of the colloidal suspension. Consequently, a reduction of the total charge and the size of particles is observed (from 7 to 15 nm [5, 56]).

II. Para-casein micelle aggregation

When the rate of hydrolysis of κ-caseins reaches 70 to 85% [5], the resulting para-casein micelles spontaneously aggregate and form a microscopic network. The aggregation rate depends on the concentration of free para-casein sites, implying that this stage is dependent on the rate and degree of casein proteolysis.

III. Gel network formation and aging

This third phase corresponds to the aging of the gel and is characterized by the occurrence of structural changes in the casein network. This latter phase is of primary importance because it is common to all casein gels, and also because the gel microstructure is directly related to the physical characteristics of the product. To describe this particular phase, Mellema et al. [57] proposed a general model based on several types of rearrangements that occur at different length scales: fusion of individual particles, rearrangement of particles, rearrangement of particles clusters and macroscopic syneresis. According to these authors, particle fusion and inter-particle rearrangements result in the formation of straight and progressively thinner strands, with more bonds per casein aggregate and, hence, stronger junctions. This consequently leads to stretching of strands and stiffening of the gel [57]. Although the mechanisms involved are not fully understood, all authors agree that rearrangements give rise to local matrix fusion and compaction, resulting in a gel with larger pores and higher permeability [58-65]. After network establishment, the progressive reorganization of the gel microstructure is thus accompanied by a reduction in the amount of water contained in casein particles (syneresis); the aggregates become denser.

Although the nature of the stages is different, they are not clearly separated in time. The aggregation phase always starts before the end of the enzymatic reaction [5] and occurs at an even lower degree of κ-casein hydrolysis when the casein concentration is increased [59, 66].

Nevertheless, the kinetic profiles for the different coagulation stages can be influenced by many process factors:

Factors that affect the rate of κ-casein proteolysis. The effect of temperature is relatively small and corresponds to Brownian motion (random diffusion), thereby increasing the encounter frequency between rennet molecules and κ-casein. pH has a large impact since lowering the pH increases the affinity of the rennet enzyme to the micelles, increasing the reaction rate. If the pH is too low, the reaction rate is lower, presumably because the elevated affinity is so high that it takes some time for the enzyme to release again [62, 67].

Factors that affect the rate of aggregation. Temperature has a big impact due to the increase of Brownian motion, increasing the encounter frequency between para-casein micelles, e.g., at 20°C, aggregation does not occur at all. Increasing the temperature also results in strengthening the hydrogen bridge and hydrophobic interactions between the para-casein micelles.
Ca^{2+} concentration considerably influences the aggregation rate because in addition to Van der Waal attraction forces, a sufficient Ca^{2+} concentration is required for two reasons: Ca^{2+} diminishes the electrostatic repulsion between micelles and Ca^{2+} ions can make bridges between negative sites in the para-casein micelles.
pH influences the aggregation rate in two ways: by lowering the pH, Ca^{2+} activity increases and the affinity of the enzyme increases causing thus proteolysis to occur in concentrated regions of the micelle surface as opposed to random surface positions. In this way, a free para-casein site becomes available sooner than when random surface proteolysis at a higher pH occurs. Consequently, it has been observed that aggregation begins at different degrees of proteolysis: 70%, 60% and 40%, at pH values of 6.6, 6.2 and 5.6, respectively [68-72].

Factors that affect the rate of gel formation. Temperature has an effect on Brownian motion and on the strengthening of the hydrogen bridge and hydrophobic interactions between the para-casein micelles. Consequently, the rate of gel formation is influenced [60, 62, 73].

The coagulation properties of milk also change with increasing casein concentration: (i) the aggregation phase occurs at a lower degree of κ-casein hydrolysis [66]. This is believed to be caused by a smaller mean free distance between casein micelles, which increases the collision frequency, and higher concentrations of ionic calcium, which reduces the electrostatic repulsions [66]; (ii) The elasticity and the firmness of the gel increases [74]; and (iii) less water and whey

proteins are expelled from the gel [59]. For example, Karlsson et al. [59] showed that the coagulation properties and microstructure during coagulation of ultrafiltrated skim milk concentrated at pH 5.8 are very different compared to those in unconcentrated skim milk. At the same rennet concentration, coagulation started at a lower degree of k-casein hydrolysis compared with the unconcentrated skim milk. Confocal laser scanning micrographs revealed that small aggregates developed in the concentrated skim milk during renneting. There was also a slower and less extensive rearrangement of the casein network in gels from UF concentrated skim milk due to a rigid and dense network formed at an early stage after coagulation.

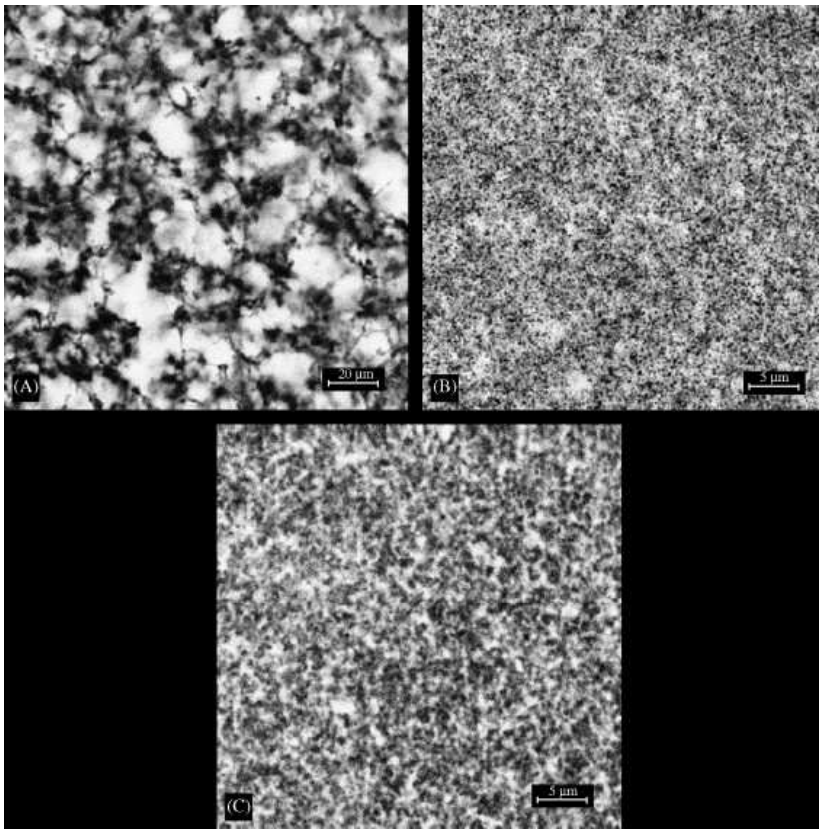

Figure 7. Confocal images of rennet-induced casein gels made from: (A) unconcentrated skim milk 24 h after rennet addition; (B) UF concentrate at 24 h; and (C) 60 days after rennet addition (extracted from Karlsson et al. [59]).

Although the coagulation mechanism remains the same, there is a big variety of gels that can be formed by rennet coagulation.

b. Acid and combined coagulation

The alteration of the milk pH and, more specifically, its acidification, is a fundamental step in many transformation processes of dairy products (yogurts, etc.). The two acidification processes used in the dairy industry result in a slow reduction of pH while remaining above 4.6 to prevent the precipitation of caseins [75]. In the traditional process, milk is acidified by bacteria that ferment lactose into lactic acid. A second process is direct acidification by the addition of a lactone such as glucono-δ-lactone (GDL) [76].

During the gradual acidification of the micelle, the binding capacity of casein for the mineral decreases due to a reduction of the negative charge of the phosphoserine residues and carboxyl groups [77]. This leads to a progressive dissolution of the CCP and calcium linked to caseins, causing a release of soluble caseins in the serum phase [78]. However, the micelle do not dissociate due to numerous intramolecular hydrophobic interactions, enabling the micelle to retain its supramolecular integrity [6]. A lowering of pH also results in an increase of the activity of Ca^{2+}, leading to a neutralization and a screening of negative charges of the micelle [79]. The result is a reduction in the electrostatic repulsion between the micelles. In addition, closer to their pH_i, κ-caseins became insoluble and tend to precipitate, which causes a total collapse of the stabilizing brush [6, 9, 80]. Moreover, the hydration of casein micelles and, therefore, their size is modified upon acidification [81-84]. More generally, acidification causes a loss of the repulsive forces and leads to the aggregation of the micelle.

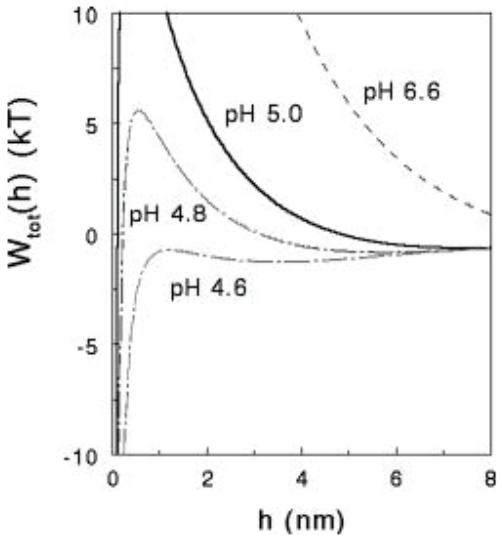

Figure 8. Calculated total interaction potential between casein micelles for various pH values. W(h) represents the potential of interaction between two micelles separated by a distance, h (extracted from Tunier et al. [85]).

Aggregation can also result from the joint action of rennet and pH. Since the action of the rennet is generally quicker than that of the acidification, this type of gel most often forms in two stages. During the first one in which the acidification has already begun, enzymatic action leads to the formation of a gel with a strong rennet character. The acidification continues and at a pH of approximately 5, when the CCP is completely soluble, the macroscopic properties of the gel change. This is the second stage that is characterized by the progressive evolution of certain properties of the gel with a strong rennet character towards that of a gel with a predominantly acid character [86-88].

As in the case of rennet gels, structural rearrangements occur and can lead to particle fusion or to increased gel permeability. Le Feunteun et al. [88-90] reported that concentrated acid gels are less subject to rearrangements than concentrated rennet gels, as illustrated by the very low and slowly evolving stiffness during gel aging. In contrast, concentrated combined gels are constituted of thicker aggregates and larger pores (**Figure 9**).

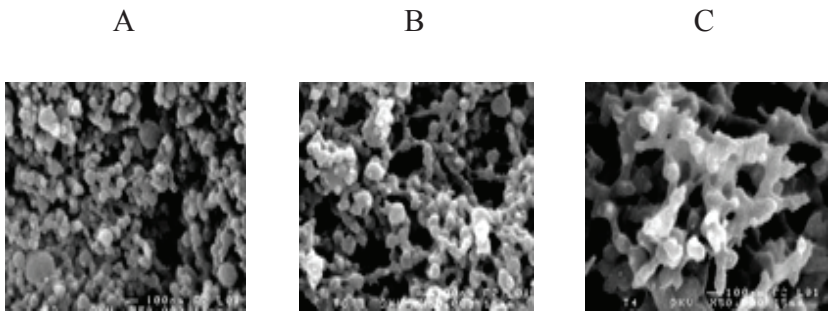

Figure 9. Different concentrated casein gel types. A: combined gel; B: rennet gel; c: Acid gel (extracted from Le Feunteun et al. [90]).

The present project did not address either acid or combined coagulation and it will not be described further.

1.3.2. Sodium caseinate

Milk caseins can be precipitated at a pH below 4.6 and then washed to remove the soluble salts, lactose and whey proteins. The precipitated caseins are then dehydrated, redissolved by re-neutralization of the system to a pH of approximately 7 with NaOH, and finally dried. The submicelles obtained are usually called sodium or calcium caseinate, depending on the counterion used in the neutralization. Sodium and calcium caseinate are widely used in industry for their excellent functional and nutritional properties, but calcium caseinate has only a limited solubility [91-92].

1.3.2.1.Characterization and behavior of sodium caseinate in solution

Sodium caseinate has been characterized in aqueous solution using static and dynamic light scattering by a number of research groups [93-100]. Casein particles are present as individual molecules at low ionic strength (3 mM NaCl) and low casein concentrations with a z-average hydrodynamic radius (R_{hz}) of 3 nm and a molecular weight (M_w) of $2.5x10^4$ g/mol. At high casein concentrations (> 80 g/L) or at high ionic strength (> 100 mM NaCl), neutral pH and room temperature, casein particles form small aggregates (R_{hz} = 11 nm; $M_w = 2.6x10^5$ g/mol) [98-99]. These well-defined aggregates that contain approximately 15 casein molecules are formed by

association of the hydrophobic parts of the casein molecules in a manner similar to the micellization of surfactants. The aggregation number (N_{agg}) increases only weakly with decreasing pH between pH 8 and 6 [99], but extensive acid-induced aggregation may occur at low pH values (below pH 5.4 at 250 mM and below pH 6.0 at 3 mM) [93, 97, 99, 101]. N_{agg} increases reversibly with increasing temperature between 10 and 50°C, but is independent of the temperature at higher values, at least up to 70°C. Like the casein micelle system, sodium caseinate is a dynamic system; its behavior depends largely on its environment.

Sodium caseinate solutions, which mainly contain α_{S1}-, α_{S2}-, β- and κ-casein in a ratio of 4:1:4:1, also contain a small weight fraction of larger particles with a radius of approximately 100 nm [93, 98-100]. The nature of the large particles is, as yet, unknown, but it is clear that they are not residual native casein since, contrary to the latter, they do not sediment during ultracentrifugation. It was suggested [99] that the particles are complexes containing both fat and proteins with ratios that make their density close to that of water.

1.3.2.2.Aggregation of sodium caseinate particles

Sodium caseinate solutions are perfectly stable over time. Their aggregation can only be brought about by the addition of calcium or through acidification. The present project has not addressed coagulation through the addition of calcium and, therefore, will not be described here.

Slow acidification of a caseinate solution causes the formation of a gel. The microstructures of acid caseinate gels have been studied by researchers using, for example, rheology [102], permeability, transmission electron microscopy (TEM) [103-104], scanning electron microscopy (**Figure 10**) [105] and confocal scanning laser microscopy (CSLM) [106]. The main factors governing the formation of acid sodium caseinate gels are the caseinate concentration, pH, temperature and ionic strength [97]. The maximum gel strength, determined using rheology, will be obtained at low ionic strength at a pH of ~ 4.6, which is around the isoelectric point of the different caseins [104]. The gels formed are not in thermodynamic equilibrium. The acid-induced gelation is reversible; adjustment of the pH from 4.6 to 7 will dissolve the gel [103]. This indicates that no covalent bonds are formed during acidification. Increasing the aging temperature results in lower moduli of the formed gels [97, 104, 107]. The acid caseinate gels are often considered as particle gels and described by a collection of fractal clusters [103].

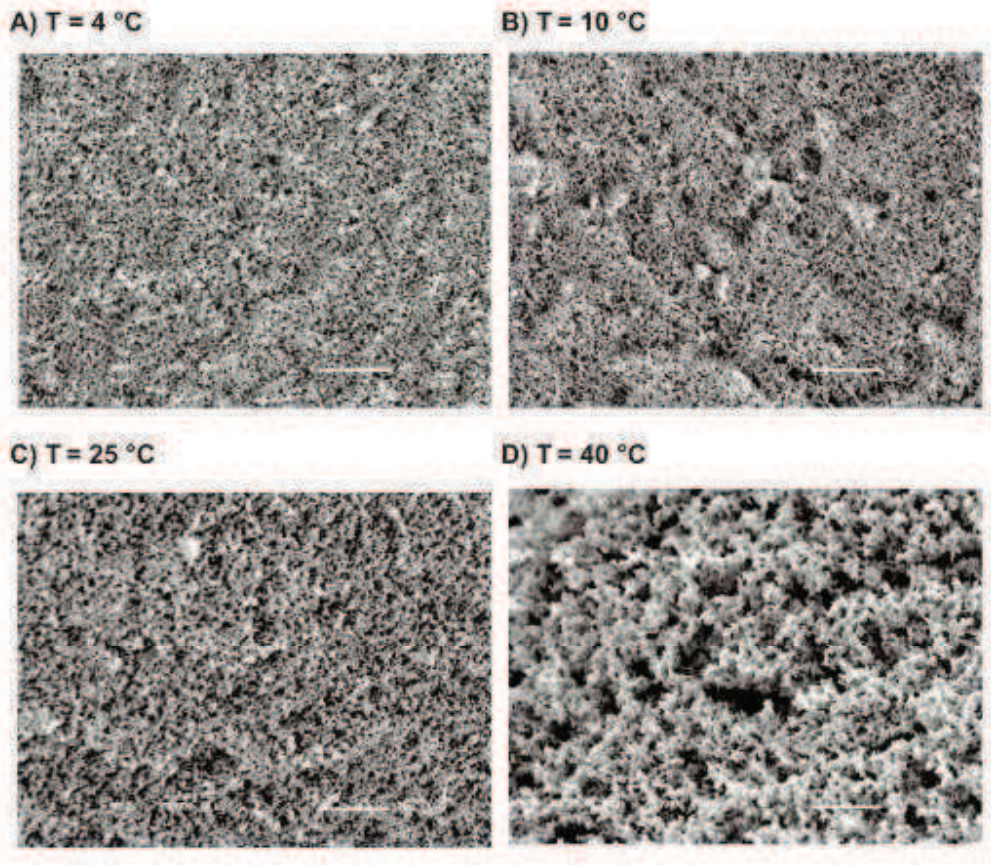

Figure 10. Scanning electron micrographs of acidified sodium caseinate gels (6% (w/w)) formed at incubation temperatures of (A) 4 ˚C, (B) 10 ˚C, (C) 25 ˚C and (D) 40 ˚C. Magnification is 2000 × and the scale bar = 10 μm for all the micrographs (extracted from Takeuchi et al. [105]).

1.4. Conclusion

Casein micelles are porous and highly hydrated macromolecular assemblies with a complex structure and properties. Upon removal of the colloidal calcium phosphate (via acid precipitation followed by a subsequent increase in pH to a physiological value of approximately 7), the large aggregates dissociate and smaller subunits of approximately 11 nm remain. These casein aggregates are very sensitive to their environment. Consequently, several changes of the latter and/or the addition of enzymes lead to their aggregation and the formation of a wide diversity of gels.

Numerous techniques can be used to study the coagulation of milk matrices but all have limitations. Many techniques are invasive and therefore do not make it possible to have access to dynamic information during the process (microscopy, ultracentrifugation, etc.). Other techniques are non-invasive and can be used for real-time investigation, but most of them are not adapted to concentrated systems such as diffusion or diffraction wave spectroscopy (i.e., turbidity measurements (< 100 g/L), etc.). Rheometry techniques are the most frequently used because they make it possible to study the coagulation processes on a continuous basis, regardless of the investigated matrix composition and concentration. However, these techniques only provide information concerning the macroscopic properties of the system. The interpretation of the results obtained in terms of internal mechanisms therefore depends on other techniques.

NMR techniques have the advantage of being non-invasive and adapted to concentrated samples. Moreover, measurements are possible whether the matrix is liquid or solid, and may therefore be performed throughout the coagulation process. For example, Le Feunteun et al. [88-89] probed the structural changes taking place in a concentrated casein suspension during rennet, acid-induced and a combined coagulation by monitoring the self-diffusivity of small and large PEG probes [88-89]. The NMR tool has a number of major assets to characterize certain phenomena that take place during the coagulation processes of milk matrices, notably when the latter are concentrated.

2. Nuclear Magnetic Resonance as a tool for studying translational and rotational diffusion

For several years now, Pulsed-Field Gradient (PFG)-NMR diffusometry and NMR relaxometry have been used as non-invasive, selective techniques to investigate structures of porous materials through the measurement of the displacement of molecules in porous systems. NMR relaxometry is sensitive to rotational diffusion, whereas the PFG method measures translational diffusion. The two methods record motions at very different time and length scales. Generally, relaxation measurements are sensitive to motions that occur at the nanometer length scale and at the picosecond-to-nanosecond time scale [108-109], whereas in PFG measurements, motion is measured over the millisecond-to-second time scale and over distances from tens of nanometers up to hundreds of microns [110-113].

2.1. Self-diffusion measurement using the PFG-NMR technique

Self-diffusion is the random translational motion of molecules driven by internal kinetic energy. Translational diffusion is the most fundamental form of transport and tends to reduce the temperature, pressure and potential gradients inside a system, as well as the action of outside forces. It is also responsible for all chemical reactions since the reacting species must collide before they can react. From a microscopic point of view, this movement of molecules is referred to as Brownian movement. Diffusion is also closely related to molecular size, viscosity and temperature, as can be seen from the Stockes-Einstein equation:

$$D = \frac{kT}{f}$$

where k is the Boltzmann constant, T is the temperature, and f is the friction coefficient. For the sample case of a spherical particle with an effective hydrodynamic radius r in a solution of viscosity η, the equation is given by:

$$D = \frac{kT}{6\pi\eta r}$$

Generally, however, molecular shapes are more complicated and may include contributions from factors such as hydration, making it necessary to modify the friction factor accordingly. As a consequence, the diffusion also provides information about the interactions and shape of the diffusing molecule.

2.1.1. Theoretical basis

All NMR theory needed for understanding the effects of B_0 gradients on nuclear spins has the Larmor equation as its origin:

$$\omega = \gamma(1-\sigma)B_0$$

where ω is the Larmor frequency (radians s^{-1}), γ is the gyromagnetic ratio (rad T^{-1} s^{-1}), B_0 (T) is the strength of the static magnetic field and σ is the shielding constant. Since B_0 is homogeneous, ω is the same throughout the sample.

In PFG-NMR, in addition to B_0, there is a spatially-dependent magnetic field gradient g (T m^{-1}). By considering that the magnetic field gradient is oriented in the z-direction (the same direction as B_0) and by neglecting the shielding constant, ω becomes spatially-dependent:

$$\omega(Z) = \gamma(B_0 + g.Z)$$

A magnetic field gradient can therefore be used to mark the position of a spin along a direction (z in this case) through the Larmor frequency. In imaging systems, which typically use equally strong magnetic field gradients in each of the x, y, and z directions, it is possible to measure diffusion along any of the x, y, or z directions (or combinations thereof). However, in standard NMR spectrometers, it is more common to measure diffusion with the gradient oriented along the z-axis (i.e., parallel to B_0). In the case of single quantum coherence and a rectangular pulse for a single spin, the cumulative phase shift is given by:

$$\Phi(t) = \underbrace{\gamma B_0 t}_{\text{Static field}} + \underbrace{\gamma g \int_0^t z(t')dt'}_{\text{Applied gradient}}$$

The degree of dephasing due to the gradient pulse is proportional to the gyromagnetic ratio of the nucleus (γ), the strength of the gradient (g), the duration of the gradient (t) and the displacement of the spin along the direction of the gradient (z). By neglecting the duration of the gradient (i.e., very short pulse) and, therefore, the movement of the spins during the gradient pulse, the degree of dephasing is a function of the spin position along the gradient axis (z). It is this dependency of the degree of dephasing to the spin position that is the basis of the measurement of a diffusion coefficient by PFG-NMR.

2.1.2. Measuring diffusion with magnetic field gradients

2.1.2.1. The Stejkal and Tanner spin echo sequence

The most common approach for measuring diffusion is to use a modification of the Hahn spin-echo pulse sequence [114] in which equal rectangular gradient pulses of duration δ are inserted into each σ period (the Stejskal and Tanner sequence [115], PFG sequence or PFG-SE (pulsed field gradient spin echo) sequence). The mechanism is shown schematically in **Figure 11**. A first π/2 rf pulse is applied, rotating the macroscopic magnetization from the z-axis into the x-y plane, and is followed by a gradient pulse of duration δ and magnitude g, which causes a progressive dephasing whose intensity depends on the position of spins in the tube. A π rf pulse is then applied that has the effect of reversing the sign of the applied gradients and static field. Finally, a second gradient pulse of equal magnitude and duration is applied.

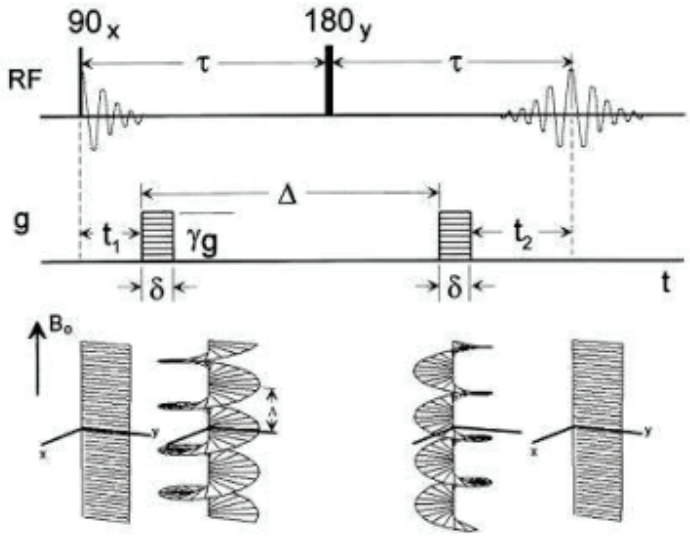

Figure 11. The Stejkal and Tanner pulsed-field gradient NMR sequence principle (extracted from Colsenet thesis [116]).

If the spins have not undergone any translational motion with respect to the z-axis, the effects of the two applied gradient pulses cancel and all spins refocus, which gives a maximum echo signal. However, if the spins have moved, the observed NMR signal will be attenuated. The greater the diffusion is, the larger the attenuation of the echo signal will be. Similarly, since the gradient strength is increased in the presence of diffusion, the echo signal attenuates, as illustrated in **Figure 12**.

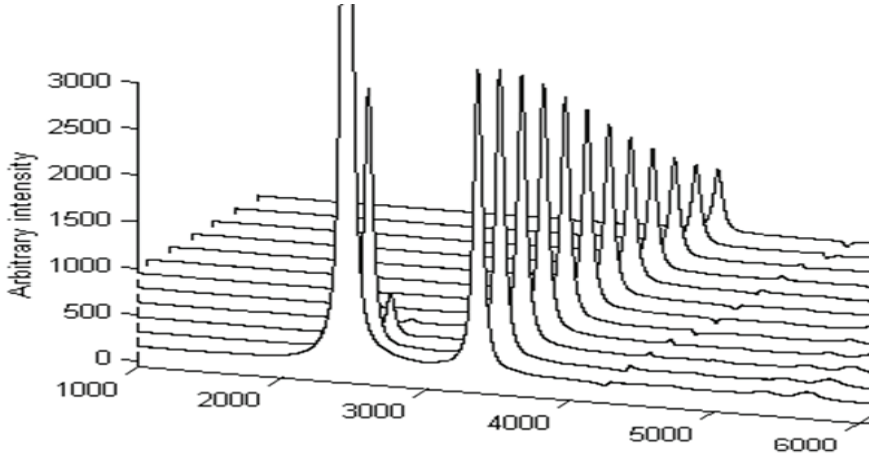

Figure 12. Example of spectra acquired during the measurement of the diffusion coefficient (extracted from Colsenet thesis [116]).

Note that the spins relax transversally throughout the experiment. The relaxation time T_2 is, therefore, part of the equation describing the spin echo signal. In contrast, the echo attenuation due to gradient is independent of the relaxation time of the sample studied. The equation representing the signal attenuation (E) is given by [115]:

$$E = \exp\left[-\gamma^2 g^2 \delta^2 \left(\Delta - \frac{\delta}{3}\right) D\right]$$

where

$$E = \exp(-KD)$$

with

$$K = \gamma^2 g^2 \delta^2 \left(\Delta - \frac{\delta}{3}\right)$$

We can therefore determine the diffusion coefficient of a molecule since all parameters, with the exception of D, are known by the experimenter: γ is the gyromagnetic ratio, g and δ are the strength and the duration of the gradient, and Δ is the time between the two gradient pulses.

Although the effects of relaxation are normalized out, the time scale of the experiment (Δ) is limited by the relaxation time of the molecules. The smallest value of Δ will be limited by the performance of the gradient system. In practice, Δ is normally between 1 ms and 1 s, δ is typically below 10 ms, the magnitude of g is machine-dependent and the largest gradient pulses at this time are on the order of 20 T m^{-1}.

2.1.2.2. Stimulated echo sequence

The stimulated echo sequence, also known as PFG-STE (pulsed field gradient stimulated echo), is shown in **Figure 13**. In this sequence, the π pulse between both gradients is replaced with two π/2 pulses, one shortly after the first gradient and the other one a little before the second gradient.

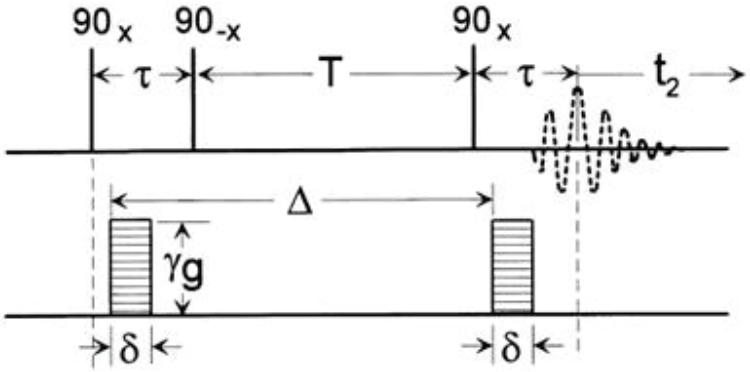

Figure 13. The stimulated echo pulse sequence (extracted from Tanner [117]).

However, the equation representing the attenuation of the signal remains the same as the one given for the PFG-SE sequence. This sequence has one extremely important difference from the standard PFG pulse sequence in that the major part of the duration can be contained in the period Δ, where the magnetization is aligned along the z-axis and where it is subject only to T_1 relaxation. This is particularly important since for many species, especially macromolecules, $T_1 >> T_2$, and, therefore, Δ may be of sufficient length. This sequence is notably used in the case of molecules with weak diffusion coefficients (large molecule and/or viscous solution) and very short transverse relaxation time. Although this sequence is not always preferable since the signal-to-noise ratio of the echo is half as intense as the one acquired with PFG-SE [117], it has been

introduced as a building block in a number of newly developed diffusion pulse sequences in an effort to extend the original method to a larger possible variety of sample types dealing with their particular problematic. In the sequences described below, it is therefore the PFG-STE scheme that will be used as the basis for these sequences.

2.1.2.3. Diffusion sequences that minimize experimental artifacts

A number of experimental factors may alter or disrupt diffusion measurements. Some of these factors such as eddy-current effects [118] and non-uniformity of gradients [119] are related to the performance of the gradient system in the probe. There are, however, other sources of artifacts caused by thermal convection currents in the sample [110], background gradients [119-121], cross-relaxation [110, 118], etc.

Although reduced by the use of active shielded probes, the eddy current-generated fields that occur in the surrounding metal structures of the probe after the application of a short gradient pulse may still be significant. Since the signal distortions caused by these effects depend on the strength of the gradient pulse applied, the result can be disastrous for a diffusion experiment that samples a range of gradient values [110, 118, 122]. The LED-BP-PFGSTE sequence [123] (gradient stimulated echo with bipolar gradients and longitudinal eddy current delay), Fig. 22, greatly alleviates this problem by incorporating gradient pulses of different polarity at both sides of a π pulse spin echo that produces a self-compensating effect for eddy currents.

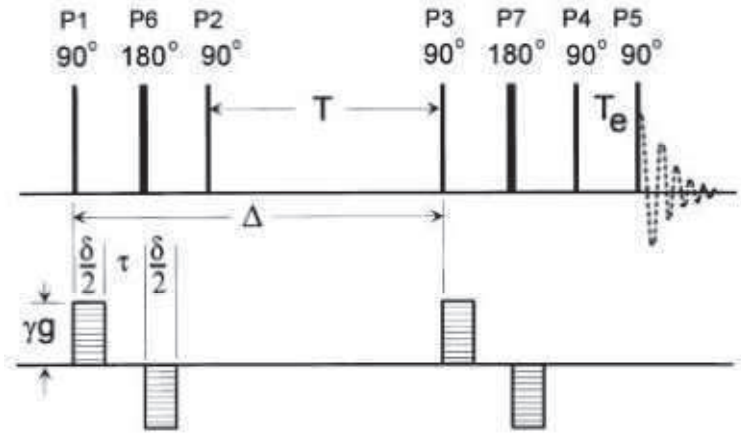

Figure 14. The LED-BP-PFGSE sequence.

The extra π pulse introduced between the BP provides other advantages: the signal acquisition is limited to within the uniform region of the gradient and results in higher quality data [110], the refocusing effect of the π pulses eliminates the effect of the steady background gradients [120-121, 124-125] and, more importantly, it serves to refocus chemical shift evolution during the gradient time [110]. In this sequence, the extra delay T_e introduced before acquisition is referred to as LED (Longitudinal Eddy Current Delay). During this period, the magnetization is stored in the z-axis until the eddy currents have dissipated. Shaping the gradient pulses, for example, as sine functions in the LED-BP-PFGSTE sequence or in any other diffusion sequence, also helps to alleviate eddy current effects [110, 118].

Although other numerous sequences are developed by using different trains and/or forms of pulses [118, 126-131], the LED-BP sequence makes it possible to effectively reduce the induction currents and has very quickly become one of the most frequently used diffusion sequences[139]. It must be emphasized that when this sequence is used, the equation describing the attenuation of the signal (Eq. 6) is slightly modified. In keeping with the scheme presented in **Figure 14**, the modified equation is as follows:

$$E = \exp\left[-\gamma^2 g^2 \delta^2 \left(\Delta - \frac{\delta}{3} - \frac{\tau}{4}\right) D\right]$$

2.1.2.4. Diffusion sequences incorporating suppression of strong signals

High intensity solvent resonances can significantly hamper diffusion estimates in pulsed gradient spin-echo NMR diffusion experiments, especially in biomolecule samples. To overcome this problem, various diffusion sequences that allow the suppression of solvent signals were proposed.

Presaturation of the solvent signal(s) can be applied prior to the PFGSTE sequence. However, the degree of suppression may not be sufficient, the solvent signal(s) may recover during the length of the PFGSTE sequence and it can result in the loss of exchangeable resonances. Some well-known solvent suppression techniques [127, 132-137] have been included in different PFGSTE sequences, affording extremely high suppression factors on the order of 10^4 without losing the information of exchangeable protons. Among the latter, those that insert a WATERGATE [136-

138] (WATER suppression by Gradient-Tailored Excitation) scheme revealed their effectiveness and have the advantage of remaining simple sequences. For example, the WATERGATE scheme can be inserted into the BP sequence at the LED delay site, or in the place of the π RF pulse in the spin echo sequence [136].

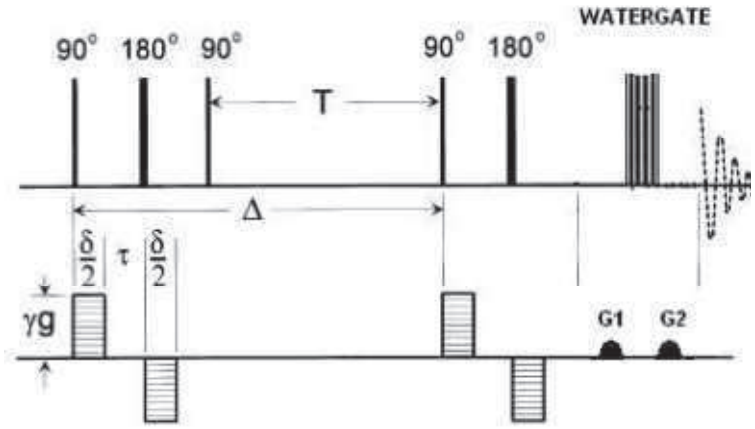

Figure 15. The BP-STE sequence with an integrated WATERGATE scheme.

The WATERGATE method is a π pulse, or a pulse train, inserted between two magnetic field gradient pulses. The equation representing the signal attenuation is the same as the one for BP-LED.

Recently, Zheng et al. [139] developed a double echo PGSTE-WATERGATE sequence (**Figure 16**) for simultaneous convection compensation and solvent signal suppression. This new sequence provides excellent convection compensation and a high solvent suppression factor in excess of 10^5 in a single scan, which is ~ 10 times higher than that of the previously developed sequences. It can be applied to diffusion measurements on a variety of solutes ranging from small molecules like amino acids to large protein aggregates.

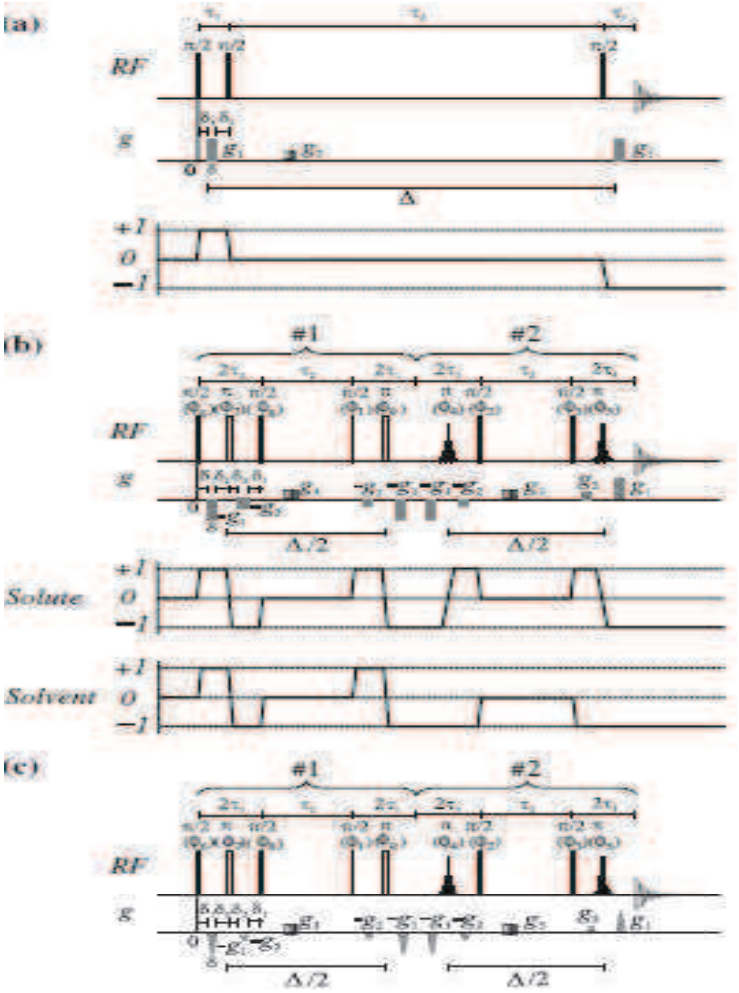

Figure 16. The standard STE based PGSE sequence (a); the double echoPGSTE WATERGATE sequence with rectangular gradients (b); and the double echoPGSTE-WATERGATE sequence with half sine shaped gradients (c) (extracted from Zheng et al. [139]).

Other sequences are also present as the specific sequences for the study of high molecular weight systems [140-141], sequences with enhanced signal dispersion or simplification in the number of signals [142-145], fast 1D diffusion sequences [146-148], etc.

2.1.3. No classical attenuation of the NMR signal

As previously explained, the signal attenuation is described by $\ln(E) = -KD$. However, there are also cases where the reduction of the signal according to k cannot be described by this simple relationship. Several reasons that may cause this phenomenon are given in the following paragraphs.

2.1.4. Free and restricted diffusion

When we use the PFG method to measure diffusion in free solution and in the absence of exchange, the diffusion coefficient is independent of the length of diffusion time Δ. This is assuming that the relaxation time(s) of the species in question is sufficiently long so that we still obtain a measurable signal and the measurements are not affected by experimental complications. However, in the case of a species diffusing within a confined space, we must be careful to properly account for the effects of the restricting geometry on the motion of the species. If a particle is diffusing within a restricted geometry (sometimes referred to as a "pore"), the displacement along the z-axis will be a function of Δ, the diffusion coefficient and the size and the shape of the restricting geometry. Consequently, if the boundary effects are not properly accounted for in the calculation of the diffusion coefficient, an apparent diffusion coefficient will be obtained instead of a self-diffusion coefficient. **Figure 17** illustrates this effect. In one case, the particle diffuses freely, while in the other case, it will be confined in a sphere of radius R. It is possible to define a variable without dimension, ξ, with which restricted diffusion can be characterized and that is written as:

$$\xi = D\Delta / R^2$$

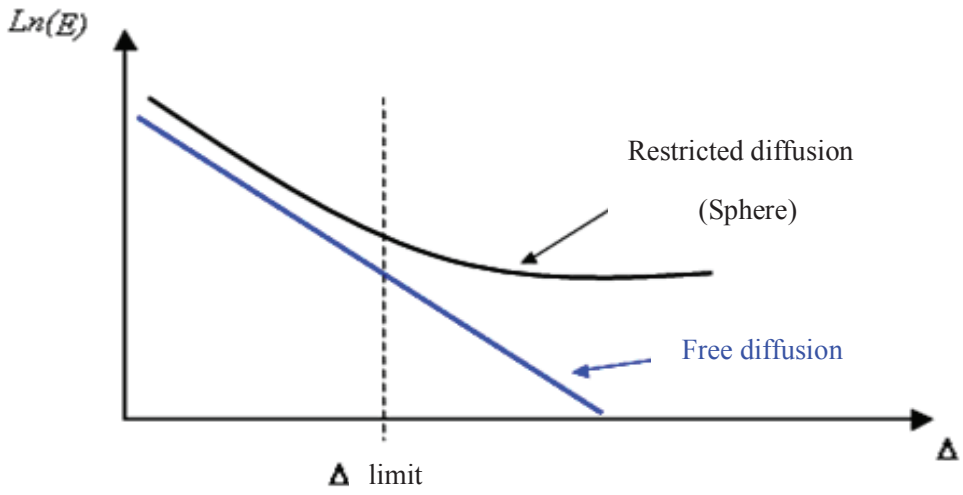

Figure 17. Schematic presentation of the NMR echo signal as a function of Δ when the diffusion is free or restricted.

The echo attenuation for diffusion in a sphere can be seen to go through three stages:

(i) when $\xi << 1$, the diffusion appears unrestricted and the result is the same as that of free diffusion;

(ii) as Δ increases, the spins begin to feel the effect of the surface. The diffusion coefficient measured will be apparent and a function of Δ;

(iii) when $\xi > 1$, the diffusion is fully restricted and the attenuation curve plateaus out.

Thus, for short values of Δ, the signal attenuation in the PFG experiment is sensitive to the diffusion of the particle. For long values of Δ, the signal attenuation becomes sensitive to the shapes and dimensions of the restricting geometry. Therefore, when the diffusion of molecules is restrained, it may reveal the size and shape of the local geometry. It is possible, for example, to determine the size distribution as well as the size of droplets in emulsions [126, 149-152] and to estimate the size of pores [153-156].

In the case of matrices that contain several phases (gels, emulsions), the diffusion of a molecule can be either free or restricted. Of course, the geometry of such matrices is not perfect in general. More or less closed holes, different sizes and forms can be found in the same matrix (matrix

polydispersity). In effect, if there are closed holes of variable sizes, even with a constant Δ, the molecules in the smallest holes may be subjected to restriction effects, whereas those located in bigger holes will have no opportunity to encounter walls. It follows that for a given value of Δ, the attenuation of the signal will deviate from the linearity [157-161].

2.1.5. Multiple diffusion coefficients

Two different molecules can have NMR signals that overlap. If these two molecules have different diffusion coefficients, then the attenuation of the signal will not be linear and the signal will be broken down into two exponentials:

$$E = P_1.\exp(-KD_1) + P_2.\exp(-KD_2)$$

Where P_1 and P_2 are the relative proportions of each molecule. In the general case of n elements, the equation is given by:

$$E = \sum_{1ton} P_n.\exp(-KD_n)$$

The figure below shows a bi-exponential NMR signal attenuation in the case of a solution containing oil and fat [162]. The authors used equation 12 to calculate the diffusion coefficients of water and fat in casein solutions.

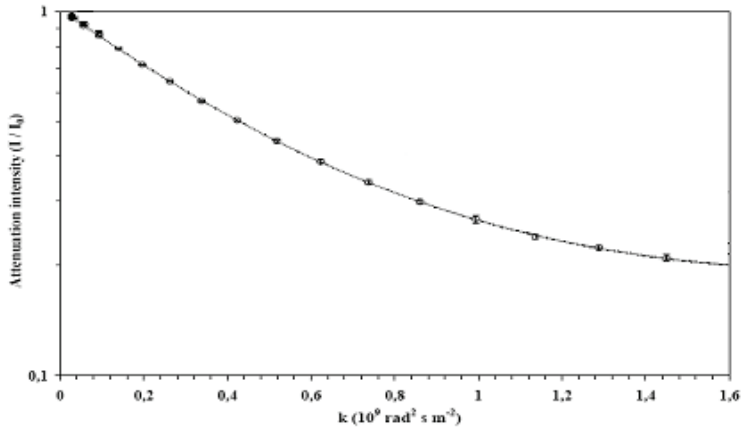

Figure 18. Echo Attenuation of NMR signal containing water and fat as a function of k in casein solutions at 40°C with $D_1 = D_{water}$ and $D_2 = D_{fat}$ (extracted from Metais thesis [162]).

2.1.6. Effect of polydispersity

Another case where attenuation cannot be linear is when we measure the diffusion coefficient of a polydisperse molecule. In the case of a polymer, the size distribution can be statistically characterized by its weight average molecular weight (M_w) and its number average molecular weight (M_n), the ratio of which is known as the polydispersity index (M_w/M_n). If this index is equal to 1, then $M_w = M_n$ and the polymer is monodisperse. Otherwise, the ratio M_w/M_n will be more greater than 1 since the dispersion in polymer weight (and therefore in diffusion coefficients) will be higher. Thus, the higher the polydispersity index of a polymer is, the more the attenuation of the NMR signal will deviate from the linearity (**Figure 19**).

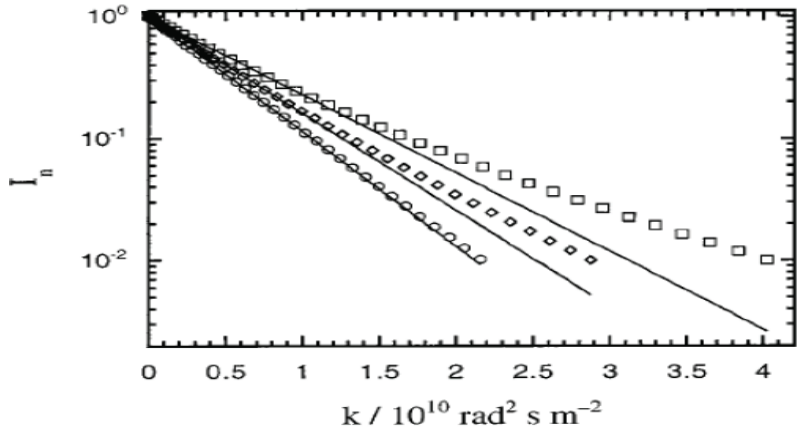

Figure 19. Echo attenuation of a polymer (106 g/mol), assuming a log-normal distribution function with different polydispersity indices (1.05, 1.4 and 2 from left to right) (extracted from Hakansson et al. [163]).

Assuming that there is no interaction between polymers of different weights, the echo signal is then given by the following equation:

$$Ln(E) = -K\left(\sum \rho_i M_i D_i / \rho_i M_i\right) = -K\langle D\rangle$$

where ρ_i is the number of molecules with a molecular weight M_i and a diffusion coefficient D_i, and $\langle D\rangle$is the average diffusion coefficient.

However, Callaghan and Pinder [164] showed that the signal attenuation of a polydisperse element could be correctly represented by the following expression:

$$Ln(E) = -K\langle D\rangle + \frac{1}{2}K^2\langle D\rangle^2\left[1-\left(M_w/M_n\right)^{-4/5}\right]$$

It is thus possible to obtain an average diffusion coefficient.

2.1.7. Diffusion measurements using other techniques

Translational diffusion can also be measured using other techniques such as fluorescence recovery after photobleaching and multiple particle tracking, which use confocal laser scanning microscopy (CLSM) to determine the displacement of particles.

2.1.7.1. Fluorescence recovery after photobleaching (FRAP)

Fluorescence recovery after photobleaching (FRAP), also referred to as (micro)photolysis, is a rather old, yet ever-evolving fluorescence technology. Its principle is to irreversibly photobleach a certain region within a fluorescently-labeled sample by irradiation with a short intense light pulse. Immediately after bleaching, a highly attenuated light beam is used to measure the recovery of fluorescence inside the bleached [165] area as a result of exchange of bleached fluorophores by unbleached molecules from the surroundings. The analysis of this process yields information about the molecular mobility and the fraction of mobile species. Performing the experiment with a confocal laser scanning microscope (CLSM) reveals this information with a high spatial resolution by collecting images of the fluorescently-labeled cell over time, while the fluorescent and photobleached molecules redistribute themselves until equilibrium is reached. By plotting the relationship between fluorescence intensity and time, the mobility of the fluorescent molecules can be directly measured [165]. This technique, in which the probe concentration remains micromolar, is microscopic, non-destructive and slightly invasive [166], and is able to cover a wide range of apparent diffusion coefficients, from 10^{-20} to 10^{-9} m^2s^{-1} [167].

FRAP has been successfully used to assess the translational mobility of all types of solutes in cytoplasm, nuclei and membranes [168-170]. In addition to its cellular applications, FRAP has also been used to study the mobility of molecules in interstitial spaces in tissues [171-172] and

extracellular matrices such as cervical mucus and biofilms [173-175]. Although FRAP was originally developed to study molecular mobility and interactions in biological samples, it has become a valuable tool in studying diffusion in all types of environments, especially in the field of polymer solutions and gels [176-179] and in food matrices. For example, Perry and al. [180] measured the diffusion coefficients of FITC-dextran probes in starch solutions. Carvajal-Rondanelli et al. [181] applied the FRAP technique to fish meat in order to model the diffusion coefficients of different fluorescein isothiocyanate (FITC)-labeled protease inhibitors between cell membranes of the muscle fibers. Balakrishnan et al. [182] measured the diffusion of FITC-dextran chains with different molecular weights (40, 500 and 2000 KDa) in a variety of beta-lactoglobulin (β-lg) gel structures prepared by heating β-lg solutions at different concentrations and different ionic strengths (**Figure 20**). More recently, Floury et al. [183] developed a FRAP protocol and analysis coupled to CSLM that allows *in situ* measurements of diffusion properties of FITC-dextran with different molecular weights and sizes (4 and 20 kDa) in a model cheese matrix based on ultrafiltrated milk.

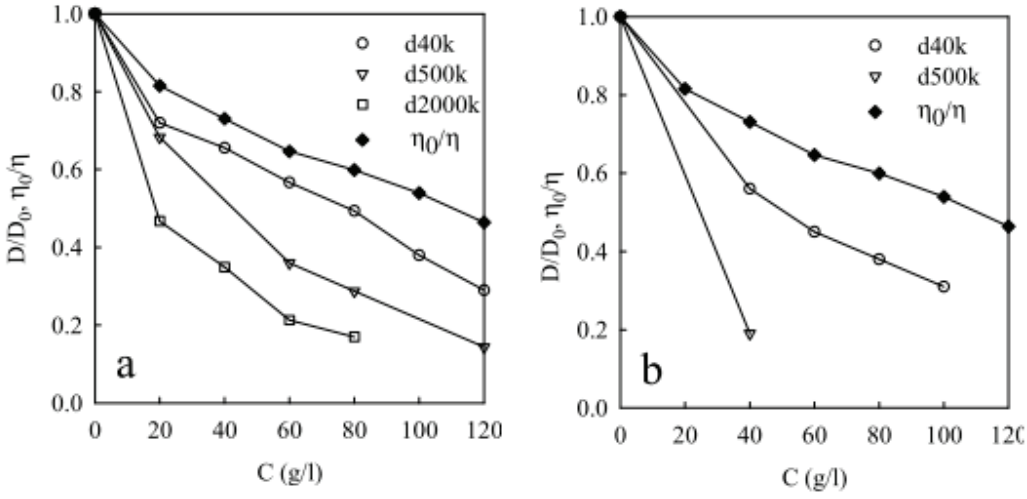

Figure 20. D/D_0 of different tracers in gels as a function of the protein concentrations at NaCl salt concentration (Cs) = 0.1 M (a) and at Cs =0.05 M (b) (extracted from Balakrishnan et al. [182]).

FRAP is a very versatile technique. It offers the possibility of microscopically examining a sample and obtaining information on molecular motion and interactions in a specific part of the sample. The main disadvantage is the need for fluorescent molecules. Labeling a molecule of

interest can change its properties [184]. Future developments in FRAP will go hand-in-hand with technological developments in microscopy, image processing and mathematics.

2.1.7.2. Multiple particle-tracking (MPT)

Multiple particle tracking (MPT) is a complementary microrheological technique in which the Brownian motion of tracer particles added to the sample (usually fluorescent latex beads) is directly recorded in real space, from which information on the rheological properties of the medium can be obtained. As an example, **Figure 21** shows individual particle trajectories for fluorescent microspheres embedded in glycerol solutions.

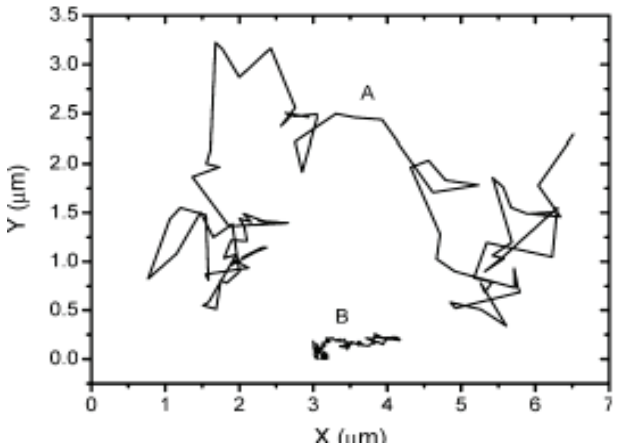

Figure 21. Representative individual particle trajectories recorded over a time period of 17 s for R = 0.25 μm fluorescent microspheres embedded in (A) 60% glycerol solution (viscosity: 0.010 Pa s) and (B) 88% glycerol solution (viscosity: 0.147 Pa s) (extracted from Moschakis et al. [185]).

Because MPT enables the study of the distribution of the motion of single probe particles, it makes it possible to obtain information regarding system heterogeneity. For example, Cucheval et al. [186] used particle tracking to probe the heterogeneity of acid milk gels and the microrheological properties of the protein network and aqueous-phase voids, in the presence and absence of pectin, by following the distribution of the displacements of added fluorescent latex beads during and after gelation. The sol-gel transition of a sodium caseinate solution that was undergoing gelation by acidification was also studied by particle tracking microrheology. The

Brownian diffusion of fluorescent microspheres with different surface coatings was used to probe spatial mechanical properties of the gels at the micron scale [185]. Balakrishnan et al. [182] also demonstrated that MPT is a powerful tool for measuring the diffusion of tracer particles in heterogeneous beta-lactoglobulin (β-lg) gels (with salt concentration > 0.15 M).

2.2. Nuclear Magnetic Resonance relaxometry as a tool for studying rotational diffusion

2.2.1. Introduction

Nuclear magnetic resonance (NMR) spectroscopy is a powerful technique for studying the dynamics of molecules using spin relaxation experiments. Thorough theoretical articles and reviews of NMR relaxation analysis are available [187-190] but are not necessarily accessible to any scientist. Although our focus is on a short description of the phenomenon, the fundamental principles are applicable.

The action of a radiofrequency pulse on a sample at thermal equilibrium perturbs the restful state of nuclear spins. Following this perturbation, it would be intuitively expected that the system would re-establish the equilibrium condition and lose the excess energy imparted to the system by the applied pulse. The lifetimes of excited nuclear spins are extremely long when compared to excited states in other spectroscopic techniques. They may last a few seconds or even minutes for nuclear spins, as opposed to less than a picosecond for electrons in optical spectroscopy, a consequence of the low transition energies associated with nuclear resonance.

Immediately after an NMR 90° pulse excitation of nuclear spins, the bulk magnetization vector is moved away from the thermal equilibrium z-axis, which corresponds to a change in the spin populations. The recovery of the magnetization along the z-axis, referred to as longitudinal relaxation, therefore corresponds to the equilibrium populations re-established and, hence, to an overall loss of energy of the spins. The energy lost by the spins is transferred into the surroundings in the form of heat, although the energies involved are so small that temperature changes in the bulk sample are undetectable. This gives rise to the original designation of this process, spin-lattice relaxation T_1.

Referring back to the situation immediately following a 90° pulse in which the transverse magnetization is on-resonance, another way in which observable magnetization can be lost also exists. The bulk magnetization vector results from the addition of many microscopic vectors for the individual nuclei that are said to possess phase coherence following pulse excitation. In fact, the magnetic field experienced by each spin in the sample is not exactly the same. Some spins will experience a slightly greater local field than the mean causing them to have a higher frequency and to thus creep ahead, whereas others will experience a slightly smaller field and start to lag behind. This results in a loosening of phase coherence fanning-out of the individual magnetization vectors, which ultimately leads to zero net magnetization in the transverse plane (**Figure 22**). It is assumed that this other form of relaxation, referred to as transverse relaxation, occurs with an exponential decay characterized by the time constant T_2.

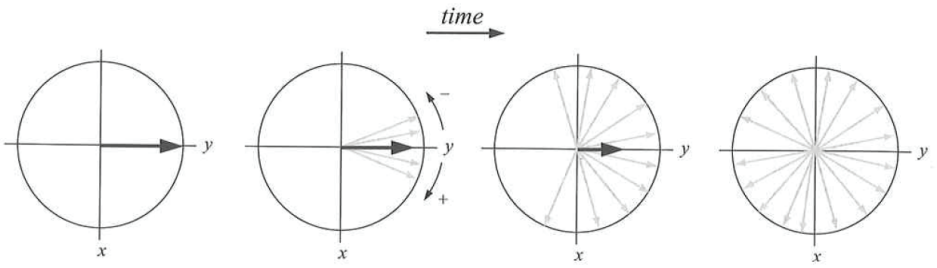

Figure 22. Scheme of the fanning-out (dephasing) of the individual magnetization vectors due to transversal relaxation (extracted from [191]).

Magnetic field differences in the sample can be considered to arise from two distinct sources. The first is simply from static magnetic field inhomogeneity throughout the sample volume, which is really an instrumental imperfection ($T_{2(\Delta B0)}$). The second is from the local magnetic fields arising from intramolecular or intermolecular interactions in the sample and represents the "genuine" or "natural" transverse relaxation processes T_2. The combination of the two sources is designated T_2^* so that:

$$\frac{1}{T_2^*} = \frac{1}{T_2} + \frac{1}{T_{2(\Delta B_0)}}$$

The decay of transverse magnetization is manifested in the observed free induction decay. Moreover, the widths of NMR resonances are inversely proportional to T_2^*.

2.2.2. Measurement of T_2

The measurement of the natural transverse relaxation time T_2 could in principle be obtained if the contribution from magnetic field inhomogeneity was removed. This can be achieved by the use of a spin echo sequence [114]. Consider a sample of spins composed of microscopically small regions so that within each region, the field is perfectly homogeneous. Magnetization vectors within any given region will precess at the same frequency. In the basic two-pulses echo sequence **(Figure 23 a**), some spins move more ahead of the mean, whereas others lag behind during the time period τ (**Figure 24**). The 180° pulse rotates the vectors toward the –y-axis, and following a further period t, the fastest moving spins coincide with the slower ones along the –y-axis. Thus, the echo has refocused the blurring in the x-y plane caused by field inhomogeneities. During the 2τ time period, some loss of phase coherence by natural transverse relaxation occurs and is not refocused by the spin echo since, in effect, there is no phase memory associated with this process to be undone. This means that at the time of the echo, the intensity of the observed magnetization will have decayed according to the natural T_2 time constant, independent of field inhomogeneity.

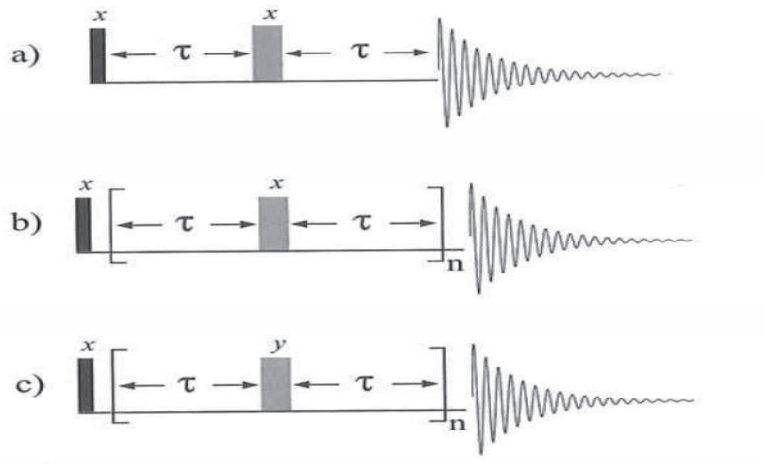

Figure 23. Spin echo sequences for measuring T_2 relaxation times: (a) a basic spin echo; (b) the Carr-Purcell sequence; and (c) the Carr-Purcell-Meiboom-Gill CPMG sequence (x and y correspond to the axis along which the pulse was applied) (extracted from [191]).

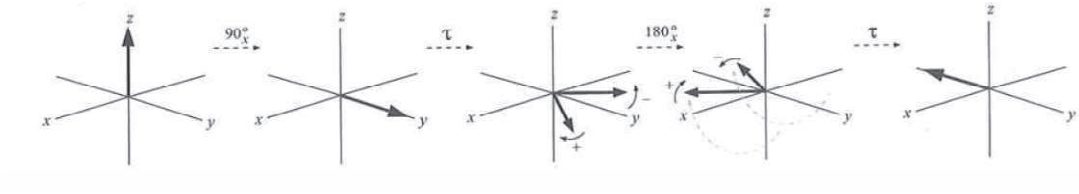

Figure 24. Evolution of the magnetization during a basic spin echo sequence (extracted from [191]).

A logical experiment for determining T_2 would be to repeat the sequence with increasing τ, and to measure the amplitude of the echo versus time. However, if any given spin diffuses during the echo (due to brownian motions), it will not be fully refocused [192]. As τ increases, the effect of diffusion become more severe and the experimental relaxation data less reliable.

A better approach to determining T_2 by minimizing the effect of diffusion is to repeat the echo sequence within a single experiment using a short τ to form multiple echoes, the decay of which follows the time constant T_2. The Carr-Purcell-Meiboom-Gill (CPMG) sequence [193] (**Figure 23 c**) causes echoes to form alternately along the –y and +y axes following each refocusing pulse. Losses from diffusion occur between the echo peaks, within time 2 τ, so if this is kept short relative to the diffusion rate (typically, $\tau < 100$ ms), some losses become negligible. The intensity of the echo over longer time periods is attenuated by repeating the – τ -180- τ - sequence many times prior to acquisition. T_2 may then be extracted by performing a series of experiments with increasing 2 τn (by increasing n) and acquiring data following the last even echo peak in each case.

2.2.3. Mechanisms for relaxation

Explicit details of the underlying mechanisms for relaxation can be found in literature focused on NMR [194-195] but here are summarized the dominant processes which influence the NMR interactions.

Nuclear spin relaxation is not a spontaneous process. It requires stimulation by a suitable local fluctuating field to induce the necessary spin transitions. There are four principal mechanisms that are able to do this: the dipole-dipole, spin rotation, chemical shift anisotropy (CSA) and quadrupolar mechanisms.

Local magnetic fields arise from a number of sources, whereas their time dependence is due to the motions of the molecule (vibration, rotation, diffusion, etc.). In fact, only chaotic tumbling of a molecule occurs at a rate that is appropriate for nuclear spin relaxation, the others being too fast or too slow. This random motion occurs with a spread of frequencies that depends on molecular collisions, associations, etc., experienced by the molecule, but is characterized by a rotational correlation time, τ_c, the average time taken for the molecule to rotate through one radian. τ_c is given by:

$$\tau_c = \frac{1}{6D_r}$$

$$D_r = \frac{k_B T}{8\pi a^3 \eta}$$

where D_r is the rotational diffusion coefficient of a spherical molecule, η the solvent viscosity, k_B the Boltzmann constant and T the temperature.

Short correlation times therefore correspond to rapid tumbling and vice-versa. Molecular motion is fundamental to the process of relaxation, but it is necessary to specify how the fields required for this arise and how these mechanisms influence spectra.

In solution, the rapid tumbling of a molecule averages the CSA so that only a single frequency for each chemically distinct site can be observed, sometimes referred to as the isotropic chemical shift. Moreover, protons exhibit a small chemical shift range and are ½ spins. They are therefore not concerned by quadrupolar mechanisms.

The most important relaxation mechanism for many ½ spin nuclei arises from the dipolar interactions between spins. Suppose that nuclei are characterized by dipoles. As two such dipoles approach, their associated magnetic fields interact; they attract or repel, depending on their relative orientations. If these dipoles were two neighboring nuclei in a molecule that is tumbling in solution, the orientation of each nucleus with respect to the static magnetic field does not vary, but their relative positions in space will alter and the local field experienced at one nucleus will fluctuate as the molecule tumbles (**Figure 25**). Tumbling at an appropriate rate can therefore induce relaxation.

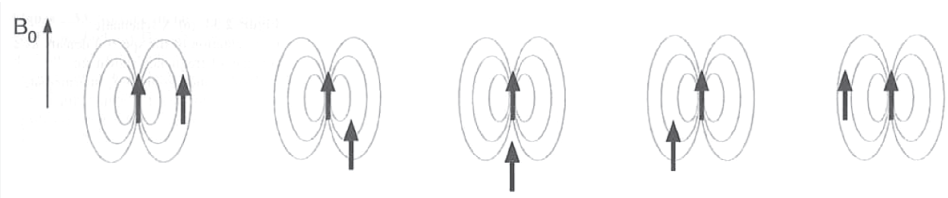

Figure 25. Through-space magnetic interaction between two spins inducing dipole-dipole relaxation (extracted from [191]).

The second relaxation mechanism deals with the spin rotation. Molecules or functional groups that rotate very rapidly associate themselves with a molecular magnetic moment generated by the rotating electronic and nuclear charges. The resulting field fluctuates as the molecule or group changes its rotational state as a result of, for example, molecular collisions, providing a further mechanism for nuclear relaxation. This is particularly effective for small, symmetrical molecules of freely rotating methyl groups, and its efficiency increases as tumbling rates increase. Thus, heating a sample enhances spin-rotation relaxation since this temperature dependence is characteristic of this mechanism and allows its presence to be established.

2.3. Conclusion

NMR experiments provide a quick and reliable tool for the precise measurement of the translational and rotational diffusion coefficients of almost every species in solution with an NMR signal. Whereas the self-diffusion coefficient reflects the displacement over micron distances of the molecule within the matrix, relaxation times T_2 reflect the rotational or local mobility of molecules at the nanometer scale. Some information can be obtained by measuring the D and T_2 values, particularly regarding the interaction/aggregation phenomenon, which occurs throughout the complicated mechanisms. Despite the interest of coupling NMR relaxometry and diffusometry, these two techniques have rarely been coupled in studies on polymer systems.

In dairy products, T_2 measurements have been focused on water molecules in order to characterize macroscopic processes such as syneresis [196], milk acidification [197-199], milk powder solubilization [200], cheese ripening or cheese moisture content [201-203]. Numerous

diffusion studies done in polymer systems and in dairy system models have been based on measuring the diffusion of polymer probe molecules of different molecular weights at different concentrations and linking them to the structure and dynamics of the matrix investigated. To facilitate the interpretation, the probe should have no specific interactions with the matrix studied. One of the most commonly used probe molecules is polyethylene glycol (PEG).

3. Mobility of probes in suspension and gel matrices

3.1.Effect of matrix, PEG size and shape on PEG self-diffusion coefficients

Poly(ethylene glycol) (PEG), otherwise known as poly(oxyethylene) or poly(ethylene oxide) (PEO), is a synthetic, water soluble, non-toxic polyether that is readily available in a range of molecular weights. PEG generally refers to oligomers and polymers with a molecular mass below 20,000 g/mol. Above this value, it is difficult to create monodisperse polymers. On the contrary, high molecular weight monodisperse polymers are synthesized when ethylene oxide is used as a monomer. PEO therefore generally refers to polymers with large molecular masses above 20,000 g/mol. PEG molecules selected as probes offer a series of key advantages. They are water soluble, available in a wide range of molecular weights with low polydispersity indices, and their NMR signal is a sharp band around 3.6 ppm. Moreover, PEGs present very weak interactions, notably with proteins [204-208], which makes it possible to observe the obstruction effects induced by proteins in various porous structures.

Some studies have reported on PEG self-diffusion in various matrices such as polymer solutions and gels [163, 209-221], whey protein systems [222], κ-carrageenan [223], cartilage [224], wet cotton [225] gastric mucin [226], agarose gels [227] and alginate samples [217, 228] measured by pulsed field gradient NMR or other techniques (release kinetics data [217], and the use of radioactive markers [221]). The results show a high dependency of PEG diffusion on the matrix structure and concentration as well as on PEG size. Independently of the investigated system and the size of the probe used, PEG diffusion decreases with increasing matrix polymer concentrations. In addition, it was found that for a given PEG molecular weight, there is a strong connection between the structure of the matrix and the probe diffusion in both κ-carrageenan [223] and whey protein gels [222]. The diffusion behavior was determined mainly by the void size, which in turn was defined by the state of aggregation of the matrix (ionic condition, cooling rate, temperature, etc.).

Another important finding arising from some of these studies was a decrease in PEG diffusion when its size increased for the same network [209, 212, 219, 224-225]. For example, in a polysaccharide gel matrix[232] at a given volume fraction of 0.07, D/D_0 was 0.56 for 1000 g/mol

PEG and 0.43 for 3350 g/mol PEG. The authors explain these results by taking the ratio between the size of the probe and the size of the gel pores into account. Larger probes are more subjected to obstruction effects. Griffiths et al. [216] studied the self-diffusion of two PEGs with the same molecular weight but different architectures (cyclic or linear) in D_2O. The behavior of these two PEGs was found to be very different. For a concentration of 5.1 g/100g, D/D_0 was 0.41 and 0.51 for the cyclic and the linear 10000 g/mol PEG, respectively. The authors attributed these differences to the fact that the friction opposing the motion of the cyclic polymer was greater than the friction opposing the motion of the linear polymer.

While many studies have been performed with polymer solutions and gels, only a few have focused on the effect of coagulation on PEG diffusion. Colsenet [222], Johansson [221, 229], Walther [223], Favre [217] and Baldursdottir [228] et al. studied the effect of gelation on PEG diffusion in whey protein systems, k-carrageenan and alginate matrices. These studies revealed that PEG diffusion was increased after the system gelation caused by the formation of a more open structure.

The two main conclusions arising from all of these studies are:

1) The sample structure has an influence on PEG diffusion. For a given molecular weight and a given matrix concentration, normalized self-diffusion coefficients can be very different according to the microstructure of the matrix.
2) The probe diffusion will be more or less sensitive to matrix structure changes, depending on its size.

The same conclusions have been drawn from studies of casein matrices. A first study was accomplished on PEG diffusion in solutions and rennet gels of casein micelles by Colsenet et al. [230]. In agreement with previous results reported in the literature, the main findings of these studies were that probe diffusion was affected by: (i) the casein concentration, i.e., PEG diffusion decreases with increasing casein concentration; (ii) the size of the PEG, i.e., for a given casein concentration, PEG diffusion decreases as polymer size increases (**Figure 26**); and (iii) the state of the matrix, solution or gel, i.e., PEG diffusion increases after coagulation (**Figure 27**). This effect was greater when the size of the probe was larger.

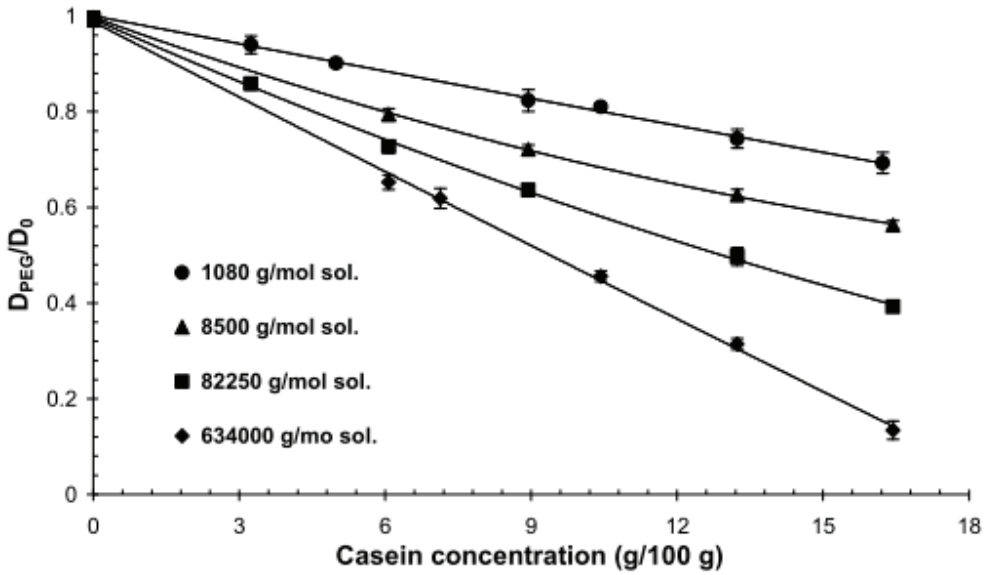

Figure 26. Plot of the normalized PEG self-diffusion coefficient in casein suspensions vs. casein concentrations for different PEG molecular masses (extracted from Colsenet et al. [230]).

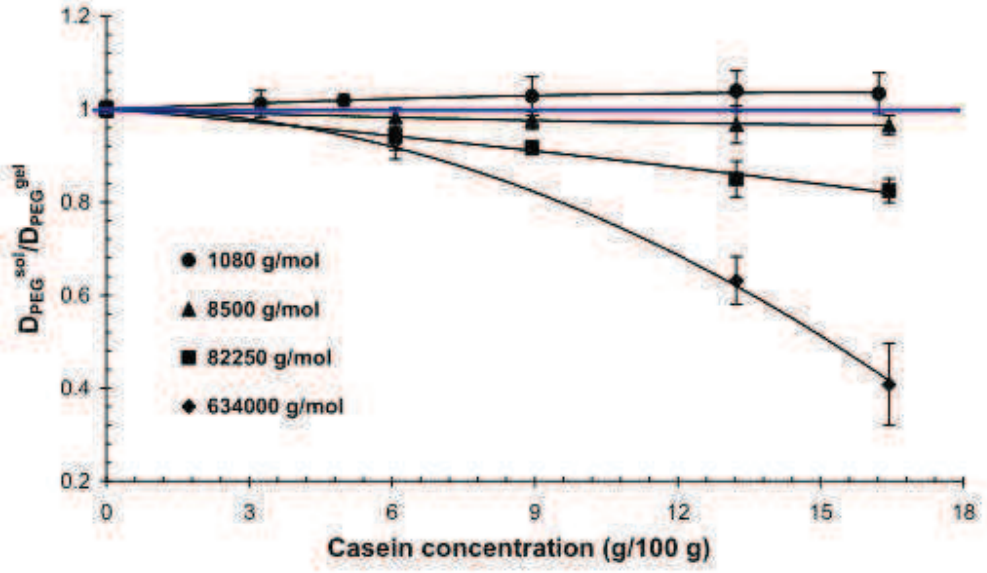

Figure 27. PEG self-diffusion coefficient in casein suspensions divided by PEG self-diffusion coefficients in casein gels vs. the casein concentration for different PEG molecular masses at 20°C (extracted from Colsenet et al. [230]).

This study was expanded by Le Feunteun et al. [90] who investigated the translational dynamics of PEG polymers with molecular weights varying from 6.10^2 to 5.10^5 in casein suspensions and in gels induced by acidification, enzyme action and a combination of both. Figure **28** gathers all the results.

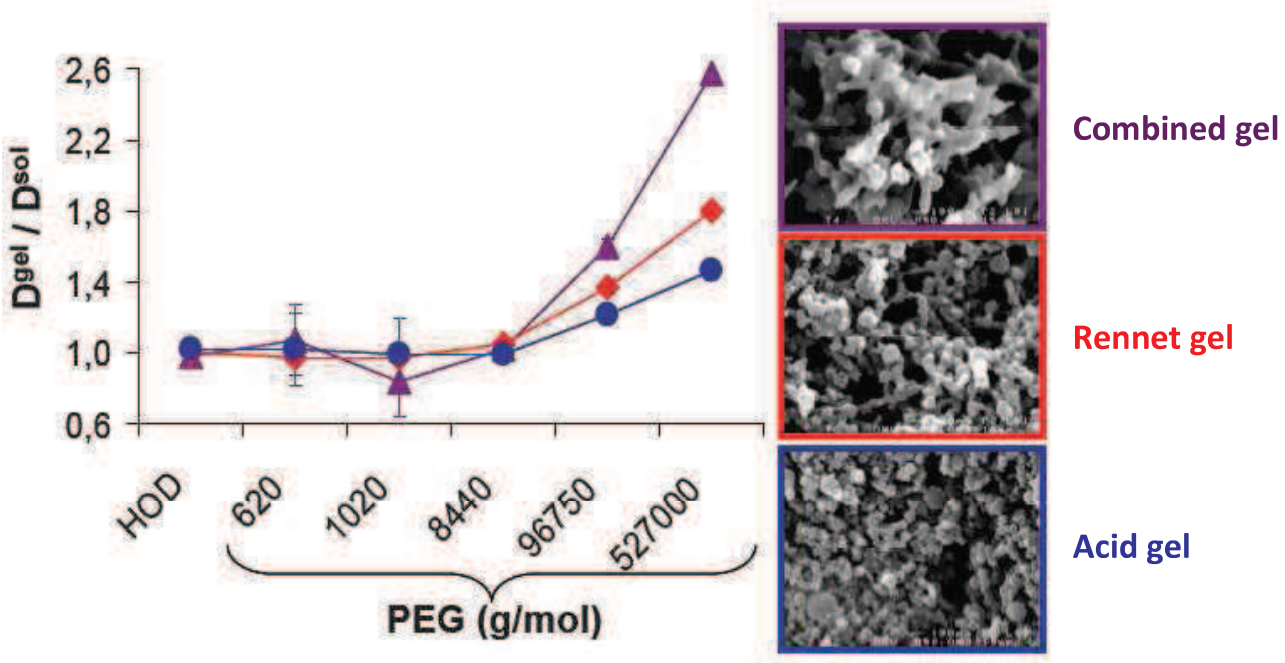

Figure 28. Dgel/Dsol ratios obtained at 20°C for HOD and all PEGs in concentrated enzymatic, acid and combined gels (extracted from Le Feunteun et al. [90]).

For PEG probes with $M_w \leq 8440$ g/mol, the diffusion was not significantly influenced by the matrix structure (solution and gel) and the type of gelation. This result seems to be quite specific to casein systems since small PEG diffusion is dependent on the structure of whey protein [222], gastric protein [226] and polysaccharide [223] matrices. However, for PEG probes with $M_w >$ 8440 g/mol, there was a strong dependence of PEG diffusion on PEG size and on the casein network structure as revealed by scanning electron microscopy images.

Nevertheless, in all the studies mentioned above, the diffusion of a molecule was measured at equilibrium, before and after the perturbation of the system. However, casein matrices undergo many changes between these two states. To acquire a better understanding of the impact of structural changes in the casein matrix during coagulation on PEG probe diffusion, Le Feunteun

et al. monitored the self-diffusion coefficients of small (620 g/mol) and large (96750 g/mol) PEG polymers during rennet [89], acid-induced and a combined coagulation [88] of a concentrated casein suspension. **Figure 29** summarizes the evolutions of the PEG diffusion and the structure of gels obtained by SEM during rennet coagulation. According to the size of the PEG, two opposed behaviors were obtained.

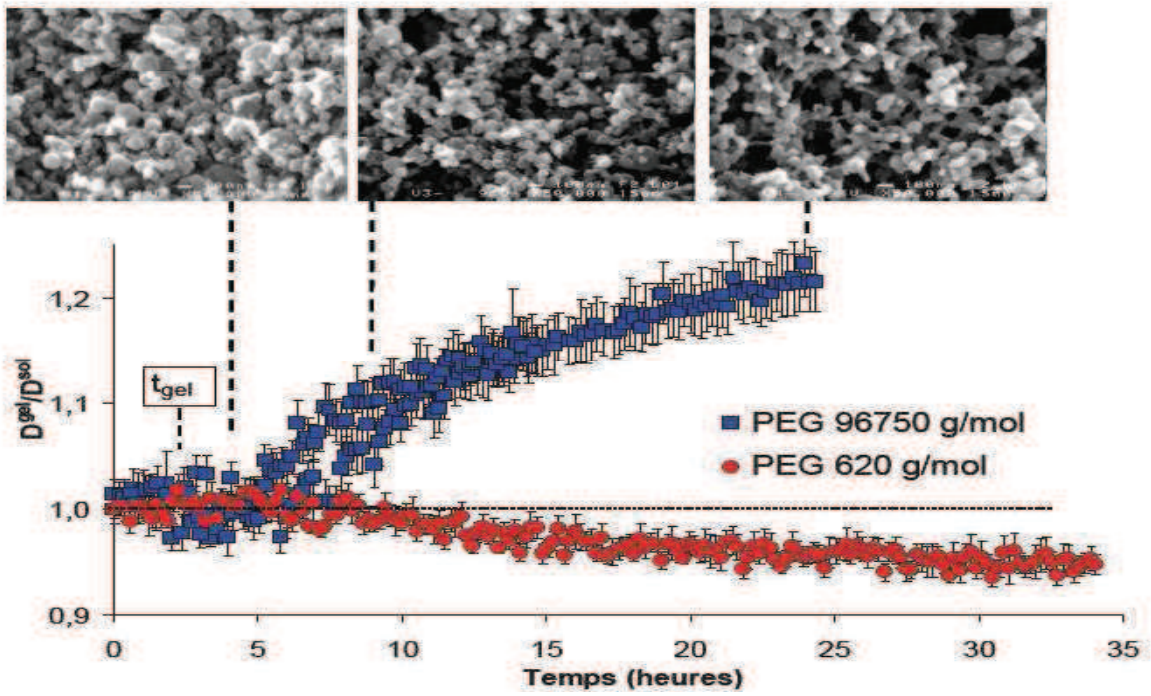

Figure 29. Evolutions of PEG diffusion and the structure of gels by SEM as a function of time after renneting (extracted from Le Feunteun et al. [89]).

The diffusion of the two probes was unaffected by the first two stages of coagulation, i.e., the enzymatic and the aggregation phases. On the other hand, beyond 5 hours when the casein aggregate compaction began, as revealed by rheometry experiments, the diffusion coefficient of the small PEG progressively decreased, in contrast to what was observed in other studies, leading to equilibrium, whereas the opposite occurred for the large PEG. These results show that only the network rearrangements, which take place during gel aging, affect probe diffusion. As illustrated by SEM images in **Figure 29**, the diffusion rate of the 96750 g/mol PEG is very sensitive to the reduction in the casein particle water content and, hence, to the progressive increase in gel porosity.

All of the results mentioned above were explained by considering that PEGs can or cannot diffuse through casein particles, depending on their size. The large probes could only diffuse around casein particles. As a result, it is assumed that they would diffuse faster after coagulation due to the intense increase in gel porosity, which is known to take place during aging, whereas the small PEG would diffuse through the casein particles. After coagulation, casein aggregates become denser and the "through the casein aggregate" diffusion component is reduced.

However, it is known that the structure of casein particles is not considerably affected by rennet action before the sol-gel transition. Le Feunteun et al. [88] chose to compare their results with the pH effects that are known to greatly change the structure of the micelle. Contrary to what was observed during rennet coagulation, in the case of the acid and the combined coagulation, the probe diffusion was changed before the sol-gel transition. The evolutions of the 96750 g/mol PEG during the acid and the combined coagulation were entirely explained by hydration changes and, therefore, by the size of the casein particles before coagulation and by the increase in network porosity after coagulation, whereas the variations of the small PEG diffusion were mainly explained by the structural reorganizations of the casein particles that take place during acidification after the removal of CCP.

In conclusion, these results show that there are two characteristic length scales of structure to be considered to explain probe diffusion. For large PEGs, the voluminosity of casein particles and the network porosity are the most important elements, whereas for small PEGs, the internal porosity of the casein particle is the preponderant factor.

Other studies performed in casein systems have focused on the dynamic properties of casein proteins in relation to the protein concentration by observing changes in their self-diffusion coefficients. For example, Mariette et al. [231] measured casein diffusion in NPC suspensions for different casein concentrations ranging from 0.03 to 0.19 g/g. Le Feunteun et al. [232] monitored the diffusion of casein particles during the renneting of a concentrated casein micelle suspension (14% w/w). This study showed that the self-diffusion of both casein particles and soluble caseins can be determined simultaneously, and explained how their evolution can be linked to the key stages of the coagulation process. Tan et al. [233] measured casein self-diffusion coefficients in SC suspensions with casein concentrations ranging from 2 to 20% w/w.

3.2. T_2 relaxation of PEG probes

Despite numerous studies concerning the diffusion of PEG/PEO probes in different matrices, there is a lack of data regarding the T_2 relaxation times of these kinds of probes. Most studies found in the literature focused on the effects of PEG/PEO polymer chain length on T_2 relaxation time in highly entangled polymer systems (reptation regime) [234-237]. To our knowledge, no studies exist concerning the effects of PEG/PEO polymer chain length on T_2 relaxation times measured in dilute and semi-dilute matrices.

3.3. Modeling of PEG probes diffusion data

Many models exist in the literature to describe the diffusion of such polymers inside systems, taking interactions between the diffusing polymer and the network into account, as well as different physical concepts such as the obstruction effect, hydrodynamic interactions, and the free volume concept in polymers. Massaro et al. [238] wrote a very detailed revue describing the main models of diffusion according to the theory to which they adhere.

Some of these models succeeded in describing PEG diffusion. However, there are limitations in the application of these physical models, particularly for large PEGs and for concentrated systems. The simplest models neglect important parameters such as the size of the probe. For example, that is why the Mackie-Meares model [239-240], which is only a function of the volume fraction of the matrix, does not make it possible to explain the diffusion of probes of different sizes. Other models are more complex and are adjusted with variable parameters that are not known or difficult to evaluate. These parameters differ from one system to another and it is generally impossible to predict their values. Moreover, the real significance of certain adjustment parameters is unclear, e.g., in the models of Amsden [241], Petit et al. [215] and Phillies [242-243]. These diffusion models can therefore not be used to estimate and predict the values of the PEG diffusion coefficient in a given system.

However, the Jonsson model [244], otherwise known as the “cell model”, contains only one adjustment parameter with real significance (volume fraction occupied by casein particles).

Without going into the details of this model, it is based on the principle that casein micelles can be assimilated to spheres that are not impermeable to PEGs. This model was used to describe the diffusion of water and PEGs in casein systems [230-231, 233]. For example, in a study by Colsenet et al. [230], this model made it possible to explain the diffusion coefficient of PEG of variable sizes in casein suspensions and gels but it did not make it possible to explain the strong increase in the large probe diffusion coefficient after the system gelation and which is explained, as mentioned above, by the increase in the empty space fraction.

On the other hand, a study carried out by Babu et al. [245] seems to support the hypothesis according to which the diffusion of PEGs would increase when more empty areas are created in the sample. They used computer simulations to show that the diffusion of a spherical probe in hard sphere suspensions and gels is mainly dependent on the volume fraction that is accessible to the diffusing particle.

This model, as well as the other diffusion models, uses the classical hard sphere concept. However, PEGs are easily deformable and can change their shape and size according to their environment [246-247], which complicates the modeling of diffusion data and the interpretation of the experimental self-diffusion results. These polymers can therefore diffuse through small spaces compared to their hydrodynamic diameter by adopting a more elongated conformation, as described by the reptation model of de Gennes [246-247] and proposed by Favre et al. [217] (**Figure 30**).

A simple power law provides a description of the solute diffusion coefficients versus molecular weight:

$$D = A.M^{-\alpha}$$

where A is a pre-exponential factor and α a characteristic exponent. This equation is often used to describe the self-diffusion of polymer chains with α varying from 0.55 for dilute systems to 2 in concentrated systems.

An intermediate mechanism was proposed by Favre et al. [217] to possibly explain the somewhat intermediate situation between negligible partial drainage of the solvent in an ideal statistical sphere (exponent value: -0.5 or 0.6) and the wormlike displacement of a linear molecule in a

network of fixed obstacles (exponent value: -2). Due to the existence of topological constraints, only solute conformations with elongated shapes are able to diffuse. Based on **Figure 30**, a gradual transition from situation a–b, reflecting an increased solute elongation, is assumed to take place when network density increases. Such a situation is expected to occur when mesh size approaches the solute hydrodynamic diameter.

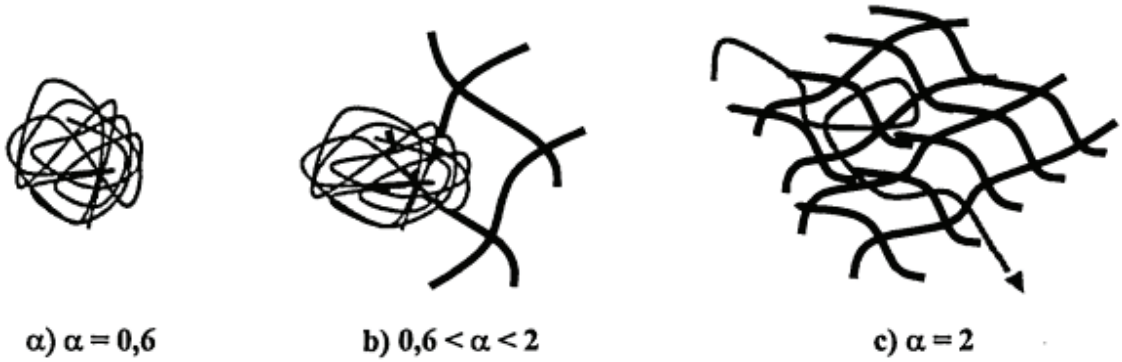

Figure 30. Schematics of different diffusion mechanisms for a macromolecular solute under dilute condition assumption. (a) In solution. Random coil with negligible solvent drainage; (c) In concentrated gels. Reptation; (b) Hypothetical mechanism for dilute networks (extracted from Favre et al. [217]).

This tentative explanation is in strong contrast with the classical hard sphere concept used in diffusion models, which make indifferent use of the equivalent spherical shape analogy (i.e., solute hydrodynamic radius). In principle, it should be possible to extend the mechanism illustrated in **Figure 30** to the other models.

Due to the difficulty of controlling the molecular size and shape of PEGs, a preferable experimental design would be to follow the diffusion of hard sphere probe particles through the matrix. In this domain, dendrimers are molecules of choice because of the good control of their molecular size and shape.

3.4. Dendrimer probes

Dendrimers, also known as starburst polymers, are spherical macromolecules and are a class of regularly branched mono-dispersed polymers [248]. Dendrimer architectures consist of three domains: (1) the core, which can be a single atom or group of atoms; (2) branch units, which divide radially grown concentric layers, referred to as generations; and (3) functional surface groups, which play a key role in determining the properties. Unlike classical polymers, dendrimers have a high degree of molecular uniformity, narrow molecular weight distribution, specific size and shape characteristics, and a highly-functionalized terminal surface [248].

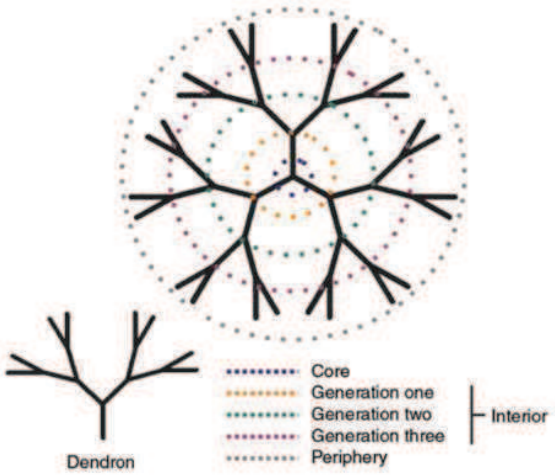

Figure 31. A dendrimer and dendron are represented with solid lines. The colored, broken lines identify the various key regions of the dendrimer (extracted from Lee et al. [249]).

Dendrimers have been recently used as diffusional probes in many systems. For example, Loren et al. [250] determined the effect of the κ-carrageenan concentration on gel microstructure and self-diffusion of two different generations (G2: "R_h = 2.82±0.06 nm", and G6: "R_h = 6.69±0.24 nm") of polyamideamine dendrimers by transmission electron microscopy (TEM), image analysis and PFG-NMR. Different salt conditions of KCl, NaCl, and mixtures thereof allowed for the formation of significantly different microstructures. Dendrimers were found to be sensitive probes to determine the effect of the gel microstructure on the molecular diffusion rate. The results showed that is possible to achieve slow or fast diffusion rates by choosing the appropriate ionic conditions and κ-carrageenan concentration. In general, the dendrimer diffusion rate

decreases with increasing κ-carrageenan concentration and increasing dendrimer size. It was shown that the dendrimer diffusion rate was influenced by obstruction. The main parameter affecting diffusion by obstruction is the void size of the gel. Small voids lead to a strongly reduced diffusion rate.

For example, **Figure 33** shows dendrimers D/D_0 as a function of increasing potassium ion concentration ranging from 20 to 200 mM KCl at constant 1 wt % κ-carrageenan concentration. The dendrimer diffusion rates increase with increasing potassium ion concentration and reaches maxima at around 100 mM KCl and decrease slightly at 150 mM KCl and even further at 200 mM KCl. These results coincide well with the balance between fine stranded and coarse gel networks in the κ-carrageenan gel structure as seen in **Figure 32**. The 20 mM KCl κ-carrageenan gel has finer strands with small voids as compared to the 100 mM KCl gel that has more aggregated strands.

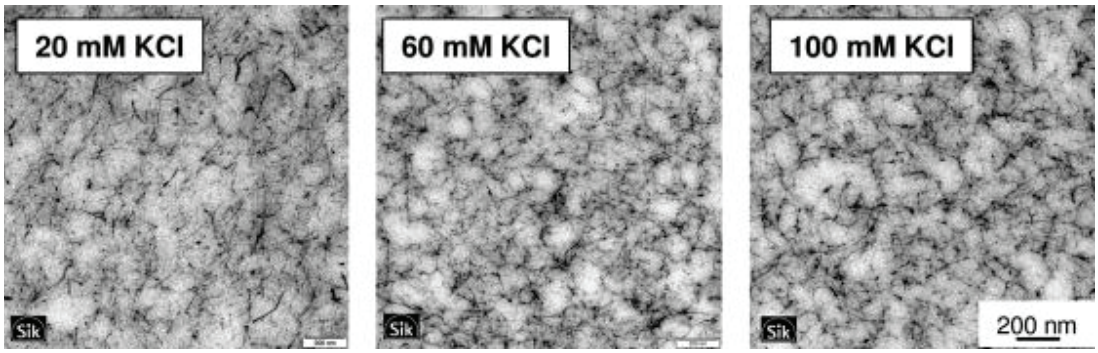

Figure 32. TEM micrographs showing 1 wt % κ-carrageenan gels at different potassium ion concentrations (extracted from Loren et al. [250]).

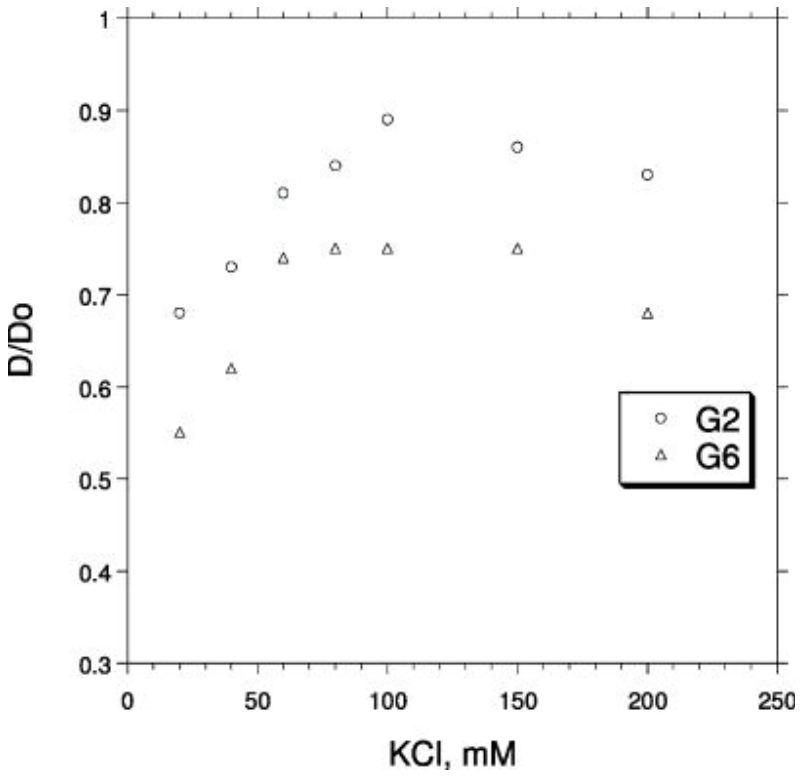

Figure 33. Normalized diffusion rate of dendrimers of generation 2 (O) and generation 6 (4) in 1 wt % κ-carrageenan gels as a function of potassium ion concentrations. Observation time = 500 ms (extracted from Loren et al. [250]).

Bernin et al. [251] studied the diffusion of different poly (amido amine) dendrimer generations in various alginate gels. The diffusion of the G2 dendrimer with a hydrodynamic radius of approximately 3 nm was only weakly affected by the gel network and appeared to be independent of the various Ca^{2+} and alginate concentrations. On the other hand, the G6 dendrimer with a radius of 8 nm experienced a large reduction in diffusion, with D_{gel}/D_0 values of 0.70 and 0.72 for 10 and 20 mmol L^{-1} Ca^{2+} gels, respectively, and 0.58 for the 30 mmol L^{-1} Ca^{2+} gel (1.5 % alginate). However, the results revealed a significant decrease in D_{gel}/D_0 for all dendrimer generations for a 5 mmol L^{-1} Ca^{2+} alginate gel in the presence of MeOH. D_{gel}/D_0 for G2 and G6 dendrimers was considerably reduced for the 10 mmol L^{-1} Ca^{2+} gel containing MeOH. These results were explained by the decrease in pore volume and, therefore, the formation of a dense network for Ca^{2+} alginate gels in water-methanol mixtures.

Baille et al. [252] studied the mobility of three different poly(propylene imine) dendrimers with hydrophilic triethylenoxy metyl ether terminal groups (generations 2, 4 and 5) in poly(vinyl alcohol) aqueous solutions and gels by NMR spectroscopy. In agreement with previous studies, dendrimer self-diffusion decreases with increasing molecular size of the diffusants and with increasing PVA concentration. These authors also measured the T_1 and T_2 relaxation times in order to study the motions of three different parts of the dendrimers (methyl and methylene protons of the terminal groups and methylene protons of the core) as a function of the generation. The results obtained show that the terminal protons are more mobile than the core protons for all dendrimers. The relaxation time measurements also reveal a decrease in mobility for all protons as the dendrimer generation increases.

3.5. Conclusion

All the results indicate that the diffusion of PEG and dendrimer probes is sensitive to the matrix microstructure. The coagulation phenomenon and other structural modifications can thus be highlighted by measuring the diffusion coefficients of these probes. Moreover, depending on its molecular weight, a probe will be more or less affected by these sample microstructure reorganizations. However, it seems difficult to predict the size that a probe molecule will have beforehand to well highlight a given structural change. Dendrimers have the advantage over PEGs in terms of shape and molecular size control.

Concerning the molecular diffusion in casein suspensions and gels, the monitoring of PEG self-diffusion coefficients during the coagulation processes made it possible to propose an interpretation model of diffusion mechanisms in relation to the casein matrix structure. It is the combination of probe size and structure length scale that should be considered. According to their size, probes can diffuse more or less easily through the casein particles. For the large probes such as the 96750 g/mol PEG, the extra-particle diffusion is the predominant mechanism. Consequently, diffusion will be mainly affected by the hydration of the casein matrix, i.e., by the size of the particles before aggregation rather than by the gel porosity. In contrast, the small probes such as the 620 g/mol PEG can diffuse through the casein particles. In this case, the diffusion depends on the internal structure of the caseins. Thus, the probe diffusion will be sensitive to different length scales of the structure, depending on its size. Finally, the amplitude of variations observed for large probes is greater because the volume available for their diffusion is highly affected by structural changes, contrary to the small probes.

All these features demonstrate that kinetic probe diffusion experiments are very valuable to study the coagulation of milk systems and might also be used to investigate the coagulation of other systems (polysaccharides, alginate, etc.), as well as certain phenomena such as the impact of various parameters on rearrangement processes.

4. Project description

The previous results of Le Feunteun et al. [88-90] have shown that the diffusion of linear and deformable polyethylene-glycol probes in NPC suspensions and gels could be explained by considering two characteristic length scales of structure. For large PEGs, the free volume fraction unoccupied by casein micelles and the matrix porosity are the most important elements, whereas for small PEGs, the internal porosity of the casein particles is the preponderant factor. This model has made it possible to explain the effect of probe size, in particular. This project aimed to validate the interpretation of Le Feunteun et al. and to improve our understanding of probe diffusion in casein systems on the basis of two approaches:

1. Modification of the casein structure

Different treatments can change the structure of the micelle and affect its porosity. Treatments such as acid precipitation of the micelle (see Section 1) lead to its dissociation and the formation of smaller subunits of approximately 11 nm, known as caseinate. The particularity of the sodium caseinate (SC) system resides in the fact that the extra-particle diffusion mechanism is the only one to be considered in these suspensions. PEGs cannot diffuse inside SC aggregates because of their small size. Thus, according to the interpretation model of Le Feunteun et al., small PEG diffusion should be more rapid in the SC system since they encounter fewer obstruction effects when diffusing around casein aggregates in SC suspensions. PEG with different molecular weights was measured in NPC and SC systems in order to compare their behavior in these two systems. The data obtained are presented in ***Chapter III***.

2. Modification of the probe

As presented in Section 3, PEGs have numerous advantages. However, these polymers are easily deformable and can change their shape according to their environment, which considerably complicates the interpretation of the diffusion results obtained in NPC suspensions and gels. However, dendrimer probes are spherical rigid molecules and, as a result, cannot diffuse inside casein particles. The main question that arises concerning this approach can be summarized as follows: “Is the molecular diffusion in systems composed of casein micelles or micellar aggregates modulated by the flexibility of the probe?”. In order to provide some answers to this

question, the translational and rotational diffusion of spherical dendrimer probes was measured and compared with that of flexible PEG probes in NPC suspensions and in a concentrated rennet casein gel (15 g /100 g H_2O) using NMR diffusometry and relaxometry. The interest of coupling the two NMR methods was to probe the investigated matrix at two different length scales. All these data are presented in ***Chapter IV***.

In ***Chapter V***, we present NMR measurements of the rotational and translational diffusion coefficients of a rigid dendrimer probe and a flexible PEG probe (R_h ~7 nm) in dilute/semi-dilute/concentrated dispersions and acid gels of a sodium caseinate polymer system. The results are discussed in an attempt to understand the respective effects of protein crowding and coagulation on translational and rotational diffusion of these probes.

All the results are discussed in C***hapter VI***. Finally, conclusions are drawn and future perspectives are considered.

5. References

1. Walstra, P., et al., *Dairy technology; principles of milk properties and processes*, edited by M. Dekker (New York, 1999).
2. Holt, C., *Structure and stability of bovine casein micelles.* Advances in Protein Chemistry, 1992. **43**: p. 63-151.
3. Fox, P.F., et al., *The casein micelle: Historical aspects, current concepts and significance.* International Dairy Journal, 2008. **18**(7): p. 677-684.
4. McMahon, D.J., et al., *Composition, Structure, and Integrity of casein micelles: a review.* Journal of Dairy Science, 1984. **67**: p. 499-512.
5. Sandra, S., et al., *The rennet coagulation mechanism of skim milk as observed by transmission diffusing wave spectroscopy.* Journal of Colloid and Interface Science, 2007. **308**(2): p. 364-373.
6. Holt, C., et al., *The hairy casein micelle: evolution of the concept and its implication for dairy technology.* Netherlands Milk and Dairy Journal, 1996. **50**: p. 85-111.
7. Davies, D.T., et al., *Variation in the protein composition of bovine casein micelles and serum casein in relation to micellar size and milk temperature.* Journal of Dairy Research, 1983. **50**(1): p. 67-75.
8. Creamer, L.K., et al., *A study of the dissociation of β-caseins from the bovine casein micelle at low temperature.* New Zealand Journal of Dairy Science and Technology, 1977. **12**: p. 58-66.
9. de Kruif, C.G., *Supra-aggregates of Casein Micelles as a Prelude to Coagulation.* Journal of Dairy Science, 1998. **81**(11): p. 3019-3028.
10. de Kruif, C.G., et al., *Casein Micelles: Size Distribution in Milks from Individual Cows.* Journal of Agricultural and Food Chemistry, 2012. **60**(18): p. 4649-4655.
11. Wade, T., et al., *Electroacoustic determination of size and zeta potential of fat globules in milk and cream emulsions.* Colloids and Surfaces B Biointerfaces, 1997. **10**(2): p. 73-85.
12. Davidson, C.M., *The use of dynamic light-scttering in monitoring rennet curd formation.* Milchwissenschaft-Milk Science International, 1990. **45**(11): p. 712-715.
13. Horne, D.S., *Studies of gelation of acidified and renneted milks using diffusing wave spectroscopy.* Milchwissenschaft-Milk Science International, 1991. **46**(7): p. 417-422.
14. Holt, C., et al., *Natural Variations in Average Size of Bovine Casein Micelles .1. Milks from Individual Ayrshire Cows.* Journal of Dairy Research, 1978. **45**(3): p. 339-345.
15. McGann, T.C.A., et al., *Composition and Size Distribution of Bovine Casein Micelles.* Biochimica Et Biophysica Acta, 1980. **630**(2): p. 261-270.
16. Dalgleish, D.G., et al., *Size-related differences in bovine casein micelles.* Biochimica et Biophysica Acta, 1989. **991**(3): p. 383-387.
17. Bloomfield, V.A., et al., *Structure of casein micelles : Physical methods.* Netherlands Milk and Dairy Journal, 1973. **27**(2/3): p. 103-120.
18. Morr, C.V., et al., *Molecular weights of fractionated bovine milk casein micelle from analytical ultracentrifugation and diffusion measurements.* Journal of dairy science, 1973. **36**(4): p. 415-418.
19. Walstra, P., *The voluminosity of bovine casein micelles and some of its applications.* Journal of Dairy Science, 1979. **46**: p. 317-323.

20. Morris, G.A., et al., *Further observations on the size, shape, and hydration of casein micelles from novel analytical ultracentrifuge and capillary viscometry approaches.* Biomacromolecules, 2000. **1**(4): p. 764-767.
21. Holt, C., *Structure and stability of bovine casein micelles.* Advenced protein Chemistry, 1992. **43**: p. 63-151.
22. Dalgleish, D.G., et al., *pH-induced dissociation of bovine casein micelles. 2. mineral solubilization and its relation to casein release.* Journal of Dairy Research, 1989. **56**: p. 727-735.
23. De Kruif, C.G., et al., *Physicochemical study of kappa- and beta-casein dispersions and the effect of cross-linking by transglutaminase.* Langmuir, 2002. **18**(12): p. 4885-4891.
24. O'Connell, J.E., et al., *beta-casein micelles; cross-linking with transglutaminase.* Colloids and Surfaces A: Physicochemical and Engineering Aspects, 2003. **216**(1-3): p. 75-81.
25. Rollema, H.S., et al., *^{1}H-NMR studies of bovine k-casein and casein micelles.* Netherlands Milk and Dairy Journal, 1988. **42**: p. 233-248.
26. Walstra, P., *On the stability of casein micelles.* Journal of Dairy Science, 1990. **73**: p. 1968-1979.
27. Walstra, and R. Jenness, *Dairy Chemistry and Physics*. 1984, John Wiley and Sons: New-York. p. 229-253.
28. Morr, C.V., *Effect of oxalate and urea upon ultracentifugation properties of raw and heated skim milk casein micelles.* Journal of Dairy Science, 1967. **50**: p. 1744-1751.
29. Ono, T.a.O., et al., *A model for the assembly of bovine casein micelles from F2 ans F3 subunits.* Journal of Dairy Research, 1989. **56**: p. 453-461.
30. Walstra, P., *Casein sub-micelles: do they exist?* International Dairy Journal, 1999. **9**(3-6): p. 189-192.
31. Horne, D.S., *Casein micelle structure: Models and muddles.* Current Opinion in Colloid & Interface Science, 2006. **11**(2-3): p. 148-153.
32. Garnier, J., et al., *Structure of the casein micelle. A proposed model.* Journal of Dairy Research, 1970. **37**: p. 493-504.
33. Horne, D.S., *Casein interactions: Casting light on the black boxes, the structure in dairy products.* International Dairy Journal, 1998. **8**(3): p. 171-177.
34. Slattery, C.W., et al., *A model for the formation and structure of casein micelles from subunits of variable composition.* Biochemica et Biophysica Acta, 1973. **317**(2): p. 529-538.
35. Slattery, C.W., *Model calculations of casein micelle size distributions.* Biophysical Chemistry, 1976. **6**(1): p. 59-64.
36. Schmidt, D.G., *Colloidal aspects of caseins.* Netherlands Milk and Dairy Journal, 1980. **34**(1): p. 42-64.
37. Farrell, H.M., et al., *Casein micelle structure: What can be learned from milk synthesis and structural biology?* Current Opinion in Colloid & Interface Science, 2006. **11**(2-3): p. 135-147.
38. McMahon, D.J., et al., *Rethinking casein micelle structure using electron microscopy.* Journal of Dairy Science, 1998. **81**(11): p. 2985-2993.
39. Marchin, S., et al., *Effects of the environmental factors on the casein micelle structure studied by cryo transmission electron microscopy and small-angle x-ray scattering/ultrasmall-angle x-ray scattering.* Journal of Chemical Physics, 2007. **126**(4).

40. Phippstodd, B.E., et al., *Milk gel structure .13. Rotary shadowing of casein micelles for electron-microscopy.* Milchwissenschaft-Milk Science International, 1982. **37**(9): p. 513-518.
41. Schmidt, D.G., et al., *Elektronenmikroskopische untersuchung der feinstruktur von caseinmicellen in kuhmilch.* Milchwissenschaft-Milk Science International, 1970. **25**: p. 596-600.
42. Dalgleish, D.G., et al., *A possible structure of the casein micelle based on high-resolution field-emission scanning electron microscopy.* International Dairy Journal, 2004. **14**: p. 1025-1031.
43. Pignon, F., et al., *Structure and rheological behavior of casein micelle suspensions during ultrafiltration process.* The Journal of Chemical Physics, 2004. **121**(16): p. 8138-8146.
44. De Kruif, C.G. and C. Holt, *in advanced dairy chemistry proteins*, edited by P.F. Fox and P.L.H. McSweeney (Kluwer, New York, 2003), vol. 1, p. 233.
45. Heertje, I., et al., *Structure formation in acid milk gels.* Food Microstructure, 1985. **4**(2): p. 267-277.
46. Karlsson, A.O., et al., *Influence of pH and NaCl on rheological properties of rennet-induced casein gels made from UF concentrated skim milk.* International Dairy Journal, 2007. **17**(9): p. 1053-1062.
47. Hojou, K., et al., *Some Applications of Ion-Beam Sputtering to High-Resolution Electron-Microscopy.* Micron, 1977. **8**(3): p. 151-170.
48. McMahon, D.J., et al., *Supramolecular structure of the casein micelle.* Journal of Dairy Science, 2008. **91**(5): p. 1709-1721.
49. Horne, D.S., *Casein micelles as hard spheres: limitations of the model in acidified gel formation.* Colloids and Surfaces a-Physicochemical and Engineering Aspects, 2003. **213**(2-3): p. 255-263.
50. Lucey, J.A., *Formation and physical properties of milk protein gels.* Journal of Dairy Science, 2002. **85**(2): p. 281-294.
51. Horne, D.S., *Casein structure, self-assembly and gelation.* Current Opinion in Colloid & Interface Science, 2002. **7**(5): p. 456-461.
52. Choi, J., et al., *Effect of insoluble calcium concentration on rennet coagulation properties of milk.* Journal of Dairy Science, 2007. **90**(6): p. 2612-2623.
53. Marchin, S., *Dynamique de la micelle de caséines : caractérisation structurale*. 2007, Agrocampus Rennes. p. 203.
54. Smiddy, M.A., et al., *Stability of Casein Micelles Cross-Linked by Transglutaminase.* Journal of Dairy Science, 2006. **89**(6): p. 1906-1914.
55. Dalgleish, D.G., *The enzymatic coagulation of milk*, *in*, *Cheese: Chemistry*, *Physics and Microbiology: vol. 1: General Aspects,* Fox, P.E. ed., Chapman & Hall: London, UK. p. 69-100.
56. Alexander, M., et al., *Application of transmission diffusing wave spectroscopy to the study of gelation of milk by acidification and rennet.* Colloids and Surfaces B-Biointerfaces, 2004. **38**(1-2): p. 83-90.
57. Mellema, M., et al., *Effects of structural rearrangements on the rheology of rennet-induced casein particle gels.* Advances in Colloid and Interface Science, 2002. **98**(1): p. 25-50.

58. Schorsch, C., et al., *Cross-linking casein micelles by a microbial transglutaminase conditions for formation of transglutaminase-induced gels.* Internatioanl Dairy Journal, 2000. **10**(8): p. 519-528.
59. Karlsson, A.O., et al., *Rheological properties and microstructure during rennet induced coagulation of UF concentrated skim milk.* International Dairy Journal, 2007. **17**(6): p. 674-682.
60. Lagoueyte, N., et al., *Temperature affects microstructure of renneted milk gel.* Journal of Food Science, 1994. **59**(5): p. 956-959.
61. Lucey, J.A., et al., *Effect of heat treatment on the physical properties of milk gels made with both rennet and acid.* International Dairy Journal, 2001. **11**(4-7): p. 559-565.
62. Mellema, M., et al., *Structure and scaling behavior of aging rennet-induced casein gels examined by confocal microscopy and permeametry.* Langmuir, 2000. **16**(17): p. 6847-6854.
63. Bauer, R., et al., *The Structure of Casein Aggregates During Renneting Studied by Indirect Fourier Transformation and Inverse Laplace Transformation of Static and Dynamic Light-Scattering Data, Respectively.* Journal of Chemical Physics, 1995. **103**(7): p. 2725-2737.
64. Lucey, J.A., et al., *Properties of acid casein gels made by acidification with glucono-[delta]-lactone. 2. Syneresis, permeability and microstructural properties.* International Dairy Journal, 1997. **7**(6-7): p. 389-397.
65. Lucey, J.A., et al., *Rheological properties of milk gels formed by a combination of rennet and glucono-delta-lactone.* Journal of Dairy Research, 2000. **67**(3): p. 415-427.
66. Sharma, S.K., et al., *Effect of milk concentration, pH and temperature on kappa-casein hydrolysis at aggregation, coagulation and curd cutting times of ultrafiltered milk.* Milchwissenschaft Milk Science International, 1994. **49**(8): p. 450-453.
67. Zoon, P., et al., *Rheological properties of rennet-induced skim milk gels. 4. The effect of pH and NaCl.* Netherlands Milk and Dairy Journal, 1989. **43**: p. 17-34.
68. Brinkhuis, J., et al., *the influence of temperature on the flocculation rate of renneted casein micelles.* Biophysical Chemistry, 1984. **19**(1): p. 75-81.
69. Dalgleish, D.G., *Coagulation of renneted coagulation of renneted bovine casein micelles-Dependence on temperature, calcium-ion concentration and ionic-strength.* Journal of Dairy Research, 1983. **50**(3): p. 331-340.
70. Daviau, C., et al., *Rennet coagulation of skim milk and curd drainage: Effect of pH, casein concentration, ionic strength and heat treatment.* Lait, 2000. **80**(4): p. 397-415.
71. Mehaia, M.A., et al., *The secondary phase of milk coagulation- Effect of calcium, pH and temperture on clotting activity.* Milchwissenschaft-Milk Science International, 1983. **38**(3): p. 137-140.
72. Najera, A.I., et al., *Effects of pH, temperature, CaCl2 and enzyme concentrations on the rennet-clotting properties of milk: a multifactorial study.* Food Chemistry, 2003. **80**(3): p. 345-352.
73. Vetier, N., et al., *Effect of temperature and aggregation rate on the fractal dimension of renneted casein aggregates.* Journal of Dairy Science, 2003. **86**(8): p. 2504-2507.
74. Culioli, J., et al., *Rheological aspects of renneting of milk concentrated by ultrafiltration.* Journal of Texture Studies, 1978. **9**(3): p. 257-281.

75. Lucey, J.A., et al., *A comparison of the formation, rheological properties and microstructure of acid skim milk gels made with a bacterial culture or glucono-delta-lactone.* Food Research International, 1998. **31**(2): p. 147-155.
76. De Kruif, C.G., *Skim milk acidification.* Journal of Colloid and Interface Science, 1997. **185**(1): p. 19-25.
77. Baumy, J.J., et al., *Effect of pH and ionic strength on the binding of bivalent cations to beta-casein.* Le Lait - Dairy Science and Technology, 1988. **68**(4): p. 409-417.
78. Dalgleish, D.G., et al., *pH-induced dissociation of bovine casein micelles.* Journal of Dairy Science, 1988. **55**(4): p. 529-538.
79. de la Fuente, M.A., *Changes in the mineral balance of milk submitted to technological treatments.* Trends in Food Science & Technology, 1998. **9**(7): p. 281-288.
80. De Kruif, C.G., *Casein micelle interactions.* International Dairy Journal, 1999. **9**(3-6): p. 183-188.
81. Famelart, M.H., et al., *pH-induced physicochemical modifications of native phosphocaseinate suspensions: Influence of aqueous phase.* Lait, 1996. **76**(5): p. 445-460.
82. Gastaldi, E., et al., *Acid milk gel formation as affected by total solids content.* Journal of Food Science, 1997. **62**(4): p. 671-675.
83. Vetier, N., et al., *Casein micelle solvation and fractal structure of milk aggregates and gels.* Lait, 2000. **80**(2): p. 237-246.
84. Banon, S., et al., *A Colloidal Approach of Milk Acidification by Glucono-Delta-Lactone.* Journal of Dairy Science, 1992. **75**(4): p. 935-941.
85. Tuinier, R., et al., *Stability of casein micelles in milk.* The Journal of Chemical Physics, 2002. **117**(3): p. 1290-1295.
86. Noel, Y., et al., *Comparaison des cinétiques de coagulation enzymatique et mixte du lait. Influence du calcium.* Lait, 1989. **69**: p. 479-490.
87. Tranchant, C.C., et al., *Different coagulation behaviour of bacteriologically acidified and renneted milk: the importance of fine-tuning acid production and rennet action.* International Dairy Journal, 2001. **11**(4-7): p. 483-494.
88. Le Feunteun, S., et al., *Effects of acidification with and without rennet on a concentrated casein system: A kinetic NMR probe diffusion study.* Macromolecules, 2008. **41**(6): p. 2079-2086.
89. Le Feunteun, S., et al., *PFG-NMR Techniques Provide a New Tool for Continuous Investigation of the Evolution of the Casein Gel Microstructure after Renneting.* Macromolecules, 2008. **41**(6): p. 2071-2078.
90. Le Feunteun, S., et al., *Impact of casein gel microstructure on self-diffusion coefficient of molecular probes measured by H-1 PFG-NMR.* Journal of Agricultural and Food Chemistry, 2007. **55**(26): p. 10764-10772.
91. Kumosinski, T.F., et al., *Determination of the quaternary structural states of bovine casein by small-angle X-ray scattering: Submicellar and micellar forms.* Archives of biochemistry and biophysics, 1988. **266**(2): p. 548-561.
92. Povey, M.J.W., et al., *Ultrasonic spectroscopy studies of casein in water.* International Dairy Journal, 1999. **9**(3): p. 299-303.
93. Chu, B., et al., *Laser light scattering of model casein solutions: effects of high temperature.* Journal of Colloid and Interface Science, 1995. **170**(1): p. 102-112.

94. Dickinson, E., et al., *Analysis of light scattering data on the calcium ion sensitivity of caseinate solution thermodynamics: relationship to emulsion flocculation.* Journal of Colloid and Interface Science, 2001. **239**(1): p. 87-97.
95. Farrell, H.M., et al., *Particle sizes of purified kappa-casein: Metal effect and correspondence with predicted three-dimensional molecular models.* Journal of Protein Chemistry, 1996. **15**(5): p. 435-445.
96. Lucey, J.A., et al., *Characterization of commercial and experimental sodium caseinates by multiangle laser light scattering and size-exclusion chromatography.* Journal of Agricultural and Food Chemistry, 2000. **48**(5): p. 1610-1616.
97. O'Kennedy, B.T., et al., *Factors affecting the acid gelation of sodium caseinate.* International Dairy Journal, 2006. **16**(10): p. 1132-1141.
98. Panouille, M., et al., *Dynamic mechanical properties of suspensions of micellar casein particles.* Journal of Colloid and Interface Science, 2005. **287**(2): p. 468-475.
99. HadjSadok, A., et al., *Characterisation of sodium caseinate as a function of ionic strength, pH and temperature using static and dynamic light scattering.* Food Hydrocolloids, 2008. **22**(8): p. 1460-1466.
100. Nash, W., et al., *Dynamic light scattering investigation of sodium caseinate and xanthan mixtures.* International Journal of Biological Macromolecules, 2002. **30**(5): p. 269-271.
101. Ruis, H.G.M., et al., *Relation between pH-induced stickiness and gelation behaviour of sodium caseinate aggregates as determined by light scattering and rheology.* Food Hydrocolloids, 2007. **21**(4): p. 545-554.
102. Braga, A.L.M., et al., *The effect of the glucono-delta-lactone/caseinate ratio on sodium caseinate gelation.* International Dairy Journal, 2006. **16**(5): p. 389-398.
103. Roefs, S.P.F.M., et al., *Structure of acid casein gels 1. Formation and model of gel network.* Colloids and Surfaces, 1990. **50**: p. 141-159.
104. Roefs, S.P.F.M., et al., *Structure of acid casein gels 2. Dynamic measurements and type of interaction forces.* Colloids and Surfaces, 1990. **50**: p. 161-175.
105. Takeuchi, K.P., et al., *Influence of ageing time on sodium caseinate gelation induced by glucono-delta-lactone at different temperatures.* Dairy Science and Technology, 2008. **88**(6): p. 667-681.
106. Lucey, J.A., et al., *Properties of acid casein gels made by acidification with glucono-delta-lactone. 2. Syneresis, permeability and microstructural properties.* International Dairy Journal, 1997. **7**(6): p. 389-397.
107. Lucey, J.A., et al., *Properties of Acid Casein Gels Made by Acidification with Glucono-d-lactone. 1. Rheological Properties.* International Dairy Journal, 1997. **7**(6): p. 381-388.
108. Brownstein, K.R., et al., *Importance of classical diffusion in NMR studies of water in biological cells.* Physical Review A, 1979. **19**(number 6): p. 2446-2453.
109. Kleinberg, R.L., et al., *Mechanism of NMR Relaxation of Fluids in Rock.* Journal of Magnetic Resonance, 1994. **108**: p. 206-214.
110. Johnson, C.S., *Diffusion ordered nuclear magnetic resonance spectroscopy: principles and applications.* Progress in Nuclear Magnetic Resonance Spectroscopy, 1999. **34**(3-4): p. 203-256.
111. Price, W.S., *Pulsed-field gradient nuclear magnetic resonance as a tool for studying translational diffusion .1. Basic theory.* Concepts in Magnetic Resonance, 1997. **9**(5): p. 299-336.

112. Price, W.S., *Pulsed-field gradient nuclear magnetic resonance as a tool for studying translational diffusion: Part II. Experimental aspects.* Concepts in Magnetic Resonance, 1998. **10**(4): p. 197-237.
113. Walderhaug, H., et al., *Self-diffusion in polymer systems studied by magnetic field-gradient spin-echo NMR methods.* Progress in Nuclear Magnetic Resonance Spectroscopy, 2010. **56**(4): p. 406-425.
114. Hahn, E.L., *Spin echoes.* Physical Review, 1950. **80**(4): p. 580-594.
115. Stejskal, E.O., et al., *Spin diffusion measurements : Spin echoes in the presence of time-dependent field gradient.* The Journal of Chemical Physics, 1965. **42**: p. 288-292.
116. Colsenet, R., *Etude par RMN de la diffusion moléculaire : influence de la structure des protéines laitières à l'état liquide et gélifié*. 2005, Nantes. p. 237.
117. Tanner, J.E., *Use of stimulated Echo in NMR Diffusion studies.* The Journal of Chemical Physics, 1970. **52(5)**: p. 2523-2526.
118. Price, W.S., *Pulsed-field gradient nuclear magnetic resonance as a tool for studying translational diffusion : Part II. Experimental aspects.* Concepts in Magnetic Resonance, 1998. **10**: p. 197-237.
119. Tillet, M.L., et al., *Practical aspects of the measurement of the diffusion of proteins in aqueous solution.* Journal of Magnetic Resonance, 1998. **133**: p. 379-384.
120. Price, W.S., et al., *Macroscopic background gradient and radiation damping effects on high-field PGSE NMR diffusion measurements.* Journal of Magnetic Resonance, 2001. **150**(1): p. 49-56.
121. Sun, P.Z., et al., *Background gradient suppression in pulsed gradient stimulated echo measurements.* Journal of Magnetic Resonance, 2003. **161**(2): p. 168-173.
122. Antalek, B., *Using pulsed gradient spin echo NMR for chemical mixture analysis: How to obtain optimum results.* Concepts in Magnetic Resonance, 2002. **14**(4): p. 225-258.
123. Wu, D.H., et al., *An improved diffusion-ordered spectroscopy experiment incorporating bipolar-gradient pulses.* Journal of Magnetic Resonance Series A, 1995. **115**(2): p. 260-264.
124. Galvosas, P., et al., *Background gradient suppression in stimulated echo NMR diffusion studies using magic pulsed field gradient ratios.* Journal of Magnetic Resonance, 2004. **166**(2): p. 164-173.
125. Zhang, X., et al., *Determination of molecular self-diffusion coefficient using multiple spin-echo NMR spectroscopy with removal of convection and background gradient artifacts.* Analytical Chemistry, 2001. **73**(15): p. 3528-3534.
126. Topgaard, D., et al., *Restricted self-diffusion of water in a highly concentrated W/O emulsion studied using modulated gradient spin-echo NMR.* Journal of Magnetic Resonance, 2002. **156**(2): p. 195-201.
127. Momot, K.I., et al., *Convection-compensating PGSE experiment incorporating excitation-sculpting water suppression (CONVEX).* Journal of Magnetic Resonance, 2004. **169**(1): p. 92-101.
128. Van Den Enden, J.C., et al., *Rapid determination of water droplet size distributions by PFG-NMR.* Journal of Colloid and Interface Science, 1990. **140**: p. 105-113.
129. Van Dusschoten, D.V., et al., *Flexible PFG NMR Desensitized for Susceptibility Artifacts, Using the PFG Multiple-Spin-Echo Sequence.* Journal of Magnetic Resonance Series a, 1994. **112**: p. 237-240.

130. Momot, K.I., et al., *PFG NMR diffusion experiments for complex systems.* Concepts in Magnetic Resonance Part A, 2006. **28A**(4): p. 249-269.
131. Cotts, R.M., et al., *Pulsed field gradients stimulated echo methods for improved NMR diffusion measurements in heterogeneous systems.* Journal of Magnetic Resonance, 1988. **83**: p. 252-266.
132. Altieri, A.S., et al., *Association of biomolecular systems via pulsed-field gradient nmr self-diffusion measurements.* Journal of the American Chemical Society, 1995. **117**(28): p. 7566-7567.
133. Ortner, K., et al., *Analysis of glycans in glycoproteins by diffusion-ordered nuclear magnetic resonance spectroscopy.* Analytical and Bioanalytical Chemistry, 2007. **388**(1): p. 173-177.
134. Simorellis, A.K., et al., *A PFG NMR experiment for translational diffusion measurements in low-viscosity solvents containing multiple resonances.* Journal of Magnetic Resonance, 2004. **170**(2): p. 322-328.
135. Flynn, P.F., *Multidimensional multinuclear solution NMR studies of encapsulated macromolecules.* Progress in Nuclear Magnetic Resonance Spectroscopy, 2004. **45**(1-2): p. 31-51.
136. Price, W.S., et al., *PGSE-WATERGATE, a new tool for NMR diffusion-based studies of ligand-macromolecule binding.* Magnetic Resonance in Chemistry, 2002. **40**(6): p. 391-395.
137. Nesmelova, I.V., et al., *Measuring protein self-diffusion in protein-protein mixtures using a pulsed gradient spin-echo technique with WATERGATE and isotope filtering.* Journal of Magnetic Resonance, 2004. **166**(1): p. 129-133.
138. Piotto, M., et al., *Gradient-tailored excitation for single-quantum nmr-spectroscopy of aqueous-solutions.* Journal of Biomolecular Nmr, 1992. **2**(6): p. 661-665.
139. Zheng, G., et al., *Simultaneous convection compensation and solvent suppression in biomolecular NMR diffusion experiments.* Journal of Biomolecular Nmr, 2009. **45**(3): p. 295-299.
140. Dingley, A.J., et al., *Measuring macromolecular diffusion using heteronuclear multiple-quantum pulsed-field-gradient NMR.* Journal of Biomolecular Nmr, 1997. **10**(1): p. 1-8.
141. Luo, R.S., et al., *Eliminating systematic error in multiple quantum diffusion measurements by bipolar gradient pulses.* Measurement Science & Technology, 1998. **9**(8): p. 1347-1350.
142. Dixon, A.M., et al., *NMR spectroscopy with spectral editing for the analysis of complex mixtures.* Applied Spectroscopy, 1999. **53**(11): p. 426A-440A.
143. Otto, W.H., et al., *Improved spin-echo-edited NMR diffusion measurements.* Journal of Magnetic Resonance, 2001. **153**(2): p. 273-276.
144. Hwang, T.L., et al., *Water suppression that works - excitation sculpting using arbitrary wave-forms and pulsed-field gradients.* Journal of Magnetic Resonance Series A, 1995. **112**(2): p. 275-279.
145. Stott, K., et al., *Excitation sculpting in high-resolution nuclear-magnetic-resonance spectroscopy - Application to selective noe experiments.* Journal of the American Chemical Society, 1995. **117**(14): p. 4199-4200.
146. Loening, N.M., et al., *One-dimensional DOSY.* Journal of Magnetic Resonance, 2001. **153**(1): p. 103-112.

147. Buckley, C., et al., *Applications of fast diffusion measurement using Difftrain.* Journal of Magnetic Resonance, 2003. **161**(1): p. 112-117.
148. Thrippleton, M.J., et al., *A fast method for the measurement of diffusion coefficients: one-dimensional DOSY.* Magnetic Resonance in Chemistry, 2003. **41**(6): p. 441-447.
149. Van Lent, K., et al., *Determination of water droplet size distribution in butter: Pulsed field gradient NMR in comparison with confocal scanning laser microscopy.* International Dairy Journal, 2008. **18**(1): p. 12-22.
150. Guillermo, A., et al., *In situ pulsed-field gradient NMR determination of the size of oil bodies in vegetable seeds. Analysis of the effect of the gradient pulse length.* Analytical Chemistry, 2007. **79**(17): p. 6718-6726.
151. Balinov, B., et al., *Determination of water droplet size in margarines and low-calorie spreads by nuclear magnetic resonance self-diffusion.* Journal of the American Oil Chemists' Society, 1994. **71**(5): p. 513-518.
152. Li, X., et al., *Determination of emulsion size distribution by NMR restricted diffusion measurement.* AICHE Journal, 1992. **38**(10): p. 1671-1674.
153. Ek, R., et al., *Pore characterization in cellulose beads from diffusion studies using the spin-echo Nmr technique.* Powder Technology, 1994. **81**(3): p. 279-286.
154. Nitta, K., et al., *Measurements of self-diffusion coefficients of water in porous membranes by PFG-NMR.* Desalination, 1999. **123**(1): p. 9-14.
155. Stallmach, F., et al., *The potentials of pulsed field gradient NMR for investigation of porous media.* Adsorption-Journal of the International Adsorption Society, 1999. **5**(2): p. 117-133.
156. Kimmich, R., et al., *Self-diffusion in fluids in porous glass: Confinement by pores and liquid adsorption layers.* Magnetic Resonance Imaging, 1996. **14**(7-8): p. 793-797.
157. Topgaard, D., et al., *Diffusion of water absorbed in cellulose fibers studied with H1-NMR.* Langmuir, 2001. **17**(9): p. 2694-2702.
158. Topgaard, D., et al., *Self-diffusion in two- and three-dimensional powders of anisotropic domains: An NMR study of the diffusion of water in cellulose and starch.* The Journal of Physical Chemistry B, 2002. **106**(46): p. 11887-11892.
159. Nyden, M., et al., *An NMR self-diffusion investigation of aggregation phenomena in solutions of ethyl(hydroxyethyl)cellulose.* Macromolecules, 1998. **31**(15): p. 4990-5002.
160. Nyden, M., et al., *A PFG NMR self-diffusion investigation of probe diffusion in an ethyl(hydroxyethyl)cellulose matrix.* Macromolecules, 1999. **32**(1): p. 127-135.
161. Rosen, O., et al., *Anomalous surfactant diffusion in a gel of chemically cross-linked ethyl(hydroxyethyl) cellulose.* The Journal of Physical Chemistry B, 2003. **107**(17): p. 4074-4079.
162. Métais, A., *Caractérisation des coefficients d'auto-diffusion de l'eau par RMN dans les gels laitiers en relation avec leur composition et leur structure*. 2003, ENSAR. p. 225.
163. Hakansson, B., et al., *The influence of polymer molecular-weight distributions on pulsed field gradient nuclear magnetic resonance self-diffusion experiments.* Colloid and Polymer Science, 2000. **278**(5): p. 399-405.
164. Callaghan, P.T., et al., *A pulsed field gradient NMR study of self-diffusion in a polydisperse polymer system: dextran in water.* Macromolecules, 1983. **16**(6): p. 968-973.
165. Carrero, G., et al., *Using FRAP and mathematical modeling to determine the in vivo kinetics of nuclear proteins.* Methods, 2003. **29**(1): p. 14-28.

166. Axelrod, D., et al., *Mobility measurement by analysis of fluorescence photobleaching recovery kinetics.* Biophysical Journal, 1976. **16**(9): p. 1055-1069.
167. Karbowiak, T., et al., *Effect of plasticizers (water and glycerol) on the diffusion of a small molecule in Iota-Carrageenan biopolymer films for edible coating application.* Biomacromolecules, 2006. **7**(6): p. 2011-2019.
168. Ishihara, A., et al., *A closer look at how membrane-proteins move.* Biophysical Journal, 1993. **65**(5): p. 1754-1755.
169. Seksek, O., et al., *Translational diffusion of macromolecule-sized solutes in cytoplasm and nucleus.* Journal of Cell Biology, 1997. **138**(1): p. 131-142.
170. Umenishi, F., et al., *cAMP regulated membrane diffusion of a green fluorescent protein-aquaporin 2 chimera.* Biophysical Journal, 2000. **78**(2): p. 1024-1035.
171. Chary, S.R., et al., *Direct measurement of interstitial convection and diffusion of albumin in normal and neoplastic tissues by fluorescence photobleaching.* Proceedings of the National Academy of Sciences of the United States of America, 1989. **86**(14): p. 5385-5389.
172. Ramanujan, S., et al., *Diffusion and convection in collagen gels: Implications for transport in the tumor interstitium.* Biophysical Journal, 2002. **83**(3): p. 1650-1660.
173. Saltzman, W.M., et al., *Antibody diffusion in human cervical-mucus.* Biophysical Journal, 1994. **66**(2): p. 508-515.
174. Sanders, N.N., et al., *The physical properties of biogels and their permeability for macromolecular drugs and colloidal drug carriers.* Journal of Pharmaceutical Sciences, 2000. **89**(7): p. 835-849.
175. Olmsted, S.S., et al., *Diffusion of macromolecules and virus-like particles in human cervical mucus.* Biophysical Journal, 2001. **81**(4): p. 1930-1937.
176. Cheng, Y., et al., *Diffusion of mesoscopic probes in aqueous polymer solutions measured by fluorescence recovery after photobleaching.* Macromolecules, 2002. **35**(21): p. 8111-8121.
177. Pajevic, S., et al., *Diffusion of linear polymer-chains in methyl-methacrylate gels.* Macromolecules, 1993. **26**(2): p. 305-312.
178. Seiffert, S., et al., *Diffusion of linear macromolecules and spherical particles in semidilute polymer solutions and polymer networks.* Polymer, 2008. **49**(19): p. 4115-4126.
179. Pluen, A., et al., *Diffusion of macromolecules in agarose gels: Comparison of linear and globular configurations.* Biophysical Journal, 1999. **77**(1): p. 542-552.
180. Perry, P.A., et al., *Fluorescence recovery after photobleaching as a probe of diffusion in starch systems.* Biomacromolecules, 2006. **7**(2): p. 521-530.
181. Carvajal-Rondanelli, et al., *Diffusion of active proteins into fish meat to minimize proteolytic degradation.* Journal of Agricultural and Food Chemistry, 2010. **58**(9): p. 5300-5307.
182. Balakrishnan, G., et al., *Particle diffusion in globular protein gels in relation to the gel structure.* Biomacromolecules, 2011. **12**(2): p. 450-456.
183. Floury, J., et al., *First assessment of diffusion coefficients in model cheese by fluorescence recovery after photobleaching (FRAP).* Food Chemistry, 2012. **133**(2): p. 551-556.
184. Meyvis, T.K.L., et al., *Fluorescence recovery after photobleaching: A versatile tool for mobility and interaction measurements in pharmaceutical research.* Pharmaceutical Research, 1999. **16**(8): p. 1153-1162.

185. Moschakis, T., et al., *Particle tracking using confocal microscopy to probe the microrheology in a phase-separating emulsion containing nonadsorbing polysaccharide.* Langmuir, 2006. **22**(10): p. 4710-4719.
186. Cucheval, A.S.B., et al., *Multiple particle tracking investigations of acid milk gels using tracer particles with designed surface chemistries and comparison with diffusing wave spectroscopy studies.* Langmuir, 2009. **25**(19): p. 11827-11834.
187. Levitt, M.H., *Spin Dynamics: Basics of Nuclear Magnetic Resonance*. 2008, John Wiley & Sons: New York
188. Bloch, F., *Nuclear Induction.* Physical Review, 1946. **70**: p. 460-473
189. Abragam, A., *The Principles of Nuclear Magnetism*. 1961, Clarendon Press, London: Oxford.
190. Bloembergen, N., et al., *Relaxation Effects in Nuclear Magnetic Resonance Absorption.* Physical Review, 1948. **73**(7): p. 679.
191. Claridge, T.D.W., *High resolution NMR techniques in Organic Chemistry*, edited by J.E. Balwin, F.R.S. and R.M. Williams (Oxford, UK, 1999), Vol. 19.
192. Carr, H.Y., et al., *Effects of Diffusion on Free Precession in Nuclear Magnetic Resonance experiments.* Physical Review, 1954. **94**(3): p. 630-638.
193. Meiboom, S., et al., *Modified Spin-Echo Method for Measuring Nuclear Relaxation Times.* Review of Scientific Instruments, 1958. **29(8)**: p. 688-691.
194. Harris, K.R., *Nuclear Magnetic resonance Spectroscopy*. 1986, Longman: Harlow.
195. Armando, A.-C., *Beyond excitation NMR relaxation.* Concepts in magnetic resonance part A, 2008. **32A**(3): p. 168-182.
196. Hinrichs, R., et al., *Characterisation of different treated whey protein concentrates by means of low-resolution nuclear magnetic resonance.* International Dairy Journal, 2004. **14**(9): p. 817-827.
197. Famelart, M.H., et al., *Acidification of pressure-treated milk.* International Dairy Journal, 1997. **7**(5): p. 325-330.
198. Roefs, S.P.F.M., et al., *Pulse NMR of Casein Dispersions.* Journal of Food Science, 1989. **54**: p. 704-708.
199. Mariette, F., et al., *NMR relaxation studies of dairy processes.* Journal of Magnetic Resonance Analysis, 1996. **2**(4): p. 290-296.
200. Davenel, A., et al., *NMR relaxometry as a non-invasive tool to characterize milk powders.* Lait, 2002. **82**(4): p. 465-473.
201. Budiman, M., et al., *Moisture measurement in cheese analogue using stretched and multi-exponential models of the magnetic resonance T-2 relaxation curve.* Journal of Dairy Research, 2002. **69**(4): p. 619-632.
202. Gianferri, R., et al., *A low-resolution and high-resolution nuclear magnetic resonance integrated approach to investigate the physical structure and metabolic profile of Mozzarella di Bufala Campana cheese.* International Dairy Journal, 2007. **17**(2): p. 167-176.
203. Gianferri, R., et al., *Proton NMR transverse relaxation measurements to study water dynamic states and age-related changes in Mozzarella di Bufala Campana cheese.* Food Chemistry, 2007. **105**(2): p. 720-726.
204. Atha, D.H., et al., *Mechanism of precipitation of proteins by polyethylene glycols-Analysis in terms of excluded volume.* Journal of Biological Chemistry, 1981. **256**(23): p. 2108-2117.

205. Bhat, R., et al., Timasheff, *Steric exclusion is the principal source of the preferential hydration of proteins in the presence of polyethylene glycols.* Protein Science : A Publication of the Protein Society, 1992. **1**(9): p. 1133-1143.
206. Hancock, T.J., et al., *Thermal stability studies of a globular protein in aqueous poly(ethylene glycol) by H-1 NMR.* Biotechnology & Bioengineering, 1996. **51**(4): p. 410-421.
207. Hermans, J., *Excluded-volume theory of polymer-protein interactions based on polymer chain statistics.* Journal of Chemical Physics, 1982. **77**(4): p. 2193-2203.
208. Knoll, D., et al., *Polymer-protein interactions - Comparison of experiment and excluded volume theory.* Journal of Biological Chemistry, 1983. **258**(9): p. 5710-5715.
209. Brown, W., et al., *Self-Diffusion of Poly(Ethylene Oxide) in Aqueous Dextran Solutions Measured Using Ft-Pulsed Field Gradient Nmr.* Polymer, 1983. **24**(2): p. 188-192.
210. Masaro, L., et al., *Self-diffusion of oligo- and poly(ethylene glycol)s in poly(vinyl alcohol) aqueous solutions as studied by pulsed-gradient NMR spectroscopy.* Macromolecules, 1998. **31**(12): p. 3880-3885.
211. Masaro, L., et al., *Study of the self-diffusion of poly(ethylene glycol)s in poly(vinyl alcohol) aqueous systems.* Journal of Polymer Science Part B-Polymer Physics, 1999. **37**(17): p. 2396-2403.
212. Walderhaug, H., et al., *Diffusion of poly(ethylene oxide) chains in gelling and nongelling aqueous mixtures of ethyl(hydroxyethyl)cellulose and a surfactant by pulsed field gradient NMR.* Journal of Physical Chemistry B, 1997. **101**(44): p. 8892-8897.
213. Walderhaug, H., et al., *A pulsed field gradient NMR study of poly(oxyethylene) diffusion in aqueous solutions and gels of ethyl (hydroxyethyl) cellulose-sodium dodecyl sulphate systems.* Colloids and Surfaces a-Physicochemical and Engineering Aspects, 1999. **149**(1-3): p. 379-387.
214. Jo, B.W., et al., *Self-diffusion of poly (ethylene oxide) - modified paclitaxel in dilute aqueous solutions.* Materials Research Innovations, 2003. **7**(3): p. 178-182.
215. Petit, J.M., et al., *Solute probe diffusion in aqueous solutions of poly(vinyl alcohol) as studied by pulsed-gradient spin-echo NMR spectroscopy.* Macromolecules, 1996. **29**(1): p. 70-76.
216. Griffiths, P.C., et al., *Role of Molecular Architecture in Polymer Diffusion - a Pgse-Nmr Study of Linear and Cyclic Poly(Ethylene Oxide).* Journal of Physical Chemistry, 1995. **99**(45): p. 16752-16756.
217. Favre, E., et al., *Diffusion of polyethyleneglycols in calcium alginate hydrogels.* Colloids and Surfaces a-Physicochemical and Engineering Aspects, 2001. **194**(1-3): p. 197-206.
218. Skirda, V.D., et al., *Investigation of translational motion of poly(ethylene glycol) macromolecules in poly(methacrylic acid) hydrogels.* Macromolecular Chemistry and Physics, 1999. **200**(9): p. 2152-2159.
219. Kwak, S., et al., *Self-diffusion of macromolecules and macroassemblies in curdlan gels as examined by PFG-SE NMR technique.* Colloids and Surfaces a-Physicochemical and Engineering Aspects, 2003. **221**(1-3): p. 231-242.
220. Matsukawa, S., et al., *Study of self-diffusion of molecules in a polymer gel by pulsed-gradient spin-echo H-1 NMR. 2. Intermolecular hydrogen-bond interaction between the probe polymer and network polymer in N,N-Dimethylacrylamide-acrylic acid copolymer gel systems.* Macromolecules, 1997. **30**(26): p. 8310-8313.

221. Johansson, L., et al., *Diffusion and interaction in gels and solutions. 2. Experimental results on the obstruction effect.* Macromolecules, 1991. **24**(22): p. 6019-6023.
222. Colsenet, R., et al., *Pulsed Field Gradient NMR Study of Poly(ethylene glycol) Diffusion in Whey Protein Solutions and Gels.* Macromolecules, 2006. **39**(3): p. 1053-1059.
223. Walther, B., et al., *Influence of kappa-Carrageenan Gel Structures on the Diffusion of Probe Molecules Determined by Transmission Electron Microscopy and NMR Diffusometry.* Langmuir, 2006. **22**(19): p. 8221-8228.
224. Trampel, R., et al., *Self-diffusion of polymers in cartilage as studied by pulsed field gradient NMR.* Biophysical Chemistry, 2002. **97**(2-3): p. 251-260.
225. Newling, B., et al., *Pulsed field gradient NMR study of the diffusion of H2O and polyethylene Glycol polymers in the supramolecular structure of wet cotton.* The Journal of Physical Chemistry B, 2003. **107**(45): p. 12391-12397.
226. Lafitte, G., et al., *PFG-NMR diffusometry: A tool for investigating the structure and dynamics of noncommercial purified pig gastric mucin in a wide range of concentrations.* Biopolymers, 2007. **86**(2): p. 165-175.
227. Weng, L.H., et al., *Transport of Glucose and Poly(ethylene glycol)s in Agarose Gels Studied by the Refractive Index Method.* Macromolecules, 2005. **38**(12): p. 5236-5242.
228. Baldursdottir, S.G., et al., *The effect of riboflavin-photoinduced degradation of alginate matrices on the diffusion of poly(oxyethylene) probes in the polymer network.* European polymer journal, 2006. **42**(11): p. 3050-3058.
229. Johansson, L., et al., *Diffusion and interaction in gels and solutions. 3. Theoretical results on the obstruction effect.* Macromolecules, 1991. **24**(22): p. 6024-6029.
230. Colsenet, R., et al., *Effect of casein concentration in suspensions and gels on poly(ethylene glycol)s NMR self-diffusion measurements.* Macromolecules, 2005. **38**(22): p. 9171-9179.
231. Mariette, F., et al., *^{1}H NMR diffusometry study of water in casein dispersions and gels.* Journal of Agricultural and Food Chemistry, 2002. **50**(15): p. 4295-4302.
232. Le Feunteun, S., et al., *The rennet coagulation mechanisms of a concentrated casein suspension as observed by PFG-NMR diffusion measurements.* Food Hydrocolloids, 2012. **27**(2): p. 456-463.
233. Tan, H.L., et al., *The microstructural and rheological properties of Na-caseinate dispersions.* Journal of Colloid and Interface Science, 2010. **342**(2): p. 399-406.
234. Brosseau, C., et al., *NMR observation of poly(ethylene oxide) dynamics in a poly(methyl methacrylate) matrix: effect of chain length variation.* Macromolecules, 1992. **25**(18): p. 4535-4540.
235. Guillermo, A. et al., *Quantitative nuclear magnetic resonance characterization of long-range chain dynamics: Polybutadiene, polyethylene-oxide solution.* Journal of Chemical Physics, 2002. **116**(7): p. 3141-3151.
236. Cohen-Addad, J.P. et al., *Nuclear magnetic resonance investigations into long range chain fluctuations in molten poly(ethylene-oxide).* Journal of Chemical Physics, 1999. **111**(15): p. 7131-7138.
237. Brereton, M.G., et al., *Nature of the proton NMR transverse relaxation function of polyethylene melts. 1. Monodispersed polyethylenes.* Macromolecules, 1991. **24**(8): p. 2068-2074.
238. Masaro, L., et al., *Physical models of diffusion for polymer solutions, gels and solids.* Progress in Polymer Science, 1999. **24**(5): p. 731-775.

239. Muhr, A.H., et al., *Diffusion in gels.* Polymer, 1982. **23**: p. 1012-1026.
240. Mackie, J.S., et al., *The diffusion of electrolytes in a cation-exchange resin membrane.I. Theoritical. Proceedings of the royal society of London.* 1955. **Series A 232**: p. 498.
241. Amsden, B., *Solute diffusion in hydrogels. An examination of the retardation effect.* Polymer Gels and Networks, 1998. **6**(1): p. 13-43.
242. Phillies, G.D.J., *Universal Scaling Equation for Self-Diffusion by Macromolecules in Solution.* Macromolecules, 1986. **19**: p. 2367-2376.
243. Phillies, G.D.J., *Dynamics of Polymers in Concentrated Solutions: The Universal Scaling Equation Derived.* Macromolecules, 1987. **20**: p. 558-564.
244. Jonnsson, B., et al., *Self-diffusion of small molecules in colloidal systems.* Colloid & Polymer Science, 1986. **264**(1): p. 77-88.
245. Babu, S., et al., *Tracer Diffusion in Colloidal Gels.* The Journal of Physical Chemistry B, 2008. **112**(3): p. 743-748.
246. De Gennes, P.G., *Reptation of a polymer chanin in the presence of fixed obstacles.* The journal of chemical physics, 1971. **55**(2): p. 572 -579.
247. De Gennes, P.G., *Brownian motions of flexible poymer chains.* Nature, 1979. **282**: p. 367 - 370.
248. Tomalia, D.A., *Birth of a new macromolecular architecture: dendrimers as quantized building blocks for nanoscale synthetic polymer chemistry.* Progress in Polymer Science, 2005. **30**(3-4): p. 294-324.
249. Lee, C.C., et al., *Designing dendrimers for biological applications.* Nature Biotechnology, 2005. **23**(12): p. 1517-1526.
250. Loren, N., et al., *Dendrimer Diffusion in kappa-Carrageenan Gel Structures.* Biomacromolecules, 2009. **10**(2): p. 275-284.
251. Bernin, D., et al., *Microstructure of polymer hydrogels studied by pulsed field gradient NMR diffusion and TEM methods.* Soft Matter, 2011. **7**(12): p. 5711-5716.
252. Baille, W.E., et al., *Self-Diffusion of Hydrophilic Poly(propyleneimine) Dendrimers in Poly(vinyl alcohol) Solutions and Gels by Pulsed Field Gradient NMR Spectroscopy.* Macromolecules, 2003. **36**(3): p. 839-847.

Chapter II

Materials and Methods

1. Solutions et gels étudiés

1.1. Poudres de caséines et sondes utilisées

Deux poudres de caséines différentes ont été utilisées dans cette étude : (i) Une poudre de phosphocaséinate natif (PPCN), fournie par le laboratoire STLO (Laboratoires de Recherches en Sciences et Technologie du lait et des Ovoproduits) de l'INRA de Rennes (ii) une poudre de Caséinate de Sodium (CaNa) fournie par Armor protéines (Saint-Brice en Coglès, France). La composition chimique de ces deux poudres figure dans le **Tableau 1**.

	Matière sèche (g/Kg)	Azote total (g/Kg)	Azote non caséinique (g/Kg)	Azote non protéique (g/Kg)	Caséines pures (g/Kg)
PPCN (%)	100	88,20	6,90	0,20	81,30
CaNa (%)	100	95,20	0,84	0,17	94,36

Tableau 1. Composition chimique de la poudre PPCN et CaNa en gramme par gramme de matière sèche

Les polymères de polyéthylène glycol (PEG) ou polyéthylèneoxyde (PEO) ont été obtenus de Varian Laboratories (Massy, France), avec différents poids moléculaires (M_w = 615, 7920 et 21300 g/mol pour les PEGs et M_w = 32530 et 93000 g/mol pour les PEOs) et des faibles indices de polydispersité (respectivement M_w/M_n = 1,07 ; 1,04 ; 1,06 ; 1,06 et 1,06) indiqués par le fournisseur. Les dendrimères polyamidoamine composés d'un noyau d'éthylène diamine et d'une surface couverte de chaines de polyéthylèneglycol ont été obtenus de Dendritic Nanotechnologies, Inc. (USA). Quatre générations (G2 (DNT-315), G3 (DNT-316), G5 (DNT-318) et G6 (DNT-319)) ont été utilisées dans cette étude. Des conditions spéciales de stockage ont été dédiées aux polymères de polyéthylèneoxyde et aux dendrimères qui ont été conservés, respectivement, à 4°C et à -20°C.

1.2. Préparation des solutions

Toutes les solutions ont été préparées à l'aide d'une solution saline contenant de l'eau ultrapure et 0,1 M de NaCl. De l'azidure de sodium (NaN_3, 0,02% w/w) a été ajouté comme agent bactériostatique.

La poudre de caséines a été dispersée dans la solution saline par agitation magnétique pendant 36h à température ambiante pour la poudre de PPCN et pendant 24h à 45°C quand la concentration en caséine était supérieure à 20 g/100 g H_2O. La poudre de CaNa a été réhydratée pendant 24h à 45°C pour toutes les concentrations. Ces solutions ont été analysées sans ajustement de pH. La teneur en extrait sec de chaque solution est contrôlée par séchage de trois coupelles, contenant quelque mL de chaque échantillon, dans une étuve à 103°C pendant 24 heures. Les concentrations en protéines sont alors calculées avec le pourcentage de protéines pures de chaque poudre.

Après hydratation des dispersions de caséines, 0,1% (w/w) de chaque PEG y a été ajoutée. Le méthanol, dans lequel les dendrimères ont été dissous, a été évaporé à sec sous flux d'azote. Ensuite, les dendrimères ont été dispersés dans une quantité appropriée d'eau saline (H_2O + 0,1 M NaCl) et ajoutés aux dispersions de caséines de façon à obtenir une concentration finale de 0,1% (w/w) en dendrimères.

1.3. Coagulation des solutions protéiques

- Les gels présure ont été réalisés en ajoutant de la chymosine Chymax-Plus (Chr Hansen, Arpajon, France). Tous les gels présure avaient une concentration égale à 15 g/100g H_2O. Ces gels ont été réalisés à 30°C pendant 2h30min par ajout de 4 µL de chy-max à 10 g de la suspension concentrée. Toutefois, ces gels étaient formés trop rapidement pour permettre de suivre la diffusion des PEGs pendant la coagulation. Aussi, afin de pouvoir réaliser des suivis cinétiques par PFG-NMR, les coagulations présure ont été ralenties. Pour cela, la température a été réduite à 20°C ainsi que la quantité d'enzyme ajoutée à 10 g de la suspension concentrée. Cette dernière était égale à 70 µl prélevée à partir d'une solution mère diluée au 1/100ème. Les études en cinétique étaient quant à elles réalisées sur des périodes d'environ 23 h. En parallèle des mesures RMN, les processus de coagulation ont été caractérisés par rhéométrie avec les mêmes conditions de coagulation.

- Tous les gels acides de CaNa ont été obtenus par ajout de Glucono-Delta-Lactone (GDL) de manière à ce que les gels aient un pH final d'environ 4.6. Les gels étudiés avaient des concentrations égales à 7,23 9,73 et 15,3 g/100g H_2O et sont obtenus par ajout de 88, 118 et 176 mg de GDL, respectivement, à 10g de chaque suspension. Après ajout du GDL, les

solutions ont été agitées pendant 5 minutes à l'aide d'un agitateur magnétique. Ensuite, une petite quantité a été transférée dans un tube RMN. Les données de diffusion ont été confrontées aux structures de ces gels par l'intermédiaire d'images de MEB.

Les gels ont été analysés par RMN le lendemain de l'ajout des agents gélifiants pour les gels présure, et le surlendemain pour les gels acides. Aucune synérèse n'a été constatée sur la durée de ces expériences.

2. Méthodes de mesure RMN

Les mesures RMN ont été effectuées sur un spectromètre Bruker 500 MHz équipé d'une sonde à gradient de champ pulsé Diff-30. Toutes les mesures ont été réalisées à 20°C. Le tube référence Bruker de méthanol (4% MeOH dans MeOD) a été utilisé pour calibrer la température à 20°C qui a été déterminée à partir de l'écart entre les déplacements chimiques des pics du OH et du CH_3 du méthanol.

2.1. Mesures du coefficient de diffusion

Les coefficients de diffusion ont été déterminés avec la séquence STE-BPP qui intègre un schéma WATERGATE 3-9-19 et qui a été présenté dans le paragraphe **2.2.2.4** du ***chapitre I***. Le coefficient de diffusion est donné par la relation suivante:

$$\frac{I(\delta,\Delta,g)}{I_0} = \sum_i p_i \exp\left[-\gamma^2 g^2 \delta^2 \left(\Delta - \frac{\delta}{3} - \frac{\tau}{4}\right) D_i\right] \qquad \textbf{(1)}$$

La **Figure 1** présente un spectre RMN obtenu durant une mesure de diffusion. Il résulte d'une suspension de caséine concentrée qui contient 0,1% (w/w) d'un PEG et 12 g/100 g H_2O de caséine. Notons que le signal qui a été mesuré dans le cas de dendrimères est le signal du PEG qui apparaissait à 3,6 ppm.

Les résultats de diffusion obtenus pour :

- La sonde (PEG et dendrimère) ont été acquis en utilisant 16 ou 32 valeurs de gradients allant de 20 à 1200 G/cm et en variant la durée d'impulsion de gradient entre 1 et 2 ms. Selon le poids moléculaire de la sonde, l'intervalle de diffusion Δ était ajusté de manière à sonder une

distance proche de 1.5 µm, en accord avec l'équation d'Einstein $z = (2.D.\Delta)^{1/2}$. Les coefficients de diffusion des sondes dans les suspensions et gels présure de caséine ont été calculés en ajustant l'équation 1, avec i=1, aux données brutes de RMN.

- Les caséines ont été acquis en variant l'intégrale des pics entre 0,4 et 2,3 ppm. Seize valeurs de gradients allant de 20 à 1200 G/cm étaient utilisées et la durée d'impulsion de gradient variait entre 1 et 2,2 ms. Les coefficients de diffusion ont été calculés en ajustant l'équation 1 avec i=2. Les deux coefficients de diffusion, D_1 et D_2, obtenus ont été attribués respectivement aux particules de caséine et aux composés solubles.

Seize scans étaient acquis et le délai de recyclage était fixé à cinq T_1. Les fichiers bruts de mesures sont traités avec le logiciel Table Curve.

Notons également que chaque jour d'expériences, le coefficient de diffusion du PEG de 32530 g/mol ($3{,}06.10^{-11}$ m^2s^{-1}) dans du H_2O était mesuré afin de s'assurer de la répétabilité des mesures dans le temps. L'écart type sur ces mesures est d'environ 3% (sur une période d'environ 1 an et demi).

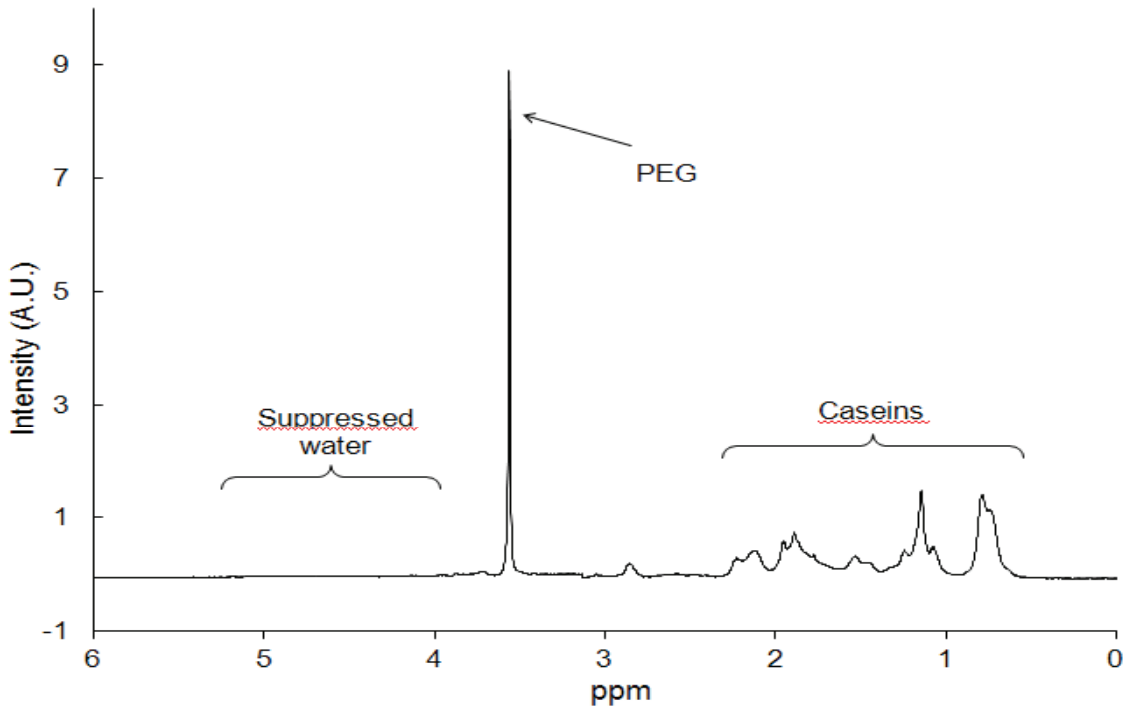

Figure 1. Exemple d'un spectre RMN obtenu durant une mesure d'auto-diffusion.

2.2. Mesure de la relaxation transversale T_2

La séquence d'excitation qui a été utilisée pour la mesure de T_2 est une séquence de Carr-Purcell-Meiboom-Gill (CPMG) (**Figure 2**) couplée avec une séquence de présaturation pour la suppression de l'eau.

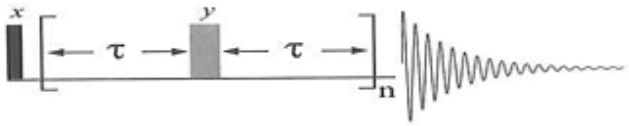

Figure 2. La séquence de Carr-Purcell-Meiboom-Gill (CPMG)

La courbe de décroissance de la relaxation transversale T_2 a été correctement ajustée, pour toutes les sondes, avec la fonction suivante:

$$I(2\tau) = \sum_{i=i}^{i} I_i x \exp\left(-\frac{2\tau}{T_{2i}}\right) \quad \textbf{(2)}$$

Avec $I(2\tau)$ l'intensité du signal RMN donné à τ, T_{2i} le temps de relaxation du composant i et I_i l'intensité du composant i à l'équilibre pour $\tau = 0$. Les mesures de T_2 ont été effectuées avec une valeur de τ égale à 1 ms. Seize valeurs ont été collectées pour chaque CPMG avec seize scans et le délai de recyclage était fixé à 5 T_1. Les temps de relaxation des sondes dans les suspensions et gels présures de caséine ont été calculés en ajustant l'équation 2 avec i=1.

2.3. Effet de l'acide gluconique

Dans les spectres de diffusion des gels acides, il s'est avéré que l'acide gluconique (provenant de l'hydrolyse de la GDL) présentait un signal RMN qui se superposait avec la raie de la sonde à 3,6 ppm comme illustré en **Figure 3**. Ainsi, les données brutes de RMN ont été analysées en utilisant l'équation 1 et 2 avec i = 2.

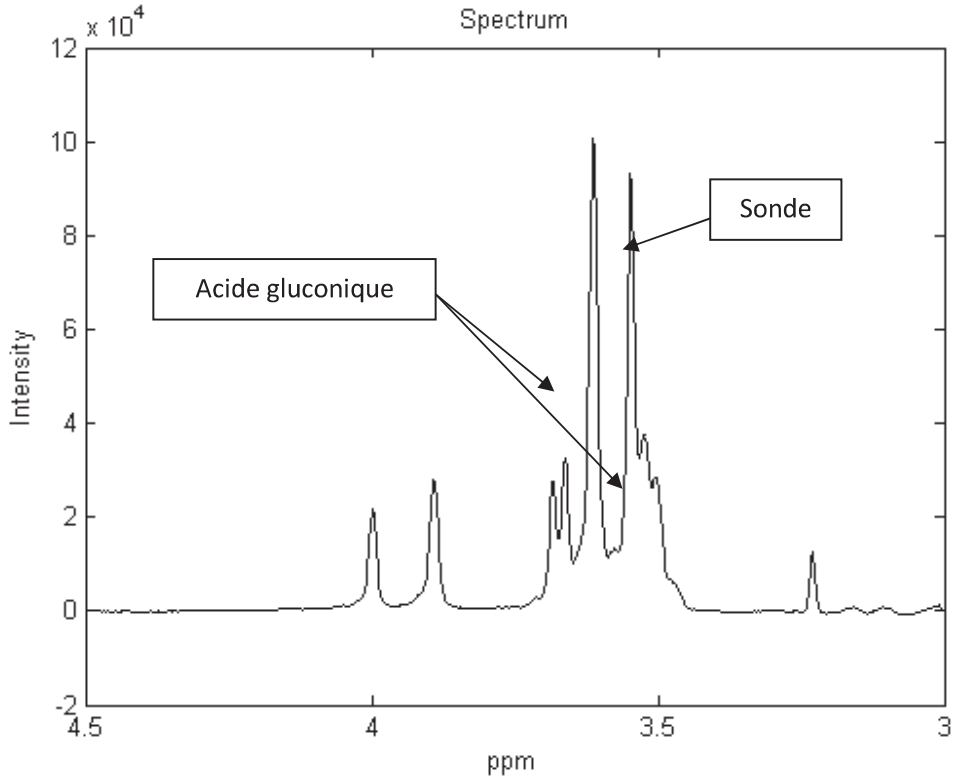

Figure 3. Superposition du signal de la sonde et du signal de l'acide gluconique à 3,6 ppm

D'autre part, Les quantités de GDL ajoutées aux échantillons pour atteindre un pH d'environ 4,6 représentaient entre 0 et 2% de la matière sèche totale de l'échantillon. Aussi, nous avons cherché à déterminer l'influence de ces ajouts sur la diffusion et la relaxation du PEG 32530 g/mol et du dendrimère G6. Comme illustré en **Figure 4** et **Figure 5**, l'effet de ces ajouts sur la diffusion et la relaxation des sondes était négligeable.

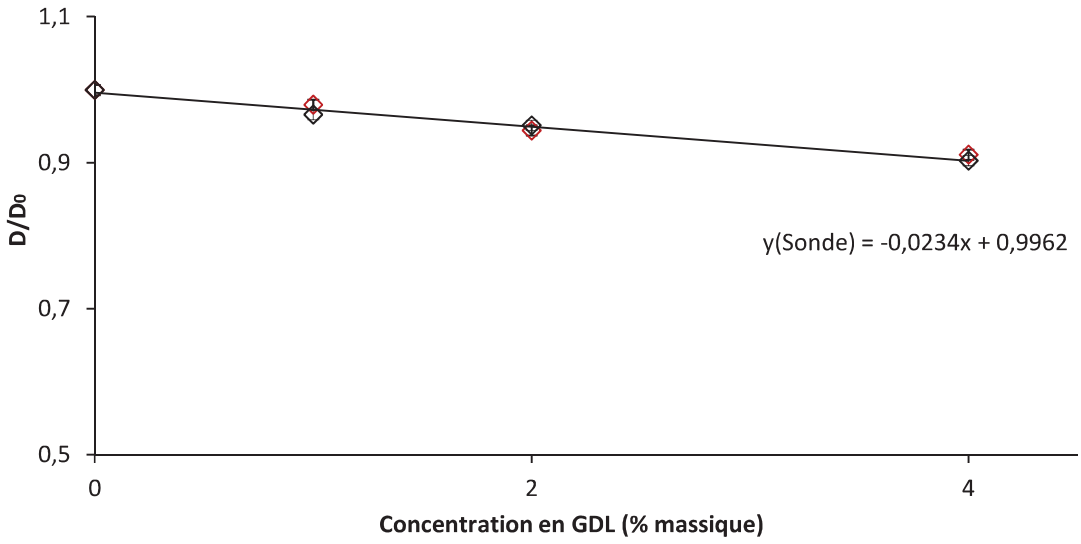

Figure 4. Effet de l'ajout de l'acide gluconique sur la diffusion du PEG 32530 g/mol (rouge) et du dendrimère G6 (noir)

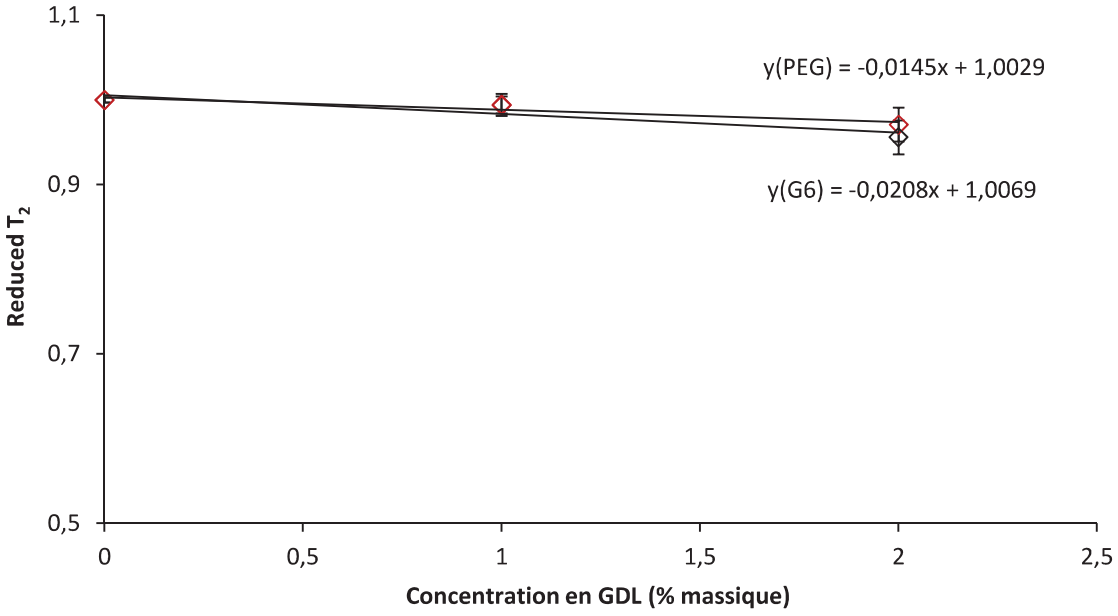

Figure 5. Effet de l'ajout de l'acide gluconique sur la diffusion du PEG 32530 g/mol (rouge) et du dendrimère G6 (noir)

3. La rhéologie

Les propriétés rhéologiques des produits peuvent être caractérisées en régime permanent ou en régime dynamique.

3.1. Régime permanent

Il s'agit d'appliquer un ensemble de forces sur un échantillon. Il en résulte une contrainte de cisaillement τ parallèle à la surface de la couche de produit. La variation de déplacement des couches de matériau les unes sur les autres correspond à la déformation γ. Sa dérivée par rapport au temps $\dot{\gamma}$ est le gradient de vitesse, autrement appelé taux de cisaillement.

La **Figure 6** présente les principaux comportements rhéologiques des fluides tels que :

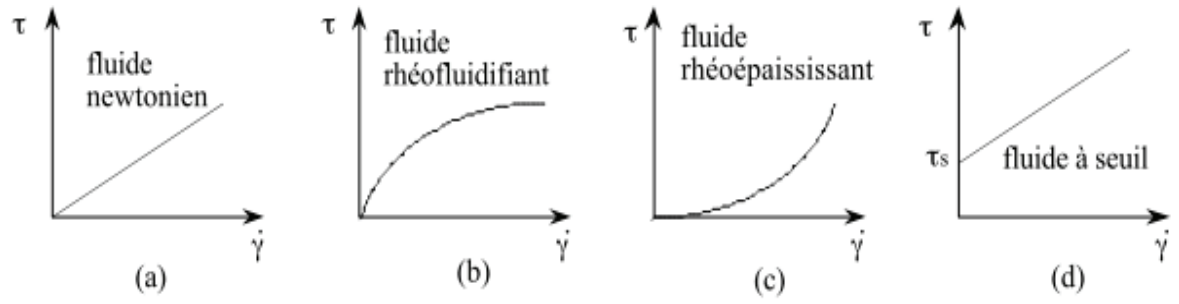

Figure 6. Rhéogrammes caractéristiques des différents comportements

- Un fluide est dit "newtonien" si sa viscosité est constante en fonction du taux de cisaillement.
- Un fluide est dit "rhéofluidifiant" si sa viscosité diminue lorsque le taux de cisaillement augmente.
- Un fluide est dit "rhéoépaississant" si sa viscosité augmente lorsque le taux de cisaillement augmente.
- Un fluide est dit à seuil s'il faut dépasser un seuil en contrainte τ_S avant qu'il ne puisse s'écouler.

3.2. Régime dynamique et viscoélasticité linéaire

On impose, dans le cas d'un rhéomètre à déformation imposée, une déformation sinusoïdale $\gamma(t)$ et on mesure une contrainte sinusoïdale $\tau(t)$ de la forme :

$$\gamma(t) = \gamma_0 \sin(\omega t)$$

$$\tau(t) = \tau_0 \sin(\omega t + \delta)$$

Où ω est la pulsation des oscillations. δ représente le déphasage et est appelé angle de perte. δ est égale à 90° dans le cas d'un liquide purement visqueux ou à 0 pour un solide purement élastique. On peut également imposer, dans le cas d'un rhéomètre à contrainte imposée, une contrainte sinusoïdale et mesurer la déformation sinusoïdale résultante.

On définit les modules de conservation G' et de perte G'', relatifs respectivement à l'élasticité et au caractère dissipatif de l'échantillon, comme étant :

$$G' = \frac{\tau_0}{\gamma_0} \cos\delta$$

$$G'' = \frac{\tau_0}{\gamma_0} \sin\delta$$

On obtient alors :

$$\tan\delta = \frac{G''}{G'}$$

Faire varier la fréquence des oscillations permet d'explorer le comportement mécanique du produit à différents échelles de temps d'observation (inversement proportionnel à ω). On peut ainsi observer des structures avec des temps de relaxation différents. Cette technique est donc particulièrement intéressante pour étudier des phénomènes de gélification et donc de structuration d'un produit.

3.3. Appareils utilisés

3.3.1. TA instruments AR 2000 (Guyancourt, France)

Ce rhéomètre à contrainte imposé a été utilisé pour les expériences en régime permanant avec des géométries cône-plan de 4 cm de diamètre et un angle de 2°. Ils disposent d'un système de régulation de température à effet Peltier. Afin d'éviter l'évaporation du produit lors des expériences, de l'huile de paraffine a été ajoutée sur l'échantillon et maintenue en place grâce à un piège en silicone.

3.3.2. A contrives Low-Shear 30 viscometer (Ruislip, United Kingdom)

Il s'agit d'un rhéomètre fonctionnant à vitesse imposée, avec une géométrie composée de cylindres coaxiaux. Il permet de mesurer des couples de forces faibles et il est donc particulièrement adapté à la mesure de faibles viscosités.

4. La Microscopie Electronique à Balayage (MEB)

Des gels acides de caséinate de sodium à deux concentrations 7,75 et 17 g/100 g H_2O étaient préparées dans des béchers de diamètres 5 cm d'après le protocole défini précédemment. Les gels étaient découpés à l'aide d'un cutter en petits cubes (5 x 5 x 5 mm) et immergés dans du glutaraldéhyde dilué à 2,5 % (v/v) dans une solution tampon phosphate 0,1 M, à pH égal environ à 7, à 4°C pendant 48 heures. Au cours des 48h le fixateur (glutaraldéhyde dilué à 2,5 %) est changé deux fois. Les échantillons étaient ensuite rincés plusieurs fois dans la solution tampon 0,1 M. Enfin, les échantillons étaient déshydratés dans une série de bains d'éthanol/eau à 10, 30, 50, 70, 80, 90, 95 et 100 % d'éthanol (v/v) pendant 20 minutes à chaque étape, avant de finir par un bain d'acétone 100% (v/v).

Les échantillons étaient ensuite apportés au Centre de Microscopie Electronique à Balayage et microAnalyse (CMEBA) de Rennes (France) où ils subissaient un séchage par la méthode du point critique du CO_2 (CPD 010, Balzers Union Ltd, Liechtenstein). Les échantillons, une fois séchés, étaient collés sur des supports métalliques en laiton ou en aluminium avec un adhésif double-face, de la laque d'Argent ou une autre colle pâteuse pouvant sécher rapidement à l'air. Ils sont ensuite métallisés à l'or ou à l'or-palladium par pulvérisation cathodique ou " sputtering ".

Les échantillons étaient alors observés avec un microscope électronique à balayage à effet du champ (Jeol JSM 6301F) opérant à 7 kV.

5. Diffusion dynamique de la lumière

La diffusion dynamique de la lumière (DLS) est une technique d'analyse spectroscopique non destructive permettant d'accéder à la taille de particules en suspension dans un liquide ou de chaînes de polymères en solution de 1 à 500 nm de diamètre environ.

Lorsque la lumière d'un laser atteint des petites particules dans une microcuvette, la lumière diffuse dans toutes les directions (différence d'indice). Ce phénomène est principalement de la diffusion de Rayleigh, diffusion élastique où les particules sont plus petites que la longueur d'onde considérée. On peut mesurer l'intensité de la lumière diffusée par les particules à un angle considéré (90° typiquement) au cours du temps. Cette dépendance en temps vient du fait que les particules dans un liquide sont soumises au mouvement Brownien à cause de l'agitation thermique. La distance entre les diffuseurs (concentration locale) change en permanence. Il en résulte des interférences constructives ou destructives et l'intensité totale mesurée contient des informations sur la vitesse de mouvement des particules.

Un traitement mathématique est mis en œuvre. On définit la fonction d'autocorrélation qui permet de comparer le signal mesuré à lui-même, mais avec un petit décalage temporel. Une modélisation graphique permet d'extraire un temps caractéristique de décroissance de cette fonction. Si l'autocorrélation décroit rapidement (tau faible), c'est que le signal mesuré varie rapidement. C'est le cas lorsque les particules se déplacent assez vite, donc qu'elles sont de petites tailles (plus mobiles). L'inverse de ce temps caractéristique (dit temps de relaxation) est lié au coefficient de diffusion des particules par la relation suivante:

$$\frac{1}{\tau} = Dq^2$$

avec D le coefficient de diffusion, q le vecteur d'onde et τ le temps de relaxation. L'équation de Stokes-Einstein permet alors d'obtenir le rayon hydrodynamique des particules:

$$R_h = \frac{k_B T}{6\pi\eta_s D}$$

où k_B désigne la constante de Boltzmann et η_s la viscosité du fluide.

Le rayon hydrodynamique est le rayon d'une sphère théorique qui aurait le même coefficient de diffusion que la particule considérée. Dans le cas d'une pelote statistique, ce rayon correspond au rayon d'une sphère dans laquelle le solvant ne pénètre pas. Pour une particule chargée, la sphère considérée contient la particule entourée de sa couche diffuse, ce qui entraine une surestimation par rapport à une mesure de taille par microscopie. En réalité, il existe une dispersité des tailles rencontrées et différentes méthodes sont mises en œuvre pour extraire l'intensité diffusée des différentes populations. Les différences sont très marquées en intensité et la présence d'impuretés ou d'agrégats sont très visibles même en très petit nombre. On obtient donc un rayon hydrodynamique, un indice de polydispersité et des indices sur l'allure du profil de distribution des tailles de particules de l'échantillon, en nombre, volume ou intensité.

5.1. Appareil utilisé

Les mesures de diffusion dynamique de la lumière des particules de caséines ont été réalisées à l'aide du Zetasizer Nano ZS (Malvern Instruments, Worcestershire, UK). La distribution de taille des particules de caséine a été obtenue en mesurant la lumière diffusée par ces particules, illuminées avec un faisceau laser (angle de diffusion = 173°, T° = 20°C), en utilisant la méthode d'analyse NNLS (nonnegative least squares).

Chapter III: Effect of casein microstructure

Publication n°1: PFG-NMR self-diffusion in casein dispersions: effects of probe size and protein aggregate size

PFG-NMR self-diffusion in casein dispersions: effects of probe size and protein aggregate size

Souad Salami[1,2], Corinne Rondeau[1,2], John van Duynhoven[3,4] and Francois Mariette[1,2,]*

[1] Irstea, UR TERE, 17 avenue de Cucillé, CS 64427, 35044 Rennes, France

[2] Université Européenne de Bretagne, France

[3]Unilever R&D, Olivier van Noortlaan 120, P.O. Box 114, 3130AC Vlaardingen, The Netherlands

[4] Laboratory of Biophysics, Wageningen University, Dreijenlaan 3, 6703HA Wageningen, The Netherlands

* Corresponding author: François Mariette, Irstea, UR TERE, CS 64426, 17 avenue de Cucillé, 35044 Rennes, Cedex, France; Tel.: +33 (0)2 23 48 21 21; Fax: +33 (0)2 23 48 21 15.

E-mail address: Francois.Mariette@irstea.fr

Abstract

The self-diffusion coefficients of different molecular weight PEGs (Polyethylene glycol) and casein particles were measured, using a pulsed-gradient nuclear magnetic resonance technique (PFG-NMR), in native phosphocaseinate (NPC) and sodium caseinate (SC) dispersions where caseins are not structured into micelles. The dependence of the PEG self-diffusion coefficient on the PEG size, casein concentration, the size and the mobility of casein obstacle particles are reported. Wide differences in the PEG diffusion coefficients were found according to the casein particle structure. The greatest reduction in diffusion coefficients was found in sodium caseinate suspensions. Moreover, sodium caseinate aggregates were found to diffuse more slowly than casein micelles for casein concentrations > 9 g/100 g H_2O. Experimental PEG and casein diffusion findings were analyzed using two appropriate diffusion models: the Rouse model and the Speedy model, respectively. According to the Speedy model, caseins behave as non-interacting hard spheres below the onset of the close packing limit (10 g/100 g H_2O for SC (Farrer & Lips, 1999) and 15 g/100 g H_2O for NPC (Bouchoux et al., 2009)) and as soft particles above this limit. Our results provided a consistent picture of the effects of diffusant mass, the dynamics of the host material and of the importance of the casein structure in determining the diffusion behavior of probes in these systems.

Keywords: Diffusion, casein micelle, sodium caseinate aggregates, PEG, Rouse model, Speedy model.

Introduction

Molecular transport, as characterized by diffusion coefficients, is a key feature of food processes and particularly of dairy processes. For example, the transformation of milk into cheese involves many operations such as coagulation, draining, salting and ripening, in which water and solute diffusion are important parameters that affect the microbiological and sensorial stability of cheese. Molecular transport behavior will obviously be different depending on the composition and microstructure of the dairy matrix. Caseins make up to 80% of the protein content of milk (Holt, 1992). Native phosphocaseinate (NPC) and sodium caseinate (SC) are two casein systems that exhibit differences in structure. In a native phosphocaseinate solution, caseins exist as large colloidal particles called "casein micelles", which contain the four caseins, α_{s1}, α_{s2}, β and κ, in the proportions of 3:1:3:1, and ~8% in mass of phosphate and calcium ions (Holt, 1992). The structure of the casein micelle has been studied for over 40 years and quite precise descriptions are available, although they are still controversial (Horne, 2006). It is commonly accepted that micelles are roughly spherical core-shell particles with outer diameters ranging from 50 to 500 nm (Dalgleish, Spagnuolo, & Douglass Goff, 2004; de Kruif, 1998; McMahon & McManus, 1998). The core is now generally described as a homogeneous network of caseins in which calcium phosphate nanoclusters are uniformly distributed (Horne, 2002; Marchin, Putaux, Pignon, & Leonil, 2007; McMahon & Oommen, 2008). The shell is essentially made of κ-casein parts with C-terminal sides, which protrude into the aqueous phase of the milk and provide steric and electrostatic stabilization of the particles (Horne, 1996; Sandra, Alexander, & Dalgleish, 2007). Casein micelles are very porous, highly hydrated and sponge-like colloidal particles containing approximately 3.4 g H_2O/g protein (Morris, Foster, & Harding, 2000). Even if these two systems contain the same relative amount of caseins, SC systems are quite different from casein micelles with respect to structure (HadjSadok, Pitkowski, Nicolai, Benyahia, & Moulai-Mostefa, 2008; Lucey, Srinivasan, Singh, & Munro, 2000; Radford & Dickinson, 2004) and interactions because they do not contain calcium phosphate nanoclusters (Farrer et al., 1999). Caseins are present as individual molecules in these dispersions, or as reversible self-assembled aggregates with a radius of ~ 11 nm (HadjSadok et al., 2008; Lucey et al., 2000; Radford et al., 2004).

Among the different methods of approach, pulsed field gradient nuclear magnetic resonance (PFG-NMR) provides a convenient means for measuring translational diffusion (Price, 1997). This technique was used because it permits nondestructive, fast and precise polymer self-diffusion coefficient measurements. Numerous PFG-NMR studies have been performed on dairy matrices such as NPC and SC systems. Some of these studies have focused on investigating the dynamic properties of casein proteins in relation to the protein concentration by observing changes in their self-diffusion coefficients. For example, (Tan & McGrath, 2010) measured casein self-diffusion coefficients in SC suspensions with casein concentrations ranging from 2 to 20% w/w. (Mariette, Topgaard, Jonsson, & Soderman, 2002) measured casein diffusion in NPC suspensions for different casein concentrations ranging from 0.03 to 0.19 g/g. (Le Feunteun, Ouethrani, & Mariette, 2012) monitored the diffusion of casein particles during the renneting of a concentrated casein micelle suspension (14% w/w). Other studies, however, have concentrated on measuring self-diffusion coefficients of PEG polymer probes of different molecular weights in NPC suspensions and gels. A first study was accomplished in NPC suspensions and rennet gels by (Colsenet, Soderman, & Mariette, 2005). This study was expanded by (Le Feunteun & Mariette, 2007) who investigated the translational dynamics of PEG polymers with molecular weights varying from 6.10^2 to 5.10^5 in casein suspensions and in gels induced by acidification, enzyme action and a combination of both. The main findings of these studies were that probe diffusion was affected by: (i) the casein concentration, i.e., PEG diffusion decreases with increasing casein concentration; (ii) the size of the PEG, i.e., for a given casein concentration, PEG diffusion decreases as polymer size increases; and (iii) the state of the matrix, solution or gel, i.e., PEG diffusion increases after coagulation. This effect was greater when the size of the probe was larger.

The diffusion coefficients of PEG observed in NPC suspensions and gels were explained by assuming a model with two diffusion pathways, one around and one through the casein particles. According to the "two pathways" diffusion model, variations in the diffusion rate of a molecule depend only on its ability to diffuse through the casein particles and the volume fraction occupied by them. This model implies that the diffusion of larger molecules is more affected by the presence of casein particles because they can less easily diffuse through them. These large probes could diffuse only around casein micelles.

The aim of the study presented here was to improve the understanding of PEG diffusion in casein systems (NPC and SC) both from the experimental and theoretical points of view. In this paper, PEGs with different molecular weights and casein protein self-diffusion coefficients were measured in both casein systems in order to provide some answers to the following questions:

(i) Does the intra-micellar diffusion mechanism adopted in NPC suspensions exist? This question is tackled by comparing the diffusion behavior of PEGs in NPC and SC dispersions. The particularity of the SC system resides in the fact that the extra-micellar diffusion mechanism is the only one to be considered in these suspensions. PEGs cannot diffuse inside SC aggregates because of their small size. Thus, according to the interpretation cited above, small PEG diffusion should be more rapid in the SC system since they encounter fewer obstruction effects when diffusing around casein aggregates in SC suspensions.

(ii) What is the effect of casein protein size and mobility in determining the diffusion behavior of PEG probes?

Experimental

Materials. Native phosphocaseinate powder was prepared at the INRA laboratory (Rennes) and the sodium caseinate powder was provided by Armor Protéines (Saint-Brice en Coglès, France). The detailed composition of the powder is given in **Table 1**. PEGs with different molecular weights (M_w) and low polydispersity indices (M_w/M_n) were obtained from Varian Laboratories (Massy, France). Sodium azide (Merck, Darmstadt, Germany) and sodium chloride (Sigma-Aldrich, Steinheim, Germany) with purities above 99% were used without purification.

	Total solids (g/Kg)	Total nitrogen matter (g/Kg)	Non-casein nitrogen (g/Kg)	Non-protein nitrogen (g/Kg)	Pure caseins (g/Kg)
NPC (%)	100	88.20	6.90	0.20	81.30
SC (%)	100	95.20	0.84	0.17	94.36

Table 1. Composition of NPC and SC powders.

Dispersion preparation. Rehydration of the powders with NaCl/water solution (0.1 M) was performed at room temperature over 36 h under constant stirring for micellar casein, and at 40°C over 24 h for sodium caseinate. Sodium azide was added (0.02% w/w) to each solution to prevent bacterial development. The solutions were studied without pH adjustment. The pH of SC solutions was 6.6±0.04 for casein concentrations ranging from 1 to 24 g/100 g H_2O, while the pH of the micellar casein dispersion was higher, ranging from 7.1 at 3 g/100 g H_2O to 6.9 at 22 g/100 g H_2O. Once the powder was totally rehydrated, 0.1% w/w of PEG was added to casein suspensions, regardless of the molecular weight. The dry matter of all casein suspensions was controlled by measuring variations in weight after drying in an oven for 24 h at 103°C. Casein

concentrations were calculated from values of dry matter content in each casein suspension and the pure casein percentage of the dry matter (**Table 1**).

Dynamic light scattering. Dynamic light scattering measurements of casein particles in NPC and SC solutions were performed on a Malvern Zetasizer Nano ZS instrument (Malvern Instruments, Worcestershire, UK). Size distribution of casein particles in solutions was obtained by measuring the light scattered by casein particles illuminated with a laser beam (scattering angle = 173°, T° = 20°C) using the NNLS analysis method (nonnegative least squares). The measured data were reported in a log-normal intensity distribution.

NMR measurements. A PFG-NMR experiment yields a series of decaying 1D-spectra. The chemical shift resolution of NMR, which enables identifying the different chemical environments that exist within a molecule and/or studying the different constituents of a mixture is thus preserved. As an example, **Figure 1** presents a ^{1}H-PFG-NMR spectrum of the casein suspension we studied. It shows that the three main constituents of our sample were well-separated by ^{1}H-NMR. The signal coming from water molecules, which was suppressed with the PFG-NMR sequence we used, resonate at 4.7 ppm. The sharp peak at 3.6 ppm is the signal coming from the 0.1 % (w/w) of a 32530 g/mol polyethylene glycol (PEG). All the other signals come from the protons of the casein molecules.

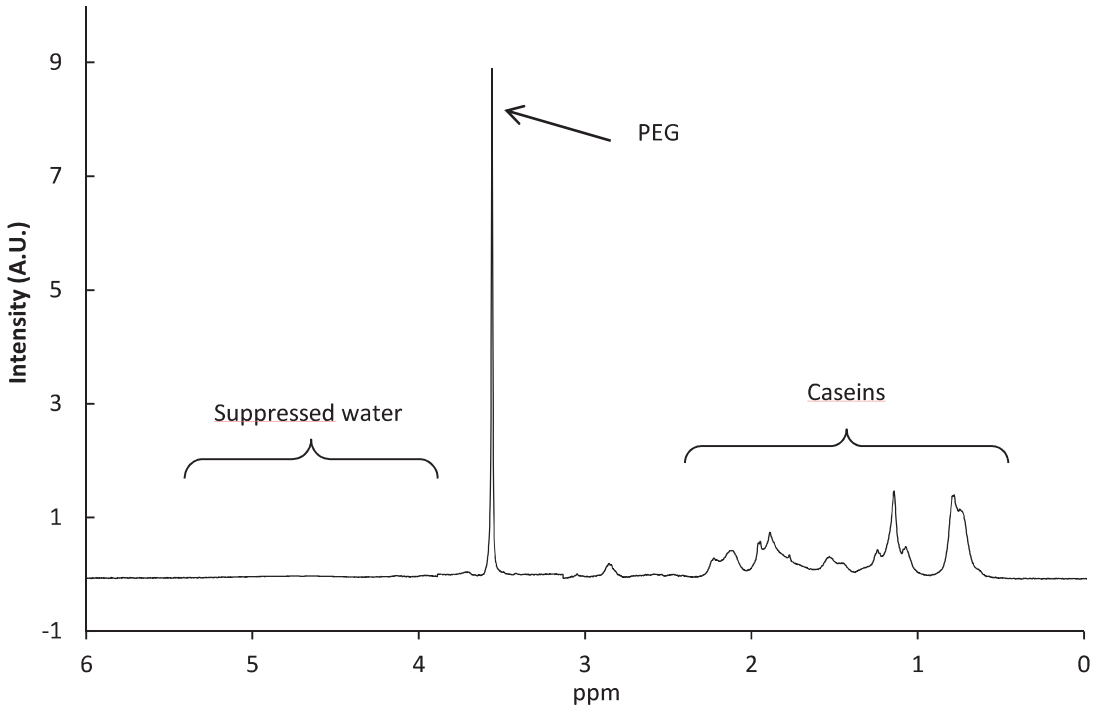

Figure 1. Example of an NMR spectrum obtained during a self-diffusion measurement. It stems from a concentrated casein suspension that contains 0.1 % (w/w) of a PEG polymer and 12 g/100g H_2O of caseins.

PEG and casein self-diffusion measurements were performed on a 500 MHz spectrometer equipped with a dedicated field gradient probe (DIFF30 from Bruker, Wissembourg, France) with a static gradient strength of 1200 (±0.2) G/cm for an amplifier output of 40 A. Diffusion spectra were acquired with a stimulated echo sequence using bipolar gradients (STE-BPP) and a 3-9-19 WATERGATE pulse scheme to suppress the water signal. Experiments were carried out with 16 different values of g, ranging from 20 to 900 G/cm, with δ = 1 ms (for PEG measurements) and δ values ranging from 1 to 2.2 ms (for casein measurements). Sixteen scans were carried out and the recycle delay was set at 5 T_1. Depending on the molecular weight of the PEG studied, Δ was adjusted to obtain a diffusion distance z of ~1.5 µm in the casein suspension, in accordance with the Einstein equation, $z = (2 \Delta D_{PEG})^{1/2}$. This procedure enabled the molecular probes to cover much greater distances than the casein micelle diameter.

NMR processing methods. All the data processing was performed with Matlab and Table Curve software. Monte-Carlo simulations were used for error calculations with 200 iterations. In a PFG-NMR experiment using the BPP sequence, the echo intensity, I, is described by:

$$I / I_0 = \sum_i p_i \exp(-k\, D_i) \quad (1)$$

with

$$k = \gamma^2 g^2 \delta^2 (\Delta - \delta/3 - \tau/4) \quad (2)$$

where I_0 is the signal intensity in the absence of gradients, γ the gyromagnetic ratio (for protons, $\gamma = 26.7520 \times 10^7$ rad.T^{-1} .s^{-1}), g the amplitude of the gradient pulse, δ the gradient pulse duration, Δ the time between the leading edges of gradient pulses, τ the time between the end of each gradient and the next radiofrequency pulse, D_i the self-diffusion coefficient of the ith component, and p_i the fractional proton number of the ith component. The magnetization decay was analyzed using a monoexponential fitting (i=1) for PEGs and a biexponential fitting (i=2) for casein self-diffusion. The standard error in PEG and casein diffusion coefficients estimated by the fitting procedure was less than 10%.

Normalization of diffusion coefficients. The self-diffusion coefficients presented in **Table 2** were used to normalize the diffusion coefficients measured in SC suspensions. Since the amount of soluble compounds is greater in NPC powder than in SC powder, their contribution to PEG diffusion hindrance in the aqueous phase cannot be neglected in NPC suspensions. To consider the effects of casein alone, we normalized the probe self-diffusion coefficients measured in NPC samples by the probe self-diffusion coefficient measured in the aqueous phase that includes these soluble compounds.

Results and Discussion

Dynamic light scattering

DLS was used to determine the size distribution of particles in suspensions of native phosphocaseinate (3 g/100 g water) as well as sodium caseinate (1 g/100 g water) containing 100 mM NaCl. **Figure 2** indicated that particles of native phosphocaseinates presented a single broad population distribution from ~ 68 to ~ 459 nm in diameter. The mean casein micelle diameter was 187 nm. These results are in very good agreement with values already reported by several authors (Dalgleish et al., 2004; de Kruif, 1998; McMahon et al., 1998). In contrast, sodium caseinate solution was found to contain two distinct populations, a major one (98% of the total volume) with an average hydrodynamic diameter of approximately 22 nm, and a small weight fraction (2%) of particles with an average diameter of approximately 200 nm. Since large particles scatter more light than small particles, the relative scattering intensity of these particles can be strong, even if their weight fraction is small (Chu, Zhou, Wu, & Farrell, 1995). In the absence of NaCl salt, caseins are known to be mostly present in the form of individual molecules (HadjSadok et al., 2008). When electrostatic repulsion is screened by the addition of 100 mM NaCl, the hydrophobic parts of the casein molecules associate, leading to the formation of small micellar aggregates that are probably star-like particles (HadjSadok et al., 2008). Our results are in very good agreement with those of (HadjSadok et al., 2008; Panouille, Benyahia, Durand, & Nicolai, 2005). In the presence of 100 mM of NaCl and under the same conditions of temperature and pH, caseins were found to have a hydrodynamic diameter of approximately 22 nm. A second population of larger particles with R_h ~100 nm was also observed. However, the nature of these large particles is as yet unknown, but it is clear that they are not residual native casein as supposed by Nash et al. (Nash, Pinder, Hemar, & Singh, 2002) since they do not precipitate during ultracentrifugation.

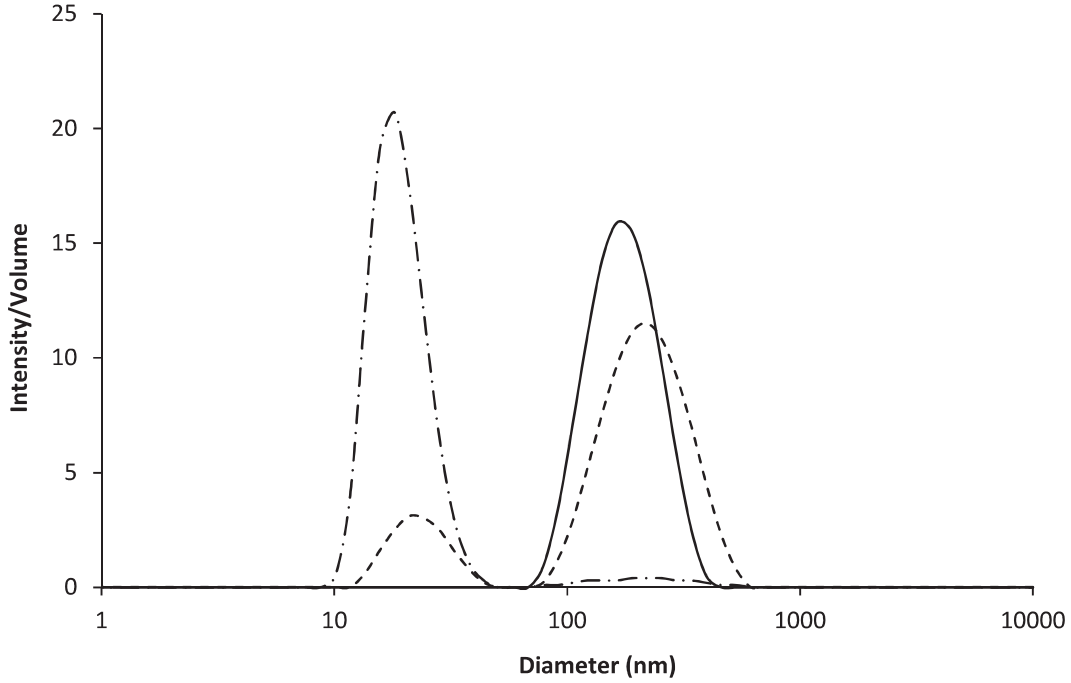

Figure 2. Lognormal particle size distribution for a NPC (solid line) and a SC (dotted line for intensity distribution/dashed-dotted line for volume distribution) suspension in the presence of 100 mM NaCl.

Diffusion by NMR

Self-diffusion of PEGs in water

The molecular weight, polydispersity index and self-diffusion coefficients measured for all PEGs studied in water/0.1M NaCl are presented in **Table 2**. Hence, the hydrodynamic diameter radius of the PEGs can be calculated with the help of the Stokes-Einstein equation:

$$R_h = \frac{k_B T}{6\pi\eta D} \quad \textbf{(3)}$$

where T is the temperature in Kelvin, K the Boltzman constant (1.38 x 10^{-23} JK^{-1}), and η the viscosity of the aqueous phase (1x10^{-3} Pa at 20°C).

M_w	M_w/M_n	D ($m^2.s^{-1}$)	R_h (nm)
615	1.07	2.70E-10	0.79
7920	1.04	6.77E-11	3.16
21300	1.06	3.99E-11	5.37
32530	1.06	3.06E-11	7
93000	1.06	1.62E-11	13.22

Table 2. Self-diffusion coefficients and the corresponding hydrodynamic radii of various PEGs. Data obtained from NMR diffusion measurements in a H_2O/NaCl solution (0.1 M) at 20°C.

Self-diffusion of PEGs in SC suspensions

The PEG self-diffusion coefficients (615, 7920, 21300, 32530 and 93000 g/mol) were measured at 20°C in SC suspensions with casein concentrations ranging from 1.26 to 24.04 g/100 g water (**Figure 3**). At high protein concentrations, the solutions became highly viscous. The absence of restricted diffusion at the length-scale studied (~1.5 µm) was verified by measuring the self-diffusion coefficients of the 93000 g/mol PEG in a concentrated casein suspension at different diffusion times, thus probing a range of distances. The results obtained (data not shown) demonstrated that the PEG self-diffusion coefficient was the same, regardless of the distance traveled between 0.65 and 1.97 µm.

PEG diffusion coefficients were found to be dependent on both casein concentration and PEG size. PEG diffusion decreased with increasing casein concentration, and for a given concentration, PEG diffusion decreased as their size was important. The change in diffusion coefficients was more significant for the probes of higher molecular weight and larger size, giving D/D_0 = 0.39, 0.13 and 0.016 for 615, 7920 and 93000 g/mol PEG, respectively, at a casein concentration of 24 g/100 g H_2O.

The effect of varying the NaCl concentration between 0 and 100 mM on the 7920 g/mol PEG self-diffusion coefficients for a fixed concentration of 5 g/100 g of H_2O was also studied. Reducing the ionic strength from 100 mM to 0.05 and 0 mM led to a decrease in the PEG-

reduced diffusion from 0.692±0.01 to 0.679±0.01 and 0.620±0.01, respectively (data not shown). As stated above, if monovalent salt is added so that electrostatic interaction is screened, the hydrophobic parts of the individual casein molecules of R_h~3 nm associate, leading to the formation of small casein aggregates of R_h~11 nm. The association number is determined by the balance of hydrophobic and electrostatic interactions, which explains the observed diffusion increase with increasing ionic strength. Thus, these results clearly showed that probe self-diffusion is dependent on the protein size: the smaller the particle size, the slower the probe diffusion rate will be. This finding is in very good agreement with numerous numerical simulations and studies in polymer systems (Colsenet et al., 2005; Gong, Hirota, Kakugo, Naria, & Osada, 2000; Saxton, 1987; Tremmel, Kirchhoff, Weis, & Farquhar, 2003), which have highlighted the effect of obstacle size or density on probe diffusion. It was found that the probe diffusion coefficient strongly decreases with decreasing protein size or increasing protein density, as the density is higher for a given composition with smaller particle sizes.

Comparison of PEG diffusion in NPC and SC suspensions

Figure 3 compares the PEG-reduced self-diffusion coefficient in NPC and SC suspensions as a function of casein concentration for different PEG molecular masses. D_{PEG} decreased with increasing casein concentrations for both NPC and SC. These results obtained in NPC suspensions are consistent with values already reported by Le Feunteun et al. (Le Feunteun & Mariette, 2008) for the 620 and 96750 g/mol PEGs in a concentrated NPC suspension (empty triangle and diamond shapes). However, the casein structure affected the intensity of the decrease. PEG diffusion was much more attenuated in the SC system. For example, at a casein concentration of 12 g/100 g H_2O, the decrease in D_r for the 615 g/mol, 7920 and 93000 g/mol PEGs was 0.76, 0.7, 0.51 in NPC suspensions and 0.61, 0.35, 0.12 in SC suspensions, respectively.

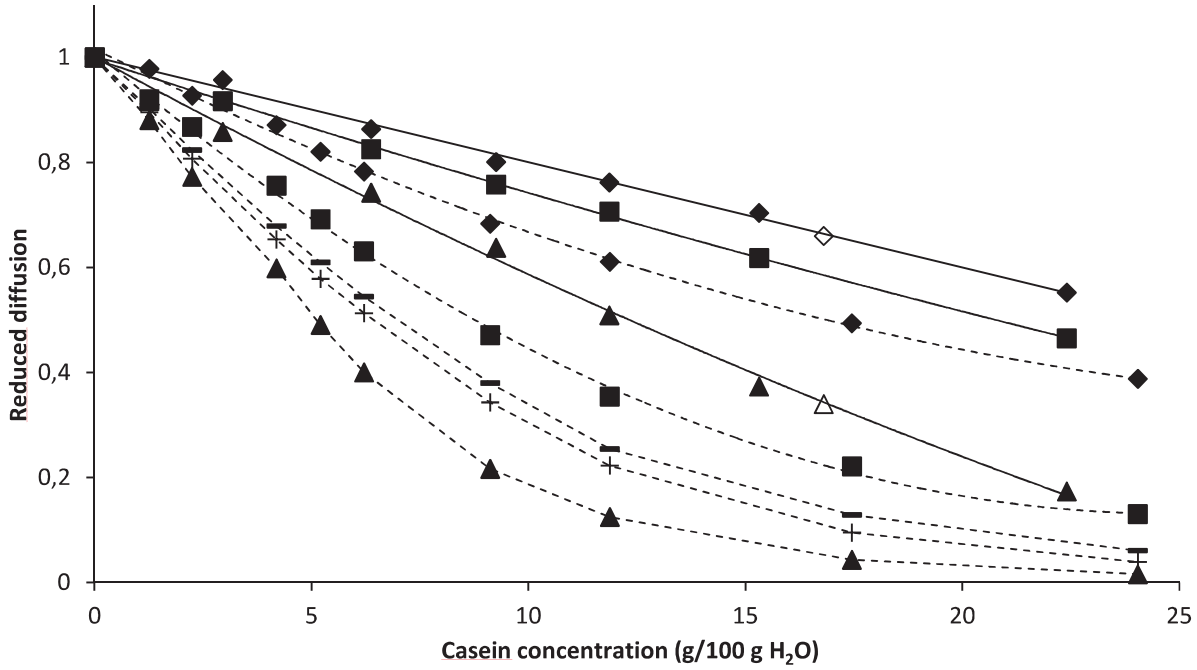

Figure 3. Reduced self-diffusion coefficients of different PEGs (615 ♦, 7920 ■, 21300 -, 32530 + and 93000 ▲) as a function of casein concentrations in NPC (solid lines) and SC (dashed lines) suspensions. Empty diamond and triangle correspond to the 620 and 93000 g/mol PEG diffusion already measured by Le Feunteun et al. in a concentrated NPC suspension (16.8 g/100 g H_2O).

All these differences in diffusion behavior may be explained by the loss of the peculiar structure of the casein micelle in SC dispersions. These differences should thus, first of all, be attributed to the difference in the casein protein size. In polymer theory, the diffusion of polymer chains can be divided into two regions based on the chain length relative to pore size R (de Gennes, 1979b; Doi & Edwards, 1986). The first region for a Gaussian chain is observed when the gyration radius of the chain $R_g < R/2$, where the diffusion is describe by the Rouse model. The second behavioral region is observed when $R_g > R/2$, where the reptation theory, proposed by de Gennes, describes the movement of an unattached chain by Brownian motion in a many-chain or gel system. A simple power law provides a description of the solute diffusion coefficients versus molecular weight:

$$D = A.M^{-\alpha} \quad (4)$$

where A is a pre-exponential factor and α a characteristic exponent.

This equation is often used to describe the self-diffusion of polymer chains with α varying from 0.55 for dilute systems to 2 in concentrated systems. The Rouse model is a well-established model for non-entangled polymer chains. The diffusion of a high molecular weight polymer in an unentangled system, or a diluted solution, is described as follows by the Rouse model: $D \sim M_w^{-1}$. The reptation theory was complementary to the works of Rouse and is expressed as $D \sim M_w^{-2}$. An intermediate mechanism was proposed by Favre et al. (Favre, Leonard, Laurent, & Dellacherie, 2001) to possibly explain the somewhat intermediate situation between negligible partial drainage of the solvent in an ideal statistical sphere (-0.5 or 0.6 exponent value) and the wormlike displacement of a linear molecule in a network of fixed obstacles (-2 exponent value). According to these authors, it can be assumed that an intermediate stage corresponding to an ellipsoidal solute shape may occur when system mesh size approaches the solute hydrodynamic diameter.

Equation 4 was applied to our data. The plots of D_{PEG} versus PEG molecular weight (M_w) in casein suspensions for different casein concentrations are given in **Figure 4**.

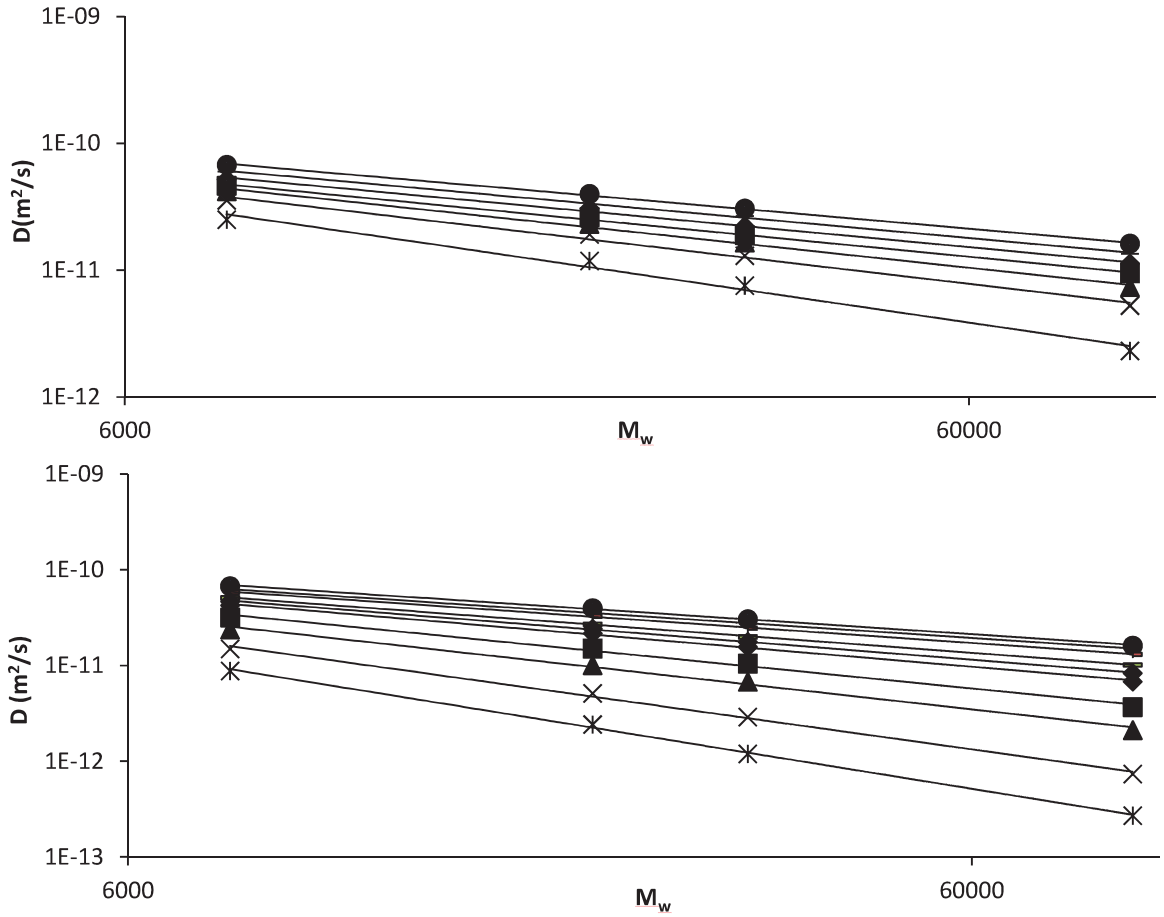

Figure 4. Power law representation of the diffusion coefficient of PEG (7920, 21300, 32530 and 93000 g/mol) showing different molecular weights in water and (A) NPC suspensions for various casein concentrations (from top to bottom): 2.88, 6.43, 9.22, 11.86, 15.35 and 22.4 g/100 g H_2O (B) in SC suspensions for various casein concentrations (from top to bottom): 1.26, 2.25, 4.19, 5.20, 6.21, 9.11, 11.87, 17.45 and 24.04 g/100 g H_2O.

All data were fitted with **Equation 4**, and values of α were extracted for each concentration. **Figure 5** shows the different α values obtained in NPC and SC suspensions with casein concentrations varying between 0 (water + NaCl) and 24 g/100 g H_2O.

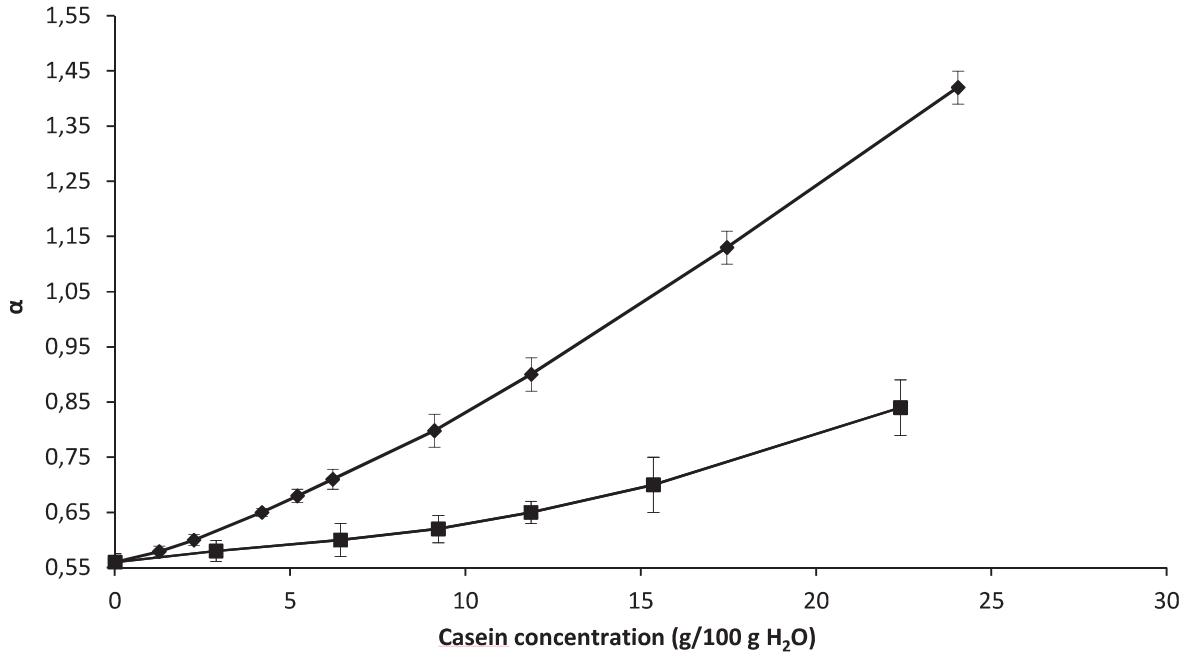

Figure 5. Exponent (α) of a power law curve fit obtained after regression of PEG diffusion coefficients (D) in NPC (■) and SC (♦) suspensions vs. molecular weight (M_w). Error bars represent the uncertainties estimated by the fitting procedure.

It can be seen that the exponent, which is close to the theoretical value of 0.6 for PEG diffusion in water (de Gennes, 1979a), gradually shifted towards higher values when the casein concentration (i.e., network density) increased. However, in the case of SC systems, the exponent shifted more rapidly towards higher values. For the NPC system, the α value varied between 0.58 and 0.84, with casein concentrations varying from 2.88 to 22.4 g/100 g water. The values of α, around 0.7, obtained for casein concentrations between 3 and 15 g/100 g H_2O, show that although the diffusion was reduced by casein micelles for these PEGs, this obstruction mechanism had no constraints on their spatial organization and they thus retained a spherical random coil form. If PEGs had diffused inside the micelle, the α values would have been higher since a PEG would be forced to change its conformation in order to diffuse inside the micelle. However, for casein concentrations > 15 g/100 g H_2O, the α values showed that PEGs adopted an ellipsoidal random coil form at this concentration and that the casein system mesh size approaches the solute diameter. For SC systems, α values varied between 0.58 and 1.42, with casein concentrations varying from 1.26 to 24.04 g/100 g water. In addition, for a casein concentration > 6 g/100 g

H_2O, PEGs assumed the aspect of statistically ellipsoidal random coils and there diameter approached the system mesh size.

The analysis above suggests that SC systems have higher densities than NPC systems for the same casein concentration, which is partially responsible for the strong reduction in the diffusion in SC suspensions with an increase in casein concentration. These results also suggest that the casein networks (NPC and SC systems) are not dense enough to induce reptation, but are dense enough so that the solute conformations corresponding to elongated shapes are favored for the diffusion step to be effective.

Protein diffusion in NPC and SC suspensions

The diffusion coefficient of casein micelles (NPC) and sodium caseinate aggregates (SC) were also measured as a function of casein concentration. Due to the presence of a small amount of soluble compounds (amino acids, peptides) in the NPC and SC powders, their contribution to the proton NMR signal of casein can therefore not be neglected. Consequently, all attenuation curves of the NMR echo signal for casein particles showed a non-linear decay and were fitted with a bi-exponential model providing two diffusion coefficients. A first diffusion coefficient with a value of approximately 10^{-11} m^2s^{-1} was calculated in both systems. According to the Stokes Einstein (SE) relation, this diffusion coefficient corresponds to particles with a hydrodynamic radius equal to approximately 3 nm. Diffusion coefficients of the same order have also been measured in NPC suspensions by other authors using the PFG-NMR technique (Le Feunteun et al., 2012; Mariette et al., 2002). This diffusion coefficient was attributed to the soluble compounds, a conclusion supported by diffusion measurements of these compounds in the serum phase extracted by ultracentrifugation. The diffusion coefficient obtained ($6.44e^{-11}$ m^2s^{-1}) was equal to the value estimated at zero casein concentration. The second diffusion coefficient, which represented the main fraction of the echo attenuation, can therefore be attributed to the casein particles. **Figure 6** shows the variation of casein particle diffusion coefficients as a function of casein concentrations in NPC and SC systems. Diffusion data were extrapolated to infinite dilution in order to estimate the casein particle size from the SE relation. The radii obtained using this equation were consistent with the casein size distribution determined by DLS and were equal to 12 nm for sodium caseinate aggregates and 96 nm for casein micelles. These findings are in very good

agreement with several PFG-NMR (Le Feunteun et al., 2012; Mariette et al., 2002), inelastic light scattering and dynamic wave spectroscopy studies (Alexander, Rojas-Ochoa, Leser, & Schurtenberger, 2002; Gaygadzhiev, Corredig, & Alexander, 2008) where the values of casein micelle diffusion reported ranged from $2x10^{-12}$ down to $2x10^{-13}$ m^2s^{-1}, depending on the composition of the dairy suspension and on its casein concentration. Sodium caseinate aggregate diffusion measurements were also consistent with values already measured by (Tan et al., 2010) in SC dispersions using the PFG-NMR technique.

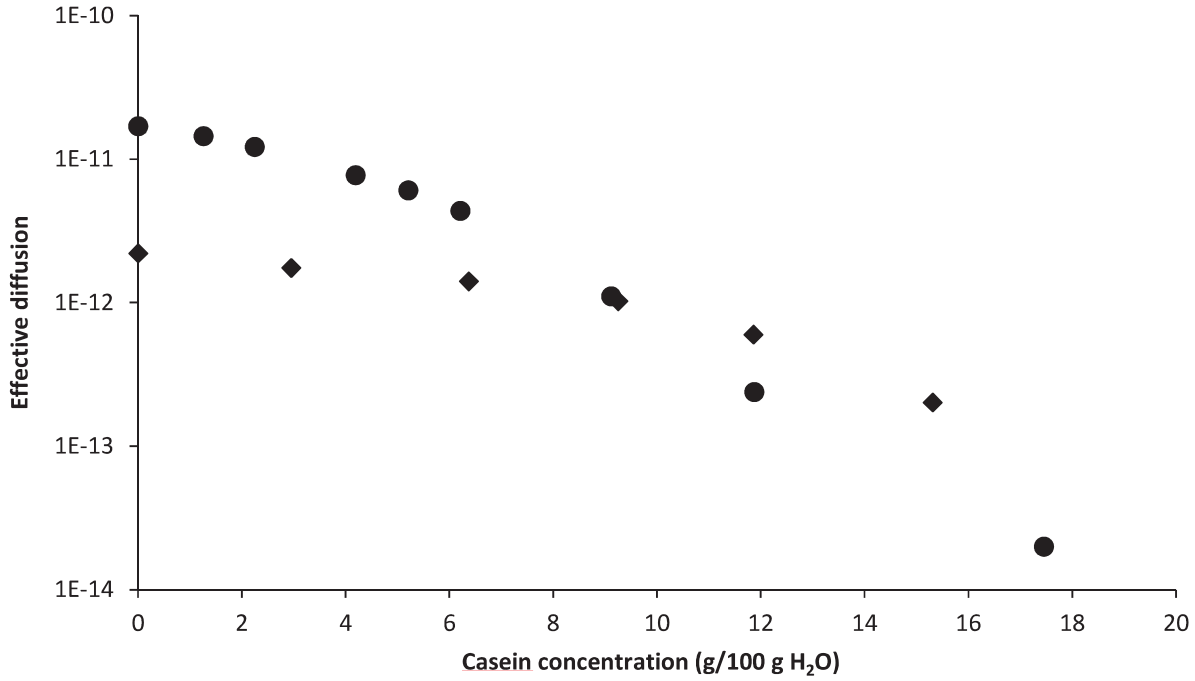

Figure 6. Comparison of casein effective diffusion in NPC (♦) and SC suspensions (•).

The experimental values of casein diffusion were fitted to the following empirical equation proposed by Speedy (Speedy, 1987) to describe the self-diffusion of non-interacting hard spheres in a hard sphere fluid:

$$D = D_0\left(1-\frac{\phi}{0.571}\right)\left(1+\phi^2(1.459-11.04\phi^2)\right) \quad \textbf{(5)}$$

The volume fraction occupied by the hard spheres is $\phi = CxV$, where C is the casein concentration (g/ml) and V is the voluminosity occupied by the casein particles (ml/g). As seen in **Figure 7**, the experimental values of casein-reduced self-diffusion coefficients as a function of casein concentration can be fitted with the Speedy model up to a casein concentration of approximately 9 g/100 g H_2O for the SC system and 15 g/100 g H_2O for the NPC system. Above these concentrations, the model failed to describe the casein diffusion data. These results suggest that SC and NPC dispersions still behave as non-interacting hard-sphere fluids up to a casein concentration that matches the onset of random-close packing of these two systems. This is in accordance with findings from previous studies that showed that the hard sphere model could be a valuable model for casein micelles (Bouchoux et al., 2009; Gaygadzhiev et al., 2008; Anne Pitkowski, 2007) and aggregating sub-micelles (Farrer et al., 1999; Panouille et al., 2005; Pitkowski, Durand, & Nicolai, 2008). At higher concentrations, there is another regime (soft spheres) in which casein micelles and casein submicelles deform, deswell and interpenetrate as the casein concentration increases. The values of voluminosity calculated from the fitting for casein micelles and sodium caseinate aggregates were 3.4±0.05 and 7±0.4 ml/g, respectively, in close agreement with previously estimated values. Reported voluminosity values for casein micelles at the pH of milk vary widely, i.e., V= 1.5 to 7.1 ml/g (Walstra, 1979), depending on the method employed. Recently, (De Kruif & Huppertz, (2012); Jeurnink & De Kruif, (1993); Morris, Foster, & Harding, 2000) reported a voluminosity of 4.2-4.4 ml/g on the basis of viscosity measurements. Moreover, voluminosity values varying between 4 and 6 ml/g for casein submicelles estimated by neutron scattering and measurement of the intrinsic viscosity have been reported (Panouille et al., 2005; Stothart & Cebula, 1982).

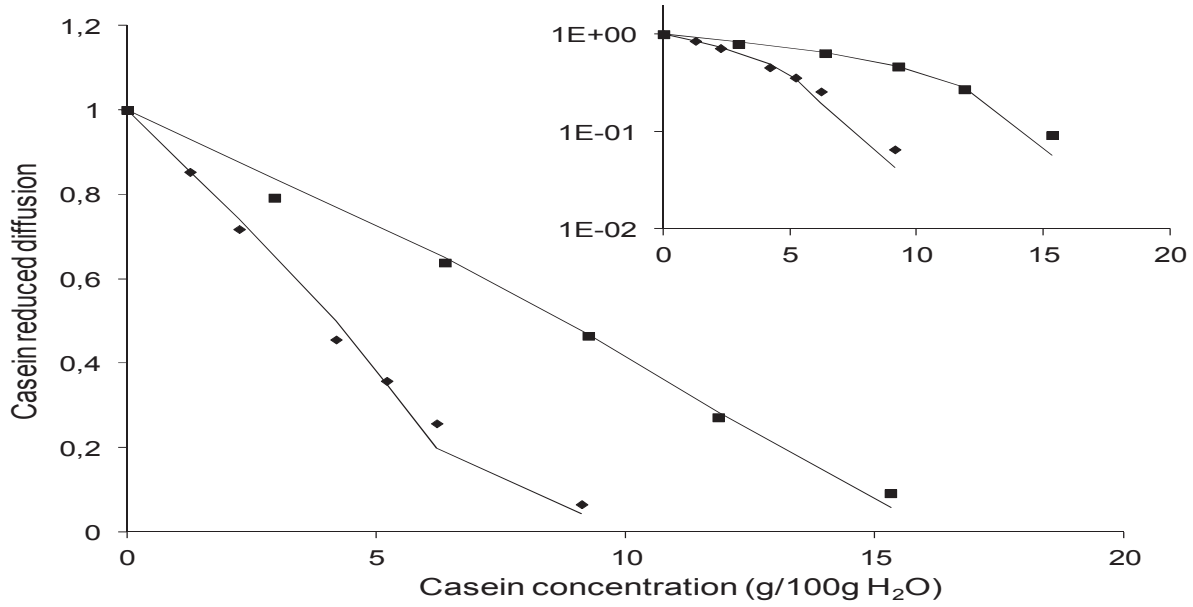

Figure 7. Casein-reduced diffusivity D/D_0 vs. casein concentration in NPC (■) and SC (♦) systems has been fitted to the Speedy model (solid line). In the insert panel we show the same behavior but in log-linear scale.

Analysis of the casein self-diffusion coefficients measured (**Figure 6**) revealed that for casein concentrations < 9 g/100g H_2O, caseins diffused faster in SC suspensions than in NPC dispersions due to their differences in size. Increasing the concentration resulted in a rapid decrease in the self-diffusion coefficient of sodium caseinate aggregates (SC). The rate of change slowed down considerably once the level of approximately 10 g/100 g H_2O sodium caseinate was reached. However, above this concentration, sodium caseinate aggregates are known to close pack, leading to a strong increase in the viscosity (Farrer et al., 1999; Pitkowski et al., 2008). Using previously measured NPC and SC solution viscosities (Pitkowski et al., 2008; Anne Pitkowski, 2007), the inverse normalized viscosities were compared with our normalized diffusion coefficient. As shown in **Figure 8**, casein micelles and sodium caseinate aggregates diffused in both systems according to the SE relation. A positive deviation from this relation was observed for sodium caseinate aggregates with casein concentrations > 12 g/100 g H_2O. The differences in diffusion behavior between casein micelles and sodium caseinate aggregates can thus be attributed to differences in protein size and dispersion viscosity.

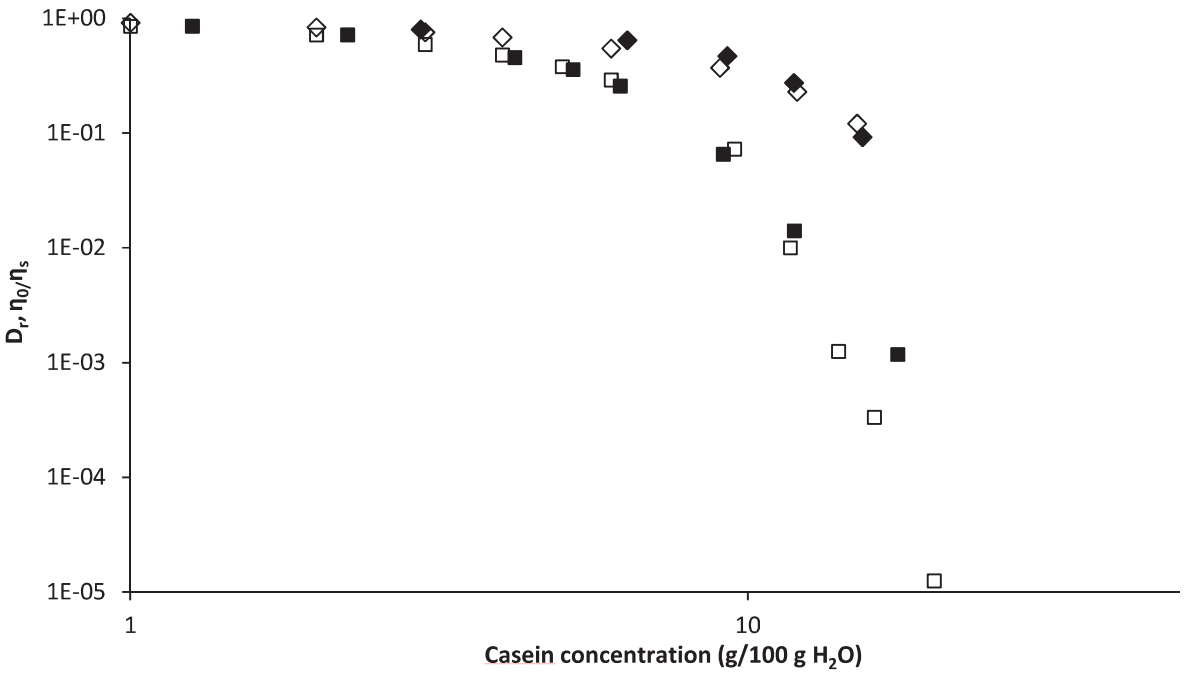

Figure 8. Casein concentration dependencies of the casein-normalized diffusivities D_r (filled shapes) and the inverse suspension viscosities (η_s) normalized by the solvent viscosity (η_0) (empty shapes) for SC (square) and NPC suspensions (diamonds).

PEG-reduced diffusion data were also compared with the SE relation (data not shown). In both casein systems, PEGs were found to diffuse faster than expected from the solution viscosity. This indicates that the reduction in the PEG diffusion coefficient was largely a function of the space occupied by the matrix and minorly affected by the macroviscosity of the dispersions. Moreover, obstacle mobility should be taken into account for a complete description of probe diffusion. This issue has been investigated, via simulations methods, by many authors (Saxton, 1987; Tremmel et al., 2003). When the obstacles are immobile, their effect may be described by percolation theory, which states that the long-range diffusion constant of the tracers goes to zero when the area fraction of the obstacles is greater than the percolation threshold (critical concentration). In contrast, if the obstacles are themselves mobile as for caseins, the diffusion constant of the tracers depends on the area fraction of obstacles and the relative jump rate of tracers and obstacles. In this case, long-range diffusion of a tracer is not prevented, but only retarded. The extent of the diffusion retardation certainly depends on the diffusion coefficient of the obstacles and the size of the tracer. This may explain the fact that long-range diffusion occurred at all of the casein

concentrations studied, even though the onset of close-packing of the casein sub-micelles (SC) and casein micelles (NPC) occurs at casein concentrations of approximately ~10 g/100 g H_2O and ~ 15 g/100 g H_2O, respectively.

In light of these results, the question arises as to whether the intra-micellar diffusion mechanism already adopted in NPC suspensions exists or not. Previous studies have shown that the PEG diffusion in NPC suspensions could be explained by considering two characteristic length scales of structure (Colsenet et al., 2005; Le Feunteun et al., 2007). For large PEGs, the free volume fraction unoccupied by casein micelles is the prevailing element, whereas for small PEGs, the micelle internal porosity is the preponderant factor. This model has made it possible to explain the effect of probe size in particular. Such an explanation was proposed because casein particles cannot be considered as impenetrable particles since they are known to be porous and highly hydrated (Morris et al., 2000). On the other hand, PEGs are flexible, easily deformable and can change their shape according to their environment, as shown in this study and proven by (Griffiths, Stilbs, Yu, & Booth, 1995). They can therefore diffuse through small spaces compared to their hydrodynamic diameter by adopting a more elongated conformation. However, our experimental results show that an extra-micellar mechanism, which is the only one to be considered in the case of SC suspensions, is sufficient to explain the difference in the values of the observed diffusion coefficient according to the probe size. These results therefore let us assume that intra-micellar diffusion would be negligible and that the data can be simply explained by taking probe size, obstacle size and mobility into account.

Conclusion

The aim of this work was to critically examine the diffusion of PEGs and caseins in NPC and SC dispersions by combining both experimental and theoretical approaches. It has been shown that in NPC and SC systems:

- Caseins behave as hard spheres in a fluid and their self-diffusion is inversely proportional to the solution viscosity measured macroscopically up to a casein concentration that matches the onset of random-close packing of these two systems. Consequently, sodium caseinate aggregates diffuse more slowly than casein micelles when the casein concentration exceeds 9 g/100 g H_2O. Casein voluminosity values obtained by fitting the casein experimental diffusion data to the Speedy model were found to be in close agreement with previous values found in the literature.

- Two drastically different diffusion behaviors of PEGs were obtained in relation to differences in casein obstacle size (inter-particle distance) and mobility between the two casein systems. A SC suspension with a casein particle size equal to 12 nm and slow mobility has a considerably stronger hindering effect than a NPC suspension with a casein particle size equal to approximately 100 nm. Diffusion data were explained using the classical power law used in the Rouse model.

The results obtained challenge the "two pathways" diffusion model already proposed to explain the diffusion of a probe in NPC suspensions (Colsenet et al., 2005; Le Feunteun et al., 2007) and indicate that the extra-micellar diffusion mechanism is the only mechanism to be considered, regardless of the size of the probe.

Acknowledgements

The authors thank the Regional Council of Brittany and Unilever (Netherlands) for their financial support. We are grateful to Arnaud Bondon (PRISM Research Platform, Rennes, France) for his help with NMR experiments. We also thank Marie-Helene Famelart, Florence Rousseau and Valerie Gagnaire (INRA Laboratory, Rennes) for helpful discussions and assistance with the rheological, dynamic light scattering and ultracentrifugation experiments. IRM-Food team has been awarded ISO 9001 certification for its activities related to research.

References

Alexander, M., Rojas-Ochoa, L. F., Leser, M., & Schurtenberger, P. (2002). Structure, dynamics, and optical properties of concentrated milk suspensions: an analogy to hard-sphere liquids. *Journal of Colloid and Interface Science, 253*(1), 35-46.

Bouchoux, A., Debbou, B., Gesan-Guiziou, G., Famelart, M. H., Doublier, J. L., & Cabane, B. (2009). Rheology and phase behavior of dense casein micelle dispersions. *Journal of Chemical Physics, 131*(16).

Chu, B., Zhou, Z., Wu, G., & Farrell, H. M., Jr. (1995). Laser light scattering of model casein solutions: effects of high temperature. *Journal of Colloid and Interface Science, 170*(1), 102-112.

Colsenet, R., Soderman, O., & Mariette, F. (2005). Effect of casein concentration in suspensions and gels on poly(ethylene glycol)s NMR self-diffusion measurements. *Macromolecules, 38*(22), 9171-9179.

Dalgleish, D. G., Spagnuolo, P., & Douglass Goff, H. (2004). A possible structure of the casein micelle based on high-resolution field-emission scanning electron microscopy. *International Dairy Journal, 14*, 1025-1031.

de Gennes, P. G. (1979a). Brownian motions of flexible polymer chains. *Nature, 282*, 367-370.

de Gennes, P. G. (1979b). Scaling concepts in polymer physics. In. Ithaca, New York: Cornell University Press.

de Kruif, C. G. (1998). Supra-aggregates of casein micelles as a prelude to coagulation. *Journal of Dairy Science, 81*(11), 3019-3028.

de Kruif, C. G., & Huppertz, T. (2012). Casein Micelles: Size Distribution in Milks from Individual Cows. *Journal of Agricultural and Food Chemistry, 60*(18), 4649-4655.

Doi, M., & Edwards, S. F. (1986). The theory of polymer dynamics. In. Oxford: Oxford University Press.

Farrer, D., & Lips, A. (1999). On the self-assembly of sodium caseinate. *International Dairy Journal, 9*(3-6), 281-286.

Favre, E., Leonard, M., Laurent, A., & Dellacherie, E. (2001). Diffusion of polyethyleneglycols in calcium alginate hydrogels. *Colloids and Surfaces a-Physicochemical and Engineering Aspects, 194*(1-3), 197-206.

Gaygadzhiev, Z., Corredig, M., & Alexander, M. (2008). Diffusing wave spectroscopy study of the colloidal interactions occurring between casein micelles and emulsion droplets:comparison to hard-sphere behavior. *Langmuir, 24*(8), 3794-3800.

Gong, J. P., Hirota, N., Kakugo, A., Narita, T., & Osada, Y. (2000). Effect of aspect ratio on protein diffusion in hydrogels. *The Journal of Physical Chemistry B, 104*(42), 9904-9908.

Griffiths, P. C., Stilbs, P., Yu, G. E., & Booth, C. (1995). Role of molecular architecture in polymer diffusion: a PGSE-NMR study of linear and cyclic poly(ethylene oxide). *The Journal of Physical Chemistry, 99*(45), 16752-16756.

HadjSadok, A., Pitkowski, A., Nicolai, T., Benyahia, L., & Moulai-Mostefa, N. (2008). Characterisation of sodium caseinate as a function of ionic strength, pH and temperature using static and dynamic light scattering. *Food Hydrocolloids, 22*(8), 1460-1466.

Holt, C. (1992). Structure and stability of bovine casein micelles. *Advances in Protein Chemistry, 43*, 63-151.

Horne, D. S. (1996). The hairy casein micelle: Evolution of the concept and its implications for dairy technology. *Netherlands Milk and Dairy Journal, 50*(2), 85-111.

Horne, D. S. (2002). Casein structure, self-assembly and gelation. *Current Opinion in Colloid & Interface Science, 7*(5), 456-461.

Horne, D. S. (2006). Casein micelle structure: Models and muddles. *Current Opinion in Colloid & Interface Science, 11*(2-3), 148-153.

Jeurnink, T. J. M., & De Kruif, K. G. (1993). Changes in milk on heating: viscosity measurements. *Journal of Dairy Research, 60*(2), 139-150.

Le Feunteun, S., & Mariette, F. (2007). Impact of casein gel microstructure on self-diffusion coefficient of molecular probes measured by H-1 PFG-NMR. *Journal of Agricultural and Food Chemistry, 55*(26), 10764-10772.

Le Feunteun, S., & Mariette, F. (2008). PFG-NMR techniques provide a new tool for continuous investigation of the evolution of the casein gel microstructure after renneting. *Macromolecules, 41*(6), 2071-2078.

Le Feunteun, S., Ouethrani, M., & Mariette, F. (2012). The rennet coagulation mechanisms of a concentrated casein suspension as observed by PFG-NMR diffusion measurements. *Food Hydrocolloids, 27*(2), 456-463.

Lucey, J. A., Srinivasan, M., Singh, H., & Munro, P. A. (2000). Characterization of commercial and experimental sodium caseinates by multiangle laser light scattering and size-exclusion chromatography. *Journal of Agricultural and Food Chemistry, 48*(5), 1610-1616.

Marchin, S., Putaux, J.-L., Pignon, F., & Leonil, J. (2007). Effects of the environmental factors on the casein micelle structure studied by cryo transmission electron microscopy and small-angle x-ray scattering/ultrasmall-angle x-ray scattering. *Journal of Chemical Physics, 126*(4), 45101.

Mariette, F., Topgaard, D., Jonsson, B., & Soderman, O. (2002). ^{1}H NMR diffusometry study of water in casein dispersions and gels. *Journal of Agricultural and Food Chemistry, 50*(15), 4295-4302.

McMahon, D. J., & McManus, W. R. (1998). Rethinking casein micelle structure using electron microscopy. *Journal of Dairy Science, 81*(11), 2985-2993.

McMahon, D. J., & Oommen, B. S. (2008). Supramolecular structure of the casein micelle. *Journal of Dairy Science, 91*(5), 1709-1721.

Morris, G. A., Foster, T. J., & Harding, S. E. (2000). Further observations on the size, shape, and hydration of casein micelles from novel analytical ultracentrifuge and capillary viscometry approaches. *Biomacromolecules, 1*(4), 764-767.

Nash, W., Pinder, D. N., Hemar, Y., & Singh, H. (2002). Dynamic light scattering investigation of sodium caseinate and xanthan mixtures. *International Journal of Biological Macromolecules, 30*(5), 269-271.

Panouille, M., Benyahia, L., Durand, D., & Nicolai, T. (2005). Dynamic mechanical properties of suspensions of micellar casein particles. *Journal of Colloid and Interface Science, 287*(2), 468-475.

Pitkowski, A. (2007). *Processus de gelification des caseines en presence de polyphosphates.* PHD thesis, University of Le Mans

Pitkowski, A., Durand, D., & Nicolai, T. (2008). Structure and dynamical mechanical properties of suspensions of sodium caseinate. *Journal of Colloid and Interface Science, 326*(1), 96-102.

Price, W. S. (1997). Pulsed-field gradient nuclear magnetic resonance as a tool for studying translational diffusion: Part 1. Basic theory. *Concepts in Magnetic Resonance, 9*(5), 299-336.

Radford, S. J., & Dickinson, E. (2004). Depletion flocculation of caseinate-stabilised emulsions: what is the optimum size of the non-adsorbed protein nano-particles? *Colloids and Surfaces A Physicochemical and Engineering Aspects, 238*(1), 71-81.

Sandra, S., Alexander, M., & Dalgleish, D. G. (2007). The rennet coagulation mechanism of skim milk as observed by transmission diffusing wave spectroscopy. *Journal of Colloid and Interface Science, 308*(2), 364-373.

Saxton, M. J. (1987). Lateral diffusion in an archipelago. The effect of mobile obstacles. *Biophysical Journal, 52*(6), 989-997.

Speedy, R. J. (1987). Diffusion in the hard-sphere fluid. *Molecular Physics, 62*(2), 509-515.

Stothart, P. H., & Cebula, D. J. (1982). Small-angle neutron scattering study of bovine casein micelles and sub-micelles. *Journal of Molecular Biology, 160*(2), 391-395.

Tan, H. L., & McGrath, K. M. (2010). The microstructural and rheological properties of Na-caseinate dispersions. *Journal of Colloid and Interface Science, 342*(2), 399-406.

Tremmel, I. G., Kirchhoff, H., Weis, E., & Farquhar, G. D. (2003). Dependence of plastoquinol diffusion on the shape, size, and density of integral thylakoid proteins. *Biochimica et Biophysica Acta-Bioenergetics, 1607*(2-3), 97-109.

Walstra, P. (1979). Voluminosity of bovine casein micelles and some of its implications. *Journal of Dairy Research, 46*(2), 317-323.

Chapter IV: Effects of probe flexibility and size

Publication n°2: Probe mobility in native phosphocaseinate suspensions and in a concentrated rennet gel: effects of probe flexibility and size

Probe mobility in native phosphocaseinate suspensions and in a concentrated rennet gel: effects of probe flexibility and size

*Souad Salami[1,2], Corinne Rondeau-Mouro[1,2], John van Duynhoven[3,4] and François Mariette[1,2]**

[1] Irstea, UR TERE, 17 avenue de Cucillé, CS 64427, F-35044 Rennes, France

[2] Université européenne de Bretagne, France

[3]Unilever R&D, Olivier van Noortlaan 120 P.O. Box 3130AC Vlaardingen The Netherlands

[4] Laboratory of Biophysics, Wageningen University, Dreijenlaan 3, 6703HA, Wageningen, The Netherlands

* Corresponding author: François Mariette, Irstea, UR TERE, CS 64426, 17 avenue de Cucillé, 35044 Rennes, Cedex, France Tel: 33 (0)223482121; fax: 33(0)223482115.

E-mail address: Francois.Mariette@irstea.fr

Abstract

Pulsed field gradient nuclear magnetic resonance and proton nuclear magnetic resonance relaxometry were used to study the self-diffusion coefficients and molecular dynamics of linear (PEGs) and spherical probes (dendrimers) in native phosphocaseinate suspensions and in a concentrated rennet gel. It was shown that both the size and shape of the diffusing molecules and the matrix topography impacted on the diffusion and relaxation rates. In suspensions, both translational and rotational diffusion decreased with increasing casein concentrations due to increased restriction in the freedom of motion. Rotational diffusion was, however, less hindered than translational diffusion. After coagulation, translational diffusion increased but rotational diffusion decreased. Analysis of the T_2 relaxation times obtained for probes of different sizes distinguished the free short-chain relaxation formed from a few monomeric units from (i) the relaxation of protons attached to long polymer chains and (ii) the short-chain relaxation attached to a rigid dendrimer core.

Keywords: PEG, dendrimer, NPC, rennet gel, diffusion, relaxation

Introduction

Caseins, a group of unique milk-specific, acid-insoluble phosphoproteins, represent around 80% of the total proteins in the milk of cattle and other commercial dairy species[1]. They are directly involved in the formation of dairy gels as they constitute the building blocks of the network. Most caseins in milk (94%) exist as large colloidal particles suspended in the aqueous phase. They are 50-600 nm in diameter (mean ≈150 nm) and called "casein micelles"[1], which are very porous, highly hydrated and sponge-like colloidal particles containing about 3.2g H_2O/g protein[2]. Due to their commercial importance and extensive use in dairy products (such as cheese and yogurt), casein suspensions and gels have been extensively studied.

Molecular diffusion in dairy systems and in models of dairy systems has been studied by the use of techniques such as diffusion wave spectroscopy (DWS), multiple particle tracking (MPT), fluorescence recovery after photobleaching (FRAP) and pulsed field gradient NMR diffusometry. For example, DWS has been used to monitor the diffusion of casein particles during the acidification[3-4] and renneting[5-9] of undiluted skim milk. Multiple particle tracking has been used in an attempt to probe heterogeneity of acid milk gels and the microrheological properties of the protein network and aqueous phase voids, in the presence and absence of pectin, during and after gelation[10]. The sol-gel transition of a sodium caseinate solution undergoing gelation by acidification has also been studied by particle tracking. The Brownian diffusion of fluorescent microspheres with different surface coatings was used to probe spatial mechanical properties of the gels at the scale of microns[11]. Floury et al.[12] have recently used the fluorescence recovery after photobleaching (FRAP) technique to measure in situ and at the microscopic scale the diffusion of FITC-dextran in a cheese model.

Several PFG-NMR self-diffusion studies have been performed on casein systems in which the self-diffusion coefficients of casein particles and polyethylene glycols (PEGs) of different molecular weights were measured at the micrometer scale for different casein concentrations. The diffusion behavior was related to the structure and dynamics of the casein matrix investigated. For example, Colsenet et al.[13] and Le Feunteun et al.[14-16] studied the effects of casein concentration and PEG size on the diffusion coefficients of PEGs in native phosphocaseinate (NPC) suspensions and gels. PEG diffusion coefficients were found to be dependent on both casein concentration and PEG size. The effects of the gel structure on PEG diffusion were also

studied by these authors. It was found that the diffusion rates of large poly-ethylene glycol (PEG) probes were enhanced after coagulation and that the rate of increase was dependent on the final gel microstructure. However, in all the studies quoted above[13-14], the diffusion of a molecule was measured at equilibrium, before and after perturbation of the system. In previous studuies, Le Feunteun et al.[15-16] reported on the time change of the self-diffusivity of a small and a large PEG probes in a casein system during rennet-induced, acid-induced and combined coagulation of a concentrated casein suspension, with the aim of investigating the structural changes taking place in the solution during coagulation. In another study[17], Le Feunteun at al. monitored the diffusion of casein particles during the renneting of a concentrated casein micelle suspension (14% w/w). This study showed that the self-diffusion of both casein particles and soluble caseins can be determined simultaneously, and explained how their evolution can be related to key stages of the coagulation process. In a previous study[18], we investigated the effects of casein structure on the diffusion behavior of PEG probes. The latter was studied in NPC and sodium caseinate (SC) suspensions where caseins are not structured into micelles but form self-assembled aggregates of 11 nm in radius. Two drastically different PEG diffusion behaviors were obtained in relation to differences in casein obstacle size (inter-particle distance) and mobility between the two casein systems. The latter was studied in NPC and SC systems by measuring the casein self-diffusion coefficients in relation to casein concentration. Casein particles were found to behave as non-interacting hard spheres in a fluid, and their self-diffusion was inversely proportional to the solution viscosity measured macroscopically, up to a casein concentration that matched the onset of random close packing of the two casein systems (15 g/100g H_2O and 10 g/100g H_2O for NPC and SC systems, respectively). At higher concentrations, there was another regime (soft spheres) in which casein micelles and casein submicelles deformed, deswelled and interpenetrated as the casein concentration increased.

Another important factor affecting the diffusion process is the shape of the diffusion molecules. For example, Wang et al.[19] have shown that star polymers, with a hydrophobic cholane core and four PEG arms, have a lower self-diffusion coefficient than linear PEGs at an equivalent hydrodynamic radius in PVA gels. In aqueous solutions of poly-vinyl alcohol (PVA), a cyclic poly-ethylene oxide (PEO) of a lower molecular weight (M_n=6000) was found to have almost the same self-diffusion coefficients as linear PEO of a higher molecular weight (M_n=10,000)[20]. This issue has not previously been explored in casein systems. In fact, the probes used to investigate

casein systems have to date been polyethylene-glycol (PEG) polymers. The advantages of this type of polymer are the absence of interaction with proteins, excellent NMR sensitivity and a low polydispersity index. However, these polymers are easily deformable and can change their shape according to their environment. They can therefore diffuse through small spaces compared to their hydrodynamic diameter by adopting a more elongated conformation, which considerably complicates the interpretation of the diffusion results obtained in NPC suspensions. A preferred experimental design would therefore be to follow the diffusion of hard sphere probe particles through the matrix. Since it is difficult to obtain NMR signals from solid particles, flexible polymers with low molecular size polydispersity are used as probes instead. However, in more recent years there has been greater interest in the use of dendrimer probes as diffusional probes[21-23]. Dendrimers, also known as starburst polymers, are spherical macromolecules and a class of regularly branched mono-dispersed polymers[24]. Dendrimer architecture consists of three domains: (1) the core, which can be a single atom or group of atoms, (2) branch units, which divide radially grown concentric layers termed generations, and (3) functional surface groups, which play a key role in determining the properties. Unlike classical polymers, dendrimers have a high degree of molecular uniformity, narrow molecular weight distribution, specific size and shape characteristics, and a highly-functionalized terminal surface[24]. Dendrimer polymers are molecules of choice because of the good control of their molecular size and shape.

The purpose of the study presented here was to elucidate the effects of the shape and size of probes on their mobility in NPC suspensions and rennet casein gels. The translational and rotational diffusion of spherical dendrimer probes were therefore measured for the first time and compared with those of flexible PEG probes in NPC suspensions and in a concentrated rennet casein gel (15 g /100 g H_2O) using NMR diffusometry and NMR relaxometry. The advantage of coupling the two NMR methods was to probe the matrix at two different length scales. Moreover, both static and real-time NMR measurements were undertaken in this study and were performed at a casein gel concentration of 15 g/ 100 g H_2O where casein micelles can be considered as hard spheres with no deformation of their shape.

Experimental

Materials. Native phosphocaseinate powder was prepared in the INRA laboratory (Rennes). The detailed composition of this powder has already been described in reference[18]. PEGs of different molecular weights M_w (615, 7920, 21300, 32530 and 93000 g/mol) and low polydispersity indices (M_w/M_n= 1.07, 1.04, 1.06, 1.06 and 1.06, respectively) were obtained from Varian Laboratories. Monodisperse polyamido-amine dendrimers with an ethylene diamine core and poly-ethylene glycol (PEG) as surface group were purchased from Dendritic Nanotechnologies Inc.(USA). Five different generations (G2 (DNT-315), G3 (DNT-316), G4 (DNT-317), G5 (DNT-318), G6 (DNT-319)) were used. Sodium azide (Merck, Darmstadt, Germany) and sodium chloride (Sigma-Aldrich, Steinheim, Germany) with purity above 99% were used without purification. The chymosin solution used was Chymax-Plus purchased from Chr-Hansen (Arpajon, Frnace).

Preparation of dispersions. Casein suspensions were prepared according to the protocol described in reference[18]. The solutions were studied without adjustment of pH, the latter was ranging from 7.1 at 2.95 g/100g H_2O to 6.9 at 29.05 g/100g H_2O.

Enzymatic coagulation. All casein gels contained 15.31 g of casein to 100 g of H_2O. For static diffusion measurements, casein gels were induced by addition of 4 µL of chymosin in 10 g of NPC suspension. NMR tubes were placed in a water bath for 2 h at 30°C and measurements were carried out 24 h after inoculation. No gel shrinkage occurred within this interval. For real-time diffusion measurements, a chymosin dilution (1 ml in 99.0 g of distilled water) was added at time t=0 s to the casein suspension (70 µL for 10 g of NPC suspension). The solution was then vigorously stirred for 3 minutes. Samples were then rapidly prepared for NMR and dynamic rheological measurements. No shrinkage of the gel was observed during the time scale of the experiments.

Dynamic light scattering. Dynamic light scattering measurements were performed on a Malvern Zetasizer Nano ZS instrument (Malvern Instruments, Worcestershire, UK). Size distribution of particles in solutions were obtained by measuring the light scattered by particles illuminated with a laser beam (scattering angle=173°, T=20°C) using the NNLS analysis method. The data measured were reported in lognormal intensity distribution.

Rheology.

- **Flow measurements.** Flow measurements were performed with a contrives Low-Shear 30 viscometer (Ruislip, United Kingdom). The instrument was operated using a Couette geometry with inner and outer radii of 5.5 and 6 mm, respectively. All rheological experiments were performed at a fixed temperature of 20°C. Measurements were repeated twice, showing very good reproducibility (within ± 10%).

- **Dynamic rheological measurements.** The viscoelastic properties of the enzymatic gels were studied with a TA instruments AR2000 rheometer (Guyancourt, France) using a cone and plate geometry (Diameter 4 cm and angle 2°). Throughout the measurements, the temperature was maintained at 20°C and the sample was covered with a film of mineral oil to prevent evaporation. The storage modulus (G') and the loss modulus (G'') were recorded at a frequency of 1 Hz and the rheometer was programed to adjust the stress automatically to provide a strain of 0.1%, which was found to be within the linear viscoelastic region of the sample.

NMR measurements. All NMR measurements were performed on a 500 MHz spectrometer (Bruker Wissembourg, France) equipped with a dedicated field gradient probe (DIFF30 from Bruker, Wissembourg, France) with a static gradient strength of 1200 (±0.2) G/cm for an amplifier output of 40A. NMR tubes (5 mm) were used and all NMR measurements were performed at 20°C.

A stimulated echo sequence using bipolar gradients (STE-BPP) and a 3-9-19 WATERGATE pulse scheme to suppress the water signal was used to measure self-diffusion coefficients. Diffusion coefficients were obtained using:

$$I(\delta,\Delta,g) = I_0 \exp\left[-\gamma^2 g^2 \delta^2 \left(\Delta - \frac{\delta}{3} - \frac{\tau}{4}\right) D\right] \quad (1)$$

where I(δ, Δ,g) and I_0 are the echo intensities in the presence of gradient pulses of strength g and the absence of gradient pulses, respectively, γ the gyromagnetic ratio (for protons, $\gamma = 26.7520 \times 10^7$ rad.T^{-1} .s^{-1}), g the amplitude of the gradient pulse, δ gradient pulse duration, Δ the time between the leading edges of gradient pulses, τ the time between the end of each gradient and the

next radiofrequency pulse, and D the self-diffusion coefficient. Diffusion experiments were carried out with 32 different values of g, ranging from 20 to 900 G/cm, with δ = 1ms. Sixteen scans were carried out and the recycle delay was set at 5 T_1. Depending on the molecular weight of the probe studied, Δ was adjusted to obtain a diffusion distance z ~1.5 µm in the casein suspensions, in accordance with the Einstein equation $z = (2 \Delta D_{Probe})^{1/2}$. This procedure enabled molecular probes to cover much greater distances than the casein micelle diameter.

All the data processing was performed with Table Curve software (Ritme, Paris).

The Carr Purcell Meiboom Gill (CPMG) sequence, coupled with a presaturation pulse scheme for water proton signal suppression, was used to measure relaxation times (T_2) of the ethoxylate methylene moieties at a chemical shift of 3.6 ppm. The relaxation decay curve for all probes was fitted accurately with a single exponential function:

$$I(2\tau) = I \exp\left[-\left(\frac{2\tau}{T_2}\right)\right] \quad (2)$$

where $I(2\tau)$ is the intensity of the NMR signal given at τ, I the intensity at equilibrium for τ=0, and T_2 the spin-spin relaxation time. T_2 measurements were undertaken with a τ-value (time between 90° and 180° pulse) of 1 ms. Sixteen data points were acquired for each CPMG with 16 scan repetitions, and recycle delay was set at 5 T_1.

The standard error in both probe self-diffusion coefficients and spin-spin relaxation times, estimated by the fitting procedure, was below 0.2%.

Normalization of diffusion coefficients and relaxation times. The effects of the soluble powder residues on probe self-diffusion were calculated according to the approach described in references 14 and 15. All the findings discussed in this paper are thus reduced self-diffusion coefficients defined as: $D_r=D/D_0$, where D is the probe self-diffusion coefficient measured in the suspension or the gel and D_0 is the probe self-diffusion coefficient measured in the serum phase extracted from NPC suspensions. Similarly, the reduced T_2 relaxation times calculated in suspensions were equal to the T_2 values obtained in NPC suspensions divided by those obtained in the serum phase.

Results

Dynamic light scattering

The size distribution of a native phosphocaseinate solution (3g/100g water + 0.1M NaCl) as determined from dynamic light scattering, presented as a single broad population distribution with casein particles from ~ 68 to ~ 459 nm in diameter (**Figure I**). The average casein micelle diameter was 187 nm. These results were in very good agreement with values already reported by several authors[25-27]. As shown in **Figure I**, the same casein size distribution was obtained in the presence of 0.1% w/w of G6 dendrimer.

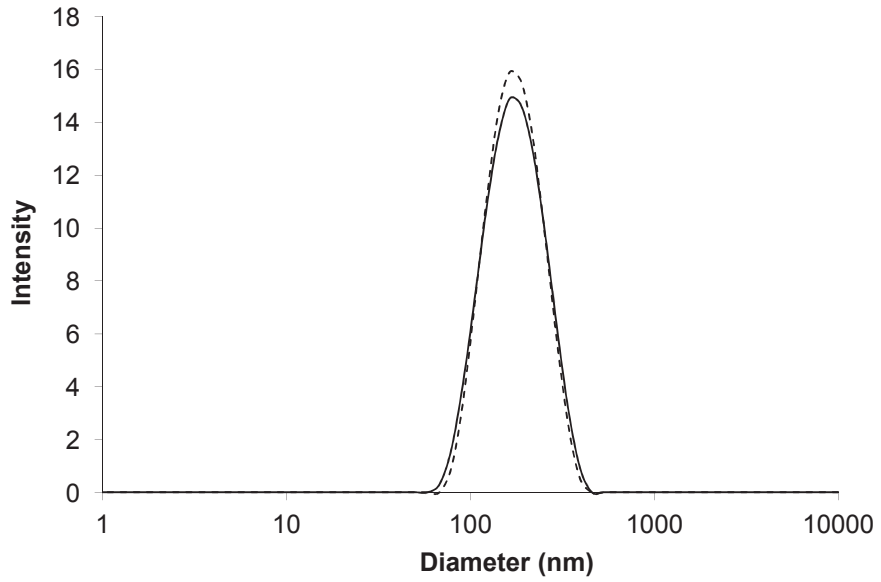

Figure I. Lognormal particle size distribution for a NPC solution in the presence (solid line) and absence (dotted line) of G6 dendrimer.

Rheology

- **Flow measurements:**

Figure II shows the shear rate dependence of the apparent viscosity for casein micelle (NPC) dispersions in H_2O/NaCl with casein concentrations of 3 and 15 g/100 g H_2O. The diluted NPC

dispersion (3 g/100 g H_2O) behaved as a Newtonian fluid over the range of shear rates investigated. At high casein concentrations, shear thinning occurred.

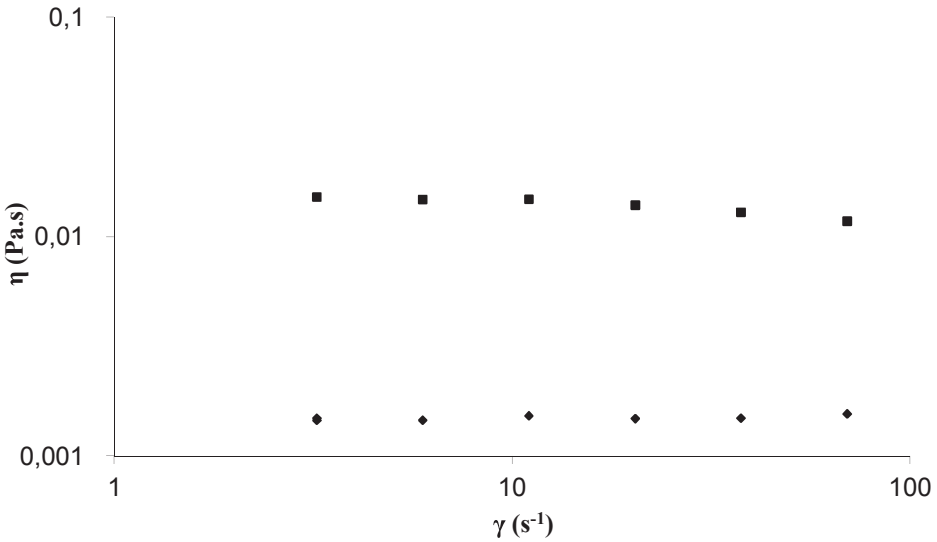

Figure II. Shear rate dependence of apparent viscosity for NPC dispersions in H_2O+NaCl without adding any probes (PEG or dendrimer). Casein concentration from top to bottom: 15 and 3 g/100g H_2O.

Viscosity values measured for the two NPC dispersions (3 and 15 g/100g H_2O) in the presence and absence of 615 g/mol PEG, and G2 and G6 dendrimers are given in **Table I**. The viscosity values for the concentrated dispersion (15g/100g H_2O) were measured at a shear rate of $3s^{-1}$. In agreement with previous studies[28], the viscosity of NPC solutions increased from 1.52 to 15 mPa s with increasing casein concentration from 3 to 15 g/100g water. The same viscosity values were obtained in the presence of 0.1% w/w of 615 g/mol PEG, G2 and G6 dendrimers, irrespective of casein concentration.

Sample	Viscosity (mPa s)/*shear rate=3s-1*
NPC (3g/100g H_2O)	1.52
NPC (3g/100g H_2O) + 615	1.51
NPC (3g/100g H_2O) + G2	1.54
NPC (3g/100g H_2O) + G6	1.53
NPC (15g/100g H_2O)	15.1

NPC (15g/100g H_2O) + 615	15.1
NPC (15g/100g H_2O) + G2	14.9
NPC (15g/100g H_2O) + G6	15

Table I. Viscosity of NPC dispersions (3 and 15g/100g H_2O) in the presence and absence of probes (615, G2 and G6) at shear rate of $3s^{-1}$.

- **Dynamic storage modulus and phase angle**

Figure III presents a typical plot of the storage modulus (G'), the loss modulus (G") and the phase angle (δ) according to reaction time during the slow gel-forming process in the presence and absence of a G6 dendrimer.

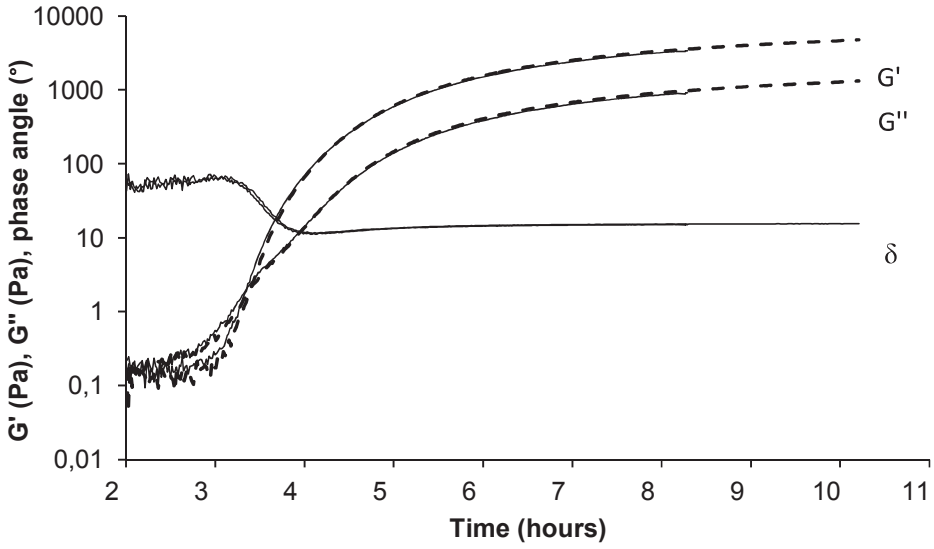

Figure III. Evolution of storage modulus (G'), loss modulus (G") and phase angle (δ) according to time after addition of chymosin in the presence (dashed line) and absence (solid line) of a G6 dendrimer.

The time at which G' and G" are equal is often used to define the "gel time" parameter. In this study, it was found to be t_{gel}= 3 h 20 min in the presence and absence of a G6 dendrimer. This indicates that the addition of low concentrations (0.1% w/w) of dendrimer has no effect on the

formation of the casein network. G' and G" continued to increase after the sol-gel transition. This indicated an increase in the gel stiffness through reorganization of the gel structure.

Diffusion and relaxation by NMR

Self-diffusion and relaxation of probe in water

^{1}H NMR T_2 relaxation times and the self-diffusion coefficients of dendrimers and PEGs in water/0.1M NaCl are presented in **Table II**. The ^{1}H NMR T_2 relaxation times pertain to the ethoxylate methylene moieties at a chemical shift of 3.6 ppm. The hydrodynamic radius of the probes was calculated from the D values using the Stokes-Einstein equation:

$$R_h = \frac{k_B T}{6\pi\eta D} \quad (4)$$

Where T is the temperature in kelvin, k_B the Boltzman constant (1.38 x 10^{-23} JK^{-1}) and η the viscosity of the aqueous phase (1x10^{-3} Pa at 20°C).

A

	D (m^2s^{-1})	R_h (nm)	T_2 (s)
G2	7.54e-11	2.84	0.485
G3	6.10e-11	3.51	0.450
G4	4.87e-11	4.40	
G5	4.16e-11	5.16	0.385
G6	3.42e-11	6.27	0.338

B

PEGs	D (m^2s^{-1})	R_h (nm)	T_2 (s)
615	2.7e-10	0.79	0.620
7920	6.77e-11	3.16	0.528
21300	3.99e-11	5.37	0.524
32530	3.06e-11	7	0.522
93000	1.62e-11	13.22	0.518

Table II. ^{1}H NMR T_2 relaxation times, self-diffusion coefficients and the corresponding hydrodynamic radii of different dendrimer generations (A) and PEG molecular weights (B). Data obtained from NMR diffusion measurements in a H_2O/NaCl solution (0.1 M) at 20°C.

Based on these results, and for clarity, PEG-dendrimer trios and couples with similar hydrodynamic radii could be recognized: (i) 7920/G2;G3 (ii) 21300/G5 (iii) 32530/G6. For the sake of simplicity, PEG and dendrimers will be called as G_X and PEG_X in the next sections, with X being equal to the hydrodynamic radius of these diffusional probes.

As seen in **Table II**, T_2 relaxation times decreased from 0.485 to 0.338 s with increasing dendrimer molecular weights (M_w) from 12628 (G2) to 207988 (G6) g/mol. T_2 relaxation times for PEGs were longer and decreased from 0.620 to 0.528 s with increasing PEG molecular weights from 615 to 7920 g/mol. However, when M_w exceeded 7920 g/mol, T_2 values exhibited minor variations, in the order of 12 ms or less.

PEG and dendrimers reduced self-diffusion in NPC suspensions and gels

The self-diffusion coefficients of a PEG/dendrimer trio and a PEG/dendrimer couple having similar hydrodynamic radii ((i) $PEG_{3.16}$ vs $G_{2.84}$ and $G_{3.51}$ (ii) PEG_7 vs $G_{6.27}$) were measured at 20° C in NPC suspensions, with casein concentrations ranging from 3 to 29 g/100g of water, and in a concentrated casein gel with a casein concentration of 15 g/100g H_2O (**Figure IV**). The absence of restricted diffusion (in suspensions and gels), at the length-scale studied (~1.5 µm), was verified for PEGs and dendrimers by varying the diffusion delay corresponding to a diffusion distance of between 0.3 and 2.4 µm in suspensions and 0.58 and 4.07 µm in gels. No variation in the diffusion coefficient measured occurred (data not shown).

A

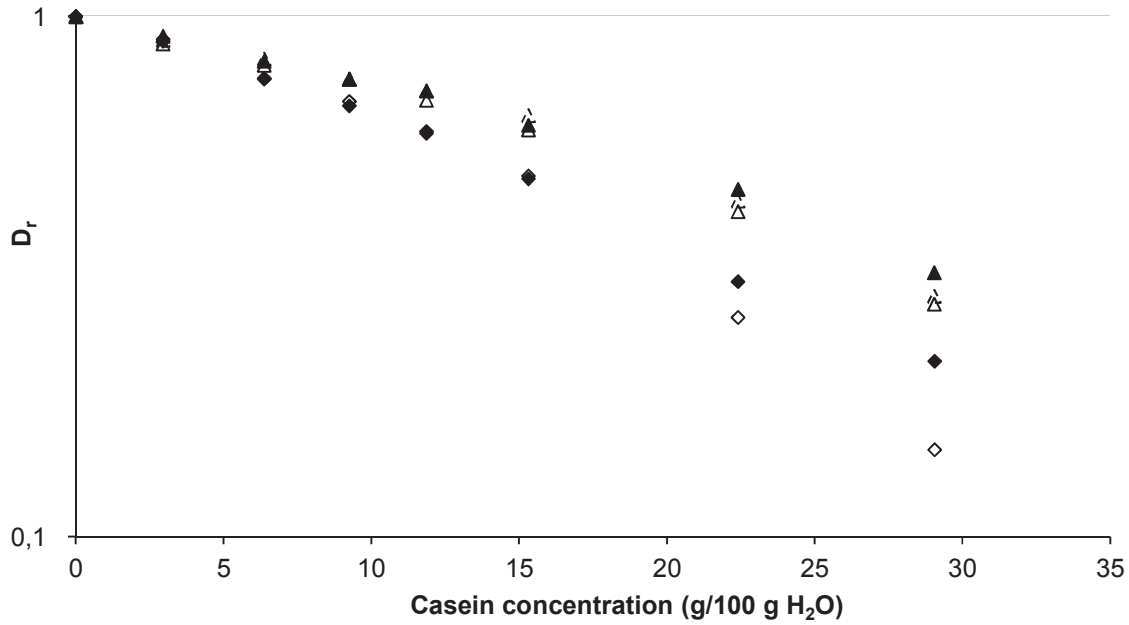

B

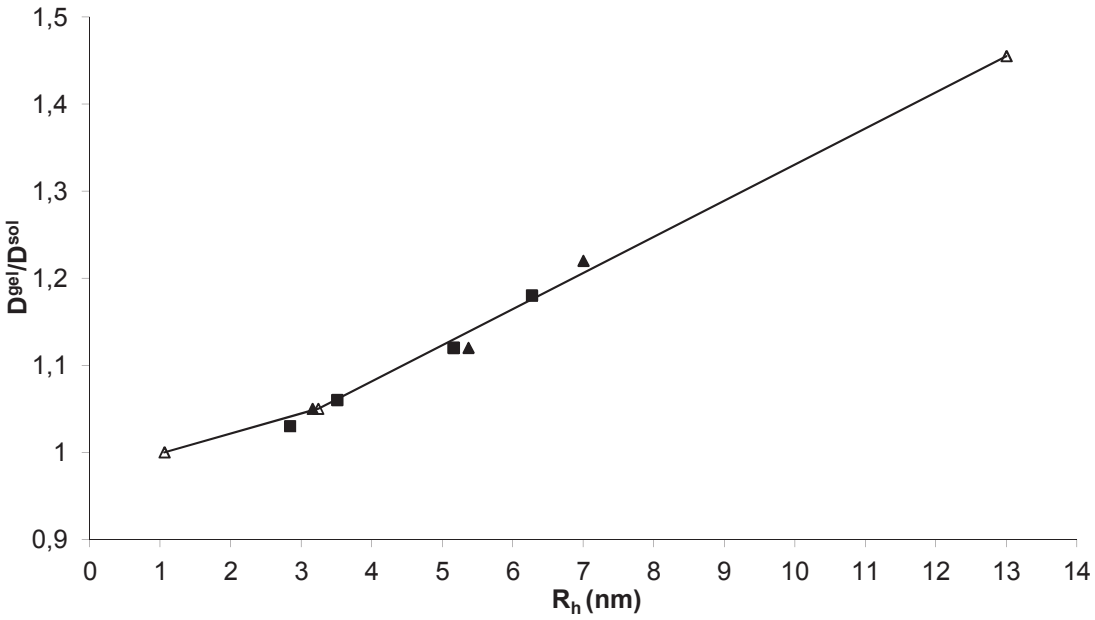

Figure IV. (A) Comparison of reduced self-diffusion coefficients of $PEG_{3.16}$ (▲)/PEG_7 (♦) and $G_{2.84}$ (⁂); $G_{3.51}$ (Δ)/$G_{6.27}$ (◊) dendrimers in relation to casein concentrations in NPC suspensions.

(B) D^{gel}/D^{sol} ratios obtained for PEGs (▲) and dendrimers (■) of various sizes in a concentrated rennet gel (15 g/100 g H_2O). Empty triangles (Δ) correspond to previously reported data[14-15] obtained in rennet casein gels prepared at the same casein concentration.

Probe self-diffusion coefficients were found to be dependent on both casein concentration and their own size; the probe diffusion decreased with increasing casein concentrations, and the probe self-diffusion reduced with size for a given concentration. This effect was observed for PEG as well as for dendrimer probes. The reduction in diffusion coefficients was greater for larger probes, giving D_r~ 0.61 and 0.49 for $PEG_{3.16}$,$G_{2.84}$;$G_{3.51}$ and PEG_7,$G_{6.27}$, respectively, at a casein concentration of 15 g/100g H_2O. However, at higher casein concentrations, the diffusion coefficient was smaller for dendrimers compared to PEGs despite the fact that the probes were of similar size. For example, at a casein concentration of 29 g/100g H_2O, the D_r of a 6.27 nm sized dendrimer and a 7 nm sized PEG ($G_{6.27}$ dendrimer and PEG_7) were 0.14 and 0.22, respectively. This highlights the effects of probe shape and flexibility on self-diffusion behavior.

After coagulation, the self-diffusion of PEG and dendrimer couples with similar R_h increased in the same manner. For the small probes (R_h ~ 3 nm), the increase was not very significant and hence the rennet coagulation had no influence on the diffusion of small probes. However, for the four largest probes (R_h ~ 5-7 nm), the effects of coagulation were greater as the size of the probe became larger. All these findings were in very good agreement with those already reported by Le Feunteun et al.[14] who studied the effects of coagulation on the diffusion of PEG probes with hydrodynamic radii of 0.8, 3.24 and 13.3 nm (**Figure IV (B)**).

PEG and dendrimer ^{1}H NMR T_2 relaxation times in NPC suspensions and gels

In parallel to self-diffusion measurements, ^{1}H NMR T_2 relaxation times were measured for each of the probes in casein suspensions with casein concentrations ranging from 3 to 22 g/100g of water. **Figure V** and **Figure VI** illustrate the dependence of the relaxation times on casein concentration and the molecular size of the probe. **Figure V (A)** and **Figure VI (A)** show that: (i) Probe ^{1}H NMR T_2 relaxation times decreased with increasing casein concentrations: the values obtained varied between 0.62 and 0.21 s for PEGs and between 0.48 and 0.18 s for dendrimers,

depending on the casein concentration and the molecular size of the probe and (ii) PEGs and dendrimers did not show a similar decreasing relaxation trend. In the case of dendrimers, T_2 relaxation followed a similar decreasing trend whatever the generation. All data collapsed onto a master curve when the reduced relaxation time was plotted as a function of casein concentration (**Figure VI (A)**). In the case of PEG probes, however, different decreasing curves were obtained depending on the molecular weight of the probe. It can clearly be seen on **Figure V (B)** and **Figure VI (B)** that two domains of chain dynamics could be determined for PEGs, while linear variations occurred for dendrimers. The crossover between the two domains labeled I and II occurred when the PEG molecular weight was about 7920 g/mol. Within the first domain, as for dendrimers, the PEG relaxation rates measured in NPC suspensions for different casein concentrations were similarly dependent on molecular weight. In contrast, the relaxation rates behaved very differently in domain II (below 7920 g/mol). At zero casein concentration and in the diluted casein system (2.95 g/100g H_2O), T_2 was almost independent of the PEG chain length, but became dependent when casein concentrations increased. A clear double break behavior was also visible for the casein concentrations greater than 12 g/100 g H_2O. Intersection of the straight line was observed at M_w=32530 g/mol.

On the other hand, ^{1}H NMR T_2 relaxation times surprisingly decreased after coagulation (**Figure V (A)** and **Figure VI (A)**), reflecting reduced rotational probe mobility in casein gels. The dependence of the relaxation times on the molecular weights of dendrimers and PEGs in the concentrated casein suspension and the rennet gel is illustrated in **Figure VII**. For dendrimer probes, T_2 relaxation times varied with increasing dendrimer molecular weight from 0.376 to 0.245 s in the casein suspension and from 0.206 to 0.160 s in the gel. For PEG probes, T_2 relaxation times varied from 0.390 s to 0.315 s in the casein suspension with increasing PEG molecular weight from 7920 to 32530. However, in the rennet gel, T_2 hardly varied (less than 10 ms) when the PEG molecular weight increased from 7920 to 32530 g/mol.

A

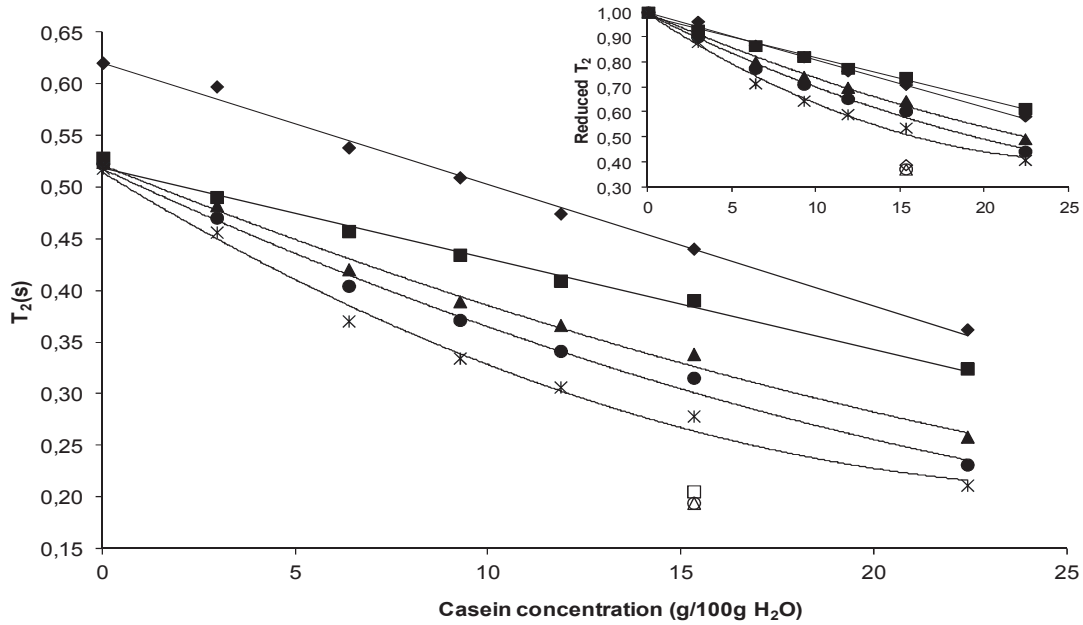

B

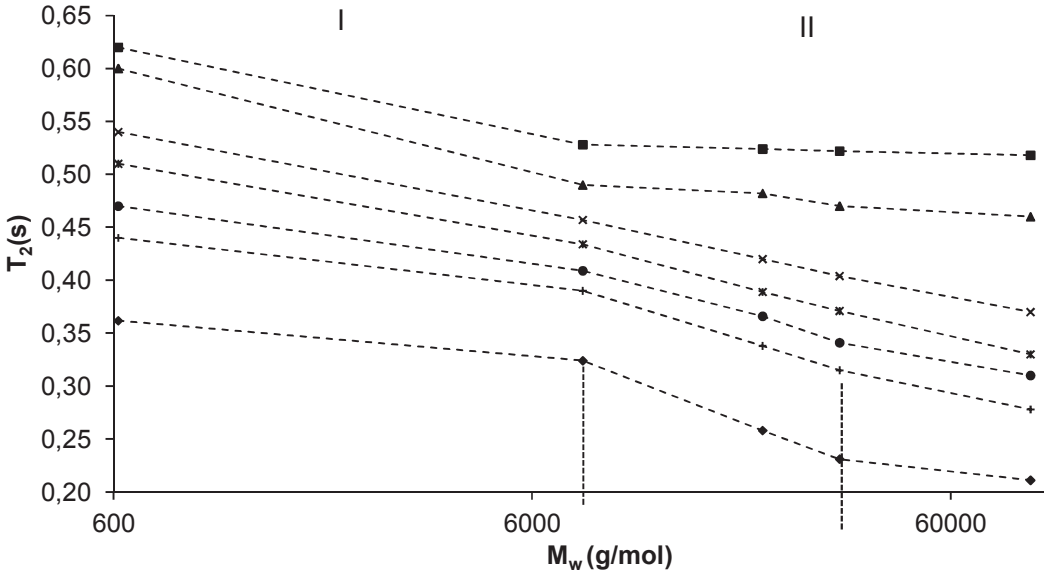

Figure V. (A) Relaxation time T_2 of PEGs as a function of casein concentrations in NPC suspensions. PEG probes from top to bottom: 615, 7920, 21300, 32530 and 93000 g/mol. Reduced T_2 relaxation times are shown in the insert panel. Solid lines are guides for the eyes.

Empty shapes correspond to the relaxation time T_2 obtained for the 7920 (□), 21300 (Δ) and 32530 (○) g/mol PEGs in the concentrated casein gel (15 g/100g H_2O) (B) Molecular weight dependence of the PEGs transverse relaxation time for various casein concentrations (from top to bottom): 0, 2.88, 6.43, 9.22, 11.86, 15.35 and 22.4 g/100g H_2O.

A

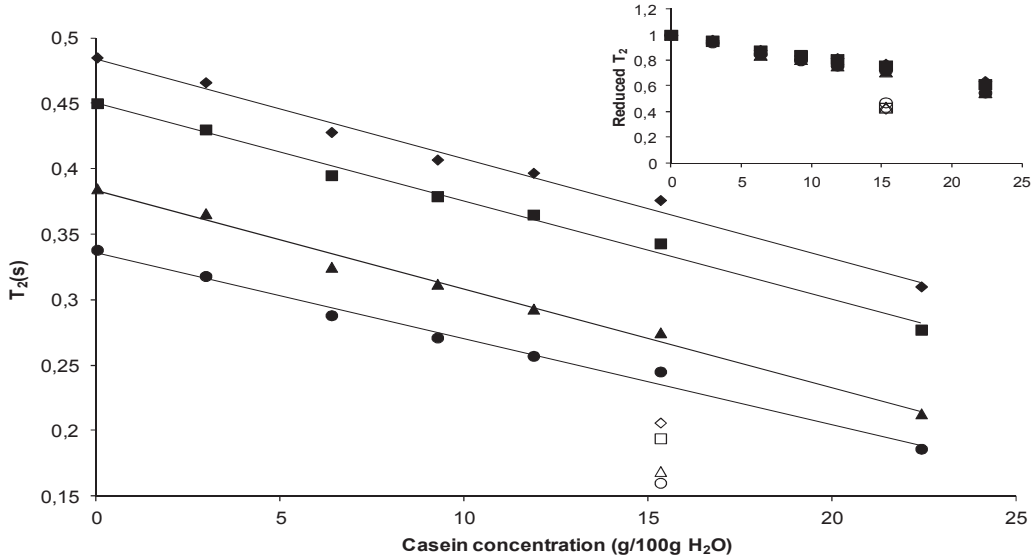

B

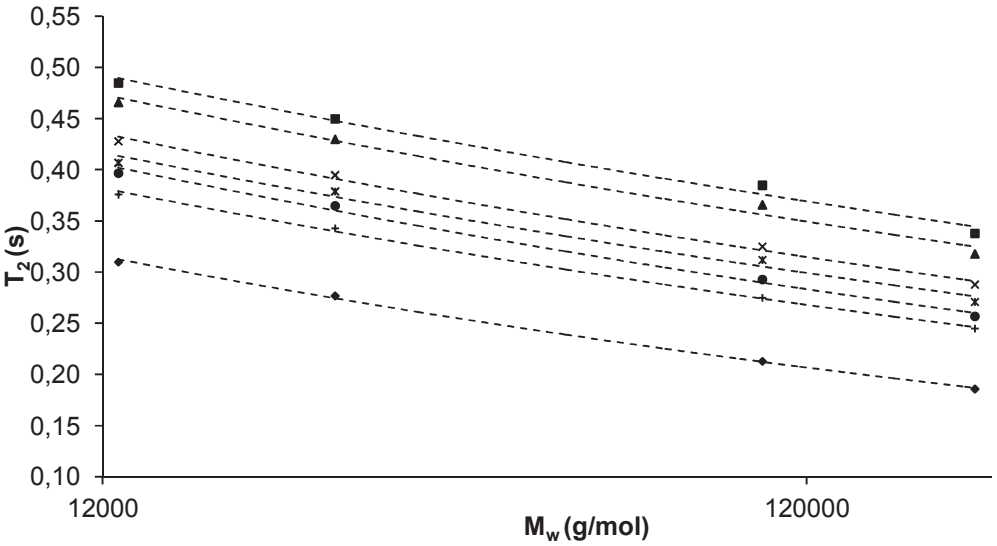

Figure VI. (A) Relaxation time T_2 of dendrimers as a function of casein concentrations in NPC suspensions. Dendrimers from top to bottom: G2, G3, G5 and G6. Reduced T_2 relaxation times are shown in the insert panel. Solid lines are guides for the eyes. Empty shapes correspond to the relaxation time T_2 obtained for the G2 (◊), G3 (□) and G5 (Δ) and G6 (○) dendrimers in the concentrated casein gel (15 g/100g H_2O) (B) Molecular weight dependence of the dendrimers transverse relaxation time for various casein concentrations (from top to bottom): 0, 2.88, 6.43, 9.22, 11.86, 15.35 and 22.4 g/100g H_2O.

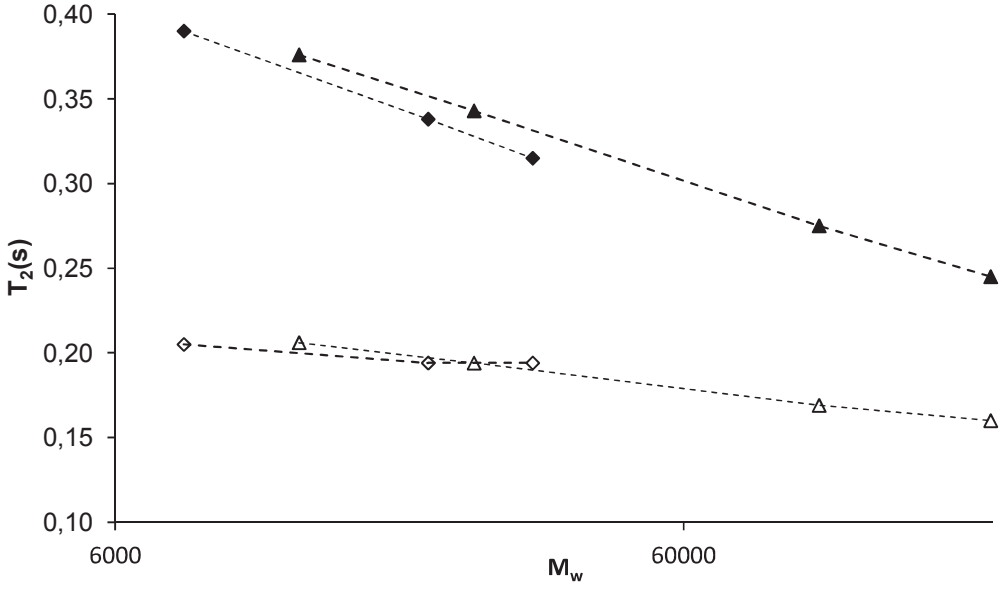

Figure VII. Molecular weight dependence of PEG (diamond) and dendrimer (triangle) transverse relaxation times in the concentrated casein suspension (solid shapes) and the gel (empty shapes) with a casein concentration of 15 g/100g H_2O.

To obtain greater understanding of the impact of structural changes in the casein matrix on probe mobility during coagulation, we monitored the self-diffusion coefficients and the relaxation rates of the G6 dendrimer during renneting of the concentrated casein micelle suspension. This revealed how and when probe diffusion and relaxation times varied during the coagulation induced by chymosin action. As shown in **Figure VIII**, relaxation of the G6 dendrimer remained stable during the first stage of coagulation, i.e. the enzymatic phase. Immediately after the

aggregation of the resulting para-casein micelles (gel formation), relaxation decreased rapidly and continued to decrease gradually throughout the experiment until it stabilized after approximately 20 h. However, diffusion of the G6 dendrimer was unaffected by the first two stages of coagulation, i.e. the enzymatic and the aggregation phases, and started to change after approximately 5 hours of coagulation, i.e. approximately two hours after gel formation. Diffusion results were in agreement with those already obtained by Le Feunteun et al.[15] who monitored the diffusion of a 96750 g/mol PEG (R_h=13.3 nm) in a concentrated rennet gel.

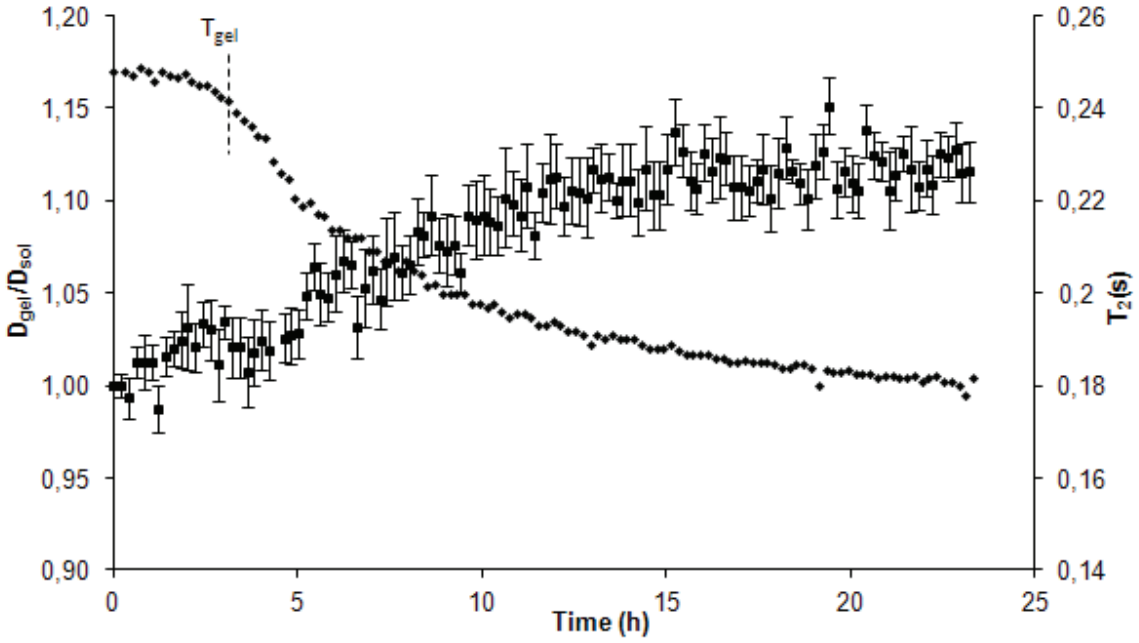

Figure VIII. Evolution of the G6 dendrimer self-diffusion coefficients (squares) and T_2 relaxation times (diamonds) over time after addition of chymosin to the concentrated casein suspension.

Discussion

Previous studies[13-14] have improved our understanding of the mechanisms of self-diffusion of linear and deformable PEG probes of various sizes in NPC suspensions and gels. It has been shown that PEG diffusion in casein suspensions is greatly dependent on both the volume fraction occupied by casein particles and the probe size. The reduction in the self-diffusion coefficient for a given volume fraction of casein particles is smaller for smaller probes. This phenomenon was first explained by assuming a model with two diffusion pathways, one around the casein particles and one through these particles. Such a model was proposed because casein particles are known to be porous and highly hydrated[29]. On the other hand, because PEGs are flexible and easily deformable, they can diffuse through small spaces compared to their hydrodynamic diameter by adopting a more elongated conformation, as described by the reptation model of De Gennes and proved by other studies[20, 30]. However, the results of our previous study[18] dealing with the effects of the casein system (NPC ($R_{h\ casein}$=100 nm) and SC ($R_{h\ casein}$=11nm) systems) on PEG diffusion indicated that the extra-particle mechanism, which is the only one to be considered in the case of SC suspensions, was sufficient to explain the differences observed in the values of the diffusion coefficients according to probe size. The results assumed that intra-micellar diffusion mechanism adopted in the NPC system would be negligible and results could be explained by taking into account the size of the probe and the density of the system. This explanation was proposed because PEG diffusion was much more attenuated in SC than in the NPC system. If intra-micellar diffusion exists, we would have observed the opposite situation, as PEG would be more constrained inside the micelle and hence would experience fewer obstruction effects when diffusing around casein aggregates in SC dispersions.

In order to further validate our hypotheses and to achieve a better understanding of probe diffusion in NPC suspensions and gels, a preferred experimental design is proposed below to follow the diffusion of hard spherical probe particles such as dendrimers with fixed dimensions through the casein matrix. Because of their spherical shape, dendrimers cannot diffuse inside the micelle. Only extramicellar diffusion is possible for this kind of probe. The results obtained for the combined study of diffusion and relaxation are discussed below.

Mobility of PEG and dendrimer probes in NPC suspensions.

(i) **Self-Diffusion**

The onset of close-packing, where casein micelles come into direct contact, occurs in NPC suspensions at a casein concentration of about 15 g/100g water[18, 31]. Below the close packing limit, PEG and dendrimer couples (with similar R_h) have similar diffusion behaviors (**Figure IX**). This finding is consistent with our previous results[18], which indicated that at a low obstacle density (between 2.88 and 15 g/100g H_2O) the obstruction mechanism induced by casein micelles has no constraints on the conformation of PEGs which remain in a spherical random coil form. If intra-micellar diffusion exists, self-diffusion of PEG should be slower than for dendrimer as it should experience more obstruction effects when diffusing inside the micelle. In the light of our results, and in agreement with our previous study[18], intra-micellar diffusion as earlier proposed for NPC systems can no longer be taken into consideration. Only an extra-micellar diffusion mechanism can exist regardless of the probe size and deformability. Above close-packing probes continued to diffuse, and differences occurred in their diffusion behavior; PEGs diffused faster than dendrimers and the differences in self-diffusion became greater as the size of the probe increased. Probe radius approached the pore size of the casein matrix with increasing casein concentrations and probe size[18]. The probes therefore diffused less freely through a dense array of obstacles which hindered their mobility in a size-dependent manner. Hindrance to PEG diffusion was less because it is capable of changing its shape to move through the concentrated casein solution by adopting an ellipsoidal random coil form[18], while a dendrimer sphere has no flexibility and thus encounters greater resistance.

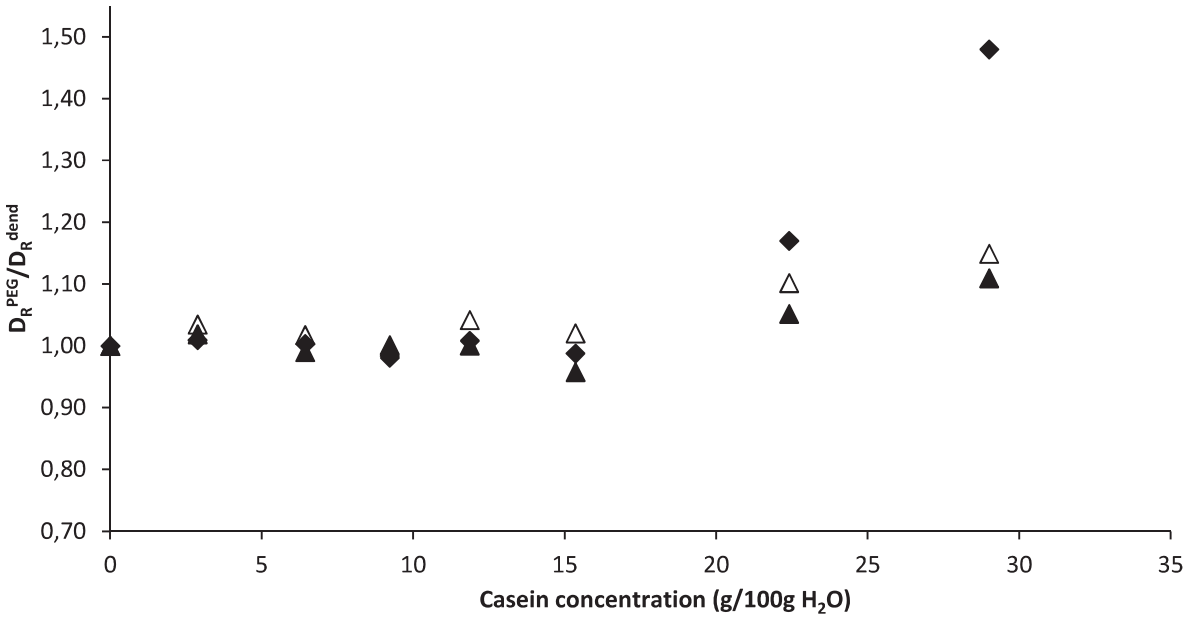

Figure IX. Variation in D_R^{PEG}/D_R^{dend} values as a function of casein concentration in NPC suspensions. (♦), (Δ) and (▲) correspond to $D_R^{PEG7}/D_R^{G6.27}$, $D_R^{PEG3.16}/D_R^{G3.51}$ and $D_R^{PEG3.16}/D_R^{G2.84}$, respectively.

(ii) ^{1}H T_2 relaxation times

While the self-diffusion coefficient reflects displacement of the molecule within the casein matrix over micron distances, the T_2 relaxation time reflects the rotational or local mobility of molecules at the nanometer scale. ^{1}H T_2 relaxation can be linked to any molecular motion that can induce fluctuating local magnetic fields. There are several distinct mechanisms occurring at the molecular level which can contribute to relaxation, but the most common mechanism is the magnetic dipole-dipole interaction which is assumed to be responsible for the relaxation of transverse magnetization in this study.

The chain length of the PEG probes used in this study increased significantly (from 615 to 93000 g/mol PEG). The results obtained at zero casein concentration (**Figure V** and **Figure VI**) reflect greater mobility for the low molecular weight PEG probes, consistent with the increasing contribution of the overall tumbling of the molecule to the relaxation. The striking result of these

experiments was the relatively low molecular weight of PEGs, corresponding to a critical size of 180 monomer units, above which the T_2 relaxation became almost size-independent. This result demonstrates the local nature of the motions responsible for the T_2 relaxation in polymer chains in an H_2O solution. Above this critical size, the overall tumbling was much slower than the local motions and, therefore, its contribution to the relaxation was negligible. Therefore, for PEG polymers in H_2O, the contribution of segmental motion to ^1H T_2 is the dominant factor rather than that of the rotational motion of a whole molecule. In contrast to PEG polymers, the dendrimer macromolecules were characterized by PEG terminal function groups located on the exterior, with a uniform chain length of 587 g/mol. Only the number of chains doubled from one generation to the next. The length of this chain was therefore short and size was close to that of the 615 g/mol PEG. As the length of this short chain does not vary, the local mobility of PEG chains was the same and only affected by the overall dendrimer tumbling which depended on the overall dendrimer size. The effect of dendrimer core rigidity manifested itself through the values of T_2 which were found to be much lower than those of the 615 g/mol PEG. The T_2 relaxation times measured thus reflected the global mobility of the dendrimer molecules.

Probe relaxation times decreased significantly in the presence of casein micelles. In many studies performed by other authors, reduction of T_2 relaxation times has been attributed to an intermolecular interaction between a probe and the network[32-33], or to changes in the network microviscosity. Attention has also focused on the effects of polymer chain length on T_2 relaxation time in entangled polymer systems and prior to reptation motion[34-37]. To our knowledge, no studies exist concerning the effects of PEG/PEO polymer chain length on T_2 relaxation times measured in dilute and semi-dilute protein systems.

In cases of interaction, there are two types of exchange processes between free PEG probes and those interacting with the casein matrix. Intercompartmental exchange can be characterized as slow and fast. Under slow exchange the relaxation will be biexponential i.e., relative components of the signal will correspond closely to the volume fractions of the physical compartments. Under fast exchange, the relaxation will be monoexponential, the single relaxation rate being the weighted volume-average of the two relaxation rates and being dependent on the pulse spacing used. However, our results showed that (i) the addition of 0.1% w/w of probes had no effect on the size of the casein particles, on the viscosity values of the suspensions or on the casein

network formation, (ii) in our ^1H T_2 experiments, PEGs and dendrimers in casein suspensions had a single component for the relaxation behavior and (iii) there was no dependence of the transverse relaxation rate of PEG on the pulse spacing for a casein concentration of 15 g/100g water. The experimental T_2 values remained stable when varying the echo time between 50 µs and 2 ms (data not shown). All these results confirm the absence of interaction between casein particles and probes and exclude the interpretation based on slow and fast exchange of molecules. Therefore, only dipole-dipole interaction was to be considered to explain the changes in T_2 values.

Taking into account the Stokes-Einstein-Debye equation, it is possible to connect the T_2 variations with changes in the solvent viscosity. However, microviscosity is not easily quantified and there is no indication of its variation in casein suspensions according to casein concentration. On the other hand, dipole-dipole interactions are known to have a considerable impact on changes in T_2 values. These dipolar effects can be influenced both by intermolecular interactions and by changes in the overall environment. The variation in relaxation times for a given polymer with increasing casein concentration can be attributed to increased restriction of its freedom of motion with increasing casein concentrations. Comparison of the reduced dendrimer self-diffusion (**Figure IV (A)**) and its T_2 relaxation times (**Figure VI (A)**) revealed that the retardation of the probe rotation was substantially less than the retardation of its translation (diffusion) in concentrated casein suspensions. This indicates that dendrimer mobility was less restricted over small distances than over large ones. This was also true for the PEG probes. In contrast to the reduced diffusion results for dendrimers, which were affected by the casein concentration and probe size, reduced dendrimer T_2 relaxation times depended similarly on the casein concentration whatever the probe size. This was not the case for PEG polymer chains because their flexibility led to variations in the contribution to the relaxation of the local segmental motion and the global or long-range motions of large chains. In diluted casein systems ($C < 6.43$ g/100g H_2O), the PEG T_2 relaxation was governed by the local mobility of the chain as in water solutions. When the casein concentration increased, the local mobility was restricted and the overall tumbling of the probe played a major role in the relaxation times even for a relatively large chain size. This result explains the dependence of T_2 relaxation times on probe molecular weights in domain II for casein concentrations ≥ 6.43 g/100 g H_2O. At higher concentrations (>12 g/100g H_2O), the mobility of the 93000 g/mol PEG was found to be greater than expected. T_2

relaxation times measured for this probe in such concentrated systems reflect either higher mobility, due to its ability to undergo conformational changes[18], or further anisotropy in the motion of probes which can be attributed to the increase in obstruction effects induced by casein proteins. The anisotropic motion of the probe chains on the NMR time scale may cause residual dipolar coupling which affects the values of the T_2 measured.

Mobility of PEG and dendrimer probes in a concentrated casein rennet gel.

(i) Self-Diffusion

The coagulation induced by chymosin action is generally broken down into three phases: enzyme action, aggregation and gel ageing[38-39]. First, the enzyme specifically splits off the κ-casein located at the surface of the supramolecular edifice. This reduces the steric and electrostatic repulsion between casein particles and the suspension becomes unstable. In the second phase, the resulting para-casein micelles spontaneously aggregate and form a microscopic network. In this study, this phenomenon was characterized by the rapid increase in G' and G" and the sudden decrease in δ between 3 and 4 hours (**Figure III**). The transition from solution to gel occurred at t=3h 20 min for slow coagulation, induced by addition of 4 µL of chymosin in 10 g of NPC suspension at 20°C, and within a few minutes for the fast coagulation induced by addition of 70 µL of a chymosin dilution (1 ml in 99.0 g of distilled water) in 10 g of NPC suspension at 30°C (data not shown). Finally, the third phase corresponds to the ageing of the gel and is characterized by the occurrence of structural changes in the casein network which give rise to local matrix fusion and compaction, resulting in a gel with larger pores and greater permeability[39-43]. Although the stages are different in nature, they are not clearly separated in time. The aggregation phase always starts before the end of the enzymatic reaction[6, 17, 44] and occurs at an even lower degree of κ-casein hydrolysis when the casein concentration is increased[17, 39, 45]. This is believed to be caused by a smaller mean free distance between casein micelles, which increases the collision frequency, and higher concentrations of ionic calcium, which reduces the electrostatic repulsion in concentrated dairy solutions[39, 45]. Based on reported results[17, 39, 45], the percentage of proteolysis at gel formation for a casein concentration of 15 g/100g H_2O is 40%. The enzymatic reaction continues to occur long past the gelation point.

As already reported by Le Feunteun et al.[14-16] and Colsenet et al.[13], the significant increase in the self-diffusion of large probes after coagulation can thus be explained on the basis of the network rearrangements that lead to particle fusion and compaction and result in a structure where molecules have more free space to diffuse. The effects of the gel structure on the solute diffusion have also previously been studied using NMR diffusometry by several authors in different matrices[21, 46-48]. Strong connection has been found between the gel structure and the probe diffusion in both κ-Carrageenan[21, 47] and whey protein[48] gels. The diffusion behavior has been determined mainly by the void size, which in turn has been defined by the state of aggregation of the matrix. The effects of coagulation have also been investigated using simulation methods[49] which have shown that the diffusion of a spherical probe in hard sphere suspensions and gels is mainly dependent on the volume fraction that is accessible to the diffusing particle.

However, the striking result of these experiments was that spherical dendrimer probes and flexible PEG probes of similar sizes showed the same increase in diffusion behavior after coagulation despite the differences in their structure. If small PEG probes could enter casein aggregates, their diffusion would be slower than that of dendrimers since they would experience more obstruction effects when diffusing inside the aggregates. In addition, during the rearrangement process, the fused particles may be accompanied by a reduction in strand porosity through shrinkage. Under the hypothesis that PEGs diffuse through the strands, these effects would lead to an increase in the obstruction effect for PEG molecules and thus a decrease in the diffusion coefficient after coagulation. In the light of our results showing an increase instead of a decrease in the probe self-diffusion coefficient, the intra-aggregate diffusion pathway already proposed in NPC rennet gels is no longer valid. Only an extra-aggregate diffusion mechanism can exist, regardless of the probe size and deformability, as in the case of NPC suspensions. The absence of significant effect of coagulation for the smallest PEGs with $R_h \leq 3$ nm may be attributed to lower sensitivity to a change in voluminosity (as observed in suspensions) because of their small size.

(ii) ^{1}H T_2 relaxation times

The local mobility of the matrix is an important issue that has to be taken into consideration. Indeed, several NMR studies have demonstrated that casein micelle, despite its large size,

contains a highly mobile protein segment which explains the narrow peak in the NMR spectra[50]. Thus the mobility of the probe molecule will most probably be affected by the motion of these segments. The coagulation of our concentrated casein sample may be visualized by the formation of a network backbone during the sol-gel transition, which was progressively reinforced upon further incorporation of particles during the aging phase. This slow casein particle aggregation process was responsible for delayed development of maximum firmness in the gel (**Figure III**). As the gel became denser, the local motion of casein particles became slower as a result of the formation of small clusters or network-like structures. This reduced motion can explain the decrease in T_2 relaxation times of probes in gels and the slope variation between suspensions and gels of the line showing the dependence of dendrimer and PEG T_2 relaxation times on molecular weight (**Figure VII**).

On the other hand, a decrease in casein mobility might be thought to result in a decrease in probe self-diffusion, but this reasoning would overlook the fact that the structural changes lead to a more open network gel structure.

Conclusion

Two independent NMR approaches were used in this study to investigate the dynamic properties of PEG and dendrimer probes: self-diffusion measurements on the one hand and spin-spin relaxation investigations on the other. We demonstrated that:

(i) The diffusion coefficient is strongly affected by the density of the casein system and also by the size and the flexibility of the probe. At low system density (below 15 g/100g H_2O), the obstruction mechanism induced by casein micelles imposed no constraints on the spatial organization of probes. Consequently, PEGs and dendrimers diffused in the same manner. Upon further confinement (above the onset of close packing 15/100g H_2O), the probe radius approached the casein mesh size. In this case, PEGs adopted an ellipsoidal random coil form in order to diffuse through the casein system. As a consequence, they diffused faster than dendrimers which encountered more resistance due to their fixed shape and lack of flexibility. In a concentrated rennet casein gel (15 g/ 100 g H_2O), PEG and dendrimer self-diffusion coefficients were found to increase in exactly the same manner due to structural changes in the casein matrix. The D^{gel}/D^{sol} ratio increased with the size of the probe. However, this could not be generalized to all the other casein concentrations. As the casein concentration increases, the casein-free volume decreases in solutions, whereas the empty volume created by the rearrangements is enhanced. Consequently, the D^{gel}/D^{sol} ratio will be higher for dendrimers than for PEGs in more concentrated casein systems.

(ii) In water and diluted casein systems, the PEG ^1H NMR T_2 relaxation time is sensitive to local motions of monomer units. T_2 exhibited minor variation when the chain molecular weight was higher than 7920 g/mol. At increasing casein concentrations polymer segmental motion was hindered. In these systems, the ^1H NMR T_2 relaxation time was mainly sensitive to long-range or global motions and strongly depended upon the chain molecular weight. The T_2 relaxation times of 587 g/mol PEG terminal function groups located on the exterior of the dendrimer macromolecules were found to be much lower than that of the free 615 g/mol PEG as they were affected by the rigidity of the dendrimer. T_2 relaxation times thus reflected the global mobility of dendrimer molecules which changed in a similar manner with increasing casein concentration. For both probes, rotational diffusion was less hindered by the casein matrix, compared to

translational diffusion. The rotational motion of the probes was retarded in the gel and this could be attributed to more restricted local mobility of the matrix as a result of the formation of small clusters or network-like structures.

In summary, the "two diffusion pathways"[13-14] model previously proposed to explain the diffusion of probes in NPC suspensions and gels is not satisfactory. The extra-micellar diffusion mechanism is the only mechanism to be taken into account, regardless of the size and the deformability of the probe.

Acknowledgements

The authors thank the Regional Council of Brittany and Unilever (Netherlands) for financial support. We are grateful to Arnaud Bondon for access to the NMR facilities of the PRISM Research Platform (Rennes, France). We also thank Marie-Helene Famelart and Florence Rousseau (INRA Rennes, UMR STLO) for their assistance with the rheological and dynamic light scattering experiments.

References

(1) Holt, C. *Adv. Protein Chem.* **1992,** 43, 63-151.
(2) de Kruif, C. G.; Huppertz, T. *J. Agric. Food Chem.* **2012,** 60 (18), 4649-4655.
(3) Cucheval, A.; Vincent, R.; Hemar, Y.; Otter, D.; Williams, M.; Vincent, R. R.; Williams, M. A. K. *Colloid Polym. Sci.* **2009,** 287 (6), 695-704.
(4) Alexander, M.; Piska, I.; Dalgleish, D. G. *Food Hydrocolloids* **2008,** 22 (6), 1124-1134.
(5) Alexander, M.; Dalgleish, D. G. *Colloids Surf. B Biointerfaces* **2004,** 38 (1), 83-90.
(6) Sandra, S.; Alexander, M.; Dalgleish, D. G. *J. Colloid Interf. Sci.* **2007,** 308 (2), 364-373.
(7) Horne, D. S. *Milchwissenschaft* **1991,** 46 (7), 417-420.
(8) Gaygadzhiev, Z.; Alexander, M.; Corredig, M. *Food Hydrocolloids* **2009,** 23 (4), 1134-1138.
(9) Hemar, Y.; Singh, H.; Horne, D. S. *Curr. Appl. Phys.* **2004,** 4 (2), 362-365.
(10) Cucheval, A. S. B.; Vincent, R. R.; Hemar, Y.; Otter, D.; Williams, M. A. K. *Langmuir* **2009,** 25 (19), 11827-11834.
(11) Moschakis, T.; Murray, B. S.; Dickinson, E. *J. Colloid Interf. Sci.* **2010,** 345 (2), 278-285.
(12) Floury, J.; Madec, M. N.; Waharte, F.; Jeanson, S.; Lortal, S. *Food Chem.* **2012,** 133 (2), 551-556.
(13) Colsenet, R.; Soderman, O.; Mariette, F. *Macromolecules* **2005,** 38 (22), 9171-9179.
(14) Le Feunteun, S.; Mariette, F. *J. Agric. Food Chem.* **2007,** 55 (26), 10764-10772.
(15) Le Feunteun, S.; Mariette, F. *Macromolecules* **2008,** 41 (6), 2071-2078.
(16) Le Feunteun, S.; Mariette, F. *Macromolecules* **2008,** 41 (6), 2079-2086.
(17) Le Feunteun, S.; Ouethrani, M.; Mariette, F. *Food Hydrocolloids* **2012,** 27 (2), 456-463.
(18) Salami, S.; Rondeau-Mouro, C.; van Duynhoven, J.; Mariette, F. *Food Hydrocolloids* ***2013,*** 31 (2), 248-225.
(19) Wang, Y. J.; Therien-Aubin, H.; Baille, W. E.; Luo, J. T.; Zhu, X. X. *Polymer* **2010,** 51 (11), 2345-2350.
(20) Griffiths, P. C.; Stilbs, P.; Yu, G. E.; Booth, C. *J. Phys. Chem.* **1995,** 99 (45), 16752-16756.
(21) Loren, N.; Shtykova, L.; Kidman, S.; Jarvoll, P.; Nyden, M.; Hermansson, A.-M. *Biomacromolecules* **2009,** 10 (2), 275-284.
(22) Baille, W. E.; Malveau, C.; Zhu, X. X.; Kim, Y. H.; Ford, W. T. *Macromolecules* **2003,** 36 (3), 839-847.
(23) Bernin, D.; Goudappel, G.-J.; van Ruijven, M.; Altskar, A.; Strom, A.; Rudemo, M.; Hermansson, A.-M.; Nyden, M. *Soft Matter* **2011,** 7 (12), 5711-5716.
(24) Tomalia, D. A. *Prog. Polym. Sci.* **2005,** 30 (3-4), 294-324.
(25) Dalgleish, D. G.; Spagnuolo, P.; Douglass Goff, H. *Int. Dairy J.* **2004,** 14, 1025-1031.
(26) de Kruif, C. G. *J. Dairy Sci.* **1998,** 81 (11), 3019-3028.
(27) McMahon, D. J.; McManus, W. R. *J. Dairy Sci.* **1998,** 81 (11), 2985-2993.
(28) Pitkowski, A. Processus de gelification des caseines en presence de polyphosphates. Universite de Maine **2007**.
(29) Morris, G. A.; Foster, T. J.; Harding, S. E. *Biomacromolecules* **2000,** 1 (4), 764-767.
(30) de Gennes, P. G. *Nature* **1979,** 282, 367-370.
(31) Bouchoux, A.; Debbou, B.; Gesan-Guiziou, G.; Famelart, M. H.; Doublier, J. L.; Cabane, B. *J. Chem. Phys.* **2009,** 131 (16).

(32) Matsukawa, S.; Ando, I.; Matsukawa, S.; Ando, I. *Macromolecules* **1999,** 32 (6), 1865-1871.
(33) Masaro, L.; Zhu, X. X. *Langmuir* **1999,** 15 (24), 8356-8360.
(34) Brosseau, C.; Guillermo, A.; Cohen-Addad, J. P. *Macromolecules* **1992,** 25 (18), 4535-4540.
(35) Brereton, M. G.; Ward, I. M.; Boden, N.; Wright, P. *Macromolecules* **1991,** 24 (8), 2068-2074.
(36) Kimmich, R.; Rosskopf, E.; Schnur, G.; Spohn, K. H. *Macromolecules* **1985,** 18 (4), 810-812.
(37) Cohen Addad, J.-P.; Guillermo, A. *Phys. Rev. Lett.* **2000,** 85 (16), 3432-3435.
(38) Zoon, P.; Vanvliet, T.; Walstra, P. *Neth. Milk Dairy J.* **1988,** 42 (3), 249-269.
(39) Karlsson, A. O.; Ipsen, R.; Ardo, Y. *Int. Dairy J.* **2007,** 17 (6), 674-682.
(40) Mellema, M.; Heesakkers, J. W. M.; van Opheusden, J. H. J.; van Vliet, T. *Langmuir* **2000,** 16 (17), 6847-6854.
(41) Lucey, J. A.; Tamehana, M.; Singh, H.; Munro, P. A. *Int. Dairy J.* **2001,** 11 (4-7), 559-565.
(42) Lucey, J. A.; van Vliet, T.; Grolle, K.; Geurts, T.; Walstra, P. *Int. Dairy J.* **1997,** 7 (6), 381-388.
(43) Lucey, J. A.; Tamehana, M.; Singh, H.; Munro, P. A. *J. Dairy Res.* **2000,** 67 (3), 415-427.
(44) Walstra, P.; Vanvliet, T. *Neth. Milk Dairy J.* **1986,** 40 (2-3), 241-259.
(45) Sharma, S. K.; Mittal, G. S.; Hill, A. R. *Milchwissenschaft* **1994,** 49 (8), 450-453.
(46) Baldursdottir, S. G.; Kjoniksen, A. L.; Nystrom, B. *Eur. Polymer J.* **2006,** 42 (11), 3050-3058.
(47) Walther, B.; Loren, N.; Nyden, M.; Hermansson, A.-M. *Langmuir* **2006,** 22 (19), 8221-8228.
(48) Colsenet, R.; Mariette, F.; Cambert, M. *J. Agric. Food Chem.* **2005,** 53 (17), 6784-6790.
(49) Babu, S.; Christophe Gimel, J.; Nicolai, T. *J. Phys. Chem. B* **2008,** 112 (3), 743-748.
(50) Rollema, H. S.; Brinkhuis, J. A.; Vreeman, H. J. *Neth. Milk Dairy J.* **1988,** 42 (2), 233-248.

Chapter V: Probe mobility in sodium caseinate dispersions and acid gels

Publication n°3: Translational and rotational diffusion of flexible PEG and rigid dendrimer probes in sodium

Translational and rotational diffusion of flexible PEG and rigid dendrimer probes in sodium caseinate dispersions and acid gels

Souad Salami[1,2], Myriam Barhoum [1,2], Corinne Rondeau[1,2], John van Duynhoven[3,4] and Francois Mariette[1,2,]*

[1] Irstea, UR TERE, 17 avenue de Cucillé, CS 64427, 35044 Rennes, France

[2] Université Européenne de Bretagne, France

[3]Unilever R&D, Olivier van Noortlaan 120, P.O. Box 114, 3130AC Vlaardingen, The Netherlands

[4] Laboratory of Biophysics, Wageningen University, Dreijenlaan 3, 6703HA Wageningen, The Netherlands

* Corresponding author: François Mariette, Irstea, UR TERE, CS 64426, 17 avenue de Cucillé, 35044 Rennes, Cedex, France; Tel.: +33 (0)2 23 48 21 21; Fax: +33 (0)2 23 48 21 15.

E-mail address: Francois.Mariette@irstea.fr

Abstract

The dynamics of rigid dendrimer and flexible PEG probes in sodium caseinate dispersions (dilute, semi-dilute and concentrated regimes) and acid gels, including both translational diffusion and rotational diffusion, were studied by NMR. In semi-dilute and concentrated regimes, translational diffusion of the probe depended on its flexibility and on the fluctuations of the matrix chains. The PEG probe diffused more rapidly than the spherical dendrimer probe. The greater conformational flexibility of PEG facilitated its motion through the crowded casein matrix. Rotational diffusion was, however, substantially less hindered than the translational diffusion and depended on the local protein-probe friction which became high when the casein concentration increased. The coagulation of the matrix led to the formation of large voids, which resulted in an increase in the translational diffusion of the probes, whereas the rotational diffusion of the probes was retarded in the gel, which could be attributed to the immobilized environment surrounding the probe.

Keywords: *Translational diffusion, rotational diffusion, PEG, dendrimer, sodium caseinate.*

Introduction

The retardation of particle transport in polymer solutions and gels plays a key role in a wide range of technological and biological processes. Accordingly, the topic has attracted much experimental and theoretical attention. Most studies have focused on the translational diffusion of tracers, commonly measured with dynamic light scattering[1-2], fluorescence recovery after photobleaching[3] and pulsed-field nuclear magnetic resonance[4-5]. Although various theoretical models for translational diffusion of tracers in polymer matrices have been proposed[6-7], the mechanisms of retardation are still incompletely understood. In contrast, experimental and theoretical studies on the rotational diffusion of tracers in polymer solutions are scarce. Rotational diffusion of spherical tracers is a local dynamic process that is less sensitive to sterical hindrance than translational diffusion. The concurrent measurement of both translational and rotational diffusion within the same matrix can, in principle, pave the way to a better understanding of the microscopic structure of a polymer network since it influences various motion and length scales. Generally, rotational diffusion is sensitive to motions that occur at the nanometer length scale and at the picosecond-to-nanosecond time scale[8-9], whereas in translational diffusion measurements, motion is measured over the millisecond-to-second time scale and over distances from tens of nanometers up to hundreds of microns[10-13]. In this context, NMR techniques have the advantage of simultaneously and non-invasively measuring the translational and rotational diffusion of molecules. Pulsed field gradient nuclear magnetic resonance diffusometry (PFG-NMR) measures translational diffusion[14], whereas NMR relaxometry is sensitive to rotational diffusion.

Sodium caseinate (SC) was chosen as a model protein in this study. Sodium caseinate has been the subject of many physico-chemical studies, partly because of its widespread use as a thickener, stabilizer and emulsifier of water-based industrial and commercial products[15]. In aqueous solutions, casein molecules are present in the form of fragile star-like aggregates of ~20 nm[16-19] in diameter containing ~ 4 to 6 g of water per gram of casein[18, 20-21]. A number of research groups have extensively characterized SC dynamics in terms of the rheological response to steady and oscillatory shear. It has been shown that SC dispersions behave like model polymeric solutions, with a hyperentanglement regime that begins above 8 g/100 g H_2O[17-18, 22].

Slow acidification of a sodium caseinate solution causes the formation of a gel. A process that has gained the attention of food industry is direct acidification by the addition of a lactone, such as glucono-δ-lactone (GDL), which slowly hydrolyzes to gluconic acid with a resulting reduction in pH. The microstructures of acid caseinate gels have been studied by researchers using, for example, rheology[23], permeability, transmission electron microscopy (TEM)[24-25], scanning electron microscopy[26] and confocal scanning laser microscopy (CSLM)[27]. The main factors governing the formation of acid sodium caseinate gels are the caseinate concentration, pH, temperature and ionic strength[28]. The maximum gel strength, determined using rheology, will be obtained at low ionic strength at a pH of ~ 4.6, which is around the isoelectric point of the different caseins[25]. Depending on the experimental conditions, different gel microstructures can thus be obtained.

In this paper, we present NMR measurements of the rotational and translational diffusion coefficients of a small rigid dendrimer probe and a small flexible PEG probe in dilute/semi-dilute/concentrated dispersions and acid gels of a sodium caseinate polymer system. The results are discussed in an attempt to understand the respective effects of protein crowding and coagulation on translational and rotational diffusion of these probes.

Experimental

Materials. Sodium caseinate powder was provided by Armor Protéines (Saint-Brice en Coglès, France). The detailed composition of this powder is described in reference[16]. Glucono-delta-lactone (GDL) was purchased from Sigma Aldrich. PEG with a molecular weight of M_w = 32530 g/mol and a hydrodynamic radius of R_h = 7 nm was obtained from Varian Laboratories. Monodisperse polyamidoamine G6 dendrimer (R_h = 6.27 nm) with an ethylene diamine core and polyethylene glycol (PEG) as a surface group was purchased from Dendritic Nanotechnologies, Inc. (USA).

Dispersion preparation. Casein suspensions were prepared according to the protocol described in reference[16]. The solutions were studied without adjustment of the pH, which was equal to 6.6±0.04 for casein concentrations ranging from 1 to 25.09 g/100 g H_2O

Acid coagulation. Depending on the casein concentration, defined amounts of GDL were added to solutions to reach a final pH of 4.6±0.05. After addition of GDL, casein suspensions were stirred for 5 min and small amounts were transferred to 5-mm NMR tubes that were maintained at 20°C for 48 h before analysis.

Scanning electron microscopy. Small cubes of the gels (5x5x5 mm) were immersed in 2.5% v/v glutaraldehyde at 20°C for 48 h in a phosphate buffer, pH 7.02. Samples were rinsed several times with distilled water before being dehydrated in a graded ethanol series (10-30-50-70-80-90-95-100 % (v/v)) in 20 min steps, and finally conserved in acetone for one night. Samples were then dried using CO_2 in a critical point dryer (CPD 010, Blazers Union ltd, Liechtenstein). Dried samples were fractured, mounted onto specimen tubes, gold-coated and microscopically analyzed using a scanning electron microscope (Jeol JSM 6301F) operated at an acceleration voltage of 7 kV. The images were produced by CMEBA (Rennes, France).

NMR measurements. All NMR measurements were performed on a 500 MHz spectrometer (Bruker Wissembourg, France) equipped with a dedicated field gradient probe (DIFF30 from Bruker Wissembourg, France) with a static gradient strength of 1200 (±0.2) G/cm for an amplifier output at 40A. NMR tubes (5 mm) were used and all NMR measurements were performed at 20°C.

Stimulated echo sequence using bipolar gradients (STE-BPP) and a 3-9-19 WATERGATE pulse scheme to suppress the water signal was used to measure self-diffusion coefficients. Diffusion coefficients were obtained using the following equation:

$$\frac{I(\delta,\Delta,g)}{I_0} = \sum_i p_i \exp\left[-\gamma^2 g^2 \delta^2 \left(\Delta - \frac{\delta}{3} - \frac{\tau}{4}\right) D_i\right] \quad (1)$$

where I(δ, Δ,g) and I_0 are the echo intensities in the presence of gradient pulses of strength g, and the absence of gradient pulses, respectively, γ is the gyromagnetic ratio (for protons, γ = 26.7520 × 10^7 rad.T^{-1} .s^{-1}), g is the amplitude of the gradient pulse, δ is the gradient pulse duration, Δ is the time between the leading edges of gradient pulses, τ is the time between the end of each gradient and the next radiofrequency pulse, D_i is the self-diffusion coefficient of the ith component, p_i is the fractional proton number of the ith component, and $\sum p_i = 1$ (in this study, i had a value of 1 or 2).

Diffusion experiments were carried out with 32 different values of g, ranging from 20 to 1100 G/cm, with δ ranging between 1 and 2 ms. Sixteen scans were carried out and the recycle delay was set at 5 T_1. Depending on the molecular weight of the PEG studied, Δ was adjusted to obtain a diffusion distance of z = ~1.5 µm under unrestricted conditions, in accordance with the Einstein equation, $z = (2 \Delta D_{Probe})^{1/2}$. Data processing was performed with Table Curve software (Ritme, Paris).

The Carr Purcell Meiboom Gill (CPMG) sequence coupled with a presaturation pulse scheme for water proton signal suppression was used to measure spin-spin relaxation times (T_2) of the ethoxylate methylene moieties at a chemical shift of 3.6 ppm. The relaxation decay curve was accurately fitted for all probes using the following equation:

$$I(2\tau) = \sum_{i=i}^{i} I_i x \exp\left(-\frac{2\tau}{T_{2i}}\right) \quad (2)$$

where I(2τ) is the intensity of the NMR signal given at τ, T_{2i} is the spin-spin relaxation time of the ith component and I_i is the intensity of the ith component at the equilibrium for τ = 0 (in this study, i had a value of 1 or 2). T_2 measurements were made with a τ-value (time between 90° and

180° pulse) of 1 ms. Sixteen data points were acquired for each CPMG with 16 scan repetitions, and the recycle delay was set at 5 T_1.

The standard error, estimated by the fitting procedure, in probe self-diffusion coefficients and T_2 relaxation times was below 2% and 0.3%, respectively.

The self-diffusion coefficients and T_2 relaxation times of the 32530 g/mol PEG and the G6 dendrimer in the dispersions were calculated by fitting **Equation 1** and **Equation 2** with i=1, to the raw NMR data. However, the gluconic acid, which is progressively formed by hydrolysis of GDL, presented an overlapping signal with those of the probes at a shift of ~3.6 ppm. The results in the presence of gluconic acid were therefore determined by fitting **Equation 1** and **Equation 2** with i=2, to the raw NMR data.

Theory: Stokes-Einstein Relationship. The Stokes-Einstein relationship relates the translational diffusion coefficient, D, of a spherical probe to its internal energy kT, the viscosity η of the medium and its radius R.

$$D = \frac{kT}{6\pi\eta R} \tag{3}$$

The Stokes-Einstein equation assumes that the probe particle is in an effective medium that can be considered as a continuum fluid of viscosity η.

Normalization of diffusion coefficients and relaxation times. The self-diffusion coefficients and T_2 relaxation times of the probes were corrected for the effect of the addition of GDL according to the approach described in reference[5]. All the data discussed in this paper are thus reduced self-diffusion coefficients defined as: $D_r=D/D_0$. D is the probe self-diffusion coefficient measured, in the dispersions or the gels, and corrected for the effect of GDL. D_0 is the probe self-diffusion coefficient measured in water. Similarly, the reduced T_2 relaxation times were equal to the T_2 values obtained in SC dispersions and gels divided by those obtained in water.

Results and discussion

Translational diffusion of probes in SC dispersions

Evolution of the reduced self-diffusion coefficients of PEG and dendrimer probes as a function of caseinate concentration is shown in **Figure 1**. The self-diffusion coefficients of the 32530 g/mol PEG and the G6 dendrimer probes in buffer solution (H_2O+0.1 M NaCl) were 3.06 x 10^{-11} m^2s^{-1} and 3.42 x 10^{-11} m^2s^{-1}, respectively. Despite their similar size, their translational diffusion decreased approximately 96.9% and 99.6%, respectively, for the 25 g/100g H_2O polymer solution. However, differences in the diffusion behavior between the probes were only observed for caseinate concentrations ≥ 12 g/100 g H_2O. Below these concentrations, the probes diffused in a similar manner.

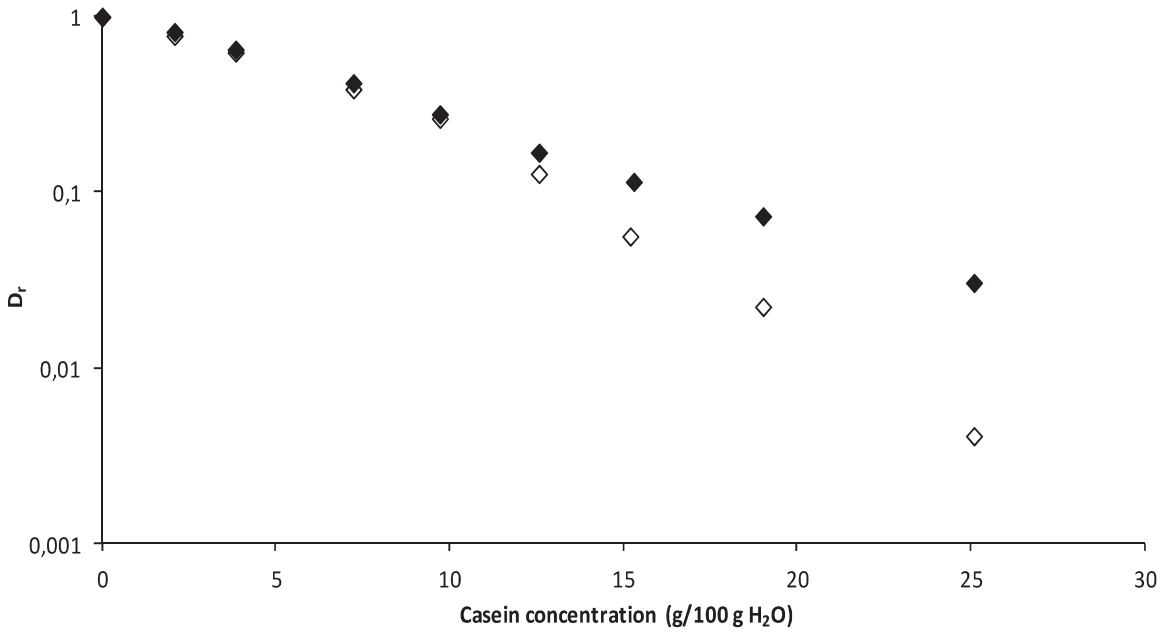

Figure 1. Comparison of the reduced self-diffusion coefficients of the PEG (♦) and the G6 dendrimer (◊) probes as a function of the SC concentration.

The bulk viscosity of the solution changes by 10^6 over the concentration range from 0 to 25 g/100 g H_2O[18]. Stokes-Einstein law (**Equation 3**) clearly does not describe diffusion of PEG and dendrimer probes through the polymer solution. Rather than the probe moving through a continuum fluid having the bulk viscosity, the probe moves through the aqueous phase,

occasionally encountering polymer strands. This regime has been designated the Ogston sieving regime[29]. On the basis of scaling theory[30], the mesh size of semi-dilute polymer solution is:

$$\xi = R_g \left(c_p / c_p^* \right)^{-\upsilon} \tag{4}$$

where R_g is the radius of gyration of the polymer, C_p^* is the critical overlap concentration and υ = 0.75 for good solvent. For the SC system used in this study, R_g = 20 nm[19] and C_p^* is ~ 12 g/100 g H_2O[18, 32]. The semi-dilute polymer regime is defined as the regime where the polymer chains are densely packed and start to overlap, which corresponds to $C_p > C_p^*$ and where the volume fraction φ_v occupied by casein particles is smaller than unity. φ_v= C x V where C is the caseinate concentration and V is the average effective specific volume of SC protein ($5x10^{-3}$ L/g).

As shown in **Table 1**, the mesh size of the SC dispersions calculated from **Equation 4** decreased from ~ 19 nm at C = 12.87 g/100 g H_2O to ~14 nm at C = 19.02 g/100 g H_2O.

Concentration (g/100g H_2O)	φ	ξ (nm)
12.57	0.62	19.3
15.3	0.76	16.7
19.02	0.95	14.2

Table 1. Concentration and volume fraction dependence of the mesh size ξ of SC solutions.

In the dilute regime (C < C*), the obstruction mechanism induced by caseins imposed no constraints on the spatial organization of probes[16]. Consequently, PEG and dendrimer probes diffused in a similar manner.

In the semi-dilute SC dispersions, probes are present in a polymer mesh with a characteristic mesh size, which is similar or equal to their hydrodynamic diameter ($2R_{G6}$ = 12.6 nm; $2R_{PEG}$ = 14 nm). The volume fraction occupied by SC exceeds unity when casein concentration is higher than 19 g/100 g H_2O. In this concentrated regime (φ > 1), SC polymer chains and the probe interpenetrate.

In both semi-dilute and concentrated regimes, the probes diffuse through a relatively dense array of obstacles. Diffusion requires either that the SC chains fluctuate or that the probe itself fluctuates and can therefore penetrate through the SC matrix. A spherical probe is rigid and

cannot change in shape, whereas the flexibility of the PEG probe enhances diffusion. To pass through the SC matrix, PEG probe can stretch to an ellipsoidal conformation, so that the cross section becomes large compared to a relaxed spherical dendrimer probe[16]. This conformational flexibility permits the PEG probe to diffuse faster than rigid spheres in SC solutions. This proposed motion can be thought of as the onset of reptation behavior[16]. The fluctuation of the polymer chains also affects probe diffusion. In both regimes, probes can still move translationally since SC chain fluctuations create voids into which the probe may jump.

Rotational diffusion of probes in SC suspension

In parallel to translational measurements, rotational diffusion was measured for the two probes in SC dispersions with SC concentration ranging from 2 to 25.09 g/100g H_2O (**Figure 2**). Reduced T_2 relaxation times are shown in **Figure 2**.

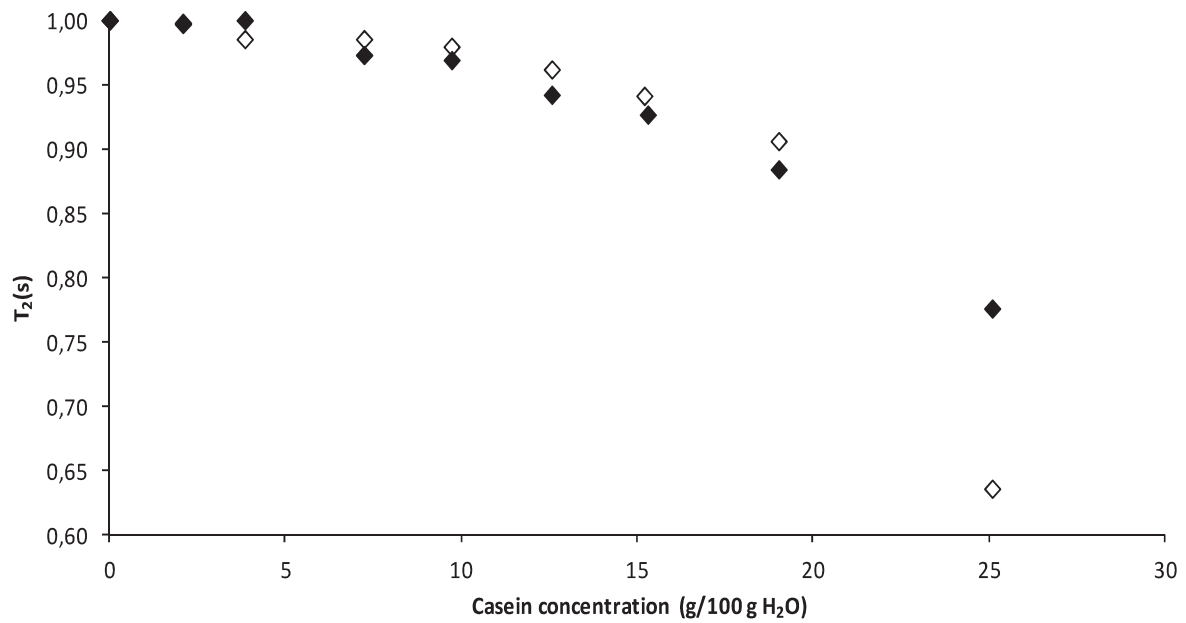

Figure 2. Reduced relaxation time T_2 of the PEG (♦) and the G6 dendrimer (◊) probes as a function of the SC concentration.

In contrast to the translational diffusion that was greatly hindered in SC dispersions (**Figure 1**), the rotational mobility was much less hindered at all concentration values. This latter decreased approximately 22.4% (for PEG) and 36.5% (for G6), respectively, for the 25 g/100 g H_2O

polymer solution, as shown in **Figure 2**. The T_2 relaxation time is particularly sensitive to the rotational or local mobility of the probes at the nanometer scale[33-34], whereas the self-diffusion coefficient reflects the displacement of the probe within the casein matrix on a distance of 1.5 μm. As a result, probe rotation was only moderately affected by the SC system at concentrations that severally hindered long-time translational self-diffusion.

The results obtained (**Figure 2)** showed that rotational diffusion of the tracer was slightly affected by the SC polymer system at concentration ($C < C^*$) where SC chains did not overlap yet. Starting from C*, rotational diffusion of the probes began to decrease significantly. In the semi-dilute SC polymer solutions, the probes used were in the vicinity of polymer chains (with $\xi \geq 2R$) and experienced thus local friction with the matrix. The extent of retardation of probe rotational motion depends on the ratio of the probe size to the mesh size (R/ξ). The higher the ratio, the greater the retardation will be.

In the concentrated polymer regime (C > 19 g/100 g H_2O where $\varphi \geq 1$) where SC chains and the probe interpenetrate, the local protein-probe friction became high and severely hindered the probe rotation. However, the decrease in rotational diffusion was more significant in the case of the dendrimer due to its fixed shape and lack of flexibility.

Effect of acid gelation on probe self-diffusion and T_2 relaxation times

Microstructure

Scanning electron microscopy (SEM) pictures of acid gels at two different concentrations (7.75 and 17 g/100g H_2O) and magnifications are presented in **Figure 3**. The structures were compact and homogeneous and had a sponge-like appearance. At the isoelectric point, SC gels exist as a coarse particulate network of casein particles linked together in clusters, chains and strands[35]. According to these images, the appearance of the network is highly dependent on the caseinate concentration. Regardless of the magnification considered, the gel with the highest caseinate concentration presented smaller pores and denser gel network.

a) 7.75 g/100 g H_2O x 10000

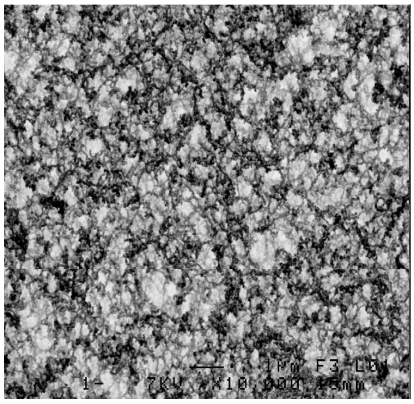

b) 17 g/100 g H_2O x 10000

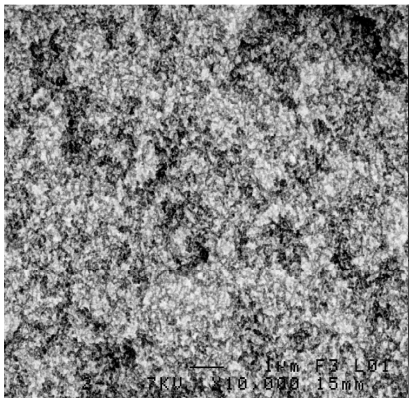

c) 7.75 g/100 g H_2O x 50000

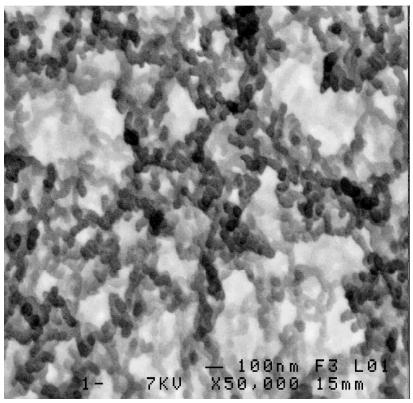

d) 17 g/100 g H_2O x 50000

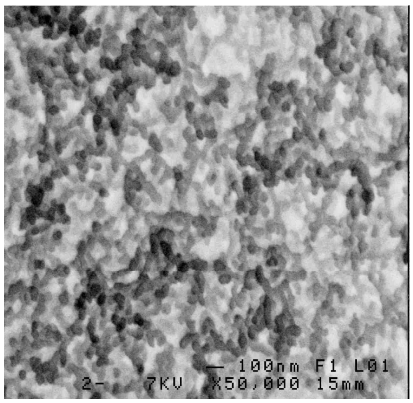

e) 7.75 g/100 g H_2O x 100000

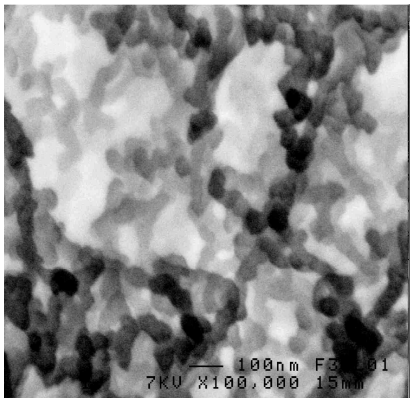

f) 17 g/100 g H_2O x 100000

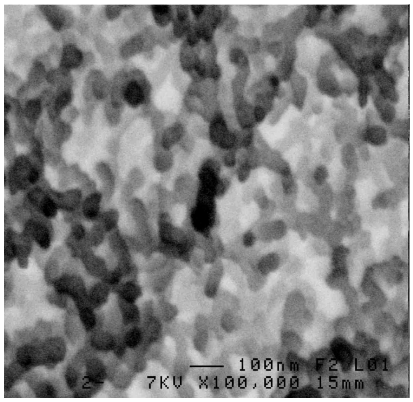

Figure 3. SEM images of acid casein gels at two magnifications and two SC concentrations. Magnifications are 10000, 20000 and 100000 × . The scale bar = 100 nm for all the micrographs.

Translational and rotational diffusion of probes in SC acid gels

Figure 4 shows the reduced PEG and dendrimer probe self-diffusion and relaxation time (T_2) in casein acid gels, divided by those obtained in dispersions, D_R^{gel}/D_R^{sol} and T_2^{gel}/T_2^{sol}, plotted as a function of SC concentration. D_R^{gel}/D_R^{sol} ratios increased from 1.88 to 2.43 and 8.02 for the $G_{6.27}$ dendrimer, and from 1.83 to 2.43 and 3.91 for the PEG_7 with increasing SC concentrations from 7.23 to 9.73 and 15.3 g/100 g H_2O.

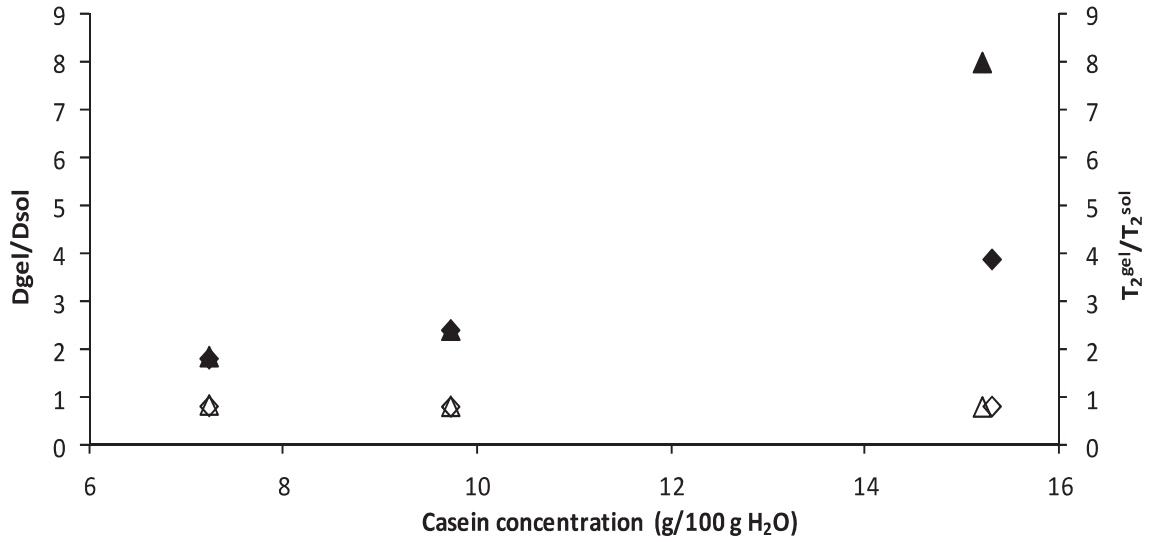

Figure 4. D^{gel}/D^{sol} (full shapes) and T_2^{gel}/T_2^{sol} ratios (empty shapes) obtained for PEG_7 (diamond) and $G_{6.27}$ (triangle) in SC acid gels prepared at different SC concentrations.

The coagulation of the matrix led to the formation of large voids (**Figure 3**), which resulted in an increase in the translational diffusion of the probes. The effect of coagulation was, however, more pronounced when samples were more concentrated since the empty volume created by the coagulation is enhanced compared to the casein-free volume available in the dispersions.

Moreover, for a given casein concentration, PEG and dendrimer probes diffused in a similar manner in the gels (**Figure 5**) as the size of the pores created in the system exceeds largely the size of the probes.

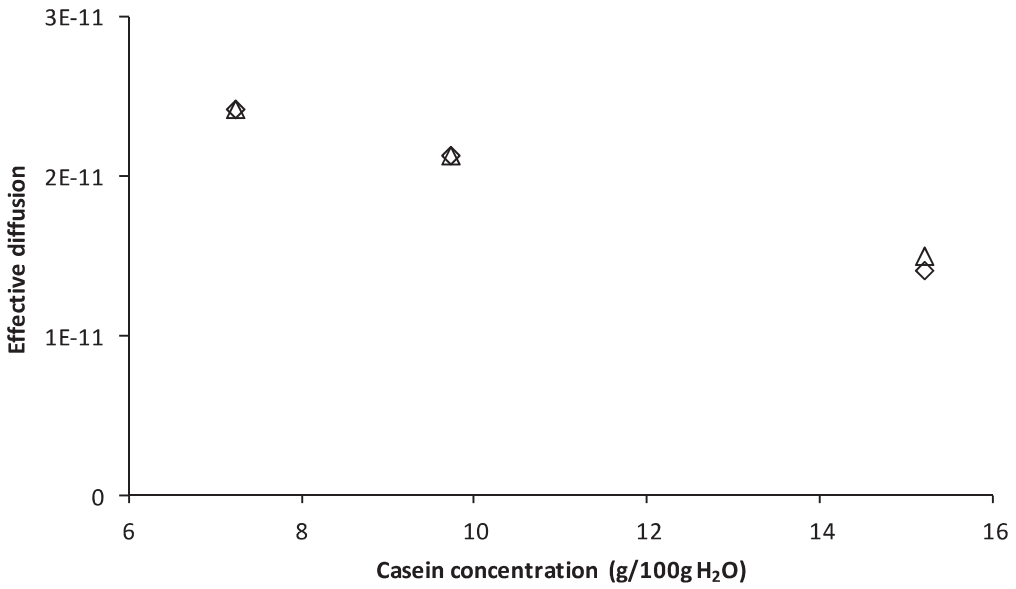

Figure 5. Variation of PEG (diamond) and dendrimer (triangle) probes effective diffusion in SC acid gels prepared at different SC concentrations.

The ratio D^{gel}/D^{sol} depended thus on the hindrance encountered by the probe in the dispersions. The greater the hindrance, the higher the ratio will be. Consequently, similar ratios were obtained at C < C* (no overlap yet of SC chains) where the probes diffused in a similar manner in the dispersions, whereas a significant difference in the ratios was observed at C > C* where the dendrimer probe encountered greater hindrance than the PEG probe in the dispersions.

On the other hand, T_2 relaxation times decreased after coagulation, reflecting reduced rotational mobility in SC gels. T_2^{gel}/T_2^{sol} ratios were approximately equal to 0.8 at all casein concentrations for both probes. This ratio indicates a weak effect of the coagulation on the rotational mobility of the probes. Moreover, these results underline the influence matrix motion on the probe rotational diffusion coefficients; a static environment or (local immobility of the casein matrix) would slow down the rotational mobility of the probe. This latter assumption is in agreement with Monte Carlo simulations of Philips et al.[36-37] performed on suspensions of both immobilized and free hard spheres using Stokesian dynamics to calculate the rotational diffusion of a free tracer sphere. These authors found that for a given average reduced free volume, the rotational diffusion in an

environment of immobilized spheres was slightly more reduced than in an environment of mobile spheres.

Conclusion

We presented experimental data for rotational and translational diffusion in dilute/semi-dilute/concentrated dispersions and gels of the semi-flexible protein, SC. Both the shape of the probe and the matrix topology were found to have a great impact on the mobility of the probe. The translational diffusion was greatly hindered in SC dispersions, and differences in the diffusion behavior between PEG and dendrimer probes were observed after the overlap of the SC chains where the mesh size of the system approaches the diameter of the probe. In this regime, PEG diffused faster than dendrimer, which encountered greater resistance due to its fixed shape and lack of flexibility. On the contrary, the rotational mobility was much less hindered in SC dispersions at all casein concentration ranges investigated and depended on the local protein-probe friction which became high when the size of the probe became comparable to the mesh size of the system. After coagulation, PEG and dendrimer translational diffusion was found to increase due to structural changes in the casein matrix, which resulted in the formation of large voids, whereas rotational diffusion of the probes was slightly retarded in the gel, which could be attributed to the immobilized environment surrounding the probe.

Acknowledgements

The authors thank the Regional Council of Brittany and Unilever (Netherlands) for financial support. We are grateful to Arnaud Bondon for access to the NMR facilities of the PRISM Research Platform (Rennes, France).

References

(1) Gold, D.; Onyenemezu, C.; Miller, W. G. *Macromolecules* **1996,** 29 (17), 5700-5709.
(2) Onyenemezu, C. N.; Gold, D.; Roman, M.; Miller, W. G. *Macromolecules* **1993,** 26 (15), 3833-3837.
(3) Cheng, Y.; Prud'homme, R. K.; Thomas, J. L. *Macromolecules* **2002,** 35 (21), 8111-8121.
(4) Colsenet, R.; Soderman, O.; Mariette, F. *Macromolecules* **2005,** 38 (22), 9171-9179.
(5) Le Feunteun, S.; Mariette, F. *J. Agric. Food Chem.* **2007,** 55 (26), 10764-10772.
(6) Masaro, L.; Zhu, X. X. *Prog. Polym. Sci.* **1999,** 24 (5), 731-775.
(7) Amsden, B. *Polymer* **2002,** 43 (5), 1623-1630.
(8) Brownstein, K. R.; Tarr, C. E. *Phys. Rev. A* **1979,** 19 (number 6), 2446-2453.
(9) Kleinberg, R. L.; Kenyon, W. E.; Mitra, P. P. *J. Magn. Reson.* **1994,** 108, 206-214.
(10) Johnson, C. S. *Prog. Nucl. Magn. Reson. Spectrosc.* **1999,** 34 (3-4), 203-256.
(11) Price, W. S. *Concepts Magn. Reson.* **1997,** 9 (5), 299-336.
(12) Price, W. S. *Concepts Magn. Reson.* **1998,** 10 (4), 197-237.
(13) Walderhaug, H.; Soderman, O.; Topgaard, D. *Prog. Nucl. Magn. Reson. Spectrosc.* **2010,** 56 (4), 406-425.
(14) Price, W. S. *Concepts Magn. Reson.* **1997,** 9 (5), 299-336.
(15) Dickinson, E.; Golding, M. *J. Colloid Interf. Sci.* **1997,** 191 (1), 166-176.
(16) Salami, S.; Rondeau-Mouro, C.; van Duynhoven, J.; Mariette, F. *Food Hydrocolloids* **2013,** 31 (2), 248-255.
(17) HadjSadok, A.; Pitkowski, A.; Nicolai, T.; Benyahia, L.; Moulai-Mostefa, N. *Food Hydrocolloids* **2008,** 22 (8), 1460-1466.
(18) Pitkowski, A.; Durand, D.; Nicolai, T. *J. Colloid Interf. Sci.* **2008,** 326 (1), 96-102.
(19) Lucey, J. A.; Srinivasan, M.; Singh, H.; Munro, P. A. *J. Agric. Food Chem.* **2000,** 48 (5), 1610-1616.
(20) Panouille, M.; Benyahia, L.; Durand, D.; Nicolai, T. *J. Colloid Interf. Sci.* **2005,** 287 (2), 468-475.
(21) Ruis, H. G. M. Structure-rheology relations in sodium caseinate containing systems Wageningen University, The Netherlands, 2007.
(22) Bouchoux, A.; Debbou, B.; Gesan-Guiziou, G.; Famelart, M. H.; Doublier, J. L.; Cabane, B. *J. Chem. Phys.* **2009,** 131 (16).
(23) Braga, A. L. M.; Menossi, M.; Cunha, R. L. *Int. Dairy J.* **2006,** 16 (5), 389-398.
(24) Roefs, S. P. F. M.; De Groot-Mostert, A. E. A.; Van Vliet, T. *Colloid. Surface.* **1990,** 50, 141-159.
(25) Roefs, S. P. F. M.; Van Vliet, T. *Colloid. Surface.* **1990,** 50, 161-175.
(26) Takeuchi, K. P.; Cunha, R. L.; Takeuchi, K.; Cunha, R. *Dairy Sci. Technol.* **2008,** 88 (6), 667-681.
(27) Lucey, J. A.; Vliet, T. V.; Grolle, K.; Geurts, T.; Walstra, P.; van Vliet, T. *Int. Dairy J.* **1997,** 7 (6), 389-397.
(28) O'Kennedy, B. T.; Mounsey, J. S.; Murphy, F.; Duggan, E.; Kelly, P. M. *Int. Dairy J.* **2006,** 16 (10), 1132-1141.
(29) Ogston, A. G.; Preston, B. N.; Wells, J. D. *Proc. R. Soc. Lond. A* **1973**, 333, 297-316..
(30) Rubinstein, M.; Colby, R. H. *Polymer Physics,* 1st ed.; oxford University Press: Oxford, 2003.

(31) Thomar, P.; Durand, D.; Benyahia, L.; Nicoali, T. *Faraday Discussion* **2012,** 158, 325-339.
(32) Bouchoux, A.; Schorr, D.; Daffe, A.; Cambert, M.; Gesan-Guiziou, G.; Mariette, F. *J. Phys. Chem. B* **2012,** 116 (38), 11744-11753.
(33) Brownstein, K.; Tarr, C. *Phys. Rev. A* **1979,** 19 (6), 2446-2453.
(34) Kleinberg, R. L.; Kenyon, W. E.; Mitra, P. P. *J. Magn. Reson. Ser. A* **1994,** 108 (2), 206-214.
(35) Kalab, M.; Allanwojtas, P.; Phippstodd, B. E. *Food Microst.* **1983,** 2 (1), 51-66.
(36) Philips, R. J.; Brady, J. F.; Bossis, G. *Phys. Fluids* **1988,** 31, 3473.
(37) philips, R. J.; Brady, J. F.; Bossis, G. *Phys. Fluids* **1988,** 31, 3462.

Chapter VI

General discussion and perspectives

The main objective of the experiments carried out during this project was to improve the understanding of the mobility of probes with different sizes and deformabilities in casein systems. In the following paragraphs, the results obtained in each casein system are compared and discussed in an attempt to understand the respective effects of protein supramolecular organization and mobility, as well as the flexibility of the probe on its mobility, with the intent to validate or invalidate the previous results of Le Feunteun et al. [1-3].

1. Description of casein matrices

Caseins have interesting association properties that make them adopt very distinct supramolecular organizations depending on their environment (**Figure 1**):

- ***Casein micelle form*** (native phosphocaseinate, NPC). In NPC dispersions, caseins are organized into so-called "casein micelles". Those micelles are complex associative colloids of approximately 100 nm in radius with a mass consisting of 8% phosphate and calcium ions in the form of ~4 nm nanoclusters that are distributed within their core [4]. Strong associative interactions exist between those calcium phosphate nanoclusters (CCP) and the calcium-sensitive, highly phosphorylated αs1- and αs2–caseins that are present in the micelle [5].

- ***Sodium caseinate form*** (SC). The mineral content of the casein micelles can be simply removed through acidification and precipitation at pH 4.6. After a subsequent increase in pH to a physiological value of ~7 through the addition of sodium hydroxide, a dispersion of sodium caseinate is obtained. In this type of dispersion, the casein molecules are no longer organized into micelles but are present in the form of fragile star-like aggregates of ~11 nm in radius [6-8].

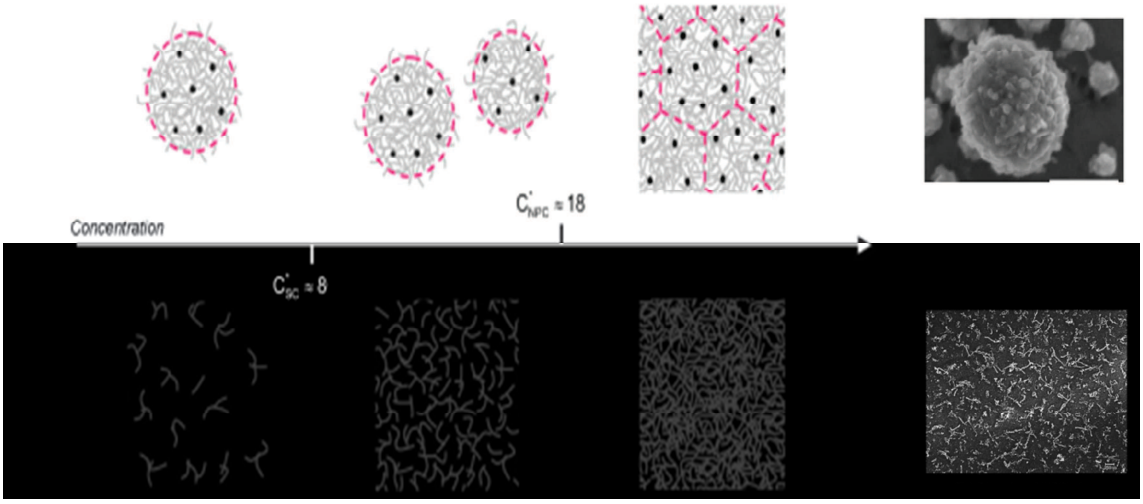

Figure 1. A schematic view of the supramolecular organization of caseins in dispersions of casein micelles (native phosphocaseinate, NPC) and sodium caseinate (SC) as a function of casein concentration. For the casein micelle representation, the CaP nanoclusters are depicted as small black dots. The dashed contour lines illustrate the fact that the micellar entity is preserved upon compression and that neighboring micelles do not interpenetrate.

These strong structural differences obviously remain as casein concentration increases. **Figure 1** gives a schematic view of the concentration process. Three distinct concentration regimes in which NPC and SC caseins respond differently to an increase in concentration can be distinguished:

1. **Diluted regime, C < 8 g/100 g H_2O**. In this first concentration regime, both NPC and SC dispersions contain the well-defined objects that are briefly described in the text below. When the concentration increases, the casein micelles (NPC) and the casein star-like aggregates (SC) move closer to each other but without coming in direct contact [9].

2. **Intermediate regime, 8 < C < 18 g/100 g H_2O.** Starting from 8 g/100 g H_2O, the SC particles are progressively forced to come into contact with each other and to interpenetrate/entangle [9-10]. A huge increase in viscosity for SC dispersions at C > 8 g/100 g H_2O was measured by different authors and was interpreted as the transition toward a "jammed" or hyperentangled regime [9-10]. Casein particles are densely packed and start to overlap at casein concentrations ≥ 12 g/100 g H_2O [7, 11]. On the other hand, a concentration

as high as 18 g/100 g H_2O is necessary to force the casein micelles to come into direct contact. The micelles are therefore still separated from each other in the range 8 − 18 g/100 g H_2O [9, 12-13].

3. **Dense regime, C > 18 g/100 g H_2O.** Starting from 18 g/100 g H_2O, the casein micelles are maximally packed and in direct contact with each other. A consequence of this is that NPC dispersions progressively turn into soft solids [9, 13]. Weak energy bonds develop between the micelles and, just like emulsion droplets, their shape changes and "deflates" as the concentration increases [9, 13].

2. Casein self-diffusion in casein dispersions

The dynamic properties of casein proteins in relation to the protein concentration were investigated in NPC and SC dispersions by observing changes in their self-diffusion coefficients. Two diffusion coefficients were measured and attributed in both casein systems to soluble compounds and casein particles. The sizes of the casein particles, estimated from the Stokes-Einstein relation (SE), were consistent with the casein size distribution determined by DLS and were equal to 12 nm in radius for sodium caseinate aggregates and 96 nm in radius for casein micelles.

Figure 2 shows the variation of casein particle normalized diffusion coefficients as a function of casein concentrations in NPC and SC dispersions. First, the data were fitted to the empirical equation proposed by Speedy [14] to describe the self-diffusion of non-interacting hard spheres in a hard sphere fluid. The results shown in **Figure 2** indicate that caseins still behave as non-interacting hard spheres up to a casein concentration of approximately 8 g/100 g H_2O for the SC system, and 15 g/100 g H_2O for the NPC system. The model failed to describe the casein diffusion data above these concentrations, at which casein particle spheres are progressively forced to come into contact with each other and, in the case of the SC system, to interpenetrate/entangle. The values of voluminosity calculated from the fitting for casein micelles and sodium caseinate aggregates were 3.4±0.05 and 7±0.4, respectively, in close agreement with previously estimated data.

Second, the normalized diffusion coefficients were compared with the inverse normalized viscosities previously measured by Pitkowski et al. [7, 15]. The results showed that the viscosity explained the diffusion behavior of casein particles in casein dispersions up to a casein concentration of approximately 20 g/100 g H_2O for the NPC system (no diffusion data was available between 15 and 22.4) and 12 g/100 g H_2O for the SC system. A clear deviation from SE prediction for sodium caseinate spheres occurs when the matrix begins to overlap and entangle. The casein particle will not sense the macroscopic solution viscosity at this stage. Instead, it encounters a reduced effective diffusivity, the microviscosity. Similarly, deviation from SE prediction for casein micelle spheres occurred when the casein particles turned into soft solids and began to interact with each other.

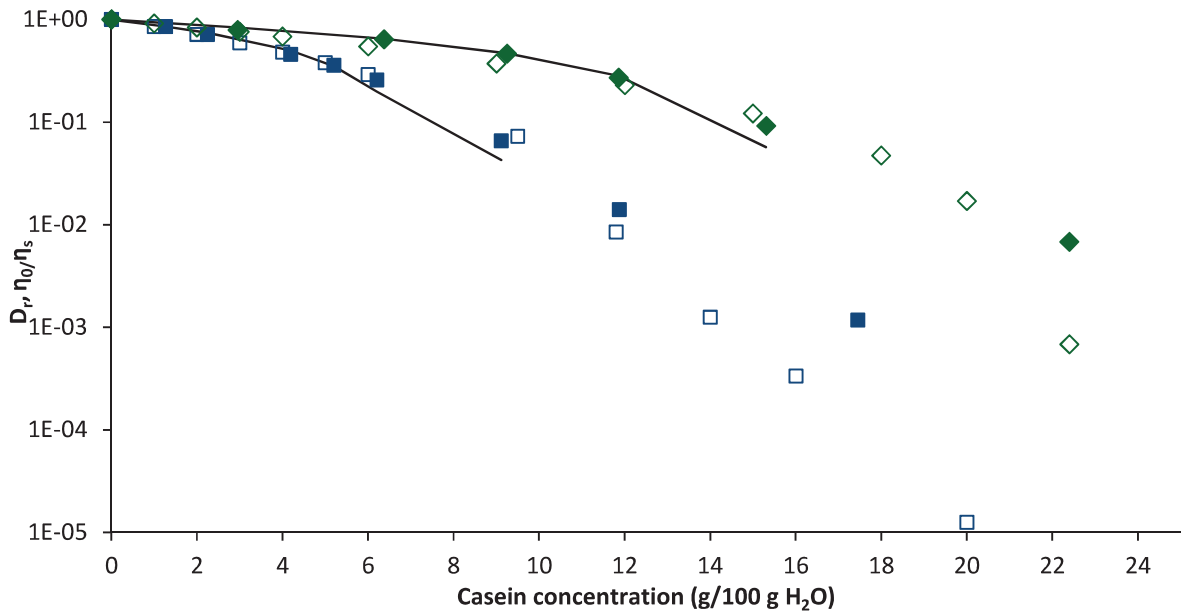

Figure 2. Casein concentration dependencies of the casein-normalized diffusivities D_r (filled shapes) and the inverse suspension viscosities (η_s) normalized by the solvent viscosity (η_0) (empty shapes) for SC (squares) and NPC suspensions (diamonds). Solid lines correspond to casein-reduced diffusivity D/D_0 calculated using the Speedy model.

3. Probe mobility in casein matrices

The mobility of flexible PEG and rigid dendrimer probes was measured in NPC and SC dispersions and gels at two different length scales, using NMR diffusometry and relaxometry. These results are discussed in two parts: the first one concerns the self-diffusion measurements and the second one the relaxation measurements.

Table 1 shows the self-diffusion coefficients and the corresponding hydrodynamic radii of different dendrimer generations and PEG molecular weights used in this study.

Dendrimers	D (m^2s^{-1})	R_h (nm)	PEGs	D (m^2s^{-1})	R_h (nm)
G2	7.54e-11	2.84	615	2.7e-10	0.79
G3	6.10e-11	3.51	7920	6.77e-11	3.16
G5	4.16e-11	5.16	21300	3.99e-11	5.37
G6	3.42e-11	6.27	32530	3.06e-11	7
			93000	1.62e-11	13.22

Table 1. Self-diffusion coefficients and the corresponding hydrodynamic radii of different dendrimer generations and PEG molecular weights. Data obtained from NMR diffusion measurements in a H_2O/NaCl solution (0.1 M) at 20°C.

Based on these results, PEG-dendrimer trios and couples with similar hydrodynamic radii could be recognized: (i) 7920/G2;G3; (ii) 21300/G5; (iii) 32530/G6. For the sake of simplicity, PEG and dendrimers will be referred to as G_X and PEG_X in the following sections, with X being equal to the hydrodynamic radius of these diffusional probes.

3.1. Probe self-diffusion in casein matrices

Depending on the molecular weight of the probe studied, Δ was adjusted to obtain a diffusion distance of z = ~1.5 µm in the casein suspensions and gels, in accordance with the Einstein equation, $z = (2 \Delta D_{probe})^{1/2}$. The absence of restricted diffusion at the length scale studied (1.5 µm) was verified for PEGs and dendrimers in NPC and SC dispersions and gels.

3.1.1. Probe self-diffusion in casein dispersions

The diffusion of ***flexible and deformable PEG probes*** was first studied in SC and NPC dispersions with casein concentrations ranging from 1.26 to 24.04 g/100 g H_2O. The probes used were $PEG_{0.79}$, $PEG_{3.16}$, $PEG_{5.37}$, PEG_7 and $PEG_{13.22}$.

As shown in **Figure 3**, wide differences in the PEG self-diffusion coefficients were found according to the casein particle structure. The greatest reduction in diffusion coefficients was found in SC dispersions that have higher densities than NPC systems for the same casein concentration. This is due to differences in the sizes of the casein particles and the entanglement of the system at low casein concentrations compared to the NPC system. Consequently, the free volume available between the particles or the entanglement points is greater in NPC dispersions than in SC dispersions for a given casein concentration, which is partially responsible for the strong reduction in diffusion in SC dispersions with an increase in casein concentration.

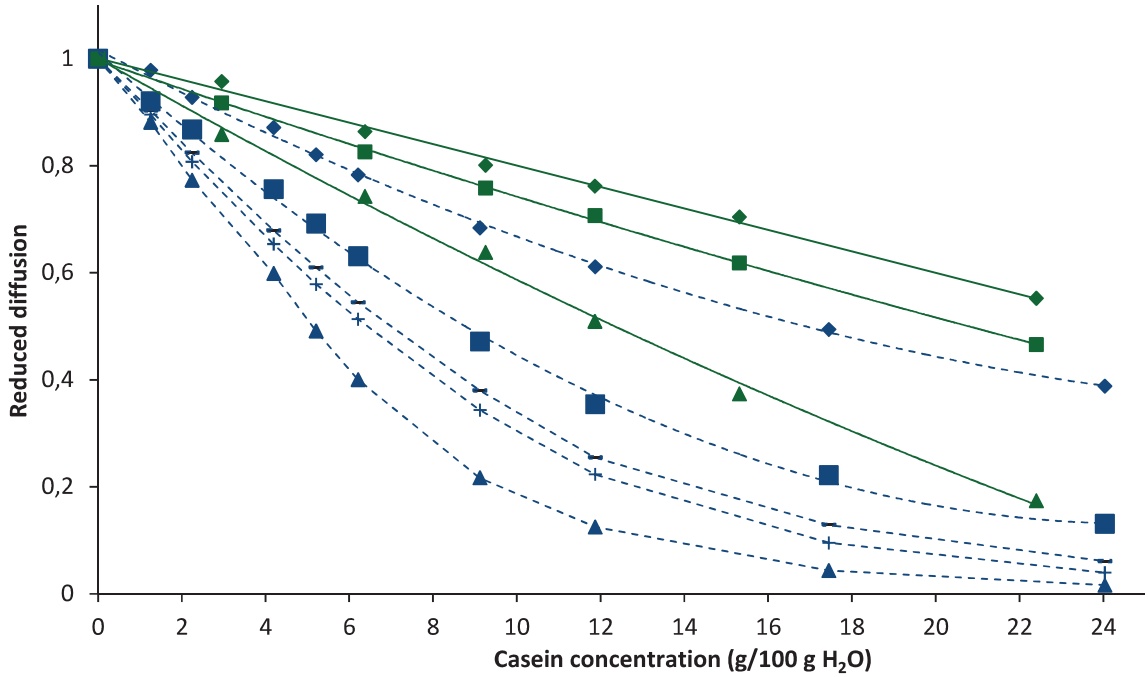

Figure 3. Reduced self-diffusion coefficients of different PEGs ($PEG_{0.79}$ ♦, $PEG_{3.16}$ ■, $PEG_{5.37}$ -, PEG_7 + and $PEG_{13.22}$▲) as a function of casein concentrations in NPC (solid lines) and SC (dashed lines) suspensions.

Secondly, ***unflexible and undeformable dendrimer probes*** were used to explore the impact of the casein matrix on the mobility of these probes. Accordingly, the diffusion of the $G_{2.84}$ dendrimer probe was compared to the diffusion of the $PEG_{3.16}$ in NPC dispersions. The diffusion of the $G_{6.27}$ dendrimer was also compared to the diffusion of the PEG_7 in NPC and SC dispersions. The results obtained in both casein dispersions are summarized in **Figure 4** with casein concentrations ranging from 1.26 to 29 g/100 g H_2O.

In both casein systems, differences in the diffusion behavior between PEG and dendrimer probes of similar size were only observed after the casein critical interacting concentration C*. Before C*, the probes diffused in a similar manner. Moreover, **Figure 3** and **Figure 4** also show that the probe diffusion occurred at all casein concentration values and was not stopped when casein particles were maximally packed and in direct contact with each other (C > 12 and 18 g/100 g H_2O for SC and NPC dispersions, respectively). This is due to the fact that casein particles are mobile obstacles that can turn into soft particles at high casein concentrations. In the case of the SC system, these soft particles can interpenetrate/entangle, whereas in the case of NPC, these soft particles are porous and penetrable. In this case, long-range diffusion of a tracer is not prevented but only retarded. The extent of the diffusion retardation certainly depends on the diffusion coefficient of the obstacles and the tracer.

A

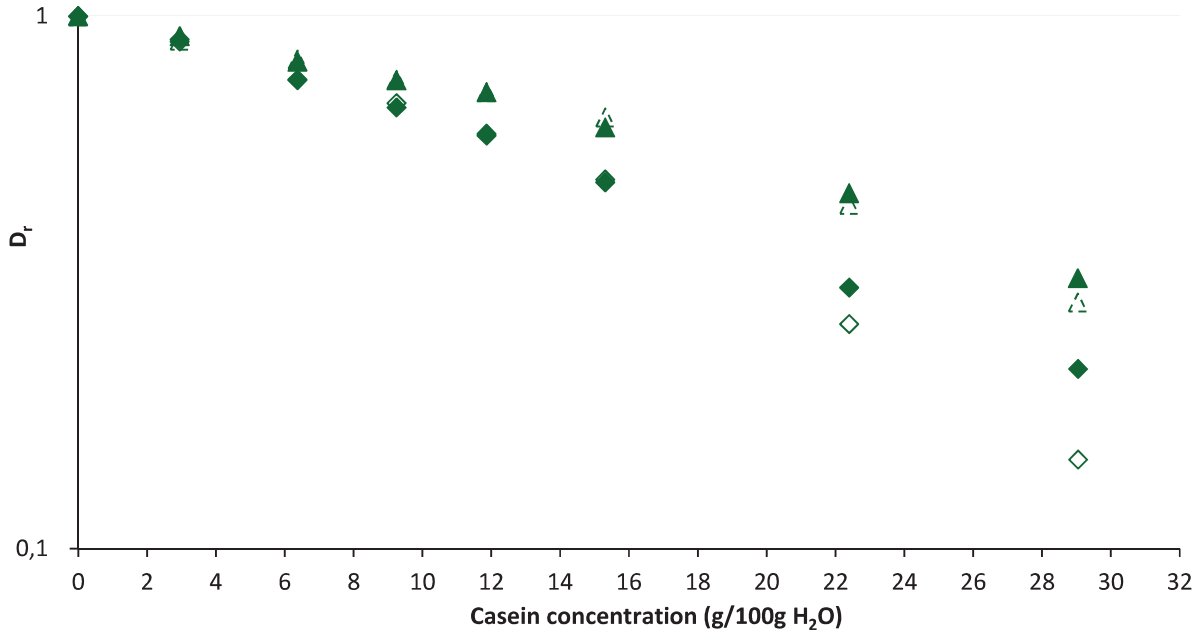
1
0,1
D_r
0
2
4
6
8
10
12
14
16
18
20
22
24
26
28
30
32
Casein concentration (g/100g H_2O)

B

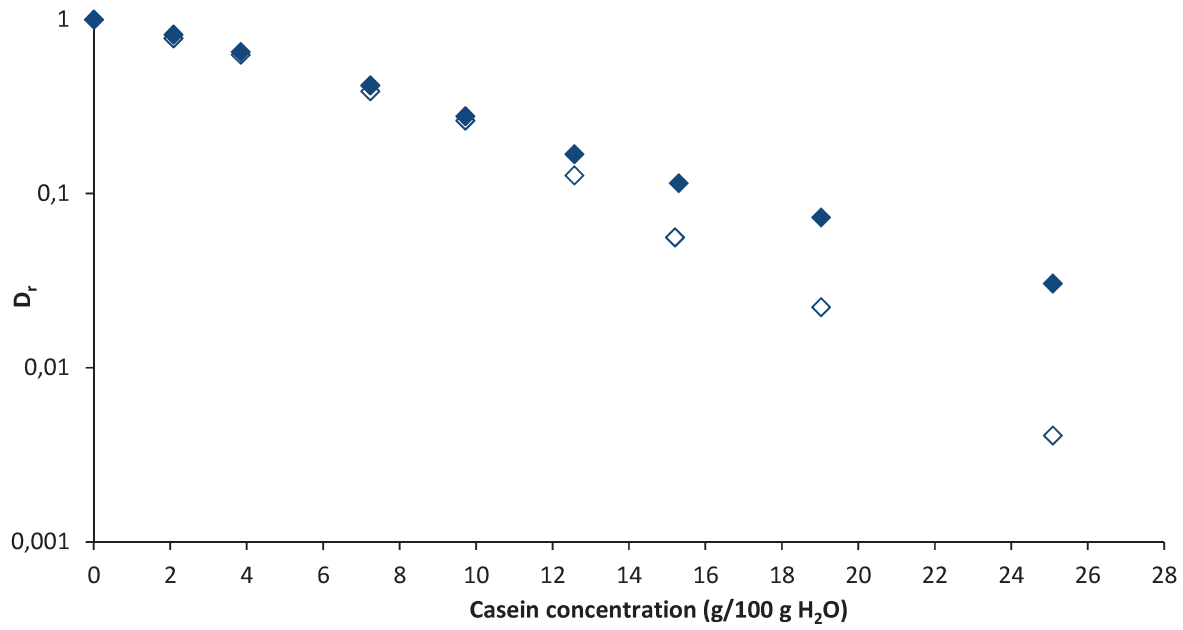
1
0,1
0,01
0,001
D_r
0
2
4
6
8
10
12
14
16
18
20
22
24
26
28
Casein concentration (g/100 g H_2O)

Figure 4. (A) Comparison of reduced self-diffusion coefficients of $PEG_{3.16}$ (▲)/PEG_7 (♦) and $G_{2.84}$ (∴)/$G_{6.27}$ (◊) dendrimers in relation to casein concentrations in NPC suspensions; (B) Comparison of the reduced self-diffusion coefficients of PEG_7 (♦) and $G_{6.27}$ (◊) dendrimers as a function of casein concentrations in SC dispersions.

Before going further into the details of these findings, it should be mentioned that as in the case of casein, probe-reduced self-diffusion data were compared with the Stokes-Einstein relation. In both casein systems, probes were found to diffuse faster than expected from the solution viscosity. This indicates that the reduction in the probe self-diffusion coefficient was minorly affected by the macroviscosity of the dispersions but assumed to depend more on the space occupied by the matrix.

The results of these experiments provided a clear answer to the main question of this thesis regarding the existence of the intra-micellar diffusion mechanism proposed earlier in NPC dispersions [1-3]. Based on this model and on those proposed in the literature [5, 16-18] that describe the casein micelle as a very porous protein that allows the diffusion of molecules with relatively high molecular weight (45,000 g/mol) [19-20], a greater reduction in diffusion coefficients should have been observed (i) in the NPC system and not in the SC system (in the first study), and (ii) for PEGs before the entanglement of the NPC system (in the second study) since the PEG should encounter greater resistance when diffusing inside the micelle. Based on these results, the intra-micellar diffusion mechanism is no longer valid. All the probes diffuse between the casein micelles, regardless of their size and deformability.

These findings do not obviate the great porosity of the casein micelle and the capability of some molecules to enter inside it, but they instead indicate that the availability of a large free volume fraction between the casein micelles does favor an extra-micellar diffusion mechanism instead of an intra-micellar diffusion mechanism.

To obtain a deeper understanding of the probe diffusion in NPC and SC systems, the PEG experimental diffusion data were modeled using a simple power law that provides a description of the solute diffusion coefficients versus molecular weight:

$$D = A.M^{-\alpha}$$

The parameter α describes the degree of probe entanglement with α varying between 0.6 and 2. The minimum value of α corresponds to the diffusion of a probe that adopts a spherical random coil form. The maximum value of α corresponds to the reptation regime in which the probe is completely "unfolded" and diffuses like a "worm" between the obstacles. The intermediate values of α correspond to changes in the shape of the probe that occur when the system mesh size approaches the probe diameter.

Figure 5 shows the different α values obtained by fitting the experimental data measured in NPC and SC suspensions.

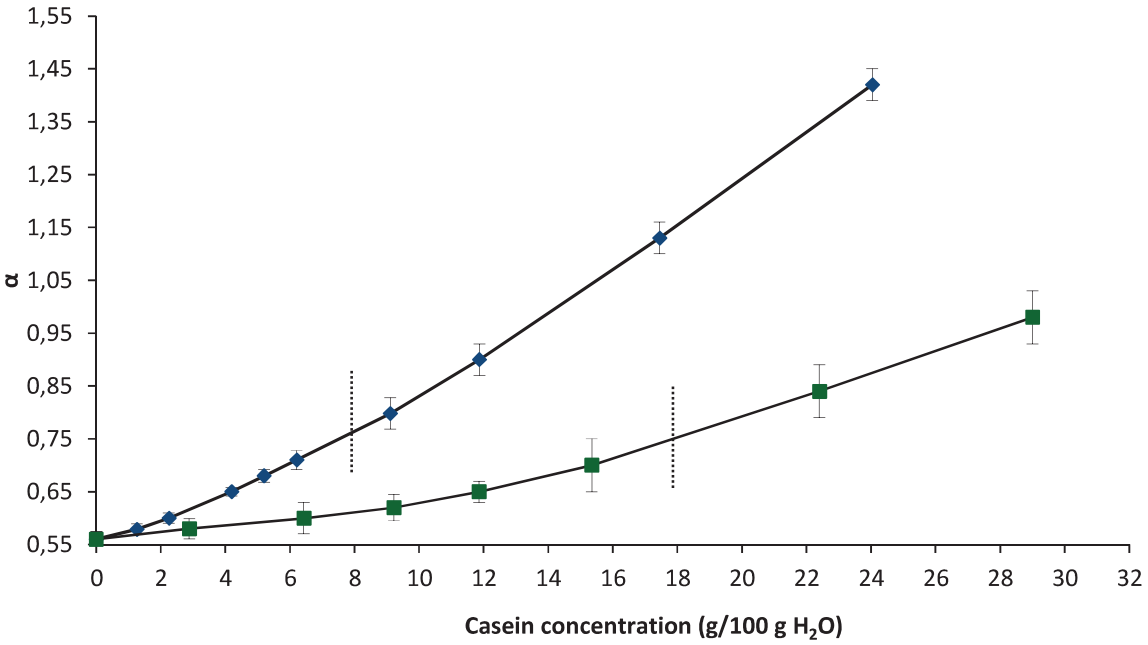

Figure 5. Exponent (α) of a power law curve fit obtained after regression of PEG diffusion coefficients (D) in NPC (■) and SC (♦) suspensions vs. molecular weight (M_w). Error bars represent the uncertainties estimated by the fitting procedure.

The results indicate that the casein networks (NPC and SC systems) are not dense enough to induce reptation (within the concentration range studied and probe size used), but are dense enough so that the solute conformations corresponding to elongated shapes are favored for the diffusion step to be effective. Before the critical casein interacting concentration (8 and 18 g/100 g H_2O for SC and NPC, respectively) where casein particles are still separated, the obstruction mechanism induced by caseins imposed no constraints on the spatial organization of probes (α <

0.7). Consequently, PEGs and dendrimers diffused in a similar manner. Beyond the critical concentration, α values shifted towards higher values (> 0.7), indicating that the size of the probe (R) approaches the pore size of the system (ξ). In this case, PEGs adopted an ellipsoidal random coil form in order to diffuse through the casein system. As a consequence, PEGs diffused faster than dendrimers, which encountered more resistance due to their fixed shape and lack of flexibility. The greater the ratio R/ξ is, the greater the difference in diffusion behavior between PEG and dendrimer will be.

Figure 6 shows that a universal curve is obtained from the data in **Figure 4 (A)** and **Figure 4 (B)** when the casein concentration was normalized using its critical casein concentration.

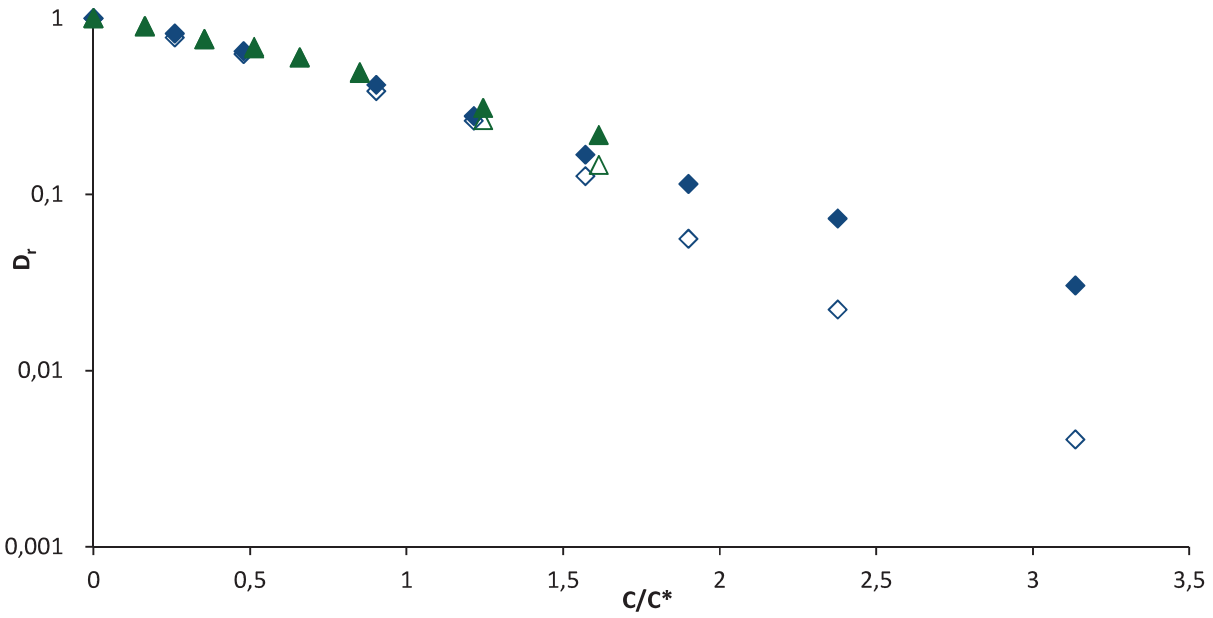

Figure 6. Plots of self-diffusion for PEG_7 and $G_{6.3}$ in NPC and SC matrices with the casein concentration normalized by its critical casein concentration, C*.

An important piece of information can be drawn from these results regarding the porosity of the casein micelle itself. Beyond the critical interacting concentration of the NPC system, the probes are forced to diffuse through the casein micelle, which is known to be open and highly porous. As shown in **Figure 4 (A)**, the diffusion of the G6 dendrimer was not stopped or severally hindered at this stage. This indicates that the size of the pore inside the micelle necessarily exceeds the diameter of G6, which is equal to 12 nm. Taking the results of **Figure 6** into account, the pore

size inside the micelle can be estimated at approximately 20 nm, the same as that estimated in SC dispersions at a casein concentration of between ~10 and 13 g/100 g H_2O (**Chapter V**).

In conclusion, it was shown that a non-interacting hard sphere model can be a valuable model for casein micelles and sodium caseinate particles up to casein concentrations that match their critical interaction concentrations. Moreover, the diffusion of these particles was found to scale inversely with the macroscopic viscosity up to a casein concentration of approximately 12 g/100 g H_2O for SC systems and 20 g/100 g H_2O for NPC systems, above which casein sphere particles turn into soft particles and interpenetrate/entangle (only in the case of the SC system). On the other hand, the diffusion of probes in NPC and SC dispersions cannot be exclusively explained by the variation in the viscosity values observed between both casein systems. Indeed, different parameters should be considered in order to explain the observed variation in the probe self-diffusion coefficients in both casein dispersions. These factors include the density and the mobility of the casein system, as well as the probe size and its flexibility. Importantly, our results showed that a connection exists between the observed changes in casein and probe molecular mobility and the already documented changes in rheological and osmotic properties of casein dispersions as concentration increases. Finally, the results obtained challenge the "two pathways" diffusion model already proposed to explain the diffusion of a probe in NPC suspensions [1-3] and indicate that the extra-micellar diffusion mechanism is the only mechanism to be considered, regardless of the size and the shape of the probe.

3.1.2. Probe self-diffusion in casein gels

The effect of coagulation was studied in rennet NPC gels at a casein concentration of 15 g/100 g H_2O, for PEG and dendrimer probes of various sizes (**Figure 7)**, and in acid SC gels at three different casein concentrations (7.23, 9.73 and 15.3 g/100 g H_2O) for the $PEG_7/G_{6.3}$ couple (**Figure 8**).

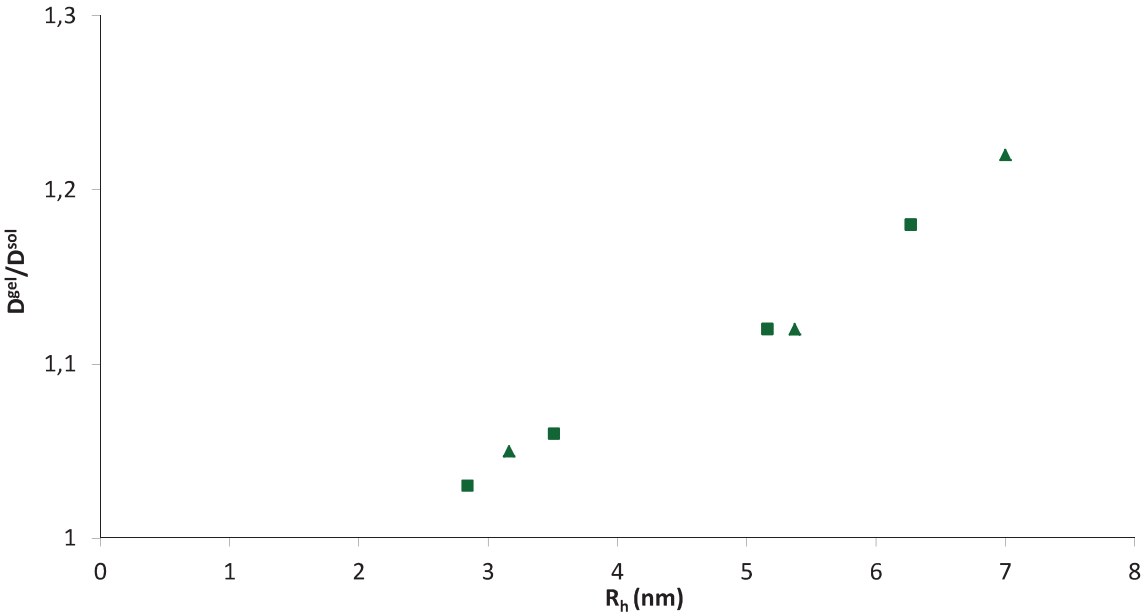

Figure 7. D^{gel}/D^{sol} ratios obtained for PEGs (▲) and dendrimers (■) of various sizes in concentrated rennet gel (15 g/100 g H_2O).

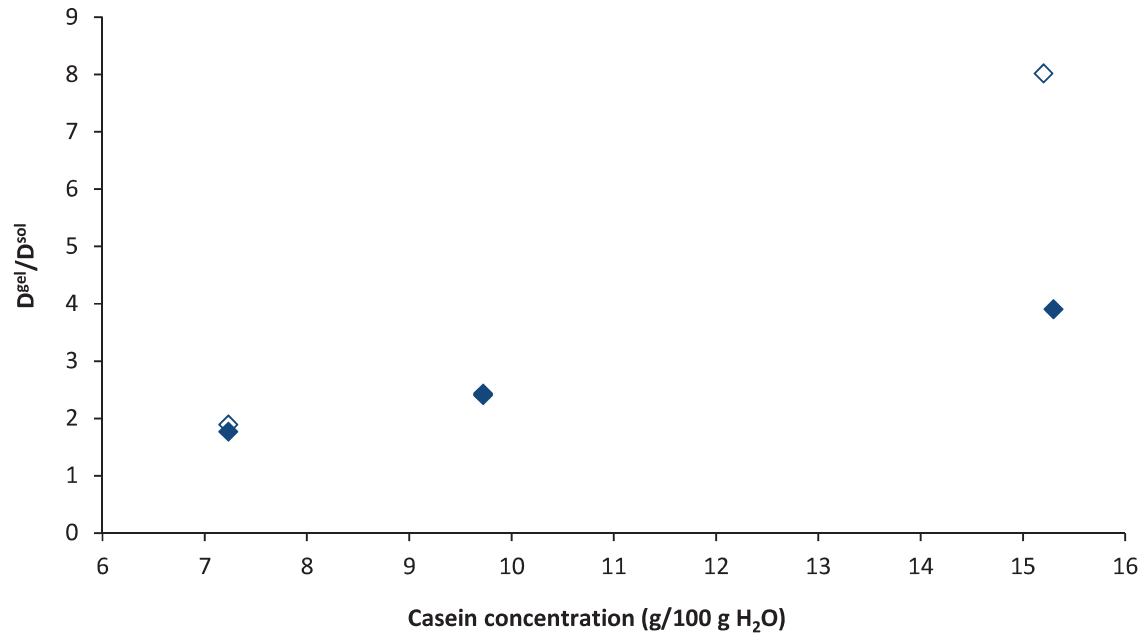

Figure 8. D^{gel}/D^{sol} obtained for PEG_7 (full shapes) and $G_{6.27}$ (empty shapes) in SC acid gels prepared at different casein concentrations.

The coagulation of the matrix led to the formation of large voids, resulting in a matrix structure with more free spaces (as shown by SEM images in **Chapter V**) and, consequently, in an increase in the self-diffusion coefficients of the probes.

The results obtained in NPC rennet gels showed that the intra-aggregate diffusion pathway already proposed in NPC gels [1-3] is no longer valid. Indeed, in this case, we should have observed (i) a decrease in the diffusion coefficient of PEG probes after coagulation due to the reduction in the strand porosity through shrinkage, and (ii) a higher diffusion in the case of dendrimer probes since they cannot enter the casein aggregates. According to these results, all the probes diffuse around the aggregates, regardless of their size and deformability.

The results obtained also showed that the effect of the coagulation was more pronounced when samples were more concentrated, since the empty volume created by the coagulation is enhanced compared to the casein-free volume available in the dispersions. Moreover, for a given casein concentration, PEG and dendrimer probes of similar size diffused in a similar manner in both types of gels (data not shown) since large pores were created in the system and whose size largely exceeds the probe size. The ratio D^{gel}/D^{sol} depended thus on the hindrance encountered by the probe in the dispersions. The greater the hindrance, the higher the ratio will be. This explains the different ratios obtained between the two casein systems and in the same system when varying the size of the probe or the concentration.

3.2. Probe relaxation in water, casein dispersions and gels

^{1}H NMR T_2 relaxation times were measured for the probes listed in **Table 1**, in water and casein systems. While the measured self-diffusion coefficients reflected translational mobility of dendrimer and PEG probes over a distance of 1.5 µm, the T_2 relaxation times reflected the rotational or local mobility of these probes at the nanometer scale.

Figure 9 and **Figure 10** illustrate the dependence of the relaxation times on the casein concentration and the molecular size of the probe in water, NPC dispersions (with casein concentration ranging from 3 to 22 g/100 g H_2O), and in a concentrated rennet NPC gel (15 g/100 g H_2O). The results showed that:

- In water, the PEG ^{1}H NMR T_2 relaxation time was sensitive to local motions of monomer units. T_2 exhibited minor variations when the chain molecular weight was higher than 7920 g/mol, which corresponds to a critical size of 180 monomer units. Above this critical size, the overall tumbling was much slower than the local motions and, therefore, its contribution to the relaxation was negligible. In contrast to PEG probes, the dendrimer macromolecules were characterized by PEG terminal function groups located on the outside, with a uniform short chain length of 587 g/mol, which is close to that of the 615 g/mol PEG. As a consequence, the local mobility of the PEG chains was the same and only affected by the overall dendrimer tumbling, which depended on the overall dendrimer size. The effect of dendrimer core rigidity manifested itself through the values of T_2, which were found to be much lower than those of the 615 g/mol PEG.
- Probe relaxation times significantly decreased in the presence of casein micelles. The extent of rotational motion retardation was, however, similar for dendrimer and PEG probes. The absence of interaction between casein micelles and probes was verified via dynamic light scattering, rheological and relaxation measurements. These variations in relaxation times for a given probe with increasing casein concentrations were attributed to increased restriction of its freedom of motion with increasing casein concentrations. The simplest case was observed for dendrimer probes that were characterized by short and uniform PEG chains. Reduced dendrimer T_2 relaxation times similarly depended on the casein concentration, regardless of probe size. However, the case was more complicated for PEG probe chains because their flexibility led to variations in the contribution to the relaxation of the local segmental motion and the global or long-range motions of large chains. In diluted casein systems ($C < 6.43$ g/100 g H_2O), the PEG T_2 relaxation was governed by the local mobility of the chain as in water solutions. When the casein concentration increased, the local mobility was restricted and the overall tumbling of the probe played a major role in the relaxation times, even for a relatively large chain size, which explains the dependence of T_2 relaxation times on probe molecular weights in domain II for casein concentrations ≥ 6.43 g/100 g H_2O.

On the other hand, the comparison of the reduced probe self-diffusion and its T_2 relaxation times in suspensions and rennet gels revealed that:

- The retardation of the probe rotation (**Figure 9 (A)** and **Figure 10 (A)**) was substantially less than the retardation of its translation (**Figure 4 (A)** and **Figure 3**) in concentrated casein suspensions. This indicates that probe mobility was less restricted over small distances than over large ones.
- While the probe self-diffusion was increased after coagulation (**Figure 7**), their ^{1}H NMR T_2 relaxation time was decreased, reflecting reduced rotational mobility in NPC rennet gels. The rotational mobility of the 7920, 21300 and 32530 g/mol (**Figure 9 (A)**) PEGs had a molecular weight dependence similar to the one obtained in water and diluted casein suspensions. T_2 hardly varied (less than 10 ms) when the PEG molecular increased from 7920 to 32530 g/mol. This indicates that the PEG ^{1}H NMR T_2 relaxation time is sensitive to local motions of monomer units in gels, which is coherent with the fact that the probe molecules are present in the liquid region of the gel with pore sizes largely exceeding the size of the probes. The pore walls are thus far away from the majority of the probe molecules and have only small perturbing effects. On the other hand, the local mobility of dendrimer probes was affected by the size of the dendrimer, but the variation of T_2 relaxation times with increasing dendrimer size was less than the variations observed in water and casein dispersions.

A

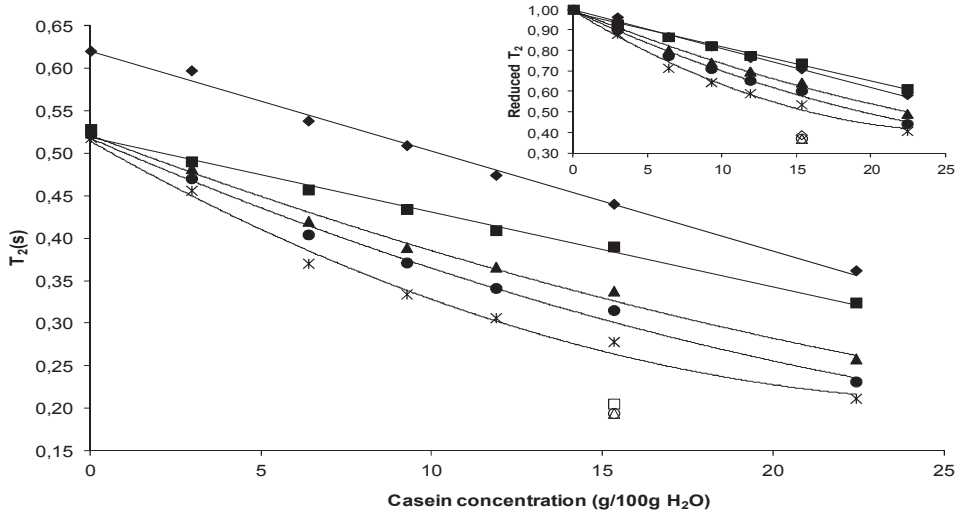

B

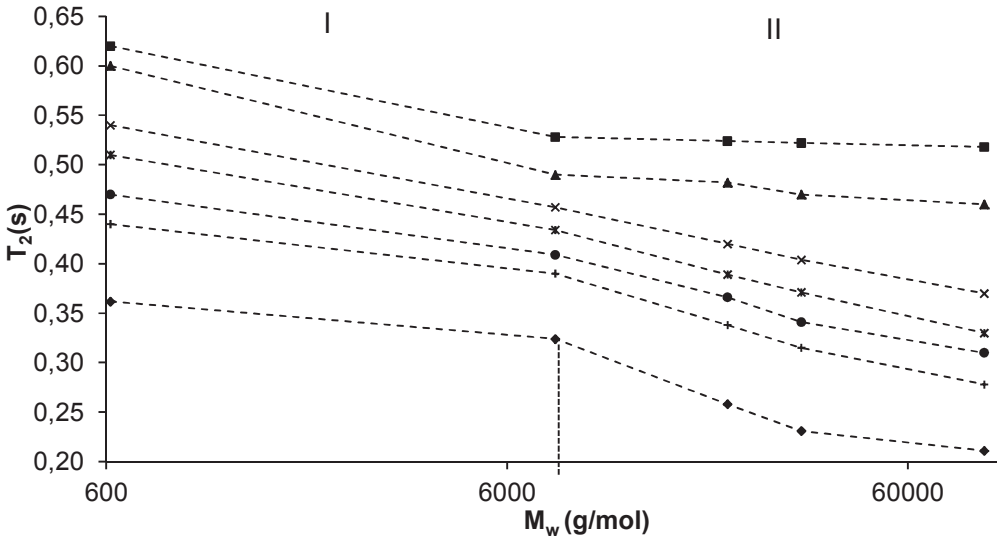

Figure 9. (A) Relaxation time T_2 of PEGs as a function of casein concentrations in NPC suspensions. PEG probes from top to bottom: 615, 7920, 21300, 32530 and 93000 g/mol. Reduced T_2 relaxation times are shown in the insert panel. Solid lines are guides for the eyes. Empty shapes correspond to the relaxation time T_2 obtained for the 7920 (□), 21300 (Δ) and 32530 (○) g/mol PEGs in the concentrated casein gel (15 g/100g H_2O) (B) Molecular weight

dependence of the PEG transverse relaxation time for various casein concentrations (from top to bottom): 0, 2.88, 6.43, 9.22, 11.86, 15.35 and 22.4 g/100 g H_2O.

A

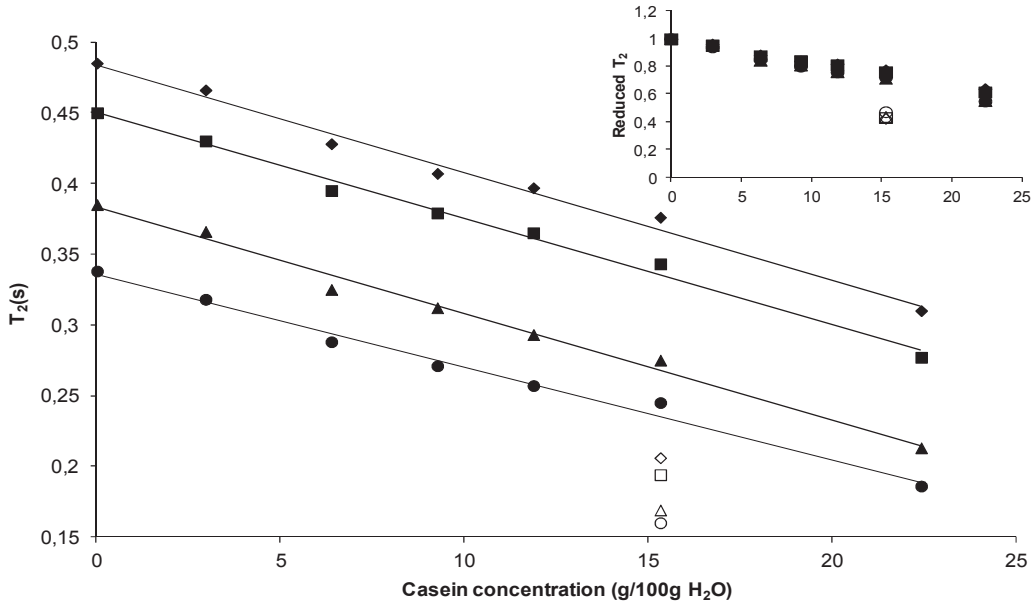

B

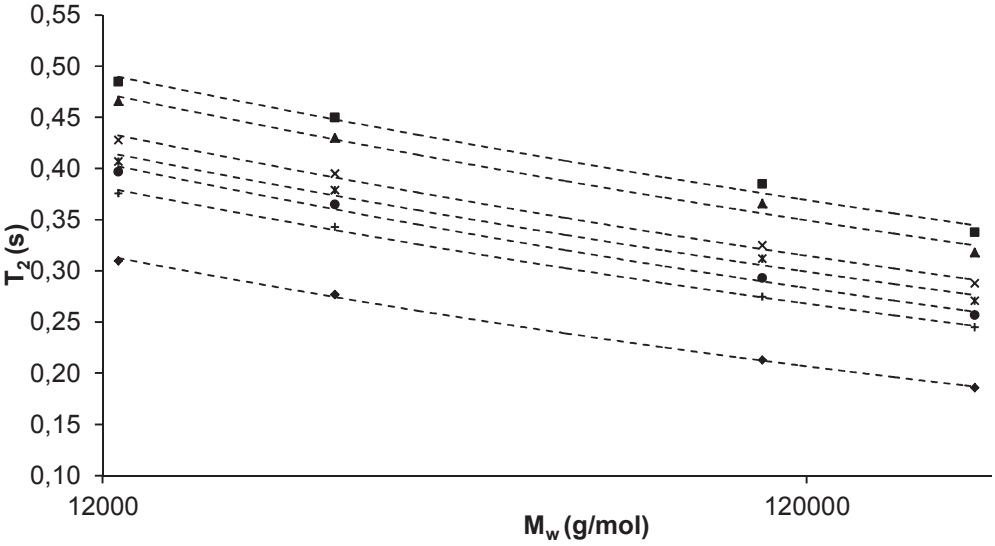

Figure 10. (A) Relaxation time T_2 of dendrimers as a function of casein concentrations in NPC suspensions. Dendrimers from top to bottom: G2, G3, G5 and G6. Reduced T_2 relaxation times are shown in the insert panel. Solid lines are guides for the eyes. Empty shapes correspond to the

relaxation time T_2 obtained for the G2 (◊), G3 (□) and G5 (Δ) and G6 (○) dendrimers in the concentrated casein gel (15 g/100 g H_2O) (B) Molecular weight dependence of the dendrimer transverse relaxation time for various casein concentrations (from top to bottom): 0, 2.88, 6.43, 9.22, 11.86, 15.35 and 22.4 g/100 g H_2O.

However, different relaxation behavior was observed in SC dispersions, as shown in **Figure 11**, which compares the variation of the T_2 relaxation times of PEG_7 (A) and $G_{6,3}$ (B) couples in SC and NPC dispersions. Although T_2 decreased with increasing casein concentration in NPC dispersions, T_2 started to decrease only when the casein concentration exceeded the critical interaction concentration (8 g/100 g H_2O). This decrease was attributed to an increase in the local matrix-friction as the mesh size of the matrix approached the size of the probe. In SC acid gels, a decrease in the rotational diffusion was also observed as in NPC rennet gels.

Although the absence of interaction between the probe and the casein matrix and, therefore, the absence of a point of contact between them was verified, the differences observed in T_2 between both casein systems are probably linked to the dynamics of the casein matrix and, more specifically, to the local mobility of the matrix. In SC dispersions, the caseins are organized into soft and fragile star-like aggregates of approximately 11 nm in radius, that are formed through weak attractive interactions between casein molecules [6-8]. Conversely, the NPC dispersions contain casein micelles that are roughly spherical, of approximately 100 nm, which are stabilized through stronger interactions between the casein chains and between the phosphoseryl residues of the α_{s1}- and α_{s2}-casein chains and the CaP nanoclusters [4-5, 18]. As a result, casein micelles are objects that are more densely packed than SC particles and have a much lower local mobility compared to them. It should be noted that the local mobility of casein micelles refers to the local mobility of the segments that extend on the outside of the micelle [22]. Furthermore, after the entanglement of the casein system, the motion of casein chains in NPC systems where CaP nanoclusters are present are much more constrained in the casein micelles than in the soft casein aggregates found in the sodium caseinate dispersions due to specific interactions that exist between caseins and minerals [11]. Taking into account the results obtained in casein gels, which show a decrease in the mobility after coagulation, a general conclusion can be drawn concerning the effect of the local matrix mobility on the motion of the probe. Highly mobile systems will allow the probe molecule to rotate, whereas lowly mobile or immobile systems will slow down

the rotation of the probe. In general, the restrictions that are experienced locally by the probe in NPC dispersions will gradually be affected by the increase in casein concentration, while in SC dispersions, the probe local mobility will be unaffected by the SC polymer matrix up to 8 g/100 g H_2O, at which point the SC particles began to come into contact and to interpenetrate/entangle. This obviously makes the local motion of the casein chains more and more difficult, which in turn explains the decrease in the probe relaxation time at this stage. The extent of retardation will therefore depend on the local mobility of the matrix, as well as on the ratio of the probe size to the pore size and on the flexibility of the probe.

A

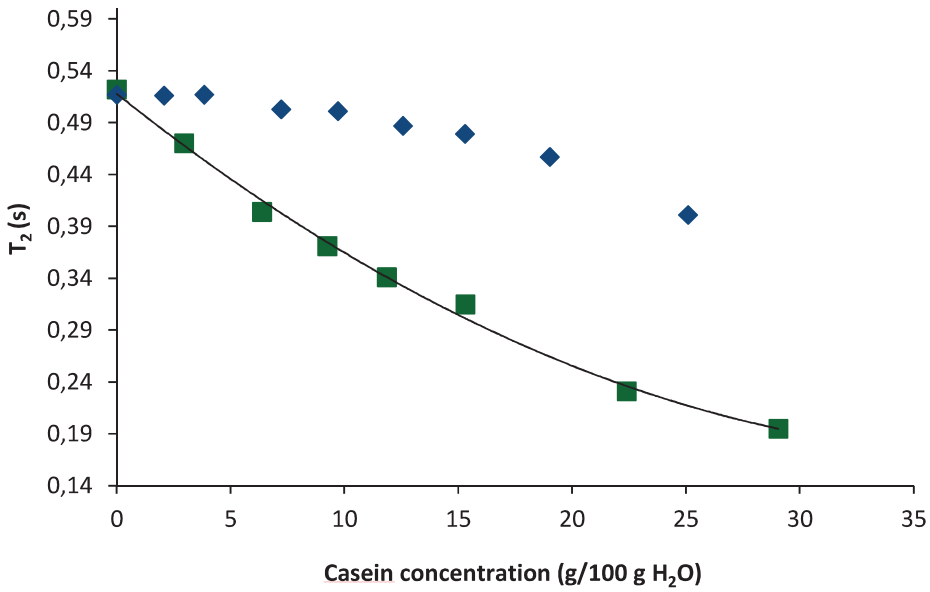

B

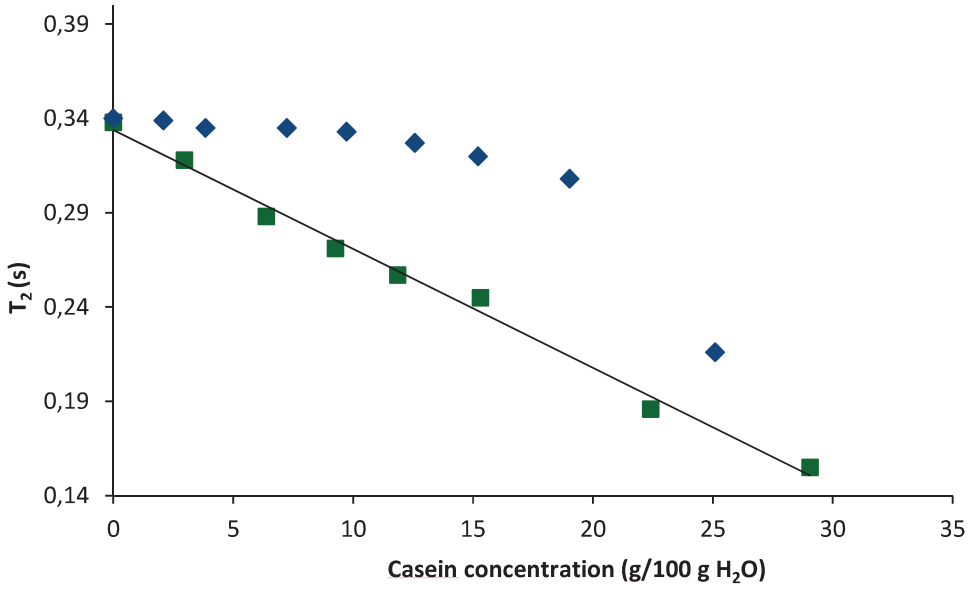

Figure 11. Variation of PEG_7 (A) and $G_{6.3}$ dendrimer (B) T_2 relaxation times in NPC (square) and SC (diamond) dispersions according to casein concentration.

4. Conclusions and perspectives

The present project made it possible to deepen our understanding of the parameters that affect the diffusion of flexible and rigid small probes in casein systems and, in particular, the impact of the microstructure of the sample.

A coherent model was used and the same mechanism was proposed to describe the diffusion of small probes in both casein dispersions (NPC and SC). It is the combination of different factors that should be considered: the ratio of the probe size to the distance between the obstructing particles or the entanglement points, the obstacle mobility and the flexibility of the probe. Before the entanglement of the casein system in which casein particles are still separated, the small PEG and dendrimer probes diffuse in a similar manner between the casein obstructing particles (casein micelles and sodium caseinate form), regardless of their deformability. An intra-micellar diffusion mechanism is not privileged by the probe in NPC dispersions due to the availability of a large free volume between the casein micelles compared to the volume available inside the

micelle. This latter was estimated to be approximately 20 nm. After the entanglement of the casein system, the probes are forced to diffuse through a dense array of obstacles where the size of the mesh (ξ) near the obstacles is similar to the size of the small probes. At this stage, PEG probes change in shape in order to diffuse through the matrix, while dendrimer probes encounter greater resistance due to their fixed shape and lack of flexibility. Differences in probe diffusion behavior between NPC and SC dispersions were linked to differences in the density between these two systems, which arise from differences in the casein particle size that was estimated via DLS and self-diffusion measurements to be equal to 12 nm in radius for SC aggregates and 96 nm in radius for casein micelles. Moreover, the diffusion of these casein particles was measured in both casein systems and was found to scale inversely with the macroscopic viscosity up to a casein concentration of about 20 g/100 g H_2O in NPC suspensions and 12 g/100 g H_2O in SC dispersions above which casein particles turn into soft solids and entangle.

The coagulation of the matrix led to the formation of large voids, which resulted in an increase in the self-diffusion coefficients of the probes. As in the case of NPC dispersions, an intra-aggregate diffusion mechanism is not privileged by the probes in rennet NPC gels. Regardless of the size and the deformability of the probe, only an inter-aggregate diffusion mechanism can exist. The effect of coagulation was more pronounced when samples were more concentrated since the empty volume created by the coagulation is enhanced compared to the casein-free volume available in the dispersions. For a given casein concentration, PEG and dendrimer probes of similar size diffused in a similar manner in the NPC rennet gel and in SC acid gels since large pores were created in the system and whose size largely exceeds the probe size. The D^{gel}/D^{sol} ratio thus depended on the resistance encountered by the probe in the dispersions.

On the other hand, the rotational diffusion of PEG and dendrimer probes was less hindered than translational diffusion in both casein systems. The interpretation of the PEG probe relaxation results involved taking the contribution to the relaxation of the local segmental motion and the long-range motions of large chains into account. It was shown that for PEG probes in H_2O and diluted casein systems, the contribution of segmental motion to ^1H T_2 is the dominant factor rather than the rotational motion of a whole molecule. T_2 exhibited minor variations when the chain molecular weight was higher than 7920 g/mol. Polymer segmental motion was hindered at increasing casein concentrations. In these systems, the ^1H NMR T_2 relaxation time was mainly

sensitive to long-range or global motions and strongly depended on the chain molecular weight. The interpretation of the results was, however, easier in the case of dendrimer probes, which were characterized by PEG terminal function groups located on the outside of the dendrimer macromolecules, with a uniform short chain length of 587 g/mol. As a consequence, the local mobility of the PEG chains was the same and only affected by the dendrimer size for a given casein concentration.

Different relaxation behaviors were observed between the two casein systems, and retardation in T_2 relaxation times was highlighted in rennet and acid casein gels. These results are probably linked to the local mobility of the matrix.

Numerous perspectives arise from this work:

- The first step could be to further improve the understanding of probe mobility in these simple matrices by:

(i) Measuring the local mobility of the casein matrix. The probe relaxation results obtained let us suggest that the local mobility of the matrix may affect the motion of the probe. Accordingly, it would be interesting to follow the variation of the casein local mobility according to casein concentration in casein dispersions and during the coagulation processes with the intent to validate the link between the matrix local motion and the probe local motion.

(ii) Proposing different experimental conditions:

- All the measurements carried out during this project were conducted at 20°C. What changes can be observed in the probe and the casein mobility at higher/lower temperatures where several modifications occur in terms of the viscosity and the structure of the dispersions? For example, at a temperature as low as 4°C, beta-casein begins to dissociate from the casein micelle, thus causing modifications in the structure of the micelle and the formation of a new type of structure. On the other hand, the aggregation number and the hydrodynamic radius of the sodium caseinate aggregates increase with increasing temperature [6]. Moreover, at high

caseinate concentrations, the viscosity strongly decreases with increasing temperature caused by a decrease of the repulsive interaction between the caseinate particles [7]. These variations in viscosity can obviously affect the diffusion of the caseinate that, in turn, will affect the diffusion of the probe.

- Knowing how concentration affects the structural and diffusional properties of food products is an essential issue in the food sciences. This thesis has addressed the dilute/semi-dilute regime where changes in osmotic, structural and rheological properties of the dispersions are still minor. An interesting perspective would be to explore the mobility of the probes and the casein particles in the concentrated regime. Following the variation of the probe and the casein particle mobility in this regime would help us to understand, in particular, the structural modification that casein micelles would undergo upon compression.

- The use of other techniques such as fluorescence recovery after photobleaching (FRAP) and multiple particle-tracking (MPT) would enable us to probe the translational mobility of PEGs and dendrimers at length scales lower (MPT) and higher (FRAP) than those probed by PFG-NMR. The combination of all three techniques should make it possible to obtain information regarding system heterogeneity and to probe the microrheological properties of the medium.

- The second step concerns the modeling of the experimental data. With the availability of more experimental data, physical diffusion models are needed for the interpretation of the results. One of the main problems of studies that aim to probe structural modifications by measuring the diffusion of probe molecules is based on the lack of models that make it possible to analyze the data. However, the experiments carried out in this thesis enabled us to identify the principal factors that explain the impact of casein matrices on probe diffusion. Thus, a promising avenue would be to construct a theoretical model that would incorporate the following elements:

  1. The mobility of the “obstructing particle”;

2. The ratio of the probe size to the mesh size of the casein matrix or to the inter-particle distance;
3. A parameter (α) that takes the variation in the PEG probe shape into account.

A theoretical model that enables us to link the diffusion of the probe to structural parameters such as the mesh size of the system would allow us to obtain information about the porosity of the casein micelle and the casein gels. The development of molecular modeling tools should, in time, make it possible to describe such phenomena. As an example, in a study by Babu et al. [23], the authors simulated tracer diffusion of colloidal particles in gels that were formed by diffusion limited cluster aggregation (DLCA) or reaction-limited cluster aggregation (RLCA) of hard spheres. It has been shown that the diffusion of tracer particles in these gels depends on the volume fraction of the gels that can be accessed by the center of mass of the particles. They investigated in detail the effects of accessible volume on the mean square displacements of tracer particles by varying the volume fraction of the gels and the structure of the gels, as well as the size of the tracers.

- Once the mobility of probes in simple matrices is fully understood, the third step could be to move as close as possible to the structure of food by making the matrix more complex. What effect will be produced by the addition of elements that contribute to the obstruction mechanism while also having an effect on the structure of the dispersions and gels? For example, the addition of fat implies additional obstruction effects, whereas the addition of polysaccharides or whey protein (accompanied by heat treatment) induces both obstruction effects and structural modifications via casein/polysaccharides or casein micelle/whey protein interactions. The presence of whey protein, fat or a polysaccharide such as carrageenan in the matrices should not be a problem for measuring the PEG and dendrimer probe self-diffusion since their chemical shifts are different from that of these probes (3.6 ppm).

5. References

1. Le Feunteun, S. and F. Mariette, *Impact of casein gel microstructure on self-diffusion coefficient of molecular probes measured by H-1 PFG-NMR.* Journal of Agricultural and Food Chemistry, 2007. **55**(26): p. 10764-10772.
2. Le Feunteun, S. and F. Mariette, *PFG-NMR techniques provide a new tool for continuous investigation of the evolution of the casein gel microstructure after renneting.* Macromolecules, 2008. **41**(6): p. 2071-2078.
3. Le Feunteun, S. and F. Mariette, *Effects of acidification with and without rennet on a concentrated casein system: A kinetic NMR probe diffusion study.* Macromolecules, 2008. **41**(6): p. 2079-2086.
4. Dalgleish, D.G., *On the structural models of bovine casein micelles-review and possible improvements.* Soft Matter, 2011. **7**(6): p. 2265-2272.
5. Horne, D.S., *Casein micelle structure: Models and muddles.* Current Opinion in Colloid & Interface Science, 2006. **11**(2-3): p. 148-153.
6. HadjSadok, A., et al., *Characterisation of sodium caseinate as a function of ionic strength, pH and temperature using static and dynamic light scattering.* Food Hydrocolloids, 2008. **22**(8): p. 1460-1466.
7. Pitkowski, A., D. Durand, and T. Nicolai, *Structure and dynamical mechanical properties of suspensions of sodium caseinate.* Journal of Colloid and Interface Science, 2008. **326**(1): p. 96-102.
8. Lucey, J.A., et al., *Characterization of commercial and experimental sodium caseinates by multiangle laser light scattering and size-exclusion chromatography.* Journal of Agricultural and Food Chemistry, 2000. **48**(5): p. 1610-1616.
9. Bouchoux, A., et al., *Rheology and phase behavior of dense casein micelle dispersions.* Journal of Chemical Physics, 2009. **131**: p. 165106-165111.
10. Thomar, P., et al., *Slow dynamics and structure in jammed milk protein suspensions.* Faraday Discussion, 2012. **158**: p. 325-339.
11. Bouchoux, A., et al., *Molecular mobility in dense protein systems: an investigation through H-1 NMR relaxometry and diffusometry.* Journal of Physical Chemistry B, 2012. **116**(38): p. 11744-11753.
12. Bouchoux, A., et al., *How to Squeeze a Sponge Casein Micelles under Osmotic Stress, a SAXS Study.* Biophysical Journal, 2010. **99**(11): p. 3754-3762.
13. Bouchoux, A., et al., *Casein Micelle Dispersions under Osmotic Stress.* Biophysical Journal, 2009. **96**(2): p. 693-706.
14. Speedy, R.J., *Diffusion in the hard-sphere fluid.* Molecular Physics, 1987. **62**(2): p. 509-515.
15. Pitkowski, A., *Processus de gelification des caseines en presence de polyphosphates*. 2007, Universite de Maine.
16. Horne, D.S., *The hairy casein micelle: Evolution of the concept and its implications for dairy technology.* Netherlands Milk and Dairy Journal, 1996. **50**(2): p. 85-111.
17. Holt, C., *Structure and stability of bovine casein micelles.* Advances in Protein Chemistry, 1992. **43**: p. 63-151.
18. Horne, D.S., *Casein interactions: Casting light on the black boxes, the structure in dairy products.* International Dairy Journal, 1998. **8**(3): p. 171-177.

19. de Kruif, C.G., et al., *Physicochemical Study of kappa- and beta-Casein Dispersions and the Effect of Cross-Linking by Transglutaminase.* Langmuir, 2002. **18**(12): p. 4885-4891.
20. O'Connell, J.E. and C.G. de Kruif, *beta-Casein micelles; cross-linking with transglutaminase.* Colloids and Surfaces A: Physicochemical and Engineering Aspects, 2003. **216**(1-3): p. 75-81.
21. Colsenet, R., O. Soderman, and F. Mariette, *Effect of casein concentration in suspensions and gels on poly(ethylene glycol)s NMR self-diffusion measurements.* Macromolecules, 2005. **38**(22): p. 9171-9179.
22. Rollema, H.S., J.A. Brinkhuis, and H.J. Vreeman, *H-1-Nmr Studies of Bovine Kappa-Casein and Casein Micelles.* Netherlands Milk and Dairy Journal, 1988. **42**(2): p. 233-248.
23. Babu, S., J. Christophe Gimel, and T. Nicolai, *Tracer Diffusion in Colloidal Gels.* The Journal of Physical Chemistry B, 2008. **112**(3): p. 743-748.

Title: NMR investigation on molecular mobility of poly(ethylene glycol/oxide) and dendrimer probes in casein dispersions and gels.

Abstract: The aim of this study was to investigate the impact of the casein microstructure on the molecular diffusion of probes with different sizes and deformabilities. The mobility of molecular flexible ('PEG') and rigid (dendrimer) probes of various sizes was studied in suspensions and gels of NPC and SC at various protein concentrations. Measurements were carried out by NMR, which makes it possible to probe translational mobilities over a distance of 1.5 microns, as well as local mobilities at the molecular scale (several nanometers) through the relaxation times, T_2. A coherent model was used and the same mechanism was proposed to describe the diffusion of small probes in both casein dispersions. It is the combination of different factors that should be considered: the ratio of the probe size to the distance between the obstructing particles or the entanglement points, as well as the flexibility of the probe. The rotational diffusion of PEG and dendrimer probes was less hindered than translational diffusion in both casein systems. Different relaxation behaviors were observed between the two casein systems and retardation in T_2 relaxation times was highlighted in rennet and acid casein gels. These results are probably related to the local mobility of the matrix. The overall results of this project led to a better understanding of probe mobility in casein systems and made it possible to propose a new model that challenges the previous one proposed by Le Feunteun et al. to describe the diffusion of probes in casein systems.

Key-words: NMR, diffusion, relaxation, poly(ethylene glycol/oxide), dendrimer, casein micelle, sodium caseinate, suspensions, rennet coagulation, acid coagulation.

Titre : Mobilité de sondes moléculaires des et des dendrimères mesurée par RMN dans des suspensions et des gels de caséine.

Résumé : L'objectif de ce travail était d'étudier l'influence qu'exerce la microstructure des caséines sur la diffusion moléculaire de petites sondes ayant des tailles et des déformabilités différentes. La mobilité de sondes moléculaires flexibles ('PEGs') et rigides (dendrimères) de taille variée a été étudiée dans des suspensions et des gels de PPCN et de CaNa à différentes concentrations en protéines. Les mesures ont été réalisées par RMN qui permet de sonder des mobilités translationnelles sur une distance de 1,5 µm, mais également des mobilités locales à l'échelle moléculaire (quelques nanomètres) à travers les temps de relaxation T_2. Un modèle cohérent a été utilisé et un mécanisme unique a été proposé pour décrire la diffusion de petites sondes dans les deux systèmes de caséine. C'est la combinaison de différents facteurs qui doivent être pris en considération : le rapport de la taille de la sonde à la distance entre les particules obstruantes ou les points d'enchevêtrement ainsi que la flexibilité de la sonde. La mobilité locale des sondes était beaucoup moins réduite que la mobilité translationnelle dans les deux systèmes de caséine. Différents comportements de relaxation ont été observés entre PPCN et CaNa et une diminution des T_2 a été mesurée dans les gels. Ces résultats ont été liés à la mobilité locale de la matrice. L'ensemble des résultats obtenus ont permis d'avoir une meilleure compréhension de la mobilité des sondes dans les systèmes caséiques et de proposer un nouveau modèle qui contredit celui déjà proposé par Le Feunteun et al. pour expliquer la diffusion des sondes dans ces systèmes.

Mots clés : RMN, diffusion, relaxation, polyéthylèneglycol, dendrimère, micelle de caséine, caséinate de sodium, suspensions, coagulation présure, coagulation acide.